Doctoral Dissertation
Doctoral Program in **Pure and Applied Mathematics** (32^{nd} Cycle)

Dipartimento di Matematica “Giuseppe Peano” - Università degli Studi di Torino
Dipartimento di Scienze Matematiche “G.L. lagrange” - Politecnico di Torino

Growth and remodelling of biological tissues, tumour masses and cellular aggregates: a theoretical and computational study

A physico-mathematical perspective encompassing Differential Geometry, Variational Methods and Configurational Forces in Continuum Mechanics

Academic Field: MAT/07 - Mathematical Physics

Salvatore Di Stefano

* * * * * *

Supervisor
Prof. Alfio Grillo

Doctoral Examination Committee:
Prof. Angela MADEO - Institut National des Sciences Appliquées de Lyon
Prof. Alessandro MUSESTI - Università Cattolica del Sacro Cuore, Brescia
Prof. Reinaldo RODRÍGUEZ-RAMOS - Universidad de la Habana, Cuba

Coordinatore del Dottorato: Prof. Riccardo Adami - Prof. Anna Maria Fino

Università degli Studi di Torino
Politecnico di Torino
A.Y. 2019/2020
September 24, 2020

I hereby declare that, the contents and organisation of this dissertation constitute my own original work and does not compromise in any way the rights of third parties, including those relating to the security of personal data.

. . . .

Salvatore Di Stefano

Turin, September 24, 2020

Summary

The main goal of this Thesis is the mathematical modelling of certain problems in the context of Biomechanics. In particular we have focused on:

- the remodelling of fibre-reinforced biological tissues, with particular attention focused on the articular cartilage of the (human) knee (we address this tissue because it is the one for which we have the largest number of experimental data);
- growth and growth-induced structural transformations in the case of tumour masses and multicellular spheroids;
- the effective behaviour of highly heterogeneous media subjected to a reorganisation of their internal structure, with particular attention to layered tissues like the bone.

The scientific activity has been conducted by developing theoretical and computational studies in the field of Nonlinear Continuum Mechanics, with the purpose of addressing different aspects of the research lines enlisted above. The main results of this Thesis can be summarised as follows.

First, we review some fundamental aspects of growth and remodelling, by switching to non-local theories of inelastic processes to capture phenomena that, otherwise, is not possible to catch.

Second, we adapt some models of growth and remodelling available in the literature to more realistic benchmarks, with the possibility to disclose results which, to best of our knowledge, were not accounted for by other Authors.

Third, we enrich models of growth and remodelling by selecting suitable variables describing the structural transformations of a tissue and by studying their evolution. Such an evolution is respectful of some mathematical restrictions, predicted by our theoretical framework.

This Thesis is mainly conceived for the broad and growing intersection between the Physico-Mathematical and Engineering communities that focuses on biomechanical problems from the theoretical, computational and experimental point of view. In this respect, the mathematical models proposed for this class of problems require, or could require, the development of dedicated numerical procedures,

which could bring to the opening of new research lines in the field of computational mechanics (for studying the robustness and the stability of algorithms, multi-grid techniques, solution of coupled problems, discretisation, linearisation methods and solvers for very large linear systems), but also new interpretations of theories already present in the literature, as well as conceptual generalisations to include and investigate some aspects of theirs that are hidden in them and not sufficiently explored. An example is given by the standard theories of growth, which often only rely on decompositions of the deformation gradient tensor of the BKL-type, without resolving explicitly the point dependence of the involved tensor fields. With this attitude in mind, the purpose of this Thesis is not the investigation of "biomechanical applications", but rather the study of a modelling process of logic-deductive type that tries to describe a certain class of phenomena of biomechanical interest that are often left out from the majority of models available in the literature. Only later the mathematical models developed and presented in this Thesis are specialised to cases of interest, for which we know all the necessary experimental data. In the chapters of this Thesis, we will refer to articular cartilage, as an example of fibre-reinforced soft tissue, to tumour masses, as a reference medium in which growth and (growth-induced) remodelling take place, and to the bone tissue, as a prototype of highly heterogeneous layered medium, undergoing a transformation of its internal structure.

The present Thesis is based on the following list of papers:

1. Ramírez-Torres, A., **Di Stefano, S.**, Grillo, A., Rodríguez-Ramos, R., Merodio, J., Penta, R. *An asymptotic homogenization approach to the microstructural evolution of heterogeneous media.* International Journal of Non-Linear Mechanics, 2018, **106**, 245-257. DOI: 10.1016/j.ijnonlinmec.2018.06.012

2. **Di Stefano, S.**, Ramírez-Torres, A., Penta, R., Grillo, A. *Self-influenced growth through evolving material inhomogeneities.* International Journal of Non-Linear Mechanics, 2018, **106**, 174-187. DOI: 10.1016/ j.ijnonlinmec.2018. 08.003

3. Crevacore, E., **Di Stefano, S.**, Grillo, A. *Coupling among deformation, fluid flow, structural reorganisation and fibre reorientation in fibre-reinforced, transversely isotropic biological tissues.* International Journal of Non-Linear Mechanics, 2019, **111**, 1-13. DOI: 10.1016/j. ijnonlinmec.2018.08.022

4. Grillo, A., **Di Stefano, S.**, Federico, S. *Growth and remodelling from the perspective of Noether's theorem.* Mechanics Research Communications, 2019, **97**, 89-95. DOI: 10.1016/j.mechrescom.2019.04.012

5. Grillo, A., **Di Stefano, S.**, Ramírez-Torres, A., Loverre, M. *A study of growth and remodelling in isotropic tissues, based on the Anand-Aslan-Chester theory*

of strain-gradient plasticity. GAMM-Mitteilungen, e201900015, 2019. DOI: 10.1002/gamm.201900015

6. **Di Stefano, S.**, Carfagna, M., Knodel, M. M., Hashlamoun, K., Federico, S., Grillo, A. *Anelastic reorganisation of fibre-reinforced biological tissues.* Computing and Visualization in Science, 2019, **20**(3-6), 95-105. DOI: 10.1007/s00791-019-00313-1

For space requirements, the following published works

7. Giverso, C., **Di Stefano, S.**, Grillo, A., Preziosi, L. *A three dimensional model of multicellular aggregate compression.* Soft Matter, 2019, **15**, 10005 - 10019. DOI: 10.1039/C9SM01628G

8. **Di Stefano, S.**, Miller, L., Grillo, A., Penta, R. *Effective balance equations for electrostrictive composites.* Accepted in *Zeitschrift für Angewandte Mathematik und Physik.*

are not directly present in this Thesis.

Acknowledgements

This Thesis represents the result of three years of work under the supervision of Prof. Alfio Grillo. Nothing could have been possible without his guidance, support, dedication and love. With his patience, motivation, and immense knowledge, he guided me in doing research, writing papers, having a talk, being a better researcher and a better human being. I could not have imagined having a better advisor and mentor for my PhD studies. Rather, I could not have imagined having a better master and a better example of what a scientist, a professor and a man should be. And, when a master is so great to give the possibility to his disciple to avoid the mistakes he did when he was young, even without blood ties, he is a father, a scientific father or a Doktorvater, as we both like to say.

I would like to thank all the people with whom I collaborated during my PhD studies. In particular, I would like to say thank you to Dr. Melania Carfagna, Dr. Eleonora Crevacore, Dr. Kotaybah Hashlamoun, Dr. Mawafag Alahasadi and Dr. Markus Knodel.

There are no words to express my gratitude to Dr. Ariel Ramírez-Torres, for his invaluable support, scientific collaboration and friendship. I hope to always deserve a place in his scientific and personal life.

I thank Michele Loverre, a great colleague and a great friend, who inspired and helped me in several occasions, even without being aware of it.

I would like to thank Prof. Salvatore Federico, Prof. Gabriel Wittum and Dr. Raimondo Penta, for the opportunity to join their research groups during my visiting period. I would like to thank also Prof. Luigi Preziosi and Dr. Chiara Giverso, with whom we have recently collaborated.

Finally, I would not have been able to reach this result without the love and help of my parents, my family, my friends Alberto, Andrea and Antonio, who are close to me, in spite of the geographical distance.

A nonna Lina e a mamma, che mi hanno insegnato l'amore, la resilienza e ad essere buono.

A nonna Concetta e a papà, che mi hanno insegnato il coraggio delle proprie idee, la forza di volontà e la capacità di ripartire dai propri errori.

Al mio maestro, Alfio, che ogni giorno mi trasmette come fare il mestiere che amo nella maniera migliore in assoluto, la capacità di perdonare gli altri e se stessi, il modo per essere sempre un uomo migliore.

Contents

List of Tables

List of Figures

Chapter 1

General Introduction: An overview of the main topics of the Thesis

This Thesis focuses on the study of some aspects of remodelling of fibre-reinforced biological tissues, as is the case of articular cartilage (Part I), and growth and remodelling of tumour masses (Part II).

With the term "remodelling" we refer to a class of transformations occurring in a biological tissue and pertaining to the evolution of its internal structure (we do not consider phase transitions among those transformations). In general, this transformation results in a change of the tissue's macroscopic mechanical properties. As reported in Chapters 2, 3 and 4, in this Thesis we consider two different types of remodelling: one consists in the manifestation, at the tissue scale, of structural rearrangements representable in terms of inelastic distortions, while the other one is the reorientation of the fibres in fibre-reinforced tissues. The former process is described, by exploiting the Bilby-Kröner-Lee decomposition of the deformation gradient tensor, in terms of a non-integrable, mixed, second-order tensor, which accompanies the change of shape of a tissue and the flow of its interstitial fluid. The latter process studies the change of the mechanical properties of a fibre-reinforced tissue in response to the evolution of the fibres' orientation. The two types of remodelling mentioned above are studied together in Chapters 2 and 3, where we highlight some possible interactions between the development of inelastic distortions and the reorientation of the fibres. In Chapter 4, instead, we focus only on the remodelling intended as production of inelastic distortions, and we address tissues that do not feature fibre reinforcement, but that are characterised by a highly heterogeneous, layered structure. We study these tissues with the aid of the Asymptotic Homogenisation Theory and we hypothesise absence of fibres in order to simplify the resulting mathematical setting.

With the term “growth”, we denote two classes of phenomena: one is referred to as *appositional, or surface, growth* and consists of the deposition or removal of material from an existing one (see e.g. [222, 17]), while the second one is said to be *volumetric growth* and consists of the redistribution and time variation of the mass density of a medium (see e.g. [210, 222, 72]). In this Thesis we consider exclusively volumetric growth. This will be introduced in Section 1.2 and in Section 1.6, and subsequently addressed in Chapters 5, 6 and 7 within different theoretical settings.

For completeness, we anticipate that the type of remodelling studied in this Thesis *does not* produce variations of mass and is characterised by time scales strongly separated from those related to volumetric growth (for instance, in tumour spheroids growth occurs over time scales of the order of days or weeks, whereas remodelling occurs on the time scale of minutes or seconds, also depending on the experiment that is considered). In addition to this consideration, we emphasise that, in none of the chapter devoted to remodelling, we shall speak of mass variation induced by remodelling. Furthermore, whereas growth may induce remodelling, due to the distortions that accompany the uptake or loss of mass, remodelling itself induces no growth.

Some parts of this introductory chapter are taken from [61, 56, 62, 114].

1.1 Remodelling of fibre-reinforced tissues

Biological tissues tend to adapt themselves to the stimuli to which they are exposed and to the environment in which they are placed [222]. By “stimulus” it is meant here any interaction, or combination of interactions, that yields an evolution of mass, composition, shape, and internal structure of a given tissue. An interaction of this kind can be genetic or epigenetic, physiological or pathological, and may be related to the occurrence of phenomena of various nature, associated with different time and length scales (see [61] and references therein).

In this work, emphasis is put on the evolution of the internal structure of fibre-reinforced soft tissues saturated with an interstitial fluid and exchanging mechanical interactions with it. For a model describing the exchange interactions between the fluid and the solid phase of a tissue experiencing anelastic phenomena, we refer, for example, to Garikipati et al. [98]. The fibres consist of collagen and are assumed to be directed according to a spatially inhomogeneous statistical distribution of orientations that makes the tissue anisotropic [151, 22, 100, 83, 79]. The fibres can be described as filiform elements with circular section. Within the mathematical models presented in this Thesis, a generic fibre is rectified in a neighbourhood of a given material point and a unit vector attached to that point is introduced to define the local direction of anisotropy of the material. On the other hand, the mechanical properties of the fibres are accounted for in the anisotropic contribution of the tissue’s energy density function. Hence, at the tissue’s scale and within a large deformation framework, our models lose the resolution of the fibres' geometry. Other details concerning the fibres' structure and mechanical properties are given in [76, 134, 158, 88]. The interactions with the fluid are usually accounted for under the hypothesis of validity of Darcy's law [138, 199, 17] (see [61] and references therein).

Within the modelling framework outlined above, we address a type of structural reorganisation that may be associated with two types of phenomena. The first one, which is often encountered in the study of cellular aggregates and tumour spheroids, occurs through the reorganisation of the extracellular matrix of the considered tissue, and leads to the change of the adhesion properties of the tissue cells [198, 104, 112]. The second phenomenon, studied in the mechanics of bone, consists of the emergence of irreversible strains in conjunction with the formation of microcracks in diseased or injured tissues [97] (we emphasise, however, that, whereas the reference to the work by Garcia et al. [97] serves to highlight the vastity of the biomechanical problems that can be addressed by suitably re-interpreting the Theory of Plasticity, no model of damage is considered in this Thesis). To give a small illustration of the type of remodelling that we investigate in this Thesis, let us consider an aggregate of cells of spherical shape. When such cellular aggregate is subjected, for instance, to centrifugation, the shape of the aggregate as a whole, as well as the shape of the cells that it contains, change, and it is possible to experimentally observe that, after a sufficiently large amount of time, the cells tend to reach a stress-free state (see [86]). Moreover, the cells change their positions and redistribute their shape and orientation in a permanent manner, so that the aggregate does not spontaneously tend to recover its original configuration, regardless of the absence of external loads. Although some Authors (as Forgacs and Co-authors in [86]) use the theory of viscoelasticity to model the experiment described so far, the inelastic behaviour of the cellular aggregate may also suggest interpretations close to viscoplasticity. Indeed, the internal structure of the aggregate changes as a consequence of the fact that the cells, relaxed or not, have modified their shape and arrangement inside the tissue. Therefore, at least in our opinion, to account for the just depicted phenomenology, it may be necessary to borrow concepts from the theories of plasticity or viscoplasticity, since these are able to describe the tissue's internal kinematics in a way that is similar to the motion of the defects in solids.

In spite of the fact that the aforementioned phenomena have different nature, both of them may be described by suitably re-interpreting some fundamental concepts of the theory of Plasticity (a general introduction to the Theory of Plasticity can be found in [161, 176]). More specifically, it is stipulated that both the remodelling of a tissue's extra-cellular matrix and the irreversible strains arising in the case of damaged or overloaded tissues can be expressed in terms of plastic-like distortions. The physical meaning of such distortions can be captured by relating them to the concept of residual stresses, which are often believed to accompany the structural changes of a tissue. The Reader is referred to [90, 92, 93, 89, 103] for a presentation of the role played by residual stresses in the study of biological tissues, with particular emphasis put on articular cartilage and to [120] for arterial walls. We also mention [6, 49, 86, 87, 91, 100, 139, 140, 144, 147, 149, 183, 219, 220] for a treatment of residual stresses in biological tissues, also with reference to growth. Since residual stresses persist even when all the loads applied to the tissue are switched off, even an unloaded configuration, taken as reference for the tissue's evolution, may happen to be in a stressed state (see [61] and references therein). We remark that there exist also other approaches to study residual stresses in biological tissues, as reported, for instance, in [49, 175].

Accordingly, it is possible to identify the plastic distortions with the transformations that bring a considered tissue (such as articular cartilage or tumour masses) from the stressed state associated with the chosen reference configuration to a stress-free state, i.e., a state reached by eliminating all applied loads and relaxing all residual stresses [176, 210]. We recall that a similar definition is given in [196] for the remodelling associated with growth. We also remark that the types of tissues addressed in this work do not comprise muscles for which the mathematical formulation, in spite of some similarities with the present one, requires to account for *active strains* (see, for instance, [102]), which are conceived within a different phenomenology.

The study of fibre-reinforced composite materials is of great interest in Biomechanics, since it permits to understand various aspects of the mechanical behaviour of biological tissues. In the literature, there are works dedicated to fundamental questions, e.g. [140, 174, 228, 170], that focus on the formulation of constitutive models for fibre-reinforced tissues with a statistical distribution of fibres (arteries, articular cartilage, etc.) and, therefore, they require a "correct" definition of suitable operators of directional averages, studies that infer the elastic and hydraulic properties of a tissue on the basis of micro-scale information, e.g. [203, 84, 83, 82, 80, 194, 195], and studies devoted to the formulation of computational methods and algorithms (see e.g. [64, 234, 79, 40, 131, 130] and [56]).

For fibre reinforced tissues, it is essential to provide a robust theoretical background to study their growth, structural reorganisation, and damage (see e.g. [157, 154, 72, 98, 13, 233]), and to relate such processes to the evolution of the material properties. This knowledge, indeed, is helpful for predicting the behaviour of injured or diseased tissues, and it may supply indications in the design of engineered tissues (see [56] and references therein).

1.2 Growth and remodelling of biological tissues

The volumetric growth of a biological tissue consists of the variation and redistribution of its mass, and is the consequence of processes that influence each other reciprocally in spite of their being characterised by different time and length scales

[55, 91, 222] (see [114] and references therein).

Besides genetic, bio-chemical, and bio-physical phenomena, which pertain to the molecular and intra-cellular scales, the growth of a tissue also depends on interactions that occur at the inter-cellular level, as well as on those that involve the tissue as a whole. The latter two types of interactions are often studied with the purpose of describing how a tissue evolves, for instance, by adapting its internal structure and material properties in response to the changes of its environment (see [114] and references therein).

In fact, the structural adaptation of a tissue may manifest itself in several different ways, and it may involve one or more classes of phenomena, which are often referred to with the common name of *remodelling*. For the types of problems addressed in this Thesis, in which a tissue is viewed as an aggregate of cells, a reorganisation of its internal structure is assumed to occur through the dissolution and reformation of the adhesion bonds among the cells [9, 198, 104], or through a rearrangement of the position, shape, and orientation of the cells in the aggregate [87, 86]. In both cases, remodelling acquires the character of a *configurational* process at the inter-cellular scale, and may result in an inelastic change of shape of the tissue as a whole. More generally, however, when the extracellular matrix (ECM) is accounted for, or in the case of fibre-reinforced tissues, the structural changes take place through the distortion of the ECM's collagenous network [200], or through the reorientation of the collagen fibres (see [114] and references therein).

The problem of fibre reorientation has been addressed in several works, sometimes in connection with growth, and for different types of tissues, these ranging from blood vessels (see e.g. [64, 127, 171, 183]) to articular cartilage (see e.g. [234, 203, 21, 116, 108, 56]). In other situations, as is the case for bone, the concept of structural adaptation is introduced to interpret the formation of cracks [97], the onset of damage, and the occurrence of inelastic distortions that are remnant of the phenomenon of plasticity in metals (see e.g. [161, 176] and [114]).

To describe the processes mentioned so far, a tissue may be viewed as a continuum, or a mixture of continua, and its dynamics may be revealed, at least *partially*, by formulating mathematical models based on the laws of continuum mechanics (see [114] and references therein).

When a tissue is modelled as a mixture of continua —typically a fluid phase and one or more solid phases— [38, 17, 11, 110, 104, 105], its growth is usually identified with an inter-phase exchange of mass. Such process is assumed to yield either an accretion of the solid mass at the expenses of the fluid or a loss of solid mass, induced by the disintegration of the tissue cells, which become necrotic and are then dissolved into the fluid. In such a framework, the solid phase is taken as a representation of the tissue cells (and, where appropriate, of the ECM), and a mathematical model of growth should be able to relate the mass variation of the solid phase with the availability of nutrients and with the structural transformations that possibly accompany growth. As already mentioned above, the latter ones are assumed to have inelastic nature and may refer to the redistribution of the solid mass, to the change of the cells' arrangement inside the tissue, so as to mimic the result of the dissolution and reformation of the cellular adhesion bonds, or to a combination of both phenomena (see [114] and references therein).

We remark that some models available in the literature study the mechanics of growth and remodelling as independent processes, with the aim of capturing the most important aspects of these two phenomena (see, for instance, [116, 5, 6, 7, 104, 38, 26]). In general, this is possible when the time scales characterising the growth and the remodelling of a biological tissue are well separated. In general, when it is not possible to appreciate such separation of scales, the two phenomena should be studied as coupled, as is the case of the problems of growth and growth-induced remodelling in tumour masses addressed in the Thesis (Chapters 5,6,7). Hence, understanding how growth and remodelling are related to each other is a necessary step towards the comprehension of the evolution of biological tissues. In this respect, we remark that the coupling of growth and remodelling has been investigated in several papers (see e.g. [9, 105, 166] and the references therein), without considering strain-gradient constitutive laws, while second-order theories have been proposed e.g. in [47, 48, 50] to investigate the transport of mass in the presence of morphogenesis (see also [72] for a discussion on this issue).

1.3 Summary of the Thesis and research questions

In this section, we give a brief presentation of the contents of each of the following chapters, and we highlight the research questions driving this Thesis.

1.3.1 Part I: Remodelling

We formulate two descriptions of remodelling for two different types of tissues.

In Chapters 3 and 4, we focus on hydrated, fibre-reinforced, soft tissues and select articular cartilage of the (human) knee as the representative member of this class of tissues. We make this choice because we are aware of many experimental data that specify the material properties of articular cartilage, such as elasticity and permeability, and that can thus be used for the numerical simulation of benchmark problems and proofs of concepts. Starting from the well-established constitutive theory of fibre-reinforced materials in biological context, especially in the case of statistical distribution of fibres (see [151, 22, 100, 83, 79]), we *conjecture* how the reorganisation of the tissue's internal structure affects its mechanical, hydraulic and structural properties in terms of stress distribution, fluid flow, pore pressure, and evolution of the structural degrees of freedom.

In Chapter 5, we consider an idealised version of a biological tissue that, within its lowest approximation, can be regarded as a layered medium (not a hydrated tissue, this time) consisting of several layers of isotropic materials, each of which is characterised by its own elastic properties. The resulting medium is highly heterogeneous and we are interested in looking at how the evolution of the micro-structure of each layers affects the overall elastic properties of the layered medium. For this purpose, we adopt the Theory of Asymptotic Homogenisation.

Research questions of Part I

In this section, we expose the specific *research questions* addressed in the forthcoming Chapters 2, 3, 4.

We rely on existing literature, in which the remodelling of a given soft tissue is understood as a continuous evolution of the tissue's mechanical properties, that is achieved through a stress-driven rearrangement of its cellular adhesion bonds [198, 104, 112] (note that, according to this vision, the identification of remodelling with the structural adaptation of the tissue is respected). Then, we *conjecture* that this approach can be "imported" to the description of remodelling of a fibre-reinforced tissue, like articular cartilage, for which, in addition to the evolution of the elastic properties, also the capability of conveying the interstitial fluid is affected by its structural reorganisation. In particular, this latter aspect is put in connection with the deformation of the solid phase of the tissue, i.e., its matrix, which, in turn, induces a variation of the porosity. Furthermore, on the basis of the previous models put forward in [176, 200, 198, 199, 104, 112, 111], and by adapting the theoretical framework proposed therein to our problem, we also *conjecture* that the above introduced inelastic distortions are triggered by stress, when it exceeds a threshold, regarded as a material property. Within this modelling framework, we set ourselves the following specific research questions:

2.1 By comparing the (hypothesised) behaviour of the considered tissue with that of well-known elastoplastic materials, can one expect that remodelling —intended as onset and development of inelastic, or plastic-like, distortions— leads to an optimised re-distribution of stress and fluid pressure? Our answer is positive, as shown in Section 2.5 (see Figures (2.2), (2.4) and (2.5)).

2.2 Since, to the best of our knowledge, inelastic distortions are often studied in the biological context for the case of isotropic materials, could there be an interplay, or a combined effect, between anisotropy and inelasticity that gives rise to new material behaviours? We answered this question in Section 2.5 (see Figures (2.1), (2.2), (2.4) and (2.5)).

2.3 Since the interstitial fluid plays a major role in the mechanical behaviour of the tissue, should one see, at least in the numerical simulations of the well-known benchmark problems addressed in the sequel, some specific phenomena concerning fluid flow? We answered this question in Section 2.5 (see Figure (2.1)).

By extending the modelling framework outlined above, we also focus on the re-orientation of the reinforcing collagen fibres embedded in the tissue's extracellular matrix. Such phenomenon consists in a structural process of remodelling, which accompanies the deformation and the structural adaptation of the tissue's extracellular matrix, as well as the evolution of the flow of the interstitial fluid. We start from different results available in the literature [21, 108, 116] in which the alignment of the fibres are described by a probability density, which measures the probability that a (rectified) fibre is aligned along a given direction. Such probability function depends constitutively on different scalar parameters. The reorientation of the fibre is determined by the evolution of such parameters. In our model, we select the so-called fibre-mean angle as structural parameter associated with the kinematics of fibres. The fibre mean angle is associated with the most probable direction, at each material point of the tissue, with respect to which the fibres tends to align themselves. In addition, we also adopt the concept of "target angle" [64, 21, 127, 183], i.e., a preferred direction that contributes to drive the direction of orientation of the fibres, and it is a functional of the deformative and/or of the stress state of the tissue.

We *conjecture* a constitutive framework in which, through the definition of a suitable energy density function, we describe the mutual interactions, at different length scales, of the structural evolution of the tissue —intended as stress-driven evolution of inelastic distortions of the matrix and fibres's reorientation— with the deformation and the fluid flow and the role played by the target angle. In particular, we answer the following *research questions:*

3.1 By comparing the model developed in our work with other published works concerning the reorientation of fibres, we ask ourselves: In which way does the coupling among the above mentioned phenomena influence the main mechanical quantities (pore pressure, deformation, hydraulic properties, stress distribution) characterising a sample of tissue? We discussed the answer to this question in Section 3.5.

3.2 What is the role played by the target angle on the reorientation of the fibres? Is it possible to find stationary solutions of the evolution equation of the fibre mean angle? The answer to this question is given in Section 3.5.

3.3 Which are the generalised forces dual to the generalised velocities associated with the structural changes that are accounted for in the model and what is the generalised force that drives the reorientation of the fibres produced by the target angle? The answer to these questions are given in Section 3.4 and in Section 3.4.1, and we anticipate that we have individuated an *effective*

Mandel stress tensor which comes from the constitutive form of the chosen strain energy density. In fact, the latter involves the coupling between the variables associated with the plastic-like distortions and the gradient of the fibre mean angle, since we are dealing with a gradient theory with respect to such variable, in order to explicitly resolve its spatial distribution within the tissue.

Finally, we focus on a class of heterogeneous materials with evolving micro-structure, which can be used to suitably model certain types of tissues, such as the bone tissue. In particular, we study materials comprising two hyperelastic media, which manifests an evolution of their internal structure. It is, in fact, this evolution that we understand here as a manifestation of *remodelling* for heterogeneous media. We assume that the evolution of the micro-structure is an inelastic process that, to a certain extent, resembles the phenomenon of Perzyna-type plasticity [176, 161]. This is done on the basis of previously published mathematical models [200, 198, 199], all showing agreement with biological evidence [86, 87]. We assume, in particular, that the tissue is a layered medium and we *conjecture* that the variation of the internal structure of a given layer is represented by the development of inelastic distortions, which are set off when the mechanical stress in that layer exceeds a certain threshold. Within this picture, the heterogeneity of the overall medium gives rise to a multi-scale problem in which a scale-dependent remodelling takes place. For such reason, we apply the asymptotic homogenisation technique to the equations describing the dynamics of a heterogeneous material with evolving micro-structure, thereby obtaining a set of upscaled, effective equations. We answer the following *research questions*:

4.1 What is the role played by plastic-like distortions in the effective form of the equations describing the dynamics of heterogeneous media whose internal structure evolves? The answer to this question is given in Section 4.5.1.

4.2 What is a suitable evolution law for inelastic distortions in this framework? The answer to this question is given in Section 4.5.2.

4.3 Also in the case of a simplified microstructure (as is the case of a layered micro-structure), which could the most suitable computational tools be to run our numerical simulations of a problem stated in this framework? The answer to this question is given in Section 4.6.

Although the results we have obtained seem to us plausible, at least from the logical and deductive point of view, there is, up to now and to the best of our knowledge, *no* experimental evidence that our predictions occur in a real tissue. However, our hope is, at least, to suggest targets for new experimental investigations.

1.3.2 Part II: Growth

We study the volumetric growth of isotropic biological tissues by adhering to three different modelling scenarios. More specifically, within this part of the Thesis, we focus on the growth of tumours in avascular stage, i.e., before the onset and development of vascularisation processes. Furthermore, as representative example of this class of tumours, we select the ductal carcinoma, a kind of tumour that develops inside the breast ducts. Such choice is motivated by the availability in the literature of experimental data and benchmark problems [167, 166, 7, 8], which we use as comparison to test our own models. The latter one, in fact, are generalisations of pre-existing models [104, 105, 66, 11, 38], and, as such, they require new parameters that are neither known nor extrapolable from those used in the previous studies which we refer to [167, 166, 7, 8, 104, 105, 66, 11, 38]. To circumvent this lack of information, we perform a sweep of the new parameters, thereby evaluating their influence on the obtained results. Starting from different models of tumour growth available in the literature, we *conjecture* how structural, or configurational, processes can affect the growth of a tumour, in addition to the well-studied ones of biological and mechanical type.

In Chapter 5, we propose a model based on a gradient theory of tumour growth. Within such a theory, in addition to the *growth tensor*, which represents the inelastic distortions induced by growth in a tumour [66, 69, 72, 47], we consider the material gradients up to the second-order of the growth tensor, thereby explicitly accounting for the resolution of inhomogeneities within the tumour. Note that, with the term "inhomogeneity", we mean that, at different material points, the growth-induced distortions are different, i.e., material points are not equivalent, and the gradients of the growth tensor capture the self-interactions between neighbouring points [66].

In Chapter 6, we enrich the model proposed in the previous chapter in the following way: we *conjecture* that, together with growth, also another type of inelastic distortions may arise in a growing medium. As discussed in [198, 104, 112] , this second type of distortions describes the reorganisation of the internal structure of the medium. In order to keep the model at a reasonable level of complexity, our theory is of grade zero in the growth-induced distortions (no gradients of the growth tensor are accounted for) and of grade one in the second type of distortions. To this end, we adapt to our purposes the theory of Anand, Aslan and Chester [15] and rephrase it for saturated porous media.

In Chapter 7, we assume that the time scale characterising the growth of a tissue is represented by a thermodynamic quantity called internal time [117, 176, 227]. We study this aspect with reference to two different theories of growth and we compare our results with phenomenological laws of growth [72, 60, 166].

Research questions of Part II

In this section, we expose the specific *research questions* addressed in the forthcoming Chapters 5, 6 and 7.

We adhere to models of tumour growth in which the tumour is described as a biphasic medium comprising a solid phase and a fluid phase. The former consists of two families of cells, the proliferating and the necrotic cells, while the latter is the interstitial fluid, which conveys various biological molecules and chemical agents to activate or deactivate several biological processes. In particular, growth is studied as a process of mass transfer among the constituents of the phases, through the definition of suitable source and sink terms. Such terms take into account, for example, the availability of nutrients within the tumour, their diffusion and transport through the interstitial fluid and mechanical interactions among the phases. In our work, we *conjecture* that the growth of the tumour gives rise to the onset and development of material inhomogeneities, which contribute in producing structural changes within the tumour tissue.

In Chapter 5, we study such material inhomogeneities by extending the standard kinematic description of growing tumours, in order to account for configurational effects associated with such material inhomogeneities, together with biological and mechanical stimuli [66, 62, 166]. To this end, we introduce a non-integrable, mixed, second-order tensor, called "growth tensor", with which we build a non-Riemannian growth-induced metric [66, 62, 235, 236, 106]. The scalar curvature of the Levi-Civita connection associated with such a metric has been employed as kinematic descriptor of our theory. We reformulate the terms describing the gain/loss of mass by introducing non-standard terms, expressed as functions of the growth-induced scalar curvature. This way, we rephrase the standard ordinary differential equation governing the growth of a tumour into a partial differential equation. Such an approach permits to capture the spatial variability of the growth and the influence of the material inhomogeneities produced by growth on the growth itself [62]. More specifically, we answer the following *research questions*:

5.1 In which way, both qualitatively and quantitatively, does the evolution of the material inhomogeneities influence the main mechanical entities (displacement, pore pressure, distribution of stress) and biological processes (tumour evolution, development of necrotic cells, distribution of nutrients) of a growing tumour? The answer to this question is given in Section 5.5.

5.2 What is the physical interpretation of the evolution of material inhomogeneities accompanying growth? The answer to this question is given in Section 5.6.

5.3 In which way does the evolution of the material inhomogeneities affect the material symmetries of the growing tissue? The answer to this question is given in Section 5.6.

In Chapter 6, in order to generalise the framework of tumour growth outlined above, we investigate the way in which a tumour grows and remodels by virtue of growth. When a tissue remodels, the cells tend to change their positions and to redistribute their shape and orientation in a permanent manner, so that the tissue does not spontaneously tend to recover its original configuration, regardless of the absence of external loads. Moreover, experiments suggest the existence of an incompatible, stress-free state in which the tumour finds itself after growth, which is consistent with the description of the tumour as an elasto-plastic material [86]. By bearing in mind such phenomena, we are interested in accurately describe the onset of development of growth-induced remodelling which, in turn, influence growth itself. More specifically, we *conjecture* that remodelling is characterised by a two-scale behaviour and we introduce a suitable kinematic variable that captures the evolution of the inhomogeneities associated with remodelling at the finer scale. In doing this, we study the growth and remodelling of a biological tissue on the basis of a strain-gradient formulation of remodelling. In particular, we recall that the type of remodelling studied in this Thesis is understood in the following two fashions: on the one hand, it can be related to the reorganisation of the adhesion bonds among the tumour cells, and, on the other hand, it leads to a visible change of shape of the tissue, which is generally not recovered when external loads are removed. For our purposes and following the model proposed by Anand, Aslan and Chester in [15], we formulate a strain-gradient framework with respect to the variable describing the fine scale remodelling. We answer the following *research questions*:

6.1 To which extent, do the onset and evolution of material inhomogeneities associated with a finer scale remodelling impact the principal physical quantities that determine the growth of the tumour (displacement, growth parameter, distribution of the stress and of the pore pressure, diffusion of the nutrients, temporal evolution of the proliferating cells)? The answer to this questions is given in Section 6.7.

6.2 In which way does the fine scale remodelling interact with the remodelling phenomena taking at the scale of the tissue? The answer to this questions is given in Section 6.7.

6.3 What kind of remodelling phenomena can be addressed by adhering to the strain-gradient framework developed in Chapter 6? The answer to this questions is given in Section 6.1.

In Chapter 7, we introduce a thermodynamic quantity, called *internal time*, in order to represent the characteristic time scale of a body's structural changes associated with growth [117, 113]. This study has been conducted by referring to

Vakulenko's Endochronic Theory [176, 227] and by employing a variational procedure based on the use of Noether's Theorem [117, 113] in the context of two different theories of growth [72, 60]. We answer the following *research questions:*

7.1 In which way does the choice of a theory of growth between the two considered in this Chapter influence the definition of the internal time? The answer to this question is given in Section 7.5.

7.2 How can Noether's Theorem help in understanding some issues related to growth mechanics? The answer to this question is given in Section 7.3.

7.3 Is it possible to recast some growth laws used in the literature in a fully variational fashion, whereas they are generally supposed to be phenomenologically written? The answer to this question is given in Sections 7.5 and 7.6.

1.4 Methodology

To use a jargon adopted in my research group, this Thesis provides the basis for building a logic-deductive *"mathematical infrastructure"* [56] for studying a "class of equivalence" of biomechanical problems. Then, for exemplification purposes, it focuses on some specific, selected problems, taken as representative elements of this class. In doing this, we worked for catching analogies and differences among several theories of biological remodelling and growth available in the literature, and for extending previous mathematical models employed for studying these topics. In this perspective, the solution of the problems presented in the forthcoming chapters has required the use of specific technical tools, but with the peculiarity of highlighting a theoretical substrate common to each of them.

The mathematical models characterising this Thesis are formulated in a rather general way, in order to cover the mechanical behaviour of a large class of tissues. Subsequently, they are specialised, by way of benchmarking, in order to address specific topics concerning, for instance, articular cartilage, tumours and idealised layered tissues, such as the bone tissue. Indeed, for these tissues, we have enough experimental information. More specifically, we refer to articular cartilage, for example of the human knee, as the prototype of the fibre-reinforced tissues in which remodelling occurs, and to tumour masses, such as tumour spheroids or ductal carcinoma, as prototypes of the tissues in which growth or the binomial remodelling and growth take place. Analogously, we refer to the bone tissue as representative of a class of strongly heterogeneous biological tissues, undergoing remodelling and whose effective behaviour is studied by means of the Asymptotic Homogenisation technique. We emphasise that our scope is not the biomechanical analysis of the tissue itself, but the establishment of a mathematical framework capable of describing the anelastic phenomena of remodelling and growth in the addressed class of tissues.

We need to clarify that the results presented in this Thesis are not ready for being employed within a medical context for therapeutic purposes, or to explain, in their complexity, the biological processes which we discuss (for instance, the growth of a tumour or the degradation of articular cartilage due to osteoarthritis). Similarly, we have not performed the experiments described in the Thesis, but we referred to standard experimental protocols reported in the literature, such as the unconfined compression test for investigating the mechanical properties of the articular cartilage of the knee. Rather, the results of the Thesis set themselves the scope of helping in the understanding of some physical aspects (more specifically, mechanical aspects) of the studied phenomena.

In fact, the results reported in the following extend some models already present in the literature, re-interpreting them, above all, from the mechanical point of view. Although such results can have, at this stage, a mainly speculative and deductive value, they are meant to give indications and suggestions for the research of new experimental goals. In this sense, it is important to underline that, mostly for the studies concerning articular cartilage, both the Thesis and the papers which it is based on, re-propose well-consolidated numerical experiments available in the literature, which have the aim of simulating laboratory experiments. Such numerical experiments are used to estimate the impact of the theoretical generalisations proposed in the Thesis on the experimental results. In this perspective, the case that can be considered as representative of this view is the "syringe effect", obtained as an outcome of the study of anisotropic remodelling of articular cartilage. To the best of our knowledge, it has not been observed in the context of "classical" experimental protocols yet (unconfined compression test of a cylindrical specimen of articular cartilage in elastic regime). In a different way, the same approach also applies to the case of tumour growth, even though, in this case, the computational cost of our models has imposed us to restrict ourselves to benchmark problems of academic rather than biological interest (growth in a cylinder duct studied as a one-dimensional problem).

In light of the above discussion, the methodology employed in this Thesis can be summarised as follows:

1. Given a biological tissue, we investigate its mechanical properties, its response to external or internal stimuli, which lead to the evolution of the internal structure of the tissue itself.

2. We individuate a class of phenomena characterising the evolution of a biological tissue. In this Thesis, we focused on remodelling and/or growth, also with the purpose of paving the way towards the study of even other types of processes, like damage and ageing.

3. We develop methodologies for describing remodelling and growth in a whole class of tissues, characterised by fibre-reinforcement, chemo-mechanical interactions and evolution of the micro-structure. This is done in a way that is kept on purpose as general as possible, in the attempt of constructing a unifying framework to the formulation of the above mentioned problems. Whereas the main drawback of this approach is the impossibility of accounting for several details, the advantage is the flexibility of the proposed models. This, in fact, can particularised in a second stage, when relevant biological facts must be considered.

4. Finally, to test our models, we specialised them to cases of interest, of which we know parameters and experimental measurements, in order to have a comparison with results available in the literature.

With respect to this last point of the list above, we highlight that the Thesis is denoted by a strong Physico-Mathematical character. Moreover, although its structure is of logic-deductive type, the Thesis is not limited to pure speculative statements. Rather, it tries to stimulate the interest of the experimental community. This is the case, for instance, for the models of tumour growth presented hereafter, which involve the derivatives of order higher than the first of the tensors of anelastic distortions associated with growth and remodelling. In this perspective, even though our models are not verified from the experimental point of view, nothing forbids, at least in principle, that experimental procedures could be developed to find evidences of the effects predicted by our models.

1.5 Main concepts and notation in the study of remodelling

In this section, we present the main concepts, definitions, modelling hypothesis and notations necessary for the development of the specific topics related to the remodelling of fibre-reinforced tissue within the forthcoming chapters.

1.5.1 Modelling hypothesis

We regard the tissue under study as a mixture comprising a solid and a fluid. The solid represents a porous medium and is assumed to feature a matrix and reinforcing collagen fibres. The matrix is composed of biological polymers and tissue cells. The fluid consists of water and several other chemical substances.

Remark 1.5.1. In spite of its major role on the tissue's dynamics, in this study we neglect the presence of chemical substances other than water. Clearly, this is just a simplifying modelling assumption, which is not meant to contradict the statement about the presence of chemical substances in the interstitial fluid. The latter, indeed, is a fact. However, to motivate our approach, we notice that, on the one hand, this modelling choice precludes the resolution of the phenomena related to the tissue's chemistry. On the other hand, however, it is capable of accounting for a strong entanglement among the flow of the fluid, the deformation of the tissue, the reorganisation of its internal structure, and the reorientation of the reinforcing fibres, while containing computational costs. Moreover, the results predicted by our model can be used as inputs for studying the evolution of chemical agents when the coupling between their dynamics and the aforementioned processes is weak enough.

We are aware of the efforts of some Authors to account for the stress contribution stemming from the ionic phases of articular cartilage. For example, Huyghe et al. [143] developed a *"quadriphasic theory"* for tissues like cartilage with the purpose of reformulating, within the context of porous media, the chemo-electro-mechanical interactions typically studied for membranes. In the context of articular cartilage, Ateshian [17] elaborated a model in which the stress of the tissue's solid phase features, apart from the classical contributions due to the pore pressure and the (assumed) hyperelastic response of the solid phase, also a contribution related to the electric potential in the tissue itself and the electric valence of its ionic constituents. More recently, Bongué-Boma et al. [32, 1] formulated a model of articular cartilage in which, under the hypothesis of Donnan equilibrium, the stress consists of a hyperelastic term, a term of electric type and a contribution due to osmotic pressure.

As reported by Ateshian [17] within the context of cartilage mechanics, great attention has been drawn on osmosis, on its relations with residual stresses, and on the issue of swelling stress. As explained in [17], this stress is attributed to the matrix of articular cartilage and is related to *"Donnan osmotic pressure in the interstitial fluid"* [17]. By re-interpreting the explanation given in [17], osmotic pressure stems from the electro-mechanical interactions between the polymers constituting the matrix of articular cartilage, which are charged negatively, and the ions (both anions and cations) dissolved in the interstitial fluid, under the constraint of electroneutrality of the overall solution. These interactions result in an *"increased pressure"*, whose main effect is to produce a nonzero-stress state in the tissue's matrix, even when the matrix itself is free of external tractions. Because of this evidence and the inhomogeneous distribution of the negatively charged polymers in the cartilage, the osmotic pressure is also distributed inhomogeneously, thereby giving rise to residual stresses [17]. Under the light shed by the preceding comments, it is possible to infer that the physics at the basis of the onset of the just defined residual stresses is different from the one that triggers those residual stresses related to the structural reorganisation (remodelling) of the solid phase of articular cartilage and to the anelastic distortions accompanying such phenomena. For this reason, and since we are currently interested in a purely mechanical model of cartilage, we have opted for a simplified description of this tissue, in which the presence of the chemical substances dissolved in the interstitial fluid is disregarded. Hence, we have concentrated our study only on the anelastic aspects of the solid phase ascribable to the transformation of its internal structure and to the mechanical interactions with the interstitial fluid.

In this Thesis, as mentioned above, we focus on the remodelling of articular cartilage, as representative example of the equivalence class of fibre-reinforced biological tissues we have in mind. To this end, the mathematical models discussed in this Thesis rest on the following main hypotheses (see [56]):

(i) the solid is hyperelastic and the fluid macroscopically inviscid;

(ii) both constituents are intrinsically incompressible, so that the change of volume of the tissue as a whole is due to the variation of porosity (since the saturation condition applies, such variation is expressed through the variation of the volumetric fraction of the solid or of the fluid);

(iii) the dynamics of the fluid adheres to Darcy's law;

(iv) all body forces acting on the solid are negligible, with the exception of those describing the momentum exchange with the fluid;

(v) growth is not accounted for in the model, so that the fluid and the solid locally preserve their mass.

1.5.2 Kinematics

We recall some concepts of the kinematics of biphasic mixtures. To this end, we adopt the theory put forward in [202], and used in [40, 108, 112, 225]. Moreover, we adopt with slight variations the covariant formalism of Continuum Mechanics presented in [165].

Accordingly, we introduce the set $\mathscr{B} \subset \mathscr{S}$ as the reference placement of the solid phase. Then, given the interval of time $\mathscr{I}$, the motion $\chi : \mathscr{B} \times \mathscr{I} \to \mathscr{S}$ is a smooth mapping such that $\mathscr{B}_{\mathrm{s}}(t) \equiv \chi(\mathscr{B}, t) \subset \mathscr{S}$ is the configuration of the solid at time $t \in \mathscr{I}$. Moreover, $\mathscr{B}_{\mathrm{f}}(t)$ is the portion of $\mathscr{S}$ occupied by the fluid at the same instant of time. Finally, $\mathscr{B}(t) := \mathscr{B}_{\mathrm{s}}(t) \cap \mathscr{B}_{\mathrm{f}}(t) \subset \mathscr{S}$ is the region of space in which the solid-fluid mixture finds itself at $t \in \mathscr{S}$. Even though $\chi(\,\cdot\,, t) : \mathscr{B} \to \mathscr{S}$ is not invertible, the map $\hat{\chi}(\,\cdot\,, t) : \mathscr{B} \to \mathscr{B}_{\mathrm{s}}(t)$, defined by $\hat{\chi}(X, t) = \chi(X, t)$ for all $(X, t) \in \mathscr{B} \times \mathscr{I}$, is invertible and such that $\mathscr{B} = \hat{\chi}^{-1}(\mathscr{B}_{\mathrm{s}}(t), t)$. In general, it occurs that $\hat{\chi}^{-1}(\mathscr{B}(t), t) \subset \mathscr{B}$. However, in all the cases studied in this Thesis, it is possible to apply the kinematical hypothesis $\hat{\chi}^{-1}(\mathscr{B}(t), t) = \mathscr{B}$, since the identity $\mathscr{B}_{\mathrm{s}}(t) = \mathscr{B}(t)$ is verified for all $t \in \mathscr{I}$ (see Figure (1.1)). For this reason, $\mathscr{B}$ can be viewed as a reference placement for the mixture as a whole [56].

With each $x \in \mathscr{B}(t)$ we associate the spatial *volumetric fractions* $\phi_{\mathrm{s}}(x, t)$ and $\phi_{\mathrm{f}}(x, t)$, which measure, respectively, the local volumetric content of solid and fluid with respect to a representative volume of the mixture. Since the mixture is assumed to be saturated, it holds that $\phi_{\mathrm{s}}(x,t) + \phi_{\mathrm{f}}(x,t) = 1$, for all $x \in \mathscr{B}(t)$ and for all t. Along with ϕ_{s} and ϕ_{f}, we also introduce $\Phi_{\mathrm{s}}(X,t) = \phi_{\mathrm{s}}(\chi(X,t),t)$ and $\Phi_{\mathrm{f}}(X,t) = \phi_{\mathrm{f}}(\chi(X,t),t)$, for $X \in \hat{\chi}^{-1}(\mathscr{B}(t),t)$ (see [56]).

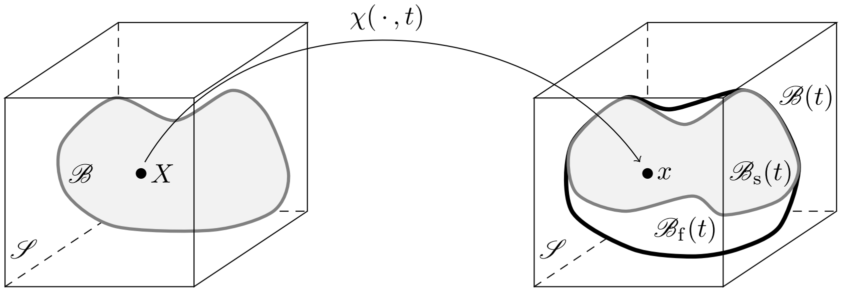

Figure 1.1: Schematic representation of the considered kinematics of mixtures [56].

For every $x \in \mathscr{S}$ and $X \in \mathscr{B}$, $T_x\mathscr{S}$ and $T_X\mathscr{B}$ are the tangent spaces of $\mathscr{S}$ and $\mathscr{B}$ at x and X, respectively. The disjoint unions $T\mathscr{S} := \sqcup_{x\in\mathscr{S}} T_x\mathscr{S}$ and $T\mathscr{B} := \sqcup_{X\in\mathscr{B}} T_X\mathscr{B}$ are the tangent bundles of $\mathscr{S}$ and $\mathscr{B}$. The spaces dual to $T_x\mathscr{S}$ and $T_X\mathscr{B}$ are referred to as co-tangent spaces and denoted by $T_x^\star\mathscr{S}$ and $T_X^\star\mathscr{B}$, while $T^\star\mathscr{S} := \sqcup_{x\in\mathscr{S}} T_x^\star\mathscr{S}$ and $T^\star\mathscr{B} := \sqcup_{X\in\mathscr{B}} T_X^\star\mathscr{B}$ are the co-tangent bundles (see [61] and references therein).

We identify the deformation gradient tensor of the solid phase with the tangent map of χ, i.e., $\boldsymbol{F}(\,\cdot\,,t) \equiv T\chi(\,\cdot\,,t) : T\mathscr{B} \to T\mathscr{S}$, so that, for every $X \in \mathscr{B}$, $\boldsymbol{F}(X,t) : T_X\mathscr{B} \to T_{\chi(X,t)}\mathscr{S}$ maps vectors of $T_X\mathscr{B}$ into vectors of $T_{\chi(X,t)}\mathscr{S}$. Once the two local systems of coordinates $\{X^A\}_{A=1,2,3}$ and $\{x^a\}_{a=1,2,3}$ are chosen in $\mathscr{B}$ and $\mathscr{S}$, the components of $\boldsymbol{F}$ read $F^a{}_A = \partial\chi^a/\partial X^A \equiv \chi^a{}_{,A}$, with $a, A = 1{,}2{,}3$. The determinant $J = \det \boldsymbol{F}$, called *volumetric ratio*, is strictly positive at all points $X \in \mathscr{B}$ and at all times (see [61] and references therein).

We denote by $\boldsymbol{g}$ and $\boldsymbol{G}$ the metric tensors associated with $\mathscr{S}$ and $\mathscr{B}$, respectively so that the Cauchy-Green deformation tensor, $\boldsymbol{C} = \boldsymbol{F}^{\mathrm{T}}.\boldsymbol{F} = \boldsymbol{F}^{\mathrm{T}}\boldsymbol{g}\boldsymbol{F}$, reduces to $\boldsymbol{C} = \boldsymbol{G}$ in the absence of deformation [165] (see [56] and references therein). Note that, in components, we have $C_{AB} = (\boldsymbol{F}^{\mathrm{T}})_A{}^a g_{ab} F^b{}_B = g_{ab} F^a{}_A F^b{}_B$.

1.5.3 The BKL decomposition in the case of remodelling

Inelastic distortions are, generally, incompatible [60, 176, 213], i.e., they are not expressible as the gradient of a deformation. Hence, their descriptor should be at least a non-integrable second-order tensor field over $\mathscr{B}$ (see [56] and references therein). We remark that, in this Thesis, the terms "distortions", "inelastic distortions" and "structural transformations" are regarded as synonyms of "remodelling".

Following the same line of thought as Elastoplasticity, this tensor is called *distortion tensor* and denoted by $\boldsymbol{F}_{\mathrm{p}}$, where the subscript "p" stands for "plastic-like distortions". A rationale for $\boldsymbol{F}_{\mathrm{p}}$ is given by invoking the BKL decomposition of the deformation gradient tensor (see [56] and references therein).

Consequently, $\boldsymbol{F}$ is written as $\boldsymbol{F} = \boldsymbol{F}_{\mathrm{e}}\boldsymbol{F}_{\mathrm{p}}$, where $\boldsymbol{F}_{\mathrm{e}}$ is said to be the tensor of elastic distortions and $J = J_{\mathrm{e}}J_{\mathrm{p}}$, with $J_{\mathrm{e}} := \det\boldsymbol{F}_{\mathrm{e}} > 0$ and $J_{\mathrm{p}} := \det\boldsymbol{F}_{\mathrm{p}} > 0$. In the literature, decompositions of the deformation gradient tensor have been extensively used to address problems of biomechanical interest (see e.g. [210, 72, 160, 5, 6, 96, 110, 112, 111]). The physical and geometrical meaning of the BKL decomposition have been explained in detail, for instance, in [176, 106] and they have been recently used to study the structural evolution of a growing tumour in [62]. For every pair $(X,t) \in \mathscr{B} \times \mathscr{I}$, $\boldsymbol{F}_{\mathrm{p}}(X,t)$ maps $T_X\mathscr{B}$ into a vector space, denoted by $\mathscr{N}_X(t)$ and consisting in the image of $T_X\mathscr{B}$ through $\boldsymbol{F}_{\mathrm{p}}(X,t)$ [62], whose vectors represent body elements in a stress-free state [60]. The way in which $\boldsymbol{F}_{\mathrm{p}}(X,t)$ operates on $T_X\mathscr{B}$ is illustrated in Figure (1.2).

In light of the BKL decomposition, each vector associated with the natural state $\mathbf{u}_X(t) \in \mathscr{N}_X(t)$ can be distorted elastically into $\boldsymbol{u}_x(t) = \boldsymbol{F}_{\mathrm{e}}(X,t)\mathbf{u}_X(t) \in T_x\mathscr{S}$, with $x = \chi(X,t)$. Moreover, we introduce the tensor $\boldsymbol{H}(X,t) : \mathscr{N}_X(t) \to T_X\mathscr{B}$ as the inverse of $\boldsymbol{F}_{\mathrm{p}}(X,t)$, so that the relation $\boldsymbol{U}_X = \boldsymbol{H}(X,t)\mathbf{u}_X(t) \in T_X\mathscr{B}$ holds true. Finally, we notice that, since $\boldsymbol{F}(X,t) : T_X\mathscr{B} \to T_x\boldsymbol{\mathcal{S}}$ is such that $\boldsymbol{u}_x(t) = \boldsymbol{F}(X,t)\boldsymbol{U}_X(t)$, with $x = \chi(X,t)$, it also holds true that

$$\boldsymbol{u}_x(t) = \boldsymbol{F}(X,t)\boldsymbol{U}_X = \boldsymbol{F}(X,t)\boldsymbol{H}(X,t)\mathbf{u}_X(t) = \boldsymbol{F}_{\mathrm{e}}(X,t)\mathbf{u}_X(t). \tag{1.1}$$

It follows from this chain of equalities, which has to be respected for all $\mathbf{u}_X(t) \in \mathscr{N}_X(t)$, that the elastic distortion tensor is given by $\boldsymbol{F}_{\mathrm{e}} = \boldsymbol{F}\boldsymbol{H}$[1]. We remark that this result goes far behind the simple renaming of $\boldsymbol{F}_{\mathrm{p}}^{-1}$ with $\boldsymbol{H}$, for it actually discloses the possibility of exploring some comparisons of the BKL decomposition with the theory of material uniformity [70, 169, 72, 69, 197] (quoting *verbatim* from [72] "*a body is said to be materially uniform if all its points are made of the same material*"). However, we do not speculate here on this comparison because it is out of the scope of this Thesis (see [61]). Similarly to $\boldsymbol{F}_{\mathrm{p}}$, we introduce the determinant of $\boldsymbol{H}$, $J_{\boldsymbol{H}} := \det\boldsymbol{H} > 0$, such that $J_{\mathrm{e}} = JJ_{\boldsymbol{H}}$.

Finally, we introduce the metric tensor $\boldsymbol{\eta}$, associated with the tissue's natural state, which allows to define the tensors $\boldsymbol{C}_{\mathrm{p}} = \boldsymbol{F}_{\mathrm{p}}^{\mathrm{T}}.\boldsymbol{F}_{\mathrm{p}} = \boldsymbol{F}_{\mathrm{p}}^{\mathrm{T}}\boldsymbol{\eta}\boldsymbol{F}_{\mathrm{p}}$ and $\boldsymbol{B}_{\mathrm{p}} = \boldsymbol{C}_{\mathrm{p}}^{-1} = \boldsymbol{F}_{\mathrm{p}}^{-1}\boldsymbol{\eta}^{-1}\boldsymbol{F}_{\mathrm{p}}^{-\mathrm{T}}$. We keep $\boldsymbol{\eta}$ formally different from $\boldsymbol{g}$ and $\boldsymbol{G}$, although, in some cases, it could be taken equal to one of those (see e.g. [183]). For future use, we also define the right elastic Cauchy-Green tensor $\boldsymbol{C}_{\mathrm{e}} = \boldsymbol{F}_{\mathrm{e}}^{\mathrm{T}}.\boldsymbol{F}_{\mathrm{e}} = \boldsymbol{F}_{\mathrm{e}}^{\mathrm{T}}\boldsymbol{g}\boldsymbol{F}_{\mathrm{e}} = \boldsymbol{H}^{\mathrm{T}}\boldsymbol{C}\boldsymbol{H}$ (see [56] and reference therein).

For further use, we introduce $\boldsymbol{\Lambda}_{\mathrm{p}} := \dot{\boldsymbol{H}}\boldsymbol{H}^{-1} = -\boldsymbol{F}_{\mathrm{p}}^{-1}\dot{\boldsymbol{F}}_{\mathrm{p}}$ and $\boldsymbol{L}_{\mathrm{p}} = \dot{\boldsymbol{F}}_{\mathrm{p}}\boldsymbol{F}_{\mathrm{p}}^{-1}$ to denote two rates of anelastic distortions associated with remodelling.

[1] We highlight that the symbol $\boldsymbol{H}$, used in this Thesis, corresponds to the symbol $\boldsymbol{K}$ in [72] and to the symbol $\boldsymbol{P}$ in [169, 70, 69].

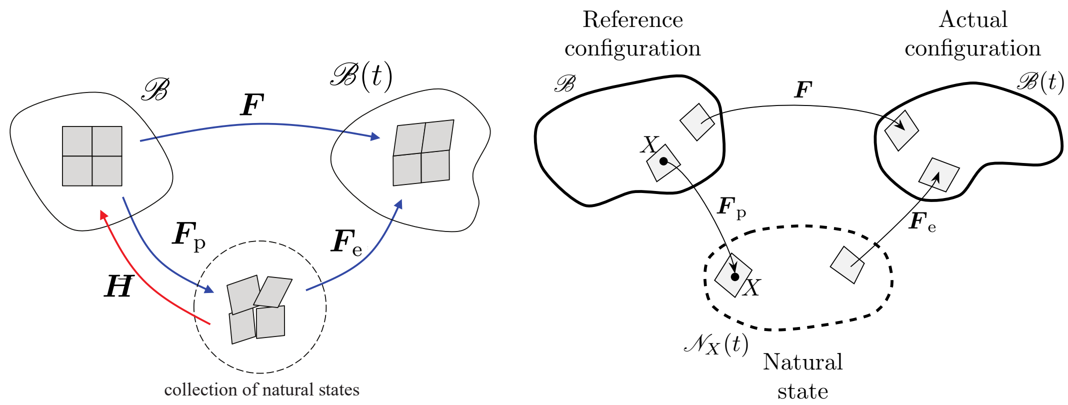

Figure 1.2: BKL decomposition in the case of remodelling ([61] and [56]).

1.5.4 The fibre pattern

Following the framework presented in [84, 80, 225, 40, 108, 107], we study fibre-reinforced tissues in which the fibres are oriented statistically. We recall that, even though the study concerning the fibre pattern could be employed to study other fibre-reinforced tissues, here we focus on articular cartilage, as reported in the previous parts of the Thesis.

The first assumption of our approach is that, at each material point X that finds itself in a natural state, the tissue is transversely isotropic with respect to the direction associated with the unit vector $\mathfrak{m}_X$, which defines the direction of local alignment of the fibre passing through X. The second assumption is that the fibres' directional distribution is such that the tissue as a whole is transversely isotropic with respect to a global symmetry axis, identified with the unit vector $\mathfrak{m}_0$. Moreover, in the sequel we restrict our attention to a sample of tissue characterised by cylindrical shape and material properties that vary only along its geometrical axis. The sample is thus homogeneous on each cross section. A consequence of this setting is that the sample's geometric axis coincides with the axis of transverse isotropy, which is then also symmetry axis of the tissue.

To account for the statistical orientation of the fibres, we adhere to the framework discussed in [80] and we introduce the function $\wp_X : \mathbb{S}^2\mathscr{N}_X(t) \to \mathbb{R}_0^+$, with

$$\mathbb{S}^2\mathscr{N}_X(t) := \{\mathfrak{m}_X \in \mathscr{N}_X(t) \colon \|\mathfrak{m}_X\| = 1\}, \tag{1.2}$$

and $\wp_X(\mathfrak{m}_X)$ measuring the probability density that a (rectified) fibre passing through X be directed along $\mathfrak{m}_X$.

With respect to an orthonormal vector basis $\{\mathfrak{e}_\alpha\}_{\alpha=1}^3$ of $\mathscr{N}_X(t)$, such that $\mathfrak{e}_3$ is parallel to $\mathfrak{m}_0$, a unit vector $\mathfrak{m}_X \in \mathscr{N}_X(t)$ can be expressed in spherical coordinates as $\mathfrak{m}_X = \check{\mathfrak{m}}_X(\vartheta, \varphi)$, where the vector-valued function $\check{\mathfrak{m}}_X : [0, \pi] \times [0, 2\pi[\to \mathbb{S}^2\mathscr{N}_X(t)$ is given by

$$\check{\mathfrak{m}}_X(\vartheta, \varphi) = \sin\vartheta \cos\varphi \, \mathfrak{e}_1 + \sin\vartheta \sin\varphi \, \mathfrak{e}_2 + \cos\vartheta \, \mathfrak{e}_3. \tag{1.3}$$

Accordingly, a physical quantity $\mathfrak{F}_X$ depending on the local direction of fibre alignment, and thus defined over the set $\mathbb{S}^2\mathscr{N}_X(t)$, can be rewritten as a function of ϑ and φ, i.e., $\mathfrak{F}_X(\boldsymbol{\mathfrak{m}}_X) = \mathfrak{F}_X(\check{\boldsymbol{\mathfrak{m}}}_X(\vartheta,\varphi)) = \check{\mathfrak{F}}_X(\vartheta,\varphi)$. In particular, the probability density becomes $\wp_X(\boldsymbol{\mathfrak{m}}_X) = \check{\wp}_X(\vartheta,\varphi)$ and, since the tissue as a whole is assumed to be transversely isotropic with respect to $\boldsymbol{\mathfrak{m}}_0$, $\check{\wp}$ is not allowed to depend on the longitude, φ. Consequently, the equality $\wp_X(\boldsymbol{\mathfrak{m}}_X) = \check{\wp}_X(\vartheta)$ must be fulfilled.

By adopting the formalism of [81], the directional average of $\mathfrak{F}_X$ is defined as

$$\langle\!\langle \mathfrak{F}_X(\boldsymbol{\mathfrak{m}}_X)\rangle\!\rangle = \int_{\mathbb{S}^2\mathscr{N}_X(t)} \mathfrak{F}_X(\boldsymbol{\mathfrak{m}}_X)\wp_X(\boldsymbol{\mathfrak{m}}_X) = \int_0^{2\pi}\!\!\int_0^{\pi} \check{\mathfrak{F}}_X(\vartheta,\varphi)\check{\wp}_X(\vartheta)\sin\vartheta\,\mathrm{d}\vartheta\mathrm{d}\varphi. \quad (1.4)$$

All physical quantities featuring in the mathematical model, including the probability density, are assumed to be invariant under the reflection $\boldsymbol{\mathfrak{m}}_X \mapsto -\boldsymbol{\mathfrak{m}}_X$, for all $\boldsymbol{\mathfrak{m}}_X$. This permits to rephrase the directional average (1.4) as

$$\langle\!\langle \mathfrak{F}_X(\boldsymbol{\mathfrak{m}}_X)\rangle\!\rangle = 2\int_{\mathbb{S}^{2+}\mathscr{N}_X(t)} \mathfrak{F}_X(\boldsymbol{\mathfrak{m}}_X)\wp_X(\boldsymbol{\mathfrak{m}}_X) = \int_0^{2\pi}\!\!\int_0^{\pi/2} \check{\mathfrak{F}}_X(\vartheta,\varphi)\check{\psi}_X(\vartheta)\sin\vartheta\,\mathrm{d}\vartheta\mathrm{d}\varphi, \quad (1.5)$$

where $\mathbb{S}^{2+}\mathscr{N}_X(t)$ is the “northern” hemisphere [40], i.e.,

$$\mathbb{S}^{2+}\mathscr{N}_X(t) := \{\boldsymbol{\mathfrak{m}}_X \in \mathbb{S}^2\mathscr{N}_X(t) : \|\boldsymbol{\mathfrak{m}}_X\| = 1,\ \boldsymbol{\mathfrak{m}}_X.\boldsymbol{\mathfrak{m}}_0 \geq 0\}, \quad (1.6)$$

and the probability density $\check{\psi}_X : [0,\pi/2] \to \mathbb{R}_0^+$ is defined by the equality $\check{\psi}_X(\vartheta) = \psi_X(\check{\boldsymbol{\mathfrak{m}}}_X(\vartheta,\varphi))$, for all $(\vartheta,\varphi) \in [0,\pi/2] \times [0,2\pi[$, with $\psi_X = 2\wp_X|_{\mathbb{S}^{2+}_X\mathscr{B}}$ [40]. As done in previous works [85, 40], we assume that $\check{\psi}_X$ is the pseudo-Gaussian distribution

$$\check{\psi}_X(\vartheta) = \frac{\check{\gamma}_X(\vartheta)}{2\pi\int_0^{\pi/2}\check{\gamma}_X(\vartheta')\sin\vartheta'\mathrm{d}\vartheta'}, \quad \check{\gamma}_X(\vartheta) = \exp\left(-\frac{[\vartheta-\mathfrak{q}]^2}{2\omega^2}\right), \quad (1.7)$$

where $\mathfrak{q}$ and ω are referred to as fibre mean angle and standard deviation, respectively. Since, as anticipated above, $\mathfrak{q}$ and ω are hypothesised to vary only along the axis of the sample, they can be written as functions of the normalised axial variable $\xi \in [0,1]$, which is zero at the sample's lower boundary and equal to one at the upper boundary. In particular, the normalised axial variable ξ is given by $\xi := \frac{X^3}{L}$, where X^3 is the coordinate along the geometrical axis of the cylindrical specimen, and L is its height in the reference configuration. Hereafter, we take the expressions [85]

$$\mathfrak{q}(\xi) = \frac{\pi}{2}\left\{1-\cos\left(\frac{\pi}{2}\left[-\frac{2}{3}\xi^2+\frac{5}{3}\xi\right]\right)\right\}, \quad \omega(\xi) = 10^3[(1-\xi)\xi]^4 + 3\cdot 10^{-2}, \quad (1.8)$$

which qualitatively reproduce the alignment of fibres in articular cartilage [179]. According to (1.8), the mean angle takes on the values $\mathfrak{q}(0) = 0$ and $\mathfrak{q}(1) = \pi/2$, and the standard deviation attains its minimum at $\xi = 0$ and $\xi = 1$. Hence, the fibres are more likely to be found aligned with the sample's symmetry axis at the bottom of the sample, and more likely to be lying on transverse plane at the top. Moreover, at $\xi = 1/2$, the standard deviation reaches its maximum, thereby tending to randomise the fibre orientation and, consequently, to make the tissue isotropic in the middle of the sample. Note that $\mathfrak{m} : \mathscr{B} \to \mathscr{N}(t)$ indicates the vector field such that $\mathfrak{m}(X) = \mathfrak{m}_X$, and $\mathscr{N}(t) := \sqcup_{X \in \mathscr{B}} \mathscr{N}_X(t)$ is the bundle of all spaces $\mathscr{N}_X(t)$.

1.6 Main concepts and notation in the study of growth and remodelling

In this section, we present the main concepts, definitions, modelling hypothesis and notation necessary for the development of the specific topics related to the growth and remodelling of biological tissues within the forthcoming chapters.

The problems under investigation involve the motion of the solid phase, the motion of the fluid phase, the distortions related to growth, and plastic-like distortions, which are associated with the reorganisation of the tissue's internal structure. The definitions supplied in this section can be encountered in many works addressing Mixture Theory, and have been recently used for establishing the theoretical framework of previous works [225, 108, 62, 56].

1.6.1 Basics of Mixture Theory

The motion of the solid phase is described by the smooth mapping $\chi : \mathscr{B} \times \mathscr{I} \to \mathscr{S}$, where $\mathscr{B}$ is the tissue's reference configuration, $\mathscr{I}$ is an interval of time and $\mathscr{S}$ is the three-dimensional Euclidean space. For each pair $(X, t) \in \mathscr{B} \times \mathscr{I}$, the spatial point occupied by the solid phase is given by $x = \chi(X, t) \in \mathscr{S}$. By differentiating χ with respect to its arguments, we obtain the deformation gradient tensor, i.e., the tangent map of χ, defined by $\boldsymbol{F}(X, t) = T\chi(X, t) : T_X\mathscr{B} \to T_{\chi(X,t)}\mathscr{S}$ [165], and the solid phase velocity $\boldsymbol{V}_{\mathrm{s}}(X, t) = \dot{\chi}(X, t)$. Here, $T_X\mathscr{B}$ and $T_{\chi(X,t)}\mathscr{S}$ are the tangent space of $\mathscr{B}$ at X and the tangent space of $\mathscr{S}$ at $\chi(X, t)$, respectively [165], and the superimposed dot means partial differentiation with respect to time. For completeness, we recall the relationship between $\boldsymbol{V}_{\mathrm{s}}$ and the Eulerian velocity of the solid phase, i.e., $\boldsymbol{v}_{\mathrm{s}}(x, t) = \boldsymbol{v}_{\mathrm{s}}(\chi(X, t), t) = \boldsymbol{V}_{\mathrm{s}}(X, t)$, so that the composition $\boldsymbol{v}_{\mathrm{s}}(\,\cdot\,, t) \circ \chi(\,\cdot\,, t) = \boldsymbol{V}_{\mathrm{s}}(\,\cdot\,, t)$ holds true for all $t \in \mathscr{I}$ (see [114] and references therein).

Remark 1.6.1. The "classical" definition of reference placement, or configuration, although widely used in Solid Mechanics, may not apply to biological tissues. To the best of our knowledge, this is particularly true for a medium undergoing appositional growth, i.e., the process in which material particles are either deposited on the growing medium, or depleted from it. In both cases, the "number" of material particles constituting the medium varies with time and, consequently, it is impossible to define a unique reference configuration for the medium, at least in the classical sense [17]. Rather, as reported in [17], *"the reference configuration of a material point is defined at the time it is deposited,"* which means that, at different times, the medium has to be associated with different reference configurations. In our setting, however, we deal with volumetric growth. This type of growth, in fact, still permits the definition of a fixed reference configuration for a growing medium if, as stated in [72], the addition or depletion of material is assumed to occur *"in such a way that material points preserve their identity"*. With the aid of this hypothesis, we can assume the existence of a fixed reference configuration for the medium under investigation (see [62] and reference therein).

The fluid motion is described by the Eulerian velocity $\boldsymbol{v}_{\mathrm{f}}(x,t)$, evaluated at every point $x \in \mathscr{S}$ occupied by the fluid and at time $t \in \mathscr{I}$. Note that, since the system under investigation is a mixture, the fluid co-exists with the solid at every point $x \in \mathscr{S}$ at which the tissue is observed. Thus, the point x can also be viewed as the image of X through the solid motion, i.e., $x = \chi(X,t)$, and the fluid motion can be studied by means of the composition $\boldsymbol{V}_{\mathrm{f}}(\,\cdot\,,t) \equiv \boldsymbol{v}_{\mathrm{f}}(\,\cdot\,,t) \circ \chi(\,\cdot\,,t)$, such that $\boldsymbol{V}_{\mathrm{f}}(X,t) = \boldsymbol{v}_{\mathrm{f}}(\chi(X,t),t)$ (see [114] and references therein).

Finally, $\boldsymbol{w} \equiv \boldsymbol{v}_{\mathrm{f}} - \boldsymbol{v}_{\mathrm{s}}$ is the velocity of the fluid relative to the solid. Note that the product $\varphi_{\mathrm{f}}\boldsymbol{w}$ is often referred to as *filtration velocity* [138], although it actually represents a specific mass flux vector [25] (see [114] and references therein).

1.6.2 Kinematics of growth and remodelling

A number of papers has been produced in which growth and remodelling have been described by adopting the language and formalism of continuum theories (see e.g. [173] and the references therein). In some works devoted to the theoretical foundations of volumetric growth (see e.g. [72, 160, 60]), emphasis is put on the necessity of defining variables that, together with the descriptors of the tissue's *standard* mechanical state, are capable of catching its structural transformations. In [72], this is done by having recourse to the theory of uniformity [67, 69], and introducing the concepts of *"archetype"* and *"transplant operator"* [72, 67, 69]. On the other hand, in several other contexts, the Bilby-Kröner-Lee (BKL) multiplicative decomposition of the deformation gradient tensor is adopted, along with its generalisations, in order to frame remodelling in terms of "plastic-like distortions" (see e.g. [112]).

Remark 1.6.2. (*Plastic-like distortions and remodelling*).
In the presence of remodelling, the structural transformations of the tissues considered in this work recall the plastic distortions of non-living, elasto-plastic materials. Sometimes, we use the adjectives "plastic" and "remodelling" interchangeably: we take this liberty when a physical quantity, historically conceived for the theory of plasticity, has to be re-interpreted in compliance with the physical context of the present work. A relevant example is the *accumulated plastic strain*, a variable for which we use both its original name and the name *accumulated remodelling strain.*

In other cases, however, we use quotation marks for "plastic" and "plasticity", if we need to recall that we are borrowing terms from the theory of plasticity. For instance, we use this convention when we speak of *micro-scale plasticity* (see [114] and references therein).

The BKL-decomposition in the case of growth

A major character of our theory is the BKL-decomposition, $\boldsymbol{F} = \boldsymbol{F}_{\mathrm{e}}\boldsymbol{F}_{\gamma}$. From the Mechanical point of view, $\boldsymbol{F}_{\gamma}$ describes the inelastic changes of the tissue's internal structure that are induced by growth, while $\boldsymbol{F}_{\mathrm{e}}$ is the accommodating part of $\boldsymbol{F}$, and is assumed to be elastic. Both $\boldsymbol{F}_{\mathrm{e}}$ and $\boldsymbol{F}_{\gamma}$ are non-singular, and their determinants, $J_{\mathrm{e}} = \det \boldsymbol{F}_{\mathrm{e}}$ and $J_{\gamma} = \det \boldsymbol{F}_{\gamma}$, are strictly positive (see [62] and references therein).

For every pair $(X, t) \in \mathscr{B} \times \mathscr{I}$, we prescribe that $\boldsymbol{F}_{\gamma}(X, t)$ maps vectors of $T_X\mathscr{B}$ into "relaxed" vectors of another tangent space. Such space is denoted by $\mathscr{N}_X(t)$, and can be identified with the image of $T_X\mathscr{B}$ through $\boldsymbol{F}_{\gamma}(X, t)$ [106]. Coherently, we write $\boldsymbol{F}_{\gamma}(X, t) : T_X\mathscr{B} \to \mathscr{N}_X(t)$, and, putting together this result and the definition of $\boldsymbol{F}(X, t)$, we express the elastic part of $\boldsymbol{F}(X, t)$ as $\boldsymbol{F}_{\mathrm{e}}(X, t) : \mathscr{N}_X(t) \to T_{\chi(X,t)}\mathscr{S}$ (see [62] and references therein).

We notice that, at this stage, $\boldsymbol{F}_{\gamma}$ is not subjected to any restriction. Hence, granted the polar decompositions $\boldsymbol{F}_{\gamma}(X, t) = \boldsymbol{R}_{\gamma}(X, t)\boldsymbol{U}_{\gamma}(X, t)$ and $\boldsymbol{F}_{\gamma}(X, t) = \boldsymbol{V}_{\gamma}(X, t)\boldsymbol{R}_{\gamma}(X, t)$, which hold true for each pair $(X, t) \in \mathscr{B} \times \mathscr{I}$, $\boldsymbol{F}_{\gamma}(X, t)$ is generally obtained by combining one of the inelastic stretches, $\boldsymbol{U}_{\gamma}(X, t) : T_X\mathscr{B} \to T_X\mathscr{B}$ and $\boldsymbol{V}_{\gamma}(X, t) : \mathscr{N}_X(t) \to \mathscr{N}_X(t)$, with the rotation tensor $\boldsymbol{R}_{\gamma}(X, t) : T_X\mathscr{B} \to \mathscr{N}_X(t)$.

In general, the tissue may find itself in a stressed state both in the current and in the reference configuration. Stresses may have different origin but, in the present context, they are generated either by growth or by the loading history undergone by the tissue. Since in our framework growth is the only process regarded as inelastic, it produces stresses that cannot be eliminated by simply switching off the applied loads. Indeed, even though all such loads were suppressed, the tissue would still occupy a configuration in which the growth-induced stresses are nonzero (see [62] and [56]).

To achieve a state in which every part of the tissue is free of stress, one should virtually disassemble the tissue into a *"conglomerate"* of completely relaxed pieces [148]. Each of such pieces can be thought of as an arbitrarily small neighbourhood of a point $x \in \mathscr{B}(t)$, and, for infinitesimally small neighbourhoods, the body piece associated with x can be identified with the tangent space $T_x\mathscr{B}(t)$. In this case, the whole relaxation can be viewed as a linear mapping between tangent spaces. In particular, since the relaxation is elastic, it is represented by $\boldsymbol{F}_{\mathrm{e}}^{-1}(x, t) : T_x\mathscr{B}(t) \to \mathscr{N}_X(t)$, with $X = \hat{\chi}^{-1}(x, t)$ (see [62] and references therein).

The vector space $\mathscr{N}_X(t)$ depends on time, and is associated with a state of the tissue characterised by an important property: it is free of stress, and is obtained by distorting the elements of $T_X\mathscr{B}$, or the elements of $T_x\mathscr{B}(t)$, in a generally incompatible way. Hence, neither $\boldsymbol{F}_\gamma(X,t)$ nor $\boldsymbol{F}_{\mathrm{e}}^{-1}(x,t)$ can be taken from the outset as the tangent maps of deformations that determine a configuration of the tissue as a subset of the Euclidean space. We recall, however, that $\mathscr{N}_X(t)$ can be assembled in a stress-free Riemannian manifold, endowed with the curved metric induced by $\boldsymbol{F}_\gamma$ (cf. e.g. [148, 147, 106]). Moreover, for all $X \in \mathscr{B}$, the vectors of $\mathscr{N}_X(t)$ are associated with the *natural*, or ground, state of the tissue, i.e., with the state in which the tissue is free of stress. Such state encompasses the whole structural evolution undergone by the tissue, which occurs from the reference configuration in the form of the distortional tensor map $\boldsymbol{F}_\gamma(X,t) : T_X\mathscr{B} \to T\mathscr{N}_X(t)$. A sketch of the explanation given so far is given in Fig. (1.3), where $\mathscr{N}_X(t)$ is represented as a *"conglomerate"* of stress-free body pieces [148].

For further use, we introduce $\boldsymbol{\mathfrak{L}}_\gamma := \boldsymbol{F}_\gamma^{-1}\dot{\boldsymbol{F}}_\gamma$ and $\boldsymbol{L}_\gamma := \dot{\boldsymbol{F}}_\gamma\boldsymbol{F}_\gamma^{-1}$ to denote the rate of anelastic distortions associated with growth.

1.6.3 Phenomenology of the growth tensor

The introduction of the growth tensor, $\boldsymbol{F}_\gamma$, produces many similarities among growth, finite strain elastoplasticity, and the theory of defects in solids (see e.g. [161, 176] for a review) and, in fact, many biological aspects of growth can be reinterpreted in terms of the evolution of inelastic distortions. One similarity with elastoplasticity is the definition of a stress-free "intermediate configuration", which exemplifies the conceptual separation between growth and deformation. Actually, the "intermediate configuration" is a collection of tissue pieces rather than a true configuration, and is obtained in two steps: First, by removing all the loads acting on the current configuration of the tissue, and then, by ideally chopping the tissue in small, stress-free pieces [176]. These can be assembled in a reference configuration by means of a transformation that is identifiable with $\boldsymbol{F}_\gamma^{-1}$. Hence, growth can be understood as the reverse process, which maps the tissue pieces from the reference configuration into the intermediate one (see [62] and references therein).

Tensor $\boldsymbol{F}_\gamma^{-1}$ is *formally* related to the existence of growth-induced inhomogeneities, [72, 66, 69, 67]. We have emphasised the adverb "formally" because, in our theory, we are not using the concept of "*archetype*" [66, 69, 67]. This notion, instead, is used to define an inhomogeneous body as a body for which it is possible to define a non-singular tensor field, whose inverse is non-integrable [72, 66].

Clearly, the way in which the inhomogeneities evolve depends on the biological problem under study and, thus, on the proposed model of growth. For instance, in [72], a prototypal evolution law for the growth inhomogeneities is set in the form of a relation between Eshelby stress and the rate at which the inhomogeneities themselves are produced. In this case, the law is obtained by following a reduction procedure that requires its compliance with the body's material symmetries, and with the principles of uniformity, objectivity, and independence of the reference configuration. A different perspective is considered e.g. in [98, 172], where some phenomenological growth laws are discussed within a chemo-mechanical framework. For arteries [183], an evolution law for the growth tensor is obtained in terms of a generalised Onsager's relation, in which the driving force of growth is identified with the difference between a suitable measure of mechanical stress and a target stress, referred to as "*homoeostatic stress*" (see [62] and references therein).

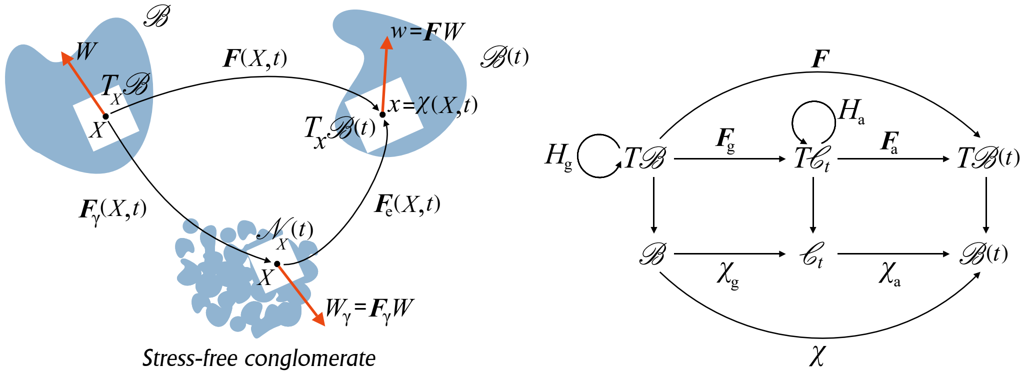

Figure 1.3: Schematic representation of the introduced mappings [62].

A different geometric picture about growth

Before going further, we mention that a different formulation of the BKL-decomposition is presented in [197, 46]. The core of such formulation is the use of two mappings that define a base and a *"target"* [46] configuration for each of the factors of the BKL-decomposition. In summary, one indicates by $\boldsymbol{F}_{\mathrm{a}}$ and $\boldsymbol{F}_{\mathrm{g}}$ the accommodating and the growth part of $\boldsymbol{F}$, so that $\boldsymbol{F} = \boldsymbol{F}_{\mathrm{a}}\boldsymbol{F}_{\mathrm{g}}$ holds true, and introduces the differentiable mappings χ_{a} and χ_{g} such that $\boldsymbol{F}_{\mathrm{a}}$ and $\boldsymbol{F}_{\mathrm{g}}$ are expressed as $\boldsymbol{F}_{\mathrm{a}} = (T\chi_{\mathrm{a}})\boldsymbol{H}_{\mathrm{a}}$ and $\boldsymbol{F}_{\mathrm{g}} = (T\chi_{\mathrm{g}})\boldsymbol{H}_{\mathrm{g}}$ [46]. Here, $T\chi_{\mathrm{a}}$ and $T\chi_{\mathrm{g}}$ are the tangent maps of χ_{a} and χ_{g}, and they represent the *compatible* contributions to $\boldsymbol{F}_{\mathrm{a}}$ and $\boldsymbol{F}_{\mathrm{g}}$. On the contrary, in general $\boldsymbol{H}_{\mathrm{a}}$ and $\boldsymbol{H}_{\mathrm{g}}$ cannot be identified with the tangent map of any deformation. Indeed, $\boldsymbol{H}_{\mathrm{g}}$ describes the generally *incompatible* structural changes due to growth, while $\boldsymbol{H}_{\mathrm{a}}$ models the elastic distortions that may have to be applied to the grown body pieces to restore a global configuration (see [62] and references therein).

For every $t \in \mathscr{I}$, the map $\chi_{\mathrm{g}}(\,\cdot\,, t)$ is identified with the diffeomorphism $\chi_{\mathrm{g}}(\,\cdot\,, t) : \mathscr{B} \to \mathscr{C}_t$, where $\mathscr{C}_t$ is referred to as *"intermediate configuration"*, while $T\chi_{\mathrm{g}}(\,\cdot\,, t)$ and $\boldsymbol{H}_{\mathrm{g}}(\,\cdot\,, t)$ are defined in terms of maps between tangent spaces, i.e., $T\chi_{\mathrm{g}}(X, t) : T_X\mathscr{B} \to T_{\chi_{\mathrm{g}}(X,t)}\mathscr{C}_t$ and $\boldsymbol{H}_{\mathrm{g}}(X, t) : T_X\mathscr{B} \to T_X\mathscr{B}$, respectively [46]. Analogous considerations hold for $\chi_{\mathrm{a}}(\,\cdot\,, t) : \mathscr{C}_t \to \mathscr{B}(t)$ and for $T\chi_{\mathrm{a}}(\,\cdot\,, t)$, and $\boldsymbol{H}_{\mathrm{a}}(\,\cdot\,, t)$ (see [46] for details). A drawing summarising the view of the BKL-decomposition presented in [46] is given in Fig. 1.3 (right). We notice that $\boldsymbol{H}_{\rm g}$ plays the same role as $\boldsymbol{F}_\gamma$ in the present context (see [62] and references therein).

We emphasise that, although we do not use here the approach by [46], we find it important to draw attention on it because, through $\chi_{\rm g}$ (or $\chi_{\rm a}$), it introduces an additional degree of freedom that, along with $\boldsymbol{F}_\gamma$, could be useful for other applications of the BKL-decomposition (see [62] and references therein).

1.6.4 The role of stress

Mathematical models of growth and remodelling should capture the "two-level" nature of the phenomena that they are meant to resolve, thereby trying to connect the visible transformations of a tissue with the chemical, electrical, and mechanical interactions occurring inside it. For instance, in the case of growth, a connection of this kind is established by *mechanotransduction* [51, 166], i.e., the modulation that mechanical stress exerts on the tissue's growth rate due to its interplay with the tissue's mass sources (see [114] and references therein).

To move forward in the comprehension of how growth and remodelling interact, an important question to answer is how to relate mechanical stress with both phenomena (see e.g. [173, 12]). For example, the tearing of the inter-cellular bonds in a tumour, which can be interpreted as an expression of remodelling [9, 198], leads to the relaxation of stress, and stress, apart from mechanotransduction, may play a role on the growth of the tumour. Indeed, a recent result presented in [166], seems to show that remodelling enhances the growth of a tumour in the avascular stage by increasing the speed at which the tumour's boundary advances in space . The observed behaviour was the consequence of the smoothing effect of the plastic-like distortions on mechanical stress, and such effect was transferred to the term describing growth through the mechanotransduction (see [114] and references therein).

The type of remodelling induced by mechanical stress can be viewed as a plastic-like behaviour and, if one assumes plastic response to be triggered by a yield stress (as is the case, for instance, in rate-independent [176, 124] or in Perzyna-like plasticity [176]), one may conclude that remodelling commences in the regions of the tissue in which the stress exceeds a certain threshold. Since in a growing tissue such regions are those in which the growth is predominant and the deformation is inhibited, it is very important to resolve accurately the plastic-like distortions. This exigency becomes stringent when the "plastic" strains accumulate in very narrow zones. In such cases, a useful tool of investigation could be to switch from a local to a *"non-local"* model of plasticity and this aspect will be discussed in the following (see [114] and references therein). We conclude by summarising some of the main symbols employed in the Thesis and introduced in the introductory chapter.

$\boldsymbol{a}$	structural tensor in the spatial configuration
$\boldsymbol{b}$	left Cauchy-Green deformation tensor
$\boldsymbol{b}_{\mathrm{e}}$	elastic left Cauchy-Green deformation tensor
$\boldsymbol{d}$	spatial diffusivity tensor
$\boldsymbol{g}$	metric tensor associated with the spatial configuration
$\boldsymbol{i}$	identity tensor associated with the spatial configuration
$\boldsymbol{k}$	permeability tensor associated with the spatial configuration
$\boldsymbol{v}_{\mathrm{s}}$	spatial solid velocity
$\boldsymbol{v}_{\mathrm{f}}$	spatial fluid velocity
$\boldsymbol{A}$	structural tensor in the reference configuration
$\boldsymbol{C}$	right Cauchy- Green deformation gradient tensor
$\boldsymbol{C}_{\mathrm{p}}$	right Cauchy-Green tensor associated with remodelling
$\boldsymbol{C}_{\gamma}$	right Cauchy-Green tensor associated with growth
$\boldsymbol{C}_{\mathrm{e}}$	elastic right Cauchy-Green tensor
$\boldsymbol{D}$	material diffusivity tensor
$\boldsymbol{F}$	deformation gradient tensor
$\boldsymbol{F}_{\mathrm{p}}$	remodelling tensor
1277 $\boldsymbol{F}_{\gamma}$	growth tensor
$\boldsymbol{F}_{\mathrm{e}}$	accommodation tensor
$\boldsymbol{G}$	metric tensor associated with the reference configuration
I_1, I_2, I_3	orthogonal invariants of $\boldsymbol{C}$
$I_{1\mathrm{e}}, I_{2\mathrm{e}}, I_{3\mathrm{e}}$	orthogonal invariants of $\boldsymbol{C}_{\mathrm{e}}$
I_4	fourth invariant of $\boldsymbol{C}$
$I_{4\mathrm{e}}$	fourth invariant of $\boldsymbol{C}_{\mathrm{e}}$
$\boldsymbol{I}$	identity tensor associated with the reference configuration
J	determinant of $\boldsymbol{F}$
J_{p}	determinant of $\boldsymbol{F}_{\mathrm{p}}$
J_{e}	determinant of $\boldsymbol{F}_{\mathrm{e}}$
J_{γ}	determinant of $\boldsymbol{F}_{\gamma}$
$\boldsymbol{H}$	inverse of the remodelling tensor
$\boldsymbol{P}$	first Piola-Kirchhoff stress tensor
$\boldsymbol{S}$	second Piola-Kirchhoff stress tensor
$\boldsymbol{Y}_{\mathrm{e}}, \boldsymbol{Y}_{\mathrm{i}}$	external and internal generalised forces
$\boldsymbol{Z}$	generalised growth velocity

$\boldsymbol{V}_{\mathrm{s}}$	material solid velocity
$\boldsymbol{V}_{\mathrm{f}}$	material fluid velocity
$\boldsymbol{V}_{\gamma}, \boldsymbol{U}_{\gamma}$	growth stretches
$\boldsymbol{R}_{\gamma}$	growth rotation tensor
$\boldsymbol{\eta}$	metric tensor associated with the natural state
χ	motion
γ	growth parameter
ω	variance
$\boldsymbol{\sigma}$	Cauchy stress tensor
$\boldsymbol{\Sigma}$	Mandel stress tensor
ϕ_{s}	spatial volumetric fraction of the solid phase
ϕ_{f}	spatial volumetric fraction of the fluid phase
Φ_{s}	referential volumetric fraction of the solid phase
Φ_{f}	referential volumetric fraction of the fluid phase
$\boldsymbol{\Lambda}_{\mathrm{p}}$	rate of anelastic distortions (reference configuration)
$\boldsymbol{L}_{\mathrm{p}}$	rate of anelastic distortions (natural state)
$\boldsymbol{\mathfrak{L}}_{\gamma}$	rate of growths (reference configuration)
$\boldsymbol{L}_{\gamma}$	rate of growth (natural state)
$\mathscr{S}$	three-dimensional Euclidean space
$\mathscr{I}$	three-dimensional Euclidean space
$\mathscr{B}$	reference placement of the solid phase
$\mathscr{B}_{\mathrm{s}}$	current configuration of the solid phase
$\mathscr{B}_{\mathrm{f}}$	current configuration of the fluid phase
$\mathscr{N}_{X}(t)$	natural state
$\boldsymbol{\mathfrak{a}}$	structural tensor in the natural state
$\boldsymbol{\mathfrak{m}}$	field of unit normal
$\boldsymbol{\mathfrak{q}}$	fibre mean angle

Chapter 2

Anelastic reorganisation of biological tissues

The work reported in this chapter has been previously published in [61].

2.1 Anelastic processes and structural changes

In this Chapter, we contribute to the study of the structural reorganisation of biological tissues in response to mechanical stimuli. We specialise our investigation to a class of hydrated soft tissues, whose internal structure features reinforcing fibres. These are oriented statistically within the tissue, and their pattern of orientation is such that, at each material point, the tissue is anisotropic. From in its natural, stress-free state, the tissue can be distorted anelastically into a global reference configuration, and then deformed under the action of external mechanical loads. The anelastic distortions are responsible for changing irreversibly the internal structure of the tissue, which, in the present context, occurs through both the rearrangement of the bonds among the tissue cells and the deformation-driven reorientation of the fibres. The anelastic strains, in addition, are assumed to model the onset and evolution of micro cracks in the tissue, which may be triggered by the mechanical loads applied to the tissue in the case of traumatic events, or diseases. For our purposes, we formulate an anisotropic model of remodelling and we consider a fully isotropic model of structural reorganisation for comparison, with the aim of studying if, how, and to what extent the evolution of anelastic distortions is influenced by the tissue's anisotropy.

Determining physically sound evolution laws for the distortions characterising the structural adaptation of biological tissues is a crucial task, which has been undertaken by several authors (see e.g. [72, 160, 98, 5, 157, 99, 183, 110]). One of the main challenges of mathematical modelling is to predict how the structural evolution of a tissue is modulated by mechanical stress. This issue is particularly relevant when also other phenomena, such as growth [200], mechano-transduction [51], and interactions with other stimuli [159, 167, 62], have to be accounted for. Moreover, since the formulation of models for the structural evolution of tissues allows for a certain freedom, and since a model that is reliable for a certain tissue may be inaccurate for another one, it is difficult to find a unified criterion for determining *a priori* how such models should be constructed. To our knowledge, however, Epstein and Maugin [72] prescribed a series of conditions that should be satisfied in order to formulate acceptable structural evolutions. These rules, in turn, are based on the theory developed, for example, in [70, 169, 69].

With the purpose of seeking for a unified form of the structural evolution laws of biological tissues, we take a phenomenological law of remodelling in isotropic media [104] and, by following the rules put forward in [72], we rephrase it for the case of an anisotropic tissue. To this end, we elaborate the anisotropic hyperelastic model of fibre-reinforced tissues developed in [84, 80, 225], in which the interaction with an interstitial fluid is considered, and we extend it to the case of nonlinear elastoplastic material behaviour. Then, after specifying the equations governing the deformation of the tissue, the fluid flow, and the evolution of the plastic-like distortions, we test our model by solving numerically dedicated benchmark problems. The main goal of our work is to evaluate the interplay between remodelling and the anisotropy of the tissue. This interplay is highlighted by comparing the results of our anisotropic model with those predicted by an isotropic model taken as reference [112].

2.2 Constitutive laws

At each material point, the solid phase of the tissue is modelled as a hyperelastic material. This hypothesis allows to describe the mechanical behaviour of the solid phase entirely in terms of a strain energy density, and to express the latter as a function of the elastic part of the deformation, only. More precisely, if we denote by $W_{\mathrm{R}} = \hat{W}_{\mathrm{R}}(\boldsymbol{C}, X, t)$ the strain energy density of the solid phase, written per unit volume of the reference configuration (note that the the material inhomogeneities and their evolution are accounted for by the explicit dependence of $\hat{W}_{\mathrm{R}}$ on the material points and time, respectively), it is possible to write [53, 72]

$$\hat{W}_{\mathrm{R}}(\boldsymbol{C}, X, t) = J_{\mathrm{p}}(X, t)\hat{W}_{\nu}(\boldsymbol{C}_{\mathrm{e}}(X, t), X) = \frac{1}{J_{\boldsymbol{H}}(X, t)}\hat{W}_{\nu}(\boldsymbol{C}_{\mathrm{e}}(X, t), X), \tag{2.1}$$

where $\hat{W}_{\nu}$ is measured per unit volume of the natural state (see the subsection *Kinematics* of Section 1.5.1 for the notation employed in (2.1) and hereafter). We remark that, in Equation (2.1), the explicit dependence of strain energy function on material points is given through ξ. In the following, however, for the sake of a lighter notation, the explicit dependence of $\hat{W}_{\nu}$ on material points, X, is omitted but understood. We adapt to the present framework a strain energy density used in previous works [84, 80, 225, 40, 111, 107], i.e.,

$$\hat{W}_\nu(\boldsymbol{C}_\mathrm{e}) = \Phi_{\mathrm{s}\nu}\hat{U}(J_\mathrm{e}) + \Phi_{0\mathrm{s}\nu}\hat{W}_0(\boldsymbol{C}_\mathrm{e}) + \Phi_{1\mathrm{s}\nu}\hat{W}_\mathrm{en}(\boldsymbol{C}_\mathrm{e}), \tag{2.2}$$

where

$$\Phi_{0\mathrm{s}\nu} = J_\mathrm{e}\phi_{0\mathrm{s}}, \tag{2.3a}$$
$$\Phi_{1\mathrm{s}\nu} = J_\mathrm{e}\phi_{1\mathrm{s}}, \tag{2.3b}$$
$$\Phi_{\mathrm{s}\nu} = \Phi_{0\mathrm{s}\nu} + \Phi_{1\mathrm{s}\nu} = J_\mathrm{e}\phi_\mathrm{s} \tag{2.3c}$$

are the volumetric fractions of the non-fibrous matrix, fibres, and solid phase as a whole, respectively, all measured per unit volume of the natural state. Similarly $\phi_{0\mathrm{s}}$ and $\phi_{1\mathrm{s}}$ are the volumetric fractions of the non-fibrous matrix and of the fibres, respectively, misured per unit volume of the actual configuration and such that $\phi_\mathrm{s} = \phi_{0\mathrm{s}} + \phi_{01\mathrm{s}}$. Moreover $\hat{U}(J_\mathrm{e})$, $\hat{W}_0(\boldsymbol{C}_\mathrm{e})$, and $\hat{W}_\mathrm{en}(\boldsymbol{C}_\mathrm{e})$ are given by

$$\hat{U}(J_\mathrm{e}) = \alpha_0\mathcal{H}(J_\mathrm{cr} - J_\mathrm{e})\frac{[J_\mathrm{e} - J_\mathrm{cr}]^{2q}}{[J_\mathrm{e} - \Phi_{\mathrm{s}\nu}]^r}, \tag{2.4a}$$
$$\hat{W}_0(\boldsymbol{C}_\mathrm{e}) = \alpha_0\left[\frac{\exp\left(\alpha_1[I_{1\mathrm{e}} - 3] + \alpha_2[I_{2\mathrm{e}} - 3]\right)}{[I_{3\mathrm{e}}]^{\alpha_3}} - 1\right], \tag{2.4b}$$
$$\hat{W}_\mathrm{en}(\boldsymbol{C}_\mathrm{e}) = \hat{W}_{1\mathrm{i}}(\boldsymbol{C}_\mathrm{e}) + \langle\!\langle \hat{W}_{1\mathrm{a}}(\boldsymbol{C}_\mathrm{e}, \mathfrak{m})\rangle\!\rangle. \tag{2.4c}$$

In (2.4a)–(2.4c), $\alpha_0 = 0.125$ MPa, $\alpha_1 = 0.778$, $\alpha_2 = 0.111$, $\alpha_3 = \alpha_1 + 2\alpha_2 = 1$, $q \geq 0$, and $r \in]0{,}1]$ are material parameters, $J_\mathrm{cr} \in]\Phi_{\mathrm{s}\nu}{,}1]$ is a critical value of J_e (in this work, we take $q = 2$, $r = 0.5$, and $J_\mathrm{cr} = \Phi_{\mathrm{s}\nu} + 0.1$), $I_{1\mathrm{e}} = \mathrm{tr}(\boldsymbol{C}_\mathrm{e})$, $I_{2\mathrm{e}} = \frac{1}{2}\{[\mathrm{tr}(\boldsymbol{C}_\mathrm{e})]^2 - \mathrm{tr}(\boldsymbol{C}_\mathrm{e}^2)\}$, and $I_{3\mathrm{e}} = \det \boldsymbol{C}_\mathrm{e}$ are the principal invariants of $\boldsymbol{C}_\mathrm{e}$, $\hat{W}_{1\mathrm{i}}$ is the isotropic part of the strain energy density of the fibres (it has the same functional form as (2.4b), but it features different coefficients), and $\hat{W}_{1\mathrm{a}}(\boldsymbol{C}_\mathrm{e}, \mathfrak{m})$ reads

$$\hat{W}_{1\mathrm{a}}(\boldsymbol{C}_\mathrm{e}, \mathfrak{m}) = \mathcal{H}(I_{4\mathrm{e}} - 1)\tfrac{1}{2}c[I_{4\mathrm{e}} - 1]^2, \tag{2.5}$$

where $I_{4\mathrm{e}} = \boldsymbol{C}_\mathrm{e} : \mathfrak{m} \otimes \mathfrak{m} = \boldsymbol{C} : (\boldsymbol{H}\mathfrak{m} \otimes \boldsymbol{H}\mathfrak{m})$ and $c = 7.46$ MPa. In (2.4a) and (2.5), $\mathcal{H}$ is the Heaviside function, i.e., $\mathcal{H}(s) = 1$ for all $s \geq 0$, and $\mathcal{H}(s) = 0$ for all $s < 0$. Finally, it is possible to define the unit vector field

$$\boldsymbol{M} = \frac{\boldsymbol{H}\mathfrak{m}}{\|\boldsymbol{H}\mathfrak{m}\|}. \tag{2.6}$$

Consequently, the structure tensor field in the natural state, i.e., $\mathfrak{a} = \mathfrak{m} \otimes \mathfrak{m}$, transforms as

$$\boldsymbol{A} = \boldsymbol{M} \otimes \boldsymbol{M} = \frac{\boldsymbol{H}\mathfrak{a}\boldsymbol{H}^\mathrm{T}}{(\boldsymbol{H}^\mathrm{T}.\boldsymbol{H}) : \mathfrak{a}}, \tag{2.7}$$

with $\boldsymbol{A}$ being the structure tensor field associated with the reference configuration, and the invariant $I_{4\mathrm{e}}$ becomes $I_{4\mathrm{e}} = I_4 I_{4\Pi}$, where we used the notation

$$I_4 = \boldsymbol{C} : \boldsymbol{A}, \quad I_{4\Pi} = (\boldsymbol{H}^{\mathrm{T}}.\boldsymbol{H}) : \mathfrak{a}. \tag{2.8a}$$

The energy $\hat{U}(J_{\mathrm{e}})$ is zero for J_{e} above the critical volume ratio J_{cr} (which, in general, is a function of material points), and diverges for J_{e} tending to $\Phi_{\mathrm{s}\nu}$ from above, thereby preventing the elastic distortions from violating the unilateral constraint $J_{\mathrm{e}} \geq \Phi_{\mathrm{s}\nu}$. The constitutive part of the first Piola-Kirchhoff stress tensor associated with the solid phase is given by

$$\boldsymbol{P}_{\mathrm{sc}} = \boldsymbol{F}\left[\frac{1}{J_{\boldsymbol{H}}}\boldsymbol{H}\left(2\frac{\partial \hat{W}_\nu}{\partial \boldsymbol{C}_{\mathrm{e}}}(\boldsymbol{C}_{\mathrm{e}})\right)\boldsymbol{H}^{\mathrm{T}}\right]. \tag{2.9}$$

Consequently, $\boldsymbol{P}_{\mathrm{sc}}$ can be expressed constitutively as a function of $\boldsymbol{F}$ and $\boldsymbol{H}$, i.e., $\boldsymbol{P}_{\mathrm{sc}} = \hat{\boldsymbol{P}}_{\mathrm{sc}}(\boldsymbol{F}, \boldsymbol{H})$. Also in this case, the explicit dependence on material points is omitted but understood.

The mathematical model presented in the following is based on the hypothesis that the interstitial fluid obeys Darcy's law. This requires the introduction of a permeability tensor for the tissue. In this work, we adapt to our problem the constitutive framework developed in [83, 82, 80, 225, 108]. Hence, we assume that the spatial permeability tensor reads [225]

$$\boldsymbol{k} = k_0 \frac{[J J_{\boldsymbol{H}} - \Phi_{1\mathrm{s}\nu}]^2}{J^2 J_{\boldsymbol{H}}^2} \boldsymbol{g}^{-1} + k_0 \frac{[J J_{\boldsymbol{H}} - \Phi_{1\mathrm{s}\nu}]\Phi_{1\mathrm{s}\nu}}{J^2 J_{\boldsymbol{H}}^2} \boldsymbol{F}\boldsymbol{H} \left\langle\!\!\left\langle \frac{\mathfrak{a}}{I_{4\mathrm{e}}} \right\rangle\!\!\right\rangle \boldsymbol{H}^{\mathrm{T}}\boldsymbol{F}^{\mathrm{T}}, \tag{2.10}$$

where k_0 is taken to be of the Holmes and Mow type [138], i.e.,

$$k_0 = k_{0\nu}\left[\frac{J J_{\boldsymbol{H}} - \Phi_{\mathrm{s}\nu}}{1 - \Phi_{\mathrm{s}\nu}}\right]^{\kappa_0} \exp\left(\frac{1}{2} m_0 [J^2 J_{\boldsymbol{H}}^2 - 1]\right), \tag{2.11}$$

where $\kappa_0 = 0.0848$ and $m_0 = 4.638$ are model parameters, and $k_{0\nu}$ is a reference permeability. As done elsewhere (e.g. in [225]), $k_{0\nu}$ is taken as a function of the axial coordinate, ξ, and its functional form is defined in (2.14). From (2.10) and (2.11) we notice that, since the product $J J_{\boldsymbol{H}} = J_{\mathrm{e}}$ has to be greater than, or equal to, $\Phi_{\mathrm{s}\nu}$, the permeability tensor is positive semi-definite for $J J_{\boldsymbol{H}} \geq \Phi_{\mathrm{s}\nu} \geq \Phi_{1\mathrm{s}\nu}$ and, in particular, it is positive definite when the strict inequality is satisfied, i.e., when $J J_{\boldsymbol{H}} > \Phi_{\mathrm{s}\nu}$.

For future use, we compute the Piola transform of $\boldsymbol{k}$, i.e., $\boldsymbol{K} = J\boldsymbol{F}^{-1}\boldsymbol{k}\boldsymbol{F}^{-\mathrm{T}}$, which reads

$$\boldsymbol{K} = k_0 \frac{[J J_{\boldsymbol{H}} - \Phi_{1\mathrm{s}\nu}]^2}{J J_{\boldsymbol{H}}^2} \boldsymbol{C}^{-1} + k_0 \frac{[J J_{\boldsymbol{H}} - \Phi_{1\mathrm{s}\nu}]\Phi_{1\mathrm{s}\nu}}{J J_{\boldsymbol{H}}^2} \boldsymbol{H} \left\langle\!\!\left\langle \frac{\mathfrak{a}}{I_{4\mathrm{e}}} \right\rangle\!\!\right\rangle \boldsymbol{H}^{\mathrm{T}}. \tag{2.12}$$

Clearly, since $\boldsymbol{k}$ is positive semi-definite, $\boldsymbol{K}$ is positive semi-definite too. Note also that $\boldsymbol{K}$ can be written as $\boldsymbol{K} = \hat{\boldsymbol{K}}(\boldsymbol{F}, \boldsymbol{H})$, where the dependence on $\boldsymbol{F}$ is through $\boldsymbol{C}$ because of objectivity, and the dependence on X is understood. In fact, in the case of inhomogeneous materials, the dependence of $k_{0\nu}$ on material points can be taken into account by expressing $k_{0\nu}$ as a function of the void ratio associated with the natural state, $e_\nu = (1 - \Phi_{\mathrm{s}\nu})/\Phi_{\mathrm{s}\nu}$, and specifying how the volumetric fraction $\Phi_{\mathrm{s}\nu}$ depends on the normalised axial coordinate ξ (we recall, indeed, that the material is assumed here to be inhomogeneous only axially). In this work, we assign the volumetric fractions of matrix and fibres in the tissue's natural state, $\Phi_{0\mathrm{s}\nu}$ and $\Phi_{1\mathrm{s}\nu}$, and we compute thus the volumetric fraction of the solid phase as $\Phi_{\mathrm{s}\nu} = \Phi_{0\mathrm{s}\nu} + \Phi_{1\mathrm{s}\nu}$. In particular, we prescribe [225]

$$\Phi_{0\mathrm{s}\nu} = \hat{\Phi}_{0\mathrm{s}\nu}(\xi) = -0.062\xi^2 + 0.038\xi + 0.046, \tag{2.13a}$$

$$\Phi_{1\mathrm{s}\nu} = \hat{\Phi}_{1\mathrm{s}\nu}(\xi) = +0.062\xi^2 - 0.138\xi + 0.204, \tag{2.13b}$$

$$\Phi_{\mathrm{s}\nu} = \hat{\Phi}_{\mathrm{s}\nu}(\xi) = -0.100\xi + 0.250. \tag{2.13c}$$

Following the constitutive framework adopted in previous works, we assume that $k_{0\nu}$ depends on e_ν as suggested by Holmes and Mow [138]. Hence, given the constant referential void ratio $e_\nu^{(0)} = 4$ and the constant referential scalar permeability $k_{0\nu}^{(0)} = 3.7729 \cdot 10^{-3}\ \mathrm{mm}^4(\mathrm{Ns})^{-1}$, we assign $k_{0\nu}$ through the expression [225]

$$\frac{k_{0\nu}}{k_{0\nu}^{(0)}} = \left[\frac{e_\nu}{e_\nu^{(0)}}\right]^{\kappa_0} \exp\left(\frac{m_0}{2}\left[\left(\frac{1+e_\nu}{1+e_\nu^{(0)}}\right)^2 - 1\right]\right). \tag{2.14}$$

In summary, the constitutive framework adopted here describes a hydrated, fibre-reinforced tissue, whose solid phase is hyperelastic, transversely isotropic with respect to a global symmetry axis (the direction of which is identified by the unit vector $\mathfrak{m}_0$), and inhomogeneous along this axis. We emphasise that, within the employed approach, the inhomogeneity is due to the fact that the volumetric fractions of matrix and fibres, $\Phi_{0\mathrm{s}\nu}$ and $\Phi_{1\mathrm{s}\nu}$, the standard deviation of the probability density, ω, and the mean angle of fibre orientation, $\mathfrak{q}$, depend on the normalised axial coordinate through the expressions (1.8), which are in qualitative agreement with the histological features of articular cartilage, as revealed by X-ray diffraction experiments [179].

2.3 Description of Remodelling

The mathematical model of the physical system under study is characterised by two dissipative phenomena. First we consider the one related to the fluid flow, which is affected by dissipative forces exchanged between the fluid and the solid phase. We prescribe that these forces depend linearly on the filtration velocity

$\boldsymbol{q} = \phi_{\mathrm{f}}[\boldsymbol{v}_{\mathrm{f}} - \boldsymbol{v}_{\mathrm{s}}]$ and, by disregarding the influence of gravity on the flow, we obtain Darcy's law, which reads $\boldsymbol{q} = -\boldsymbol{k}\,\mathrm{grad}\,p$ in spatial form [17], and $\boldsymbol{Q} = -\boldsymbol{K}\mathrm{Grad}\,p$ in the so-called "material" form. Here, $\boldsymbol{Q} := J\boldsymbol{F}^{-1}\boldsymbol{q}$ is the Piola transform of the filtration velocity, and $\mathrm{Grad}\,p = \boldsymbol{F}^{\mathrm{T}}\mathrm{grad}\,p$ is the "material" pressure gradient, obtained by differentiating p with respect to the coordinates associated with the reference configuration. We remark that the filtration velocity represents the specific mass flux vector associated with the motion of the fluid relative to the solid.

The second dissipative phenomenon addressed in this work is due to the reorganisation of the tissue's internal structure. This process is described here in analogy with the theory of finite strain plasticity through the introduction of $\boldsymbol{H}$ [72]. The rate with which the anelastic distortions associated with $\boldsymbol{H}$ evolve in time is given by $\boldsymbol{\Lambda}_{\mathrm{p}} = \dot{\boldsymbol{H}}\boldsymbol{H}^{-1}$ and it will be referred to as *tensor of rate of remodelling*. In the sequel, we shall assume that remodelling is a volume-preserving process, which yields the restriction $J_{\boldsymbol{H}} = 1$ and implies that $\boldsymbol{\Lambda}_{\mathrm{p}}$ is a deviatoric second-order tensor. Within this framework, the generalised force power-conjugate to $\boldsymbol{\Lambda}_{\mathrm{p}}$ is the Mandel stress tensor $\boldsymbol{\Sigma} = \boldsymbol{C}\boldsymbol{S}$ [70, 169], where $\boldsymbol{S} = \boldsymbol{F}^{-1}\boldsymbol{P}_{\mathrm{sc}}$ is the constitutive part of the second Piola-Kirchhoff stress tensor of the solid phase.

2.3.1 Dissipation Inequality

By accounting for the contributions due to the flow and remodelling, denoted by $\mathfrak{D}_{\mathrm{flow}}$ and $\mathfrak{D}_{\mathrm{rem}}$, respectively, the dissipation of the system under study can be written as [112]

$$\mathfrak{D}_{\mathrm{R}} = \underbrace{\boldsymbol{K} : [\mathrm{Grad}\,p \otimes \mathrm{Grad}\,p]}_{\mathfrak{D}_{\mathrm{flow}} \geq 0} \underbrace{-\boldsymbol{\Sigma} : \boldsymbol{\Lambda}_{\mathrm{p}}}_{\mathfrak{D}_{\mathrm{rem}}} \geq 0. \tag{2.15}$$

Since the positive semi-definiteness of $\boldsymbol{K}$ guarantees that $\mathfrak{D}_{\mathrm{flow}}$ is non-negative for all pressure gradients, the fulfilment of the inequality $\mathfrak{D}_{\mathrm{R}} \geq 0$ is equivalent to requiring the condition $\mathfrak{D}_{\mathrm{rem}} = -\boldsymbol{\Sigma} : \boldsymbol{\Lambda}_{\mathrm{p}} \geq 0$ for all $\boldsymbol{\Sigma}$ and $\boldsymbol{\Lambda}_{\mathrm{p}}$. Moreover, the physical observation that remodelling is triggered by stress suggests to relate $\boldsymbol{\Sigma}$ to $\boldsymbol{\Lambda}_{\mathrm{p}}$ in such a way that the aforementioned restriction is respected. This should be done, however, by exploiting the fact that $\boldsymbol{\Sigma}$ complies, by construction, with the symmetry condition $\boldsymbol{\Sigma}\boldsymbol{C} = \boldsymbol{C}\boldsymbol{S}\boldsymbol{C} = (\boldsymbol{\Sigma}\boldsymbol{C})^{\mathrm{T}}$ [70, 169]. Upon setting $\boldsymbol{Y} := \boldsymbol{C}\boldsymbol{S}\boldsymbol{C}$, this yields the chain of equalities

$$\boldsymbol{\Sigma} : \boldsymbol{\Lambda}_{\mathrm{p}} = (\boldsymbol{C}\boldsymbol{S}\boldsymbol{C}) : (\boldsymbol{\Lambda}_{\mathrm{p}}\boldsymbol{C}^{-1}) = \boldsymbol{Y} : \mathrm{sym}(\boldsymbol{\Lambda}_{\mathrm{p}}\boldsymbol{C}^{-1}), \tag{2.16}$$

which allows to rephrase $\mathfrak{D}_{\mathrm{rem}}$ as [70]

$$\mathfrak{D}_{\mathrm{rem}} = -\boldsymbol{Y} : \mathrm{sym}(\boldsymbol{\Lambda}_{\mathrm{p}}\boldsymbol{C}^{-1}) \geq 0. \tag{2.17}$$

We recall that the stress tensor $\boldsymbol{Y}$ can be obtained by expressing the strain energy density as a function of the Piola strain $\boldsymbol{\mathcal{E}} = \frac{1}{2}[\boldsymbol{G}^{-1} - \boldsymbol{C}^{-1}]$ [70, 169].

We prescribe here that $\boldsymbol{Y}$ and $\mathrm{sym}(\boldsymbol{\Lambda}_{\mathrm{p}}\boldsymbol{C}^{-1})$ are related to each other through an expression of the type

$$\mathrm{sym}(\boldsymbol{\Lambda}_{\mathrm{p}}\boldsymbol{C}^{-1}) = -\boldsymbol{\mathcal{R}}, \tag{2.18}$$

where $\boldsymbol{\mathcal{R}}$ is a tensor-valued function that has to be specified constitutively. Equation (2.18) shall also be referred to as the *remodelling law*.

To satisfy the condition $\mathfrak{D}_{\mathrm{rem}} \geq 0$, we assume here that $\boldsymbol{\mathcal{R}}$ can be written as $\boldsymbol{\mathcal{R}} = \mathbb{T} : \boldsymbol{Y}$, where $\mathbb{T}$ is a fourth-order tensor endowed with the major symmetry and such that the inequality $\mathfrak{D}_{\mathrm{rem}} = \boldsymbol{Y} : \mathbb{T} : \boldsymbol{Y} \geq 0$ (i.e., $\mathbb{T}$ has to be positive semi-definite). The constitutive expression defining $\mathbb{T}$ specifies the law of remodelling that one is interested in. It should be noticed, however, that since $\boldsymbol{\Lambda}_{\mathrm{p}}$ is deviatoric (i.e., $\mathrm{tr}\boldsymbol{\Lambda}_{\mathrm{p}} = 0$), the right-hand-side of (2.18), $\boldsymbol{\mathcal{R}}$, must comply with the restriction $\mathrm{tr}(\boldsymbol{C}\boldsymbol{\mathcal{R}}) = 0$. This requires $\mathbb{T}$ to fulfil the condition $\mathrm{tr}[\boldsymbol{C}(\mathbb{T} : \boldsymbol{Y})] = \boldsymbol{C} : \mathbb{T} : \boldsymbol{Y} = 0$, for all $\boldsymbol{Y}$.

2.3.2 Remodelling laws

Equation (2.18) is the remodelling equation and it describes how the anelastic phenomena evolve during all the deformative process. It is formulated as an evolution law for $\boldsymbol{H}$ through the tensor $\boldsymbol{\Lambda}_{\mathrm{p}} = \dot{\boldsymbol{H}}\boldsymbol{H}^{-1}$.

In this work, we assume that remodelling occurs at a given material point when the Frobenius norm $\|\mathrm{dev}\boldsymbol{\sigma}\| = \sqrt{g_{ab}[\mathrm{dev}\boldsymbol{\sigma}]^{ac}g_{cd}[\mathrm{dev}\boldsymbol{\sigma}]^{db}}$ of the deviatoric part of the constitutive solid phase Cauchy stress, $\boldsymbol{\sigma} = J^{-1}\boldsymbol{P}_{\mathrm{sc}}\boldsymbol{F}^{\mathrm{T}}$, exceeds at that point a threshold equivalent stress, σ_Y, termed “yield stress” in analogy with Plasticity. To take this requirement into account, we write $\mathbb{T}$ as $\mathbb{T} = \zeta\mathbb{L}$, where ζ is a scalar stress-dependent “remodelling switch”. Hence, following [104], we prescribe a Perzyna-like model [176]

$$\zeta = \lambda(\phi_{\mathrm{s}}) \left[\frac{\|\mathrm{dev}\boldsymbol{\sigma}\| - \sqrt{2/3}\,\sigma_Y}{\|\mathrm{dev}\boldsymbol{\sigma}\|} \right]_+ , \tag{2.19}$$

where $\lambda(\phi_{\mathrm{s}})$ is a material parameter depending on the volumetric fraction of the solid phase, and the operator $[\,\cdot\,]_+$ extracts the positive part of the function to which it is applied (see also [56]). In this work, we assume that the yield stress is constant, and we set $\sigma_Y = 0.002$ MPa. We emphasise that $\lambda(\phi_{\mathrm{s}})$ vanishes for vanishing ϕ_{s}, since no remodelling may occur if the solid phase is absent. In the following, we adopt the simple law $\lambda(\phi_{\mathrm{s}}) = \lambda_0\phi_{\mathrm{s}}^2 = \lambda_0[\Phi_{\mathrm{s}\nu}/JJ_{\boldsymbol{H}}]^2$, with $\lambda_0 = 0.5\ (\mathrm{MPa}\cdot\mathrm{s})^{-1}$. We also remark that, since the condition $J_{\boldsymbol{H}} = 1$ applies in this context, the equality $\phi_{\mathrm{s}} = \Phi_{\mathrm{s}\nu}/J$ allows to rephrase the dependence of λ on ϕ_{s} in terms of the volume ratio J alone, rather than in terms of J and $J_{\boldsymbol{H}}$.

To complete the description of remodelling, it is necessary to specify the fourth-order tensor $\mathbb{L}$. In this work, we consider the expression

$$\mathbb{L} = \mathbb{M}^* : \mathbb{D} : \mathbb{M}^{*\mathrm{T}}, \tag{2.20}$$

where $\mathbb{M}^*$ and $\mathbb{M}^{*\mathrm{T}}$ are specified in Appendix A. The fourth-order tensor $\mathbb{D}$ encodes information about the material properties of the tissue and, in general, is a function of $\boldsymbol{C}$ and $\boldsymbol{H}$. With the notation introduced in Appendix A, $\mathbb{D}$ transforms tensors of $([T\mathscr{B}]^0_2, \mathrm{sym})$ into tensors of $([T\mathscr{B}]^2_0, \mathrm{sym})$. According to (2.20), the tensor $\boldsymbol{\mathcal{R}}$ featuring in (2.18) reads

$$\boldsymbol{\mathcal{R}} = \mathbb{T} : \boldsymbol{Y} = \zeta\, \mathbb{L} : \boldsymbol{Y} = \zeta\, \mathbb{M}^* : \mathbb{D} : \mathbb{M}^{*\mathrm{T}} : \boldsymbol{Y}. \tag{2.21}$$

We remark that the double-contraction of $\mathbb{M}^{*\mathrm{T}}$ with $\boldsymbol{Y}$ extracts the deviatoric part of $\boldsymbol{Y}$ with respect to the metric $\boldsymbol{C}$, i.e.,

$$\mathbb{M}^{*\mathrm{T}} : \boldsymbol{Y} = \boldsymbol{Y} - \tfrac{1}{3}\mathrm{tr}(\boldsymbol{C}^{-1}\boldsymbol{Y})\boldsymbol{C}. \tag{2.22}$$

Moreover, by introducing the tensor $\boldsymbol{Z} := \mathbb{D} : \mathbb{M}^{*\mathrm{T}} : \boldsymbol{Y}$, the left-multiplication by $\mathbb{M}^*$ in (2.21) leads to

$$\boldsymbol{\mathcal{R}} = \zeta\, \mathbb{M}^* : \boldsymbol{Z} = \zeta\, \left[\boldsymbol{Z} - \tfrac{1}{3}\mathrm{tr}(\boldsymbol{C}\boldsymbol{Z})\boldsymbol{C}^{-1}\right], \tag{2.23}$$

which guarantees the compliance with the constraint

$$0 = \mathrm{tr}\,\boldsymbol{\Lambda}_{\mathrm{p}} = \mathrm{tr}\left[\boldsymbol{C}\,\mathrm{sym}(\boldsymbol{\Lambda}_{\mathrm{p}}\boldsymbol{C}^{-1})\right] - \mathrm{tr}(\boldsymbol{C}\boldsymbol{\mathcal{R}}) = -\zeta\,\mathrm{tr}[\boldsymbol{C}(\mathbb{M}^* : \boldsymbol{Z})] = 0. \tag{2.24}$$

For the sake of simplicity, in the following we set $\mathbb{D} = \mathbb{I}^{\sharp *}$ (see Appendix A for the definition of $\mathbb{I}^{\sharp *}$), which implies

$$\boldsymbol{Z} = \mathbb{I}^{\sharp *} : \mathbb{M}^{*\mathrm{T}} : \boldsymbol{Y} = \boldsymbol{S} - \tfrac{1}{3}\mathrm{tr}(\boldsymbol{C}\boldsymbol{S})\boldsymbol{C}^{-1} = \mathbb{M}^* : \boldsymbol{S} = \tilde{\boldsymbol{S}}, \tag{2.25a}$$

$$\mathbb{L} : \boldsymbol{Y} = \mathbb{M}^* : \boldsymbol{Z} = \mathbb{M}^* : \mathbb{I}^{\sharp *} : \mathbb{M}^{*\mathrm{T}} : \boldsymbol{Y} = \mathbb{M}^{\sharp *} : \boldsymbol{Y}, \tag{2.25b}$$

where $\tilde{\boldsymbol{S}}$ is said to be the deviatoric part of $\boldsymbol{S}$ with respect to the metric $\boldsymbol{C}$, and $\mathbb{M}^{\sharp *}$ is defined in Appendix A. Furthermore, since $\mathbb{M}^*$ is idempotent (i.e., it holds that $\mathbb{M}^* : \mathbb{M}^* = \mathbb{M}^*$), we obtain the identity

$$\mathbb{M}^* : \boldsymbol{Z} = \mathbb{M}^* : \mathbb{M}^* : \boldsymbol{S} = \mathbb{M}^* : \boldsymbol{S} = \boldsymbol{Z}. \tag{2.26}$$

Thus, Equation (2.23) reduces to

$$\boldsymbol{\mathcal{R}} = \zeta\, \mathbb{M}^* : \boldsymbol{Z} = \zeta\, \boldsymbol{Z} = \zeta\left[\boldsymbol{S} - \tfrac{1}{3}\mathrm{tr}(\boldsymbol{C}\boldsymbol{S})\boldsymbol{C}^{-1}\right], \tag{2.27}$$

and the remodelling law takes on the form

$$\mathrm{sym}(\boldsymbol{\Lambda}_{\mathrm{p}}\boldsymbol{C}^{-1}) = -\zeta\left[\boldsymbol{S} - \tfrac{1}{3}\mathrm{tr}(\boldsymbol{C}\boldsymbol{S})\boldsymbol{C}^{-1}\right] = -\zeta\,\tilde{\boldsymbol{S}}, \tag{2.28}$$

thereby satisfying the requirement (2.24).

Model M1: Fully isotropic model We use this model for comparison with the other ones, and we obtain it in the limit of vanishing volumetric fraction of the fibres. Hence, we set $\Phi_{1\mathrm{s}\nu} = 0$, which implies $\Phi_{0\mathrm{s}\nu} = \Phi_{\mathrm{s}\nu}$, and we rewrite the strain energy density (2.2) as

$$\hat{W}_\nu(\boldsymbol{C}_\mathrm{e}) = \Phi_{\mathrm{s}\nu}\hat{U}(J_\mathrm{e}) + \Phi_{\mathrm{s}\nu}\hat{W}_0(\boldsymbol{C}_\mathrm{e}). \tag{2.29}$$

Consequently, the second Piola-Kirchhoff stress tensor consists of the isotropic contribution only, i.e.,

$$\boldsymbol{S}_\mathrm{iso} = \frac{1}{J_{\boldsymbol{H}}}\boldsymbol{H}\left[2\Phi_{\mathrm{s}\nu}\left(\frac{\partial\hat{U}}{\partial\boldsymbol{C}_\mathrm{e}} + \frac{\partial\hat{W}_0}{\partial\boldsymbol{C}_\mathrm{e}}\right)\right]\boldsymbol{H}^\mathrm{T}, \tag{2.30}$$

and the permeability tensor reduces to $\boldsymbol{K}_\mathrm{iso} = Jk_0\boldsymbol{C}^{-1}$. Furthermore, we prescribe the remodelling law

$$\mathrm{sym}(\boldsymbol{\Lambda}_\mathrm{p}\boldsymbol{C}^{-1}) = -\boldsymbol{\mathcal{R}}_{(1)} = -\zeta\,\mathbb{L} : \boldsymbol{Y}_\mathrm{iso}. \tag{2.31}$$

with $\boldsymbol{Y}_\mathrm{iso} = \boldsymbol{C}\boldsymbol{S}_\mathrm{iso}\boldsymbol{C}$. By substituting $\boldsymbol{Y}_\mathrm{iso}$ into (2.31) and performing all the necessary algebraic calculations, we obtain

$$\mathrm{sym}(\boldsymbol{\Lambda}_\mathrm{p}\boldsymbol{C}^{-1}) = -\boldsymbol{\mathcal{R}}_{(1)} = -\zeta\tilde{\boldsymbol{S}}_\mathrm{iso}, \tag{2.32}$$

with $\tilde{\boldsymbol{S}}_\mathrm{iso} = \mathbb{M}^* : \boldsymbol{S}_\mathrm{iso} = \boldsymbol{S}_\mathrm{iso} - \frac{1}{3}\mathrm{tr}(\boldsymbol{C}\boldsymbol{S}_\mathrm{iso})\boldsymbol{C}^{-1}$.

Model M2: Semi-isotropic model In this model, we use the full permeability tensor defined in (2.12) and the transversely isotropic strain energy density (2.2), which produces the second Piola-Kirchhoff stress tensor

$$\boldsymbol{S} = \boldsymbol{S}_\mathrm{i} + \boldsymbol{S}_\mathrm{a}, \tag{2.33}$$

with

$$\boldsymbol{S}_\mathrm{i} = \frac{1}{J_{\boldsymbol{H}}}\boldsymbol{H}\left[2\Phi_{\mathrm{s}\nu}\frac{\partial\hat{U}}{\partial\boldsymbol{C}_\mathrm{e}} + 2\Phi_{0\mathrm{s}\nu}\frac{\partial\hat{W}_0}{\partial\boldsymbol{C}_\mathrm{e}} + 2\Phi_{1\mathrm{s}\nu}\frac{\partial\hat{W}_{1\mathrm{i}}}{\partial\boldsymbol{C}_\mathrm{e}}\right]\boldsymbol{H}^\mathrm{T}, \tag{2.34a}$$

$$\boldsymbol{S}_\mathrm{a} = \frac{1}{J_{\boldsymbol{H}}}\boldsymbol{H}\left[2\Phi_{1\mathrm{s}\nu}\frac{\partial\langle\!\langle\hat{W}_{1\mathrm{a}}\rangle\!\rangle}{\partial\boldsymbol{C}_\mathrm{e}}\right]\boldsymbol{H}^\mathrm{T}. \tag{2.34b}$$

Note that $\boldsymbol{S}_\mathrm{i}$ and $\boldsymbol{S}_\mathrm{a}$ represent, respectively, the isotropic and transversely isotropic contributions to the overall constitutive part of the second Piola-Kirchhoff stress tensor of the solid phase, $\boldsymbol{S}$.

In spite of the fact that both the elastic and the hydraulic response of the tissue are transversely isotropic, we consider the same remodelling law as in the Model M1. Hence, we set

$$\mathrm{sym}(\boldsymbol{\Lambda}_\mathrm{p}\boldsymbol{C}^{-1}) = -\boldsymbol{\mathcal{R}}_{(2)} = -\zeta\,\mathbb{L} : \boldsymbol{Y}, \tag{2.35}$$

where $\boldsymbol{Y}$ splits additively as $\boldsymbol{Y} = \boldsymbol{CSC} = \boldsymbol{CS}_{\mathrm{i}}\boldsymbol{C} + \boldsymbol{CS}_{\mathrm{a}}\boldsymbol{C}$. Analogously to the Model M1, also in this case the remodelling law can be written as

$$\mathrm{sym}(\boldsymbol{\Lambda}_{\mathrm{p}}\boldsymbol{C}^{-1}) = -\boldsymbol{\mathcal{R}}_{(2)} = -\zeta\left[\tilde{\boldsymbol{S}}_{\mathrm{i}} + \tilde{\boldsymbol{S}}_{\mathrm{a}}\right], \tag{2.36}$$

with

$$\tilde{\boldsymbol{S}}_{\mathrm{i}} = \mathbb{M}^* : \boldsymbol{S}_{\mathrm{i}} = \boldsymbol{S}_{\mathrm{i}} - \tfrac{1}{3}\mathrm{tr}(\boldsymbol{CS}_{\mathrm{i}})\boldsymbol{C}^{-1}, \tag{2.37a}$$

$$\tilde{\boldsymbol{S}}_{\mathrm{a}} = \mathbb{M}^* : \boldsymbol{S}_{\mathrm{a}} = \boldsymbol{S}_{\mathrm{a}} - \tfrac{1}{3}\mathrm{tr}(\boldsymbol{CS}_{\mathrm{a}})\boldsymbol{C}^{-1} \tag{2.37b}$$

being the deviatoric parts of $\boldsymbol{S}_{\mathrm{i}}$ and $\boldsymbol{S}_{\mathrm{a}}$, respectively, with respect to the deformed metric $\boldsymbol{C}$. We remark that, according to (2.36), the presence of the fibres supplies a direct contribution to the remodelling law through $\tilde{\boldsymbol{S}}_{\mathrm{a}}$.

Remark 2.3.1. Each remodelling law, i.e., (2.31) or (2.35), is in general equivalent to a set of six scalar differential equations in the components of $\boldsymbol{H}$. However, when the isochoric condition $J_{\boldsymbol{H}} = 1$ is enforced, as is the case in this work, the number of independent equations is five, because the constraint $\mathrm{tr}(\boldsymbol{\Lambda}_{\mathrm{p}}) = \mathrm{tr}(\dot{\boldsymbol{H}}\boldsymbol{H}^{-1}) = 0$ has to be respected. Since, in general, $\boldsymbol{H}$ possesses nine independent components, which become eight when the isochoric condition $J_{\boldsymbol{H}} = 1$ applies, the remodelling laws are not closed. To obtain the closure, we perform the polar decomposition of $\boldsymbol{H}$, i.e., $\boldsymbol{H} = \boldsymbol{V}.\boldsymbol{R} \equiv \boldsymbol{VGR}$, where $\boldsymbol{R}$ is a rotation tensor and $\boldsymbol{V}$ is a symmetric and positive-definite tensor. In this work, we impose that the rotations associated with remodelling are not allowed, so that only $\boldsymbol{V}$ is unknown. Since it has only six independent components (actually five, because it holds that $J_{\boldsymbol{H}} = \det \boldsymbol{V} = 1$), the remodelling laws become closed. We also notice that the identity $\boldsymbol{\Lambda}_{\mathrm{p}} = \dot{\boldsymbol{H}}\boldsymbol{H}^{-1} = \dot{\boldsymbol{V}}\boldsymbol{V}^{-1}$ holds true.

2.4 Benchmark test and numerical settings

We formulate a finite strain poroplastic problem for a porous medium in which the interstitial fluid obeys Darcy's law and the solid phase exhibits hyperelastic behaviour. Given the reference configuration of the tissue $\mathscr{B} \subset \mathcal{S}$ and the interval of time $\mathcal{I} \subset \mathbb{R}$, find the motion χ, pressure p, and $\boldsymbol{V}$ such that

$$\mathrm{Div}\left(\boldsymbol{K}\,\mathrm{Grad}\,p\right) = \dot{J}, \qquad \text{in } \mathscr{B}\times\mathcal{I}, \tag{2.38a}$$

$$\mathrm{Div}\left(-Jp\,\boldsymbol{g}^{-1}\boldsymbol{F}^{-\mathrm{T}} + \boldsymbol{P}_{\mathrm{sc}}\right) = \boldsymbol{0}, \qquad \text{in } \mathscr{B}\times\mathcal{I}, \tag{2.38b}$$

$$\mathrm{sym}(\boldsymbol{\Lambda}_{\mathrm{p}}\boldsymbol{C}^{-1}) = -\boldsymbol{\mathcal{R}}, \qquad \text{in } \mathscr{B}\times\mathcal{I}, \tag{2.38c}$$

where $\boldsymbol{\mathcal{R}}$ can be equal to $\boldsymbol{\mathcal{R}}_{(1)}$ or $\boldsymbol{\mathcal{R}}_{(2)}$, depending on whether the model M1 or M2 is computed. We emphasise that, by construction, both $\boldsymbol{\mathcal{R}}_{(1)}$ and $\boldsymbol{\mathcal{R}}_{(2)}$ have to be understood as functionals of χ, and $\boldsymbol{V}$, i.e., $\boldsymbol{\mathcal{R}}_{(\alpha)} = \hat{\boldsymbol{\mathcal{R}}}_{(\alpha)}(\chi, \boldsymbol{V})$, for

$\alpha \in \{1,2\}$. Whereas (2.38c) expresses the general form of the investigated remodelling law, (2.38a) and (2.38b) represent, respectively, the mass balance law and the momentum balance law for the biphasic system with which the tissue is approximated. We recall, indeed, that the tissue is assumed here to consist of a solid phase, which comprises a porous matrix and the reinforcing fibres, and an inviscid interstitial fluid obeying Darcy's law. Equations (2.38a)–(2.38c) are determined under the hypotheses that the mass densities of the solid and the fluid phase are constant (a condition implying the intrinsic incompressibility of both phases), and that all the external body forces —including the inertial ones— as well as all the quantities of order higher than the first in the relative velocity $\boldsymbol{v}_{\mathrm{fs}} := \boldsymbol{v}_{\mathrm{f}} - \boldsymbol{v}_{\mathrm{s}}$ are negligible. More specifically, the mass balance law (2.38a) implies that the opposite of the divergence of the specific (material) mass flux $\boldsymbol{Q} = -\boldsymbol{K}\,\mathrm{Grad}\, p$ is compensated for by the time derivative of the volume ratio J. Furthermore, the momentum balance law (2.38b) defines the overall stress tensor of the biphasic system under study as $\boldsymbol{P}_{\mathrm{tot}} = -Jp\,\boldsymbol{g}^{-1}\boldsymbol{F}^{-\mathrm{T}} + \boldsymbol{P}_{\mathrm{sc}}$, where the pressure p is the Lagrange multiplier associated with the incompressibility and the saturation constraints.

The logical steps leading to (2.38a) and (2.38b) have been presented elsewhere (cf. e.g. [115, 80, 225, 109, 116, 112, 40, 111]), and will not be repeated here. In addition to them, the remodelling law (2.38c) supplies a further coupling among deformation, pressure, and plastic-like distortions.

Equations (2.38a)–(2.38c) shall be solved for simulating an *unconfined compression test* of the sample under study. This test represents a typical benchmark problem for investigating the elastic and hydraulic properties of biological tissues (cf. (2.38a) and (2.38b), respectively), and has been adapted here in order to also account for the reorganisation of the sample's internal structure (cf. (2.38c)). In the experiment simulated in this work, a specimen of tissue of cylindrical shape is positioned between two rigid, parallel plates, and compressed. The two plates are impermeable to the fluid flow. The compression takes place in displacement control and, in particular, by displacing the upper plate according to a given loading ramp. The lower plate is instead kept fixed, and the specimen is clamped on it. The upper plate constitutes a frictionless glide surface for the specimen, whose upper boundary is thus allowed to deform radially in axial-symmetric way. The lateral boundary is assumed to be free of contact forces, thereby requiring that both the pressure and the radial component of the overall stress vanish on it (see (2.39b)).

By introducing a reference frame with origin O coinciding with the centre of the lower boundary of the sample, and orthonormal Cartesian basis vectors $\{\Xi_I\}_{I=1}^{3}$ emanating from O, such that Ξ_3 is the unit vector directed along the specimen's symmetry axis, the experiment described above is represented by the boundary conditions [40, 108]:

$$\begin{cases} \chi^3 = f \\ (-\boldsymbol{K}\,\mathrm{Grad}\, p).\boldsymbol{N} = 0 \end{cases} \qquad \text{on } \partial\mathscr{B}^{(u)}, \tag{2.39a}$$

$$\begin{cases} (-Jp\boldsymbol{g}^{-1}\boldsymbol{F}^{-\mathrm{T}} + \boldsymbol{P}_{\mathrm{sc}}).\boldsymbol{N} = 0 \\ p = 0 \end{cases} \qquad \text{on } \partial\mathscr{B}^{(l)}, \tag{2.39b}$$

$$\begin{cases} \chi(X,t) - \chi(X,0) = \boldsymbol{0} \\ (-\boldsymbol{K}\,\mathrm{Grad}\, p).\boldsymbol{N} = 0 \end{cases} \qquad \text{on } \partial\mathscr{B}^{(L)}. \tag{2.39c}$$

In (2.39a), χ^3 is the axial component of the motion, and f is the loading ramp

$$f(t) = \begin{cases} L - \frac{t}{T_{\mathrm{ramp}}} u_{\mathrm{T}}, & \text{for } t \in [0, T_{\mathrm{ramp}}], \\ L - u_{\mathrm{T}}, & \text{for } t \in]T_{\mathrm{ramp}}, T_{\mathrm{end}}], \end{cases} \tag{2.40}$$

where $u_{\mathrm{T}} = 0.20$ mm is the target displacement imposed to the sample and $L = 1$ mm is the sample's initial length. The initial cross section of the sample has diameter $D = 3$ mm. The target displacement is reached at the end of the loading ramp, i.e., at $T_{\mathrm{ramp}} = 20$ s, and is then kept constant until $T_{\mathrm{end}} = 300$ s. Moreover, in (2.39a)–(2.39c), $\partial\mathscr{B}^{(u)}$, $\partial\mathscr{B}^{(l)}$ and $\partial\mathscr{B}^{(L)}$ are the upper, lateral and lower part of the boundary $\partial\mathscr{B}$, such that $\partial\mathscr{B} = \partial\mathscr{B}^{(u)} \sqcup \partial\mathscr{B}^{(l)} \sqcup \partial\mathscr{B}^{(L)}$. Finally, $\boldsymbol{N}$ is the unit vector normal to $\partial\mathscr{B}$.

It is assumed that, at the initial time, the sample finds itself in an undeformed state, with zero pressure, and in the absence of anelastic distortions. These requirements lead to the initial conditions

$$\chi(X,0) = X, \qquad \forall\, X \in \mathscr{B}, \tag{2.41a}$$

$$p(X,0) = 0, \qquad \forall\, X \in \mathscr{B}, \tag{2.41b}$$

$$\boldsymbol{V}(X,0) = \boldsymbol{G}^{-1}(X) \qquad \forall\, X \in \mathscr{B}. \tag{2.41c}$$

The numerical solution of (2.38a)–(2.38c), with (2.41a)–(2.41c) and (2.39a)–(2.39c), is achieved by performing Finite Element simulations. In particular, following [112, 40], (2.38a) and (2.38b) are put in weak form, and solved according to a given Finite Element scheme, while (2.38c) is solved only at the integration points of the finite elements. To this end, by searching for the motion χ and pressure p in the Sobolev spaces $(H^1(\mathscr{B} \times \mathcal{I}, \mathcal{S}))^3$ and $H^1(\mathscr{B} \times \mathcal{I}, \mathcal{S})$, respectively, and enforcing the boundary conditions (2.39a)–(2.39c), the model equations (2.38a)–(2.38c) are reformulated as

$$\mathcal{F}_\chi = \hat{\mathcal{F}}_\chi(\chi, p, \boldsymbol{V}) = \int_{\mathscr{B}} \hat{\boldsymbol{P}}(\chi, p, \boldsymbol{V}) : \boldsymbol{g}\,\mathrm{Grad}\; \tilde{\boldsymbol{u}} = 0, \tag{2.42a}$$

$$\mathcal{F}_p = \hat{\mathcal{F}}_p(\chi, p, \boldsymbol{V}) = \int_{\mathscr{B}} \left\{ (\mathrm{Grad}\; \tilde{p}) \hat{\boldsymbol{K}}(\chi, \boldsymbol{V}) (\mathrm{Grad}\, p) + \tilde{p}\dot{J} \right\} = 0, \tag{2.42b}$$

$$\boldsymbol{\mathcal{F}}_V = \hat{\boldsymbol{\mathcal{F}}}_V(\chi, \boldsymbol{V}) = \mathrm{sym}(\dot{\boldsymbol{V}}\boldsymbol{V}^{-1}) + \hat{\boldsymbol{\mathcal{R}}}(\chi, \boldsymbol{V}) = \boldsymbol{0}, \tag{2.42c}$$

where $\tilde{\boldsymbol{u}}$ and $\tilde{p}$ are the test functions associated with the velocity and pressure and are sometimes referred to as "virtual velocity" and "virtual pressure", respectively. We notice that the functionals $\hat{\mathcal{F}}_\chi$ and $\hat{\mathcal{F}}_p$ depend linearly on the virtual fields $\tilde{\boldsymbol{u}}$ and $\tilde{p}$. However, for the sake of a lighter notation, we have omitted this dependence in their definitions.

2.5 Results

In this section, we present and discuss the main results of our simulations (see Figures 2.1–2.5). In particular, we show (i) how remodelling modulates the mechanical and hydraulic response of the tissue, and (ii) how the fibre reinforcement, which makes the tissue transversely isotropic, influences the evolution of the anelastic distortions. To highlight the consequences of remodelling, we run a set of simulations in which remodelling is switched off, and we compare the corresponding results with those stemming from the set of simulations in which the models M1 and M2 are implemented. Moreover, in order to see the role played by the fibre reinforcement, we compare the results predicted by the model M1, in which an ideal isotropic tissue without fibres is simulated, with those predicted by the model M2, in which the presence of the fibres is accounted for. In all the plots (Figures 2.1–2.5), we evaluate the physical quantity of interest at the point X_{U} of Cartesian coordinates given by (1.3,0.0,1.0) [mm], which is on the upper boundary and close to the lateral boundary of the sample. In Figure 2.1a, we report the time trend of the magnitude of the (spatial) filtration velocity, $\|\boldsymbol{q}(X_{\mathrm{U}},t)\|$, evaluated at the point X_{U} for $t \in [0, T_{\mathrm{end}}[$, where we let T_{end} be arbitrarily greater than T_{ramp}. We show both the case of no remodelling and the case of remodelling, as described by the models M1 and M2. In the absence of remodelling, the magnitude of the filtration velocity grows monotonically until the target displacement is reached, i.e., until $t = T_{\mathrm{ramp}}$. Then, it relaxes asymptotically towards zero for increasing time. When remodelling occurs, the trend of $\|\boldsymbol{q}(X_{\mathrm{U}},t)\|$ depends on whether or not the fibres are accounted for. In the simulation performed by applying the model M1, the influence of remodelling on $\|\boldsymbol{q}(X_{\mathrm{U}},t)\|_{\mathrm{M1}}$ is twofold: on the one hand, it lowers considerably the maximum value of $\|\boldsymbol{q}(X_{\mathrm{U}},t)\|$, which is however attained at $t = T_{\mathrm{ramp}}$, and, on the other hand, it leads to a much slower relaxation time. Hence, even though $\|\boldsymbol{q}(X_{\mathrm{U}},t)\|_{\mathrm{M1}}$ decreases monotonically towards zero, the curve associated with M1 intersects the curve of no remodelling, and it holds that

$$\|\boldsymbol{q}(X_{\mathrm{U}},t)\|_{\mathrm{M1}} \geq \|\boldsymbol{q}(X_{\mathrm{U}},t)\|_{\text{no-rem}}, \tag{2.43}$$

for all $t \geq T_1$, with $T_1 > T_{\mathrm{ramp}}$ being the time at which the two curves intersect each other. The simulation performed considering the model M2 leads, instead, to quite different results. First of all, the maximum value of $\|\boldsymbol{q}(X_{\mathrm{U}},t)\|_{\mathrm{M2}}$, always attained at $T = T_{\mathrm{ramp}}$, is smaller than the one reached in the case of no remodelling and bigger than the one predicted by M1. Moreover, the relaxation of $\|\boldsymbol{q}(X_{\mathrm{U}},t)\|_{\mathrm{M2}}$ towards zero is slower than that observed in the case of no remodelling, but slightly faster than the one obtained by employing the model M1. The most noticeable results, however, are given by the loss of monotonicity of $\|\boldsymbol{q}(X_{\mathrm{U}},t)\|_{\mathrm{M2}}$ in the interval $[T_{\mathrm{ramp}}, T_{\mathrm{end}}[$, and by the presence of the point of non-differentiability, hereafter denoted by T_{c}, between T_{ramp} and $t = 50\,\mathrm{s}$. This behaviour is due to the fact that, when remodelling occurs and the anisotropy of the fibre pattern is considered, the

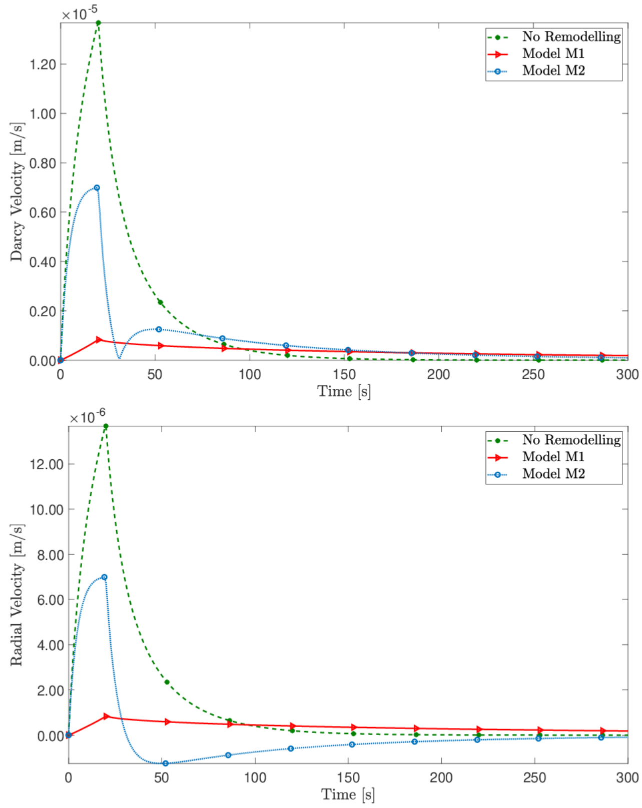

Figure 2.1: Norm of Darcy velocity vs time **(a)** and radial component of Darcy velocity vs time **(b)**, evaluated at the point X_{U} of Cartesian coordinates (1.3,0.0,1.0) [mm]. The anisotropic model predicts an inversion of the filtration velocity, which yields thus an inflow of fluid after a critical instant of time is reached. This behaviour is not captured by the isotropic model M1.

radial component of the filtration velocity decreases for $t > T_{\mathrm{ramp}}$, becomes negative until it attains a global minimum and, subsequently, it grows asymptotically towards zero for a sufficiently long time (see Figure 2.1b). The above discussion contributes to answer the research questions 2.2 and 2.3.

The change of sign in the radial velocity may be interpreted as a “syringe effect”, thereby meaning that, for $t > T_{\mathrm{c}}$, the fluid tends to flow back into the tissue. Since the fluid filtration velocity complies with Darcy’s law, this behaviour is accompanied by a change of sign of the radial pressure gradient, which implies that the pressure at X_{U} becomes smaller than zero for $t > T_{\mathrm{c}}$ (we recall, indeed, that our boundary conditions prescribe that, on the lateral boundary of the sample, the pressure is zero at all times). This observation seems to be supported by the results shown in Figure 2.2. In the absence of remodelling, pressure grows until a global maximum is reached, and it relaxes then towards zero for increasing time. A qualitatively similar trend is also observed when remodelling is switched on and the model M1 is used,

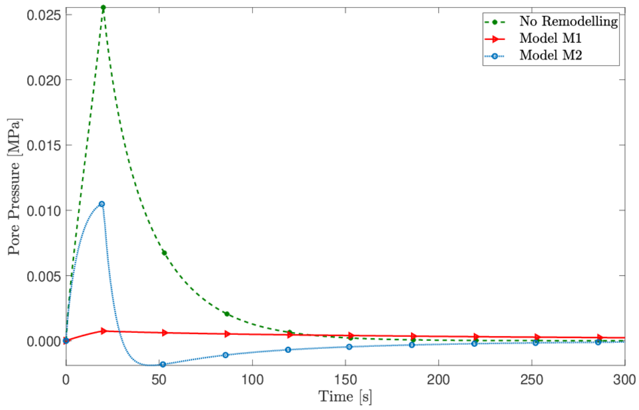

Figure 2.2: Pressure vs time, $p(X_{\mathrm{U}}, t)$, evaluated at the point X_{U} of Cartesian coordinates (1.3,0.0,1.0) [mm]. The isotropic model M1 predicts a dramatic decrease of pressure due to the progression of remodelling. In the case of the model M2, instead, the interplay between the evolution of the plastic distortions and the tissue's anisotropy contains the pressure fall and induces a loss of monotonicity in the time trend. This is consistent with the inversion of the filtration velocity observed in Figure 2.1.

even though the maximum value of pressure is much smaller than the one obtained in the case of no remodelling. The model M1 predicts, indeed, that $[p(X_{\mathrm{U}}, t)]_{\mathrm{M1}}$ consists of two monotonic branches, one increasing over the interval $[0, T_{\mathrm{ramp}}]$ and the other one decreasing over $[T_{\mathrm{ramp}}, T_{\mathrm{end}}[$. The decreasing branch intersects the relaxing branch of the pressure curve of no remodelling and tends towards zero more slowly than the latter one. The curve determined by simulating the model M2 grows rather steeply until the maximum pressure is attained, and this maximum places itself in between the values obtained in the case of no remodelling and that of model M1, respectively. Then, $[p(X_{\mathrm{U}}, t)]_{\mathrm{M2}}$ decreases much faster than it happens in the other cases, becomes negative, and reaches a global minimum. Afterwards it grows again, and it then tends to zero from below at a rate comparable with that of no remodelling. We remark that the instant of time at which pressure equals zero coincides with T_{c}, i.e., the time at which the radial component of the filtration velocity changes its sign.The above discussion contributes to answer the research questions 2.1, 2.2 and 2.3.

In Figure 2.3, we study the time trend of porosity at X_{U}. We notice that, both in the case of no remodelling and in the case of the model M1, porosity decreases monotonically in time. In the absence of remodelling, porosity varies very smoothly, and the amplitude of the variation between its initial and asymptotic values is bigger than in the other case. The model M1, in turn, predicts a rather pronounced change of slope of the porosity curve, and the asymptotic value of porosity is reached more slowly. A quite different behaviour can be observed when the tissue's anisotropy

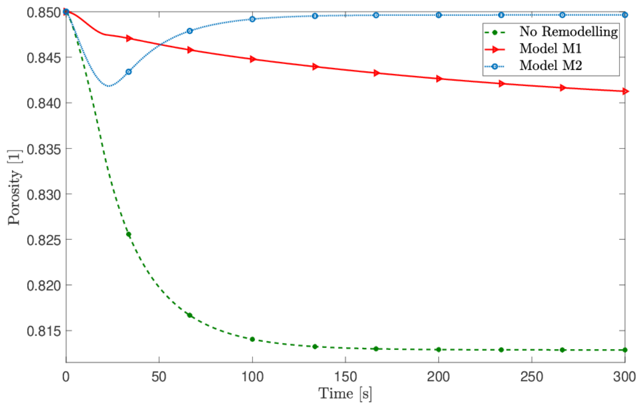

Figure 2.3: Porosity vs time, $1 - \Phi_{s\nu}(X_U)/J(X_U, t)$, evaluated at the point X_U of Cartesian coordinates (1.3,0.0,1.0) [mm]. Whereas the case of no remodelling and the model M1 predict quantitatively different, but qualitatively similar, results, the model M2 is characterised by a trend that is both quantitatively and qualitatively different from the other two. The loss of monotonicity is, in fact, consistent with that of Figures 2.1 and 2.2, and represents an opening of the tissue's pores (with corresponding increase of porosity) on the way towards the stationary state.

is accounted for. Indeed, in accordance with the inversion of the fluid filtration velocity (see Figure 2.1) and the change of sign of the pressure (see Figure 2.2), the model M2 prescribes that porosity varies in time in a non-monotonic way. More specifically, it decreases until it comes to a global minimum, which corresponds to the end of the loading ramp, and then it grows towards a stationary value. This behaviour is consistent with the fact that, to permit the inflow of fluid, the tissue must increase its porosity, and it seems to be a consequence of the interplay between the tissue's anisotropy and the evolution of the anelastic distortions. The above discussion contributes to answer the research question 2.3.

In terms of $\boldsymbol{F}_{\rm p}$, a measure of the magnitude of plastic-like distortions is the Frobenius norm of the anelastic strain tensor

$$\boldsymbol{E}_{\rm p} = \tfrac{1}{2}\left[\boldsymbol{F}_{\rm p}^{\rm T}.\boldsymbol{F}_{\rm p} - \boldsymbol{G}\right]. \tag{2.44}$$

Since it holds that $\boldsymbol{F}_{\rm p}$ is the inverse of $\boldsymbol{H}$, $\boldsymbol{E}_{\rm p}$ may be rewritten as

$$\boldsymbol{E}_{\rm p} = \tfrac{1}{2}[\boldsymbol{H}^{-\rm T}.\boldsymbol{H}^{-1} - \boldsymbol{G}] = -\boldsymbol{\mathcal{A}}_{\boldsymbol{H}}, \tag{2.45}$$

where $\boldsymbol{\mathcal{A}}_{\boldsymbol{H}}$ is the Almansi-Euler-like strain tensor associated with $\boldsymbol{H}$. Finally, by enforcing the polar decomposition $\boldsymbol{H} = \boldsymbol{V}.\boldsymbol{R}$, $\boldsymbol{E}_{\rm p}$ becomes

$$\boldsymbol{E}_{\rm p} = \tfrac{1}{2}[\boldsymbol{V}^{-1}.\boldsymbol{V}^{-1} - \boldsymbol{G}]. \tag{2.46}$$

Equation (2.45) suggests which tensor field should be used to address remodelling within the theory of uniformity [70, 169, 53, 197].

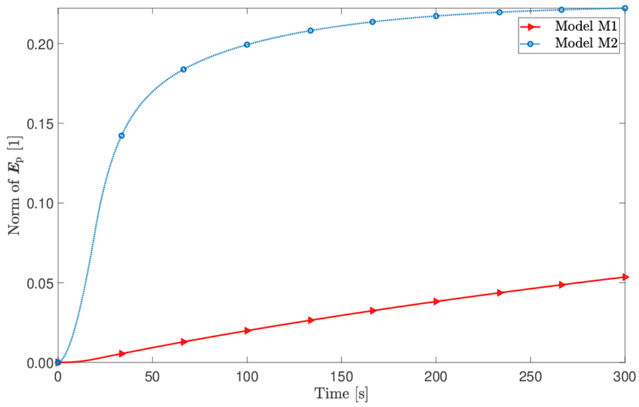

Figure 2.4: Frobenius norm of $\boldsymbol{E}_{\mathrm{p}} = \frac{1}{2}[\boldsymbol{V}^{-1}.\boldsymbol{V}^{-1} - \boldsymbol{G}]$ vs time, $\|\boldsymbol{E}_{\mathrm{p}}(X_{\mathrm{U}}, t)\|$, evaluated at the point X_{U} of Cartesian coordinates (1.3,0.0,1.0) [mm]. The magnitude of the plastic strains is bigger in the transversely isotropic model M2. In the isotropic model M1, instead, the plastic strains are rather small, but they tend to the stationary state much more slowly than predicted by the model M2.

The Frobenius norm of $\boldsymbol{E}_{\mathrm{p}}$ is now evaluated at X_{U} and its variation in time is reported in Figure 2.4. We notice that the magnitude of the anelastic distortions as predicted by the model M2 is much bigger than that obtained by the model M1. Thus, the anisotropy of the tissue seems to enhance the growth of the plastic distortions, whose magnitude increases quite rapidly and tends to approach a stationary value. In the case of the model M1, instead, $\|\boldsymbol{E}_{\mathrm{p}}(X_{\mathrm{U}}, t)\|$ grows much more slowly (and almost linearly) towards a stationary value. The above discussion contribute to answer the research questions 2.2 and 2.3.

Finally, we investigate how the onset of plastic distortions modulates the stress borne by the tissue. To this end, we plot in Figure 2.5 the von Mises equivalent stress at X_{U}, and we notice that the curve corresponding to the model M1 is, until about 200 s, bounded from above by the curve pertaining to the model M2. This means that, even though the plastic distortions are characterised by a magnitude of $\boldsymbol{E}_{\mathrm{p}}$ that is bigger in the anisotropic case than in the isotropic one, the level of stress reached in the first case is higher. We remark that the onset of remodelling occurs only when the von Mises equivalent stress, $\|\mathrm{dev}\boldsymbol{\sigma}\|$, overcomes the yield stress, σ_Y. In fact, there exists an instant of time such that the condition of incipient remodelling, i.e., $\|\mathrm{dev}\boldsymbol{\sigma}\| = \sigma_Y$, is verified, and the von Mises equivalent stress is bigger than σ_Y for all subsequent times. To highlight this behaviour, we plotted in Figure 2.5 the yield stress (which is constant in time in this work), and we showed that, in all the considered cases, the von Mises equivalent stress exceeds the yield stress after a quite short interval of time.The above discussion contributes to answer the research questions 2.1, 2.2 and 2.3.

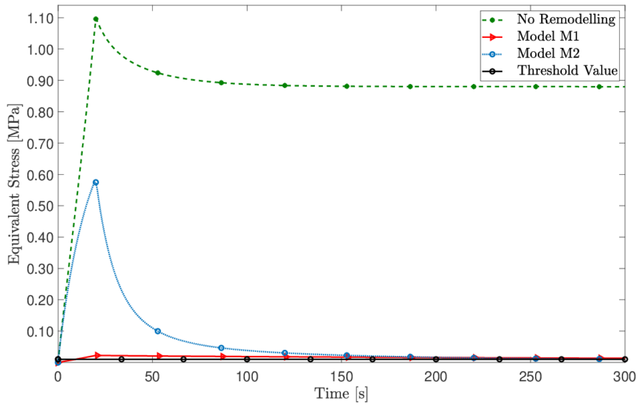

Figure 2.5: Equivalent stress vs time, evaluated at the point X_{U} of Cartesian coordinates (1.3,0.0,1.0) [mm]. The equivalent stress is the Frobenius norm of the deviatoric part of the constitutive Cauchy stress tensor, i.e., $\|\mathrm{dev}\boldsymbol{\sigma}\|$, with $\boldsymbol{\sigma} = J^{-1}\boldsymbol{F}\boldsymbol{S}\boldsymbol{F}^{\mathrm{T}}$. The 2nd Piola-Kirchhoff stress tensor $\boldsymbol{S}$ is given by (2.30) for the model M1, and by (2.33) both for the model M2 and for the case of no remodelling (in which, however, the identity $\boldsymbol{V} = \boldsymbol{G}^{-1}$ applies).

2.6 Conclusions

In this work, we employed an inhomogeneous and transversely isotropic poroplastic model of fibre-reinforced biological tissue in order to study how the variation of the tissue's internal structure (i.e., the process of remodelling), which manifests itself through the onset and evolution of anelastic distortions, is influenced by the material symmetries of the tissue itself.

For our purposes, we rephrased the poroelastic model of hydrated, fibre-reinforced tissues summarised in [80, 225] in order to account for the presence of anelastic distortions (the definition of the hyperelastic strain energy energy is developed from [84, 80] and the tissue's permeability has been adapted from [83, 82, 80, 225]). Then, we formulated and solved numerically the two different descriptions of structural remodelling denoted by model M1 and model M2. We recall that, while the tissue has been simulated as inhomogeneous and transversely isotropic both in the case of the model M2 and in the reference case of no remodelling, it has been regarded as inhomogeneous but isotropic in the model M1. We emphasise that this idealisation serves as a basis for comparison with the transversely isotropic model M2, and has been done to highlight the interplay between the tissue's material symmetries and the development of plastic distortions. These, indeed, drive an evolution of the group of material symmetries, but they do not change it (see [68, 69] for further details).

Among the obtained results, represented graphically in Figures 2.1–2.5, we give prominence to the "syringe effect" discussed in Section 2.5, which is observed in our simulations only when remodelling occurs in the tissue modelled as an inhomogeneous and transversely isotropic material (cf. model M2). Such effect seems to be an evidence of the change of the tissue's mechanical and hydraulic behaviour. Such alteration of material response could characterise a diseased or damaged tissue, and could thus also provide some indications on how the tissue might behave in non-physiological conditions.

Finally, since the observed changes of material behaviour occur both qualitatively and quantitatively in the case of anisotropy (while the change is only quantitative in the case of isotropy), our results could be used for studying the interplay between growth and remodelling in anisotropic tissues. For example, this could be of interest for elaborating more detailed and more accurate models of tumour growth, in which the onset of remodelling has appreciable consequences on the tumour evolution [167, 166].

In summary, the research questions 2.1—2.3 have been answered in the following way:

- The "syringe effect", discussed in Section 2.5, is observed in our simulations only when remodelling occurs in the tissue described as inhomogeneous and transversely isotropic material. We, thus, conclude that this behaviour is an output of the interplay between anelasticity and anisotropy.

- The observed changes of the material behaviour occur both qualitatively and quantitatively in the case of anisotropy, while the change is only quantitative in the case of isotropy.

- Changes of the tissue's mechanical properties manifest themselves through stress relaxation, loss of monotonicity in the temporal evolution of the porosity and through the production of plastic-like distortions, whereas the changes of the tissue's hydraulic properties involve the filtration velocity and the pressure distribution in time and space.

Chapter 3

Structural reorganisation and fibre reorientation in fibre-reinforced biological tissues

The work reported in this chapter has been previously published in [56].

3.1 Introduction

We highlight some mechanical aspects of the coupling among deformation, fluid flow, structural evolution, and reorientation of fibres in fibre-reinforced, hydrated, soft biological tissues. For our purposes, we elaborate a model in which the tissue's interstitial fluid is inviscid and obeys Darcy's law, and the solid constituents are transversely isotropic, hyperelastic materials. Within this setting, we consider two different types of remodelling: One consists of the reorientation of the fibres, while the other one is the manifestation, at the tissue scale, of structural rearrangements representable in terms of inelastic distortions. Our focus is on the interplay between the latter ones and the fibre reorientation. In our model, such interplay is a consequence of the constitutive framework, which resolves explicitly the space variability of a parameter, the "fibre mean angle", that determines the direction along which the fibres tend to align themselves. Our main results concern the description of a Mandel-like stress tensor, which drives the inelastic distortions when the fibre mean angle is distributed inhomogeneously throughout the tissue, and of a diffusion-like tensor depending on the inelastic distortions, which guides the evolution of the fibre mean angle.

With these motivations, we propose to improve and extend the model presented in [108], where the reorientation of fibres was studied in a transversely isotropic fibre-reinforced tissue, with fibres aligned according to a prescribed probability density. Such probability density was parametrised by an angle denominated "fibre mean angle" and determining, at each material point, the direction of the most probable fibre alignment.

In the present work, there are three relevant differences with respect to [108]. The *first* and major difference is that we now account for plastic-like distortions and study their influence on the reorientation of the collagen fibres by adhering to the formalism introduced in [61]. Plastic-like distortions are meant to describe the onset and progression of irreversible strains in the tissue, which may arise in response to diseases or injuries [97], or the reorganisation of the tissue's extracellular matrix, as is the case for cellular aggregates and tumour spheroids [198, 104, 112]. In the literature, the concept of inelastic distortions is often related to that of residual stresses, an issue typically investigated with the aid of the Bilby-Kröner-Lee decomposition of the deformation gradient tensor. A rather different point view, however, has been recently proposed in [175], where a study on the impact of residual stresses on the mechanical behaviour of tissues is presented. The *second* difference is related to the rationale with which the concept of *target angle* is accounted for. We recall that the "target angle" is a preferred angle that, depending on the deformation or stress state in the tissue, contributes to direct the evolution of the fibre mean angle. In fact, it can be thought of as the generator of an external force that drives the fibre mean angle towards the value determined by the interactions of the fibres with the environment in which they are embedded. After mentioning the approaches proposed, for example, in [64, 21, 127, 183], we select for our purposes a modification of the target angle put forward in [64]. The *third* difference is a re-definition of the constitutive framework and, in particular, of the free energy density of the Allen-Cahn type [108], which models the reorientation of the fibres and constituted the crux of [108].

The most significant contribution of our work is the enrichment of the constitutive framework through the definition of two "non-standard" terms in the total free energy density of the system, W_ν. One of these terms, denoted by W_{Grad}, is said to be the "gradient part" of W_ν since it features the material gradient of the fibre mean angle, $\mathfrak{q}$. The energy density W_{Grad} keeps track, already at the constitutive level, of the *explicit* dependence of $\mathfrak{q}$ on material points [108]. Thus, such dependence is not inherited from the quantities involved in the evolution equation of $\mathfrak{q}$. Rather, it is accounted for *a priori* by enrolling $\mathrm{Grad}\mathfrak{q}$ among the constitutive arguments of W_ν. This gives rise to a generalised force that, by embodying the inhomogeneity of $\mathfrak{q}$, contributes to drive the evolution of $\mathfrak{q}$ itself. As a consequence, the coupling of $\mathfrak{q}$ with the dynamics of the plastic-like distortions introduce a novelty with respect to [108].

The other non-standard term in W_ν is referred to as the "structural part" and is denoted by W_{str}. In our view, it represents the potential energy that pertains to a given distribution of $\mathfrak{q}$, and its existence is postulated *a priori*, regardless of the fact that the tissue is deformed elastically or distorted inelastically. In fact, W_{str} can be non trivial also in the absence of deformation and plastic-like distortions, although we do allow for its coupling with these kinematic variables. The way in which this is done here is another novelty of our work, for we strongly modify the coupling previously defined in [108]. Moreover, we compare our concept of structural energy with the one introduced in [21], within a setting rather different from ours.

The proposed constitutive framework leads to the key point of this work: The coupling among the kinematic variables is such that the dynamics of the system can be depicted as a "game among three players", i.e., the motion, the plastic-like distortions, and the fibre mean angle.

In our model, plastic-like distortions are assumed to be set off, for instance, when the tissue undergoes irreversible strains [97], when the cells of the tissue redistribute their adhesion bonds, or when the tissue's extracellular matrix rearranges the cross-links forming its structure [112]. In these cases, the solid constituent of the tissue experiences transformations that cannot be described in terms of shape changes, and that necessitate, thus, new descriptors. As suggested in [60], such descriptors should be regarded as independent kinematic variables that represent the structural degrees of freedom of the tissue. Within this picture, and by regarding the tissue as a deformable porous medium permeated by an interstitial fluid, our goal is to describe the interactions among deformation, fluid flow, and the aforementioned structural changes, emphasising the coupling between the plastic-like distortions and the fibre reorientation.

3.2 Dynamical equations

According to the mathematical model presented in Chapter 2, also in this case the flow of the fluid and the deformation of the considered tissue are accounted for by the mass balance law and the linear momentum balance law for the tissue as a whole, i.e.,

$$\dot{J} = \mathrm{Div}\,[\boldsymbol{K}\,\mathrm{Grad}\,p]\,, \qquad \text{in } \mathscr{B}\times\mathscr{I}, \tag{3.1a}$$

$$\mathrm{Div}\left[-Jp\,\boldsymbol{g}^{-1}\boldsymbol{F}^{-\mathrm{T}} + \boldsymbol{P}_{\mathrm{sc}}\right] = \boldsymbol{0}, \qquad \text{in } \mathscr{B}\times\mathscr{I}. \tag{3.1b}$$

We first consider the reorganisation of the tissue due to the production of inelastic distortions. Then, in accordance with [60], we introduce a set of generalised forces dual of the virtual velocity associated with $\boldsymbol{F}_{\mathrm{p}}$, and we distinguish between the internal and the external forces of this kind, denoted by $\boldsymbol{Y}_\nu^{\mathrm{int}}$ and $\boldsymbol{Y}_\nu^{\mathrm{ext}}$, respectively. Hence, by invoking the Principle of Virtual Powers, we obtain the force balance [60]

$$\boldsymbol{Y}_\nu^{\mathrm{int}} = \boldsymbol{Y}_\nu^{\mathrm{ext}}, \quad \text{in } \mathscr{B}\times\mathscr{I}, \tag{3.2}$$

where the subscript "ν" means that $\boldsymbol{Y}_\nu^{\mathrm{int}}$ and $\boldsymbol{Y}_\nu^{\mathrm{ext}}$ are defined with respect to the natural state of the tissue [44]. Finally, using the jargon of [60], we remark that

Eq. (3.2) is consistent with a "*grade zero*" theory, in which no gradient of $\boldsymbol{F}_{\mathrm{p}}$ is accounted for.

We now turn to the reorientation of the reinforcing fibres. As reported in [21, 108, 116], the alignment of the fibres in the tissue is governed by a probability density that depends on a given set of scalar parameters. The variation of these parameters is responsible for the reorientation of the fibres. In our model, we select one parameter only, which we indicate with $\mathfrak{q}$ and employ to describe the kinematics of the fibres. In particular, $\mathfrak{q}$ acquires the meaning of "fibre mean angle". Analogously to the reasoning that has led us to (3.2), we consider both internal and external generalised forces dual of the (scalar) virtual velocity $\mathfrak{v}$ associated with $\mathfrak{q}$. In this case, however, since we aim at resolving explicitly the point dependence of $\mathfrak{q}$, we also need to account for the kinematic descriptor $\mathrm{Grad}\,\mathfrak{q}$, along with its virtual counterpart $\mathrm{Grad}\,\mathfrak{v}$. Then, by employing again the Principle of Virtual Powers, and restricting it for brevity only to the sub-problem of the fibre reorientation, we find

$$\int_{\mathscr{B}} \left\{ y^{(0)}\mathfrak{v} + \boldsymbol{y}^{(1)}\,\mathrm{Grad}\mathfrak{v} \right\} = \int_{\mathscr{B}} h^{(0)}\mathfrak{v} + \int_{\partial\mathscr{B}_N} h^{(1)}\,\mathfrak{v}, \tag{3.3}$$

where $y^{(0)}$ and $\boldsymbol{y}^{(1)}$ are a scalar and a vector-like internal force, defined as the dual entities of $\mathfrak{v}$ and $\mathrm{Grad}\mathfrak{v}$, respectively, $h^{(0)}$ is an external force, $h^{(1)}$ is an external contact force, $\partial\mathscr{B}_N$ is the Neumann boundary of $\partial\mathscr{B}$, and the virtual velocity $\mathfrak{v}$ is assumed to vanish identically on the Dirichlet portion of $\partial\mathscr{B}$, i.e., on $\partial\mathscr{B}_D = \partial\mathscr{B}\backslash\partial\mathscr{B}_N$. Equation (3.3) leads to the balance laws

$$y^{(0)} - \mathrm{Div}\,\boldsymbol{y}^{(1)} = h^{(0)}, \qquad \text{in } \mathscr{B}\times\mathscr{I}, \tag{3.4a}$$

$$\boldsymbol{y}^{(1)}.\boldsymbol{N} = h^{(1)}, \qquad \text{on } \partial\mathscr{B}_N\times\mathscr{I}. \tag{3.4b}$$

Upon setting, in the case of isochoric plastic-like distortions,

$$\mathscr{R}_\nu^{\mathrm{ext}} \equiv h^{(0)}, \tag{3.5a}$$

$$\mathscr{R}_\nu^{\mathrm{int}} \equiv y^{(0)} - \mathrm{Div}\,\boldsymbol{y}^{(1)}, \tag{3.5b}$$

we can rephrase (3.4a) as

$$\mathscr{R}_\nu^{\mathrm{int}} = \mathscr{R}_\nu^{\mathrm{ext}}, \quad \text{in } \mathscr{B}\times\mathscr{I}, \tag{3.6}$$

thereby generalising the results in [183, 116].

Equations (3.1a), (3.1b), (3.2), reformulated for the case of isochoric plastic-like distortions, and (3.6) describe the dynamics of the system under study. Their solution determines the model unknowns, identified with p, χ, $\boldsymbol{F}_{\mathrm{p}}$, and $\mathfrak{q}$. Among those, a *true* configuration of the solid is obtained by specifying the triple of descriptors $(\chi, \boldsymbol{F}_{\mathrm{p}}, \mathfrak{q})$. In the sequel, we refer to $\mathfrak{q}$ and $\boldsymbol{F}_{\mathrm{p}}$ as to *remodelling variables*, and to $\boldsymbol{Y}_\nu^{\mathrm{int}}$, $\boldsymbol{Y}_\nu^{\mathrm{ext}}$, $\mathscr{R}_\nu^{\mathrm{int}}$, and $\mathscr{R}_\nu^{\mathrm{ext}}$ as to generalised *remodelling forces*.

3.3 Constitutive laws

To constitutively characterise the fibre-reinforced medium under study, we assign a free energy density consisting of two terms, both of which are written per unit volume of the material in its natural state, i.e. [108],

$$W_\nu = W_{\mathrm{std}} + W_{\mathrm{rem}}. \tag{3.7}$$

The term W_{std} takes into account the hyperelastic behaviour of the solid material, and relies on a mechanical model of fibre-reinforced media, in which the fibres are oriented statistically [84, 83, 80]. In this respect, we denote the corresponding strain energy density by W_{std}, where the subscript "std" stands for "standard". The other term, W_{rem}, is not standard and it has been introduced in order to specifically account for remodelling [21, 108, 138]. The energy density W_{rem} is assumed to exist independently of deformation and, in fact, it is conceived as the energetic contribution that characterises each possible directional distribution of the fibres in the tissue. For this reason, W_{rem} may be nontrivial also in the undeformed configuration of the tissue [108].

3.3.1 "Standard" Constitutive laws

Following [84, 83, 80, 108, 116], we define W_{std} as a function of $\boldsymbol{C}_{\mathrm{e}}$ and $\mathfrak{q}$, i.e., we set $W_{\mathrm{std}} = \hat{W}_{\mathrm{std}}(\boldsymbol{C}_{\mathrm{e}}, \mathfrak{q})$, with

$$\hat{W}_{\mathrm{std}}(\boldsymbol{C}_{\mathrm{e}}, \mathfrak{q}) = \Phi_{\mathrm{s}\nu}\hat{U}(J_{\mathrm{e}}) + \Phi_{0\mathrm{s}\nu}\hat{W}_0(\boldsymbol{C}_{\mathrm{e}}) + \Phi_{1\mathrm{s}\nu}\left[\hat{W}_{1\mathrm{i}}(\boldsymbol{C}_{\mathrm{e}}) + \hat{W}_{1\mathrm{a}}(\boldsymbol{C}_{\mathrm{e}}, \mathfrak{q})\right]. \tag{3.8}$$

For the expressions of $\Phi_{\mathrm{s}\nu}$, $\Phi_{0\mathrm{s}\nu}$ and $\Phi_{1\mathrm{s}\nu}$, we refer to Eqs. (2.13a)-(2.13c) and Table 3.1. The definitions of the $\hat{U}(J_{\mathrm{e}})$ and $\hat{W}_0(\boldsymbol{C}_{\mathrm{e}})$ are reported in Eqs. (2.4a) and (2.4b), respectively, while $\hat{W}_{1\mathrm{i}}(\boldsymbol{C}_{\mathrm{e}})$ has the same functional form of $\hat{W}_0(\boldsymbol{C}_{\mathrm{e}})$, but with different coefficients. For convenience of the Reader, in Table 3.1 the material parameters involved in (3.8) are reported. The latter term of (3.8), $W_{1\mathrm{a}}$, is defined through the directional average [228, 83, 80, 79, 151, 100]

$$\hat{W}_{1\mathrm{a}}(\boldsymbol{C}_{\mathrm{e}}, \mathfrak{q}) = \left\langle\!\!\left\langle \hat{\mathscr{W}}_{1\mathrm{a}}(\boldsymbol{C}_{\mathrm{e}}, \boldsymbol{\mathfrak{m}}) \right\rangle\!\!\right\rangle(\mathfrak{q}) = \int_{\mathbb{S}^2\mathscr{B}} \hat{\mathscr{W}}_{1\mathrm{a}}(\boldsymbol{C}_{\mathrm{e}}, \boldsymbol{\mathfrak{m}})\Psi(\boldsymbol{\mathfrak{m}}, \mathfrak{q}). \tag{3.9}$$

where $\hat{\mathscr{W}}_{1\mathrm{a}}(\boldsymbol{C}_{\mathrm{e}}, \boldsymbol{\mathfrak{m}})$ is the transversely isotropic strain energy density of a single fibre, and $\boldsymbol{\mathfrak{m}}$ is a field of unit vectors individuating the direction of space along which the fibres are locally oriented.

A possible explicit constitutive expressions $\hat{\mathscr{W}}_{1\mathrm{a}}(\boldsymbol{C}_{\mathrm{e}}, \boldsymbol{\mathfrak{m}})$ is given by [80, 225]

$$\hat{\mathscr{W}}_{1\mathrm{a}}(\boldsymbol{C}_{\mathrm{e}}, \boldsymbol{\mathfrak{m}}) = \check{\mathscr{W}}_{1\mathrm{a}}(I_{4\mathrm{e}}) = \check{\mathscr{V}}_{1\mathrm{a}}(I_{4\mathrm{e}})\mathcal{H}(I_{4\mathrm{e}} - 1), \tag{3.10a}$$

$$\check{\mathscr{V}}_{1\mathrm{a}}(I_{4\mathrm{e}}) = \frac{k_1}{2k_2}\left\{\exp\left(k_2[I_{4\mathrm{e}} - 1]^2\right) - 1\right\}. \tag{3.10b}$$

The constitutive expression of $\check{\mathscr{V}}_{1\mathrm{a}}$ is taken from [183, 139].

Here, the probability density function Ψ is assumed to depend only on the direction of the local fibre orientation and on the remodelling variable, $\mathfrak{q}$. However, in more general contexts, it can depend on several other parameters. It is important to remark that, in this work, it is taken transversely isotropic with respect to a direction $\mathfrak{m}_0$ for the tissue as a whole. To justify this assumption, we consider a specimen of tissue of cylindrical shape, and we assume that the symmetry axis of the cylinder coincides with $\mathfrak{m}_0$.

Symbol	Definition	Units	Symbol	Definition	Units
r	0.50	[—]	$\Phi_{0\mathrm{s}\nu}$	$0.046 + 0.038\xi - 0.062\xi^2$	[—]
q	2.00	[—]	$\Phi_{1\mathrm{s}\nu}$	$0.204 - 0.138\xi + 0.062\xi^2$	[—]
α_0	0.125	[MPa]	Γ	$1 \cdot 10^4$	[Pa s]
$\alpha_1 = \alpha_{\mathrm{i}1}$	0.778	[—]	D_0	$1 \cdot 10^{-4}$	[N(rad)$^{-1}$]
$\alpha_2 = \alpha_{\mathrm{i}2}$	0.111	[—]	ζ_0	0.50	[(MPa s)$^{-1}$]
$\alpha_{\mathrm{i}0}$	7.59	[MPa]	e_ν	$(1 - \Phi_{s\nu})/\Phi_{s\nu}$	[—]
J_{cr}	$0.1 + \Phi_{\mathrm{s}\nu}(\xi)$	[—]	$e_\nu^{(0)}$	4.0	[—]
k_1	13.00	[kPa]	κ_0	0.0848	[—]
k_2	12.20	[—]	m_0	4.6380	[—]
σ_y	0.002	[MPa]	$k_{0\nu}^{(0)}$	$3.7729 \cdot 10^{-3}$	[mm^4(N s)$^{-1}$]
$\Phi_{\mathrm{s}\nu}$	$\Phi_{0\mathrm{s}\nu} + \Phi_{1\mathrm{s}\nu}$	[—]	$\mathscr{A}_0$	$(k_1/k_2)(4.387\,\xi^{2.228} + 1)$	[kPa]

Table 3.1: Parameters used in the numerical simulations. See [80, 225], and the references therein, for the values in the first seven rows on the left.

We remark that $\hat{\mathscr{W}}_{1\mathrm{a}}(\boldsymbol{C}_\mathrm{e}, \mathfrak{m})$ depends on $\mathfrak{m}$ through the structure tensor $\mathfrak{a} := \mathfrak{m} \otimes \mathfrak{m}$ and, since $\mathfrak{a}$ is invariant under the transformation $\mathfrak{m} \mapsto -\mathfrak{m}$, it also holds that $\hat{\mathscr{W}}_{1\mathrm{a}}(\boldsymbol{C}_\mathrm{e}(X,t), \mathfrak{m}_X) = \hat{\mathscr{W}}_{1\mathrm{a}}(\boldsymbol{C}_\mathrm{e}(X,t), -\mathfrak{m}_X)$, for all $X \in \mathscr{B}$ and for all times.

While the strain energy density of a single fibre, $\hat{\mathscr{W}}_{1\mathrm{a}}(\boldsymbol{C}_\mathrm{e}, \mathfrak{m})$, is transversely isotropic with respect to $\mathfrak{m}$, the directional average (3.9) models a material that is transversely isotropic with respect to $\mathfrak{m}_0$. To guarantee this property, for all $X \in \mathscr{B}$ in the natural state, we first choose a triad $\{\mathfrak{e}_\alpha(X)\}_{\alpha=1}^3$ of basis unit vectors, with $\mathfrak{e}_3(X)$ parallel to $\mathfrak{m}_0$. Then, we introduce the polar coordinates $(\vartheta, \varphi) \in [0, \pi] \times [0,2\pi[$, so that $\mathfrak{m}_X$ reads

$$\mathfrak{m}_X \equiv \check{\mathfrak{m}}_X(\vartheta, \varphi) = \sin\vartheta\, \cos\varphi\, \mathfrak{e}_1 + \sin\vartheta\, \sin\varphi\, \mathfrak{e}_2 + \cos\vartheta\, \mathfrak{e}_3, \tag{3.11}$$

and we enforce the condition

$$\Psi(\mathfrak{m}_X, \mathfrak{q}) = \Psi(\check{\mathfrak{m}}_X(\vartheta, \varphi), \mathfrak{q}) \equiv \check{\Psi}(\vartheta, \mathfrak{q}). \tag{3.12}$$

Since the probability density $\check{\Psi}(\vartheta, \mathfrak{q})$ re-defined in (3.12) is independent of φ, the directional average (3.9) has to be transversely isotropic with respect to $\mathfrak{m}_0$. Several functional forms can be used to express $\check{\Psi}(\vartheta,\mathfrak{q})$. For example, it can be a pseudo-Gaussian distribution [21, 108, 116, 85], defined by

$$\check{\Psi}_{\mathrm{PG}}(\vartheta,\mathfrak{q}) \equiv \hat{\Psi}_{\mathrm{PG}}(\vartheta,\mathfrak{q},\omega) = \frac{\hat{\gamma}(\vartheta,\mathfrak{q},\omega)}{\mathcal{N}(\mathfrak{q},\omega)}, \tag{3.13a}$$

$$\hat{\gamma}(\vartheta,\mathfrak{q},\omega) = \exp\left(-\frac{(\vartheta-\mathfrak{q})^2}{2\omega^2}\right), \tag{3.13b}$$

$$\mathcal{N}(\mathfrak{q},\omega) = 2\pi\int_0^{\pi/2}\hat{\gamma}(\vartheta,\mathfrak{q},\omega)\sin\vartheta\,\mathrm{d}\vartheta. \tag{3.13c}$$

In (3.13a)–(3.13c), $\omega^2 > 0$ is the variance of the pseudo-Gaussian distribution, $\mathcal{N}(\mathfrak{q},\omega)$ is the normalisation factor, and the remodelling angle $\mathfrak{q}$ is the angle, taken from $\boldsymbol{\mathfrak{m}}_0$, that denotes the semi-aperture of a cone of fibres with the apex in X.

The angle $\mathfrak{q}$ is conceived in such a way that $\check{\boldsymbol{\mathfrak{m}}}(\mathfrak{q},\varphi)$ represents the set of most probable directions of fibre alignment, with φ varying in $\in [0{,}2\pi[$. We remark that, according to the definitions(3.13a)–(3.13c), the values of ϑ that are admissible for $\check{\Psi}_{\mathrm{PG}}$ range in $[0,\pi/2]$. For this reason, also $\mathfrak{q}$ is allowed to vary within the same interval only.

Other forms of the probability density can be found e.g. in [21, 100]

3.3.2 "Non-Standard" constitutive laws

The energy density associated with remodelling is given in the form [108]

$$\hat{W}_{\mathrm{rem}}(\boldsymbol{F}_{\mathrm{e}},\boldsymbol{F}_{\mathrm{p}},\mathfrak{q},\mathrm{Grad}\,\mathfrak{q}) = \Phi_{1\mathrm{s}\nu}\left[\hat{W}_{\mathrm{str}}(\boldsymbol{C}_{\mathrm{e}},\mathfrak{q}) + \hat{W}_{\mathrm{Grad}}(\boldsymbol{F}_{\mathrm{e}},\boldsymbol{F}_{\mathrm{p}},\mathrm{Grad}\,\mathfrak{q})\right], \tag{3.14}$$

where $\hat{W}_{\mathrm{str}}(\boldsymbol{C}_{\mathrm{e}},\mathfrak{q})$ and $\hat{W}_{\mathrm{Grad}}(\boldsymbol{F}_{\mathrm{e}},\boldsymbol{F}_{\mathrm{p}},\mathrm{Grad}\,\mathfrak{q})$ are referred to as the *structural* part and the *gradient* part of the strain energy density, respectively. Although (3.14) has recently been introduced in [108], in the present work the constitutive expressions of $\hat{W}_{\mathrm{str}}$ and $\hat{W}_{\mathrm{Grad}}$ are rather different from those supplied in [108].

The first difference concerns $\hat{W}_{\mathrm{str}}(\boldsymbol{C}_{\mathrm{e}},\mathfrak{q})$, which is assumed here to be transversely isotropic, and to depend on $\boldsymbol{C}_{\mathrm{e}}$ only through $\bar{\boldsymbol{C}}_{\mathrm{e}} = J_{\mathrm{e}}^{-2/3}\boldsymbol{C}_{\mathrm{e}}$, i.e.,

$$\hat{W}_{\mathrm{str}}(\boldsymbol{C}_{\mathrm{e}},\mathfrak{q}) = \mathscr{A}_0\mathscr{P}(\mathfrak{q})\left[1+\frac{k_2}{k_1}\left\langle\!\!\left\langle\check{\mathscr{V}}_{1\mathrm{a}}(\bar{I}_{4\mathrm{e}})\mathcal{H}(I_{4\mathrm{e}}-1)\right\rangle\!\!\right\rangle(\mathfrak{q})\right], \tag{3.15}$$

where $\bar{I}_{4\mathrm{e}} = \bar{\boldsymbol{C}}_{\mathrm{e}} : (\boldsymbol{\mathfrak{m}}\otimes\boldsymbol{\mathfrak{m}}) = J_{\mathrm{e}}^{-2/3}I_{4\mathrm{e}}$, $\mathscr{A}_0$ is a point-dependent material coefficient, and $\mathscr{P}(\mathfrak{q})$ a double-well function of the fibre mean angle [108], i.e.,

$$\mathscr{P}(\mathfrak{q}) = \frac{1}{(\pi/4)^4}\mathfrak{q}^2\left(\mathfrak{q}-\frac{\pi}{2}\right)^2. \tag{3.16}$$

As noticed above, a more complete constitutive approach would call for expressing $\check{\mathscr{V}}_{1\mathrm{a}}$ as a function of $I_{4\mathrm{e}}$ and $I_{5\mathrm{e}}$ [59]. However, since such a modelling choice does not change the "philosophy" of our work, we opt here for an easier form of $\check{\mathscr{V}}_{1\mathrm{a}}$.

The second difference concerns the definition of W_{Grad}, which is assumed to depend also on the plastic-like distortions through the expression

$$W_{\mathrm{Grad}} = \tfrac{1}{2}\boldsymbol{d} : \operatorname{grad}{}^{\mathrm{s}}\mathfrak{q} \otimes \operatorname{grad}{}^{\mathrm{s}}\mathfrak{q} = \tfrac{1}{2}\boldsymbol{F}_{\mathrm{p}}^{-1}\boldsymbol{F}_{\mathrm{e}}^{-1}\boldsymbol{d}\boldsymbol{F}_{\mathrm{e}}^{-\mathrm{T}}\boldsymbol{F}_{\mathrm{p}}^{-\mathrm{T}} : \operatorname{Grad}\mathfrak{q} \otimes \operatorname{Grad}\mathfrak{q}, \tag{3.17}$$

where we employed the identity $\operatorname{grad}{}^{\mathrm{s}}\mathfrak{q}(x,t) = \boldsymbol{F}^{-\mathrm{T}}(X,t)\operatorname{Grad}\mathfrak{q}(X,t)$, with ${}^{\mathrm{s}}\mathfrak{q}(\,\cdot\,,t) : \mathscr{B}(t) \to [0,\pi/2]$ being the spatial version of the fibre mean angle. Among the many possible choices for expressing the second-order tensor $\boldsymbol{d}$, which has the physical meaning of angular stiffness per unit length [108], we select $\boldsymbol{d} = D_0\boldsymbol{b}_{\mathrm{e}}$, where $\boldsymbol{b}_{\mathrm{e}} = \boldsymbol{F}_{\mathrm{e}}.\boldsymbol{F}_{\mathrm{e}}^{\mathrm{T}}$ is the elastic left Cauchy-Green deformation tensor, and the coefficient D_0 is assumed to be constant. In general, D_0 should be a function of material points. However, in this work, we attribute the dependence on material points to the "effective" coefficient $\Phi_{1\mathrm{s}\nu}D_0$, which features in the definition of W_{rem}, and is obtained by multiplying W_{Grad} by $\Phi_{1\mathrm{s}\nu}$, as done in (3.14). Upon substituting $\boldsymbol{d} = D_0\boldsymbol{b}_{\mathrm{e}}$ into (3.17), we can rephrase W_{Grad} as a function of $\boldsymbol{F}_{\mathrm{p}}$ and $\operatorname{Grad}\mathfrak{q}$, i.e.,

$$W_{\mathrm{Grad}} = \tilde{W}_{\mathrm{Grad}}(\boldsymbol{F}_{\mathrm{p}}, \operatorname{Grad}\mathfrak{q}) = \tfrac{1}{2}D_0\boldsymbol{B}_{\mathrm{p}} : \operatorname{Grad}\mathfrak{q} \otimes \operatorname{Grad}\mathfrak{q}. \tag{3.18}$$

3.4 Residual Dissipation Inequality and Remodelling Equations

We adapt the study of the dissipation inequality from [108, 110] and, to avoid lengthy calculations, we report here only the results that are most important for this work. By exploiting the identity $\boldsymbol{C}_{\mathrm{e}} = \boldsymbol{F}_{\mathrm{p}}^{-\mathrm{T}}\boldsymbol{C}\boldsymbol{F}_{\mathrm{p}}^{-1}$, we can rephrase the constitutive expression of the overall free energy density W_ν as a function of $\boldsymbol{C}$, $\boldsymbol{F}_{\mathrm{p}}$ and $\mathfrak{q}$, i.e.,

$$W_\nu = \tilde{W}_\nu(\boldsymbol{C}, \boldsymbol{F}_{\mathrm{p}}, \mathfrak{q}, \operatorname{Grad}\mathfrak{q}). \tag{3.19}$$

By assuming isochoric plastic-like distortions, i.e., $J_{\mathrm{p}} = 1$, we obtain

$$\boldsymbol{P}_{\mathrm{s}} = -\Phi_{\mathrm{s}\nu}p\,\boldsymbol{g}^{-1}\boldsymbol{F}^{-\mathrm{T}} + \boldsymbol{F}\left(2\frac{\partial\tilde{W}_\nu}{\partial\boldsymbol{C}}\right), \tag{3.20a}$$

$$\boldsymbol{P}_{\mathrm{f}} = -(J - \Phi_{\mathrm{s}\nu})p\,\boldsymbol{g}^{-1}\boldsymbol{F}^{-\mathrm{T}}, \tag{3.20b}$$

where $\boldsymbol{P}_{\mathrm{s}}$ and $\boldsymbol{P}_{\mathrm{f}}$ are the first Piola-Kirchhoff stress tensors of the solid and the fluid, respectively. Next, we write $W_{\mathrm{std}} = \tilde{W}_{\mathrm{std}}(\boldsymbol{C}, \boldsymbol{F}_{\mathrm{p}}, \mathfrak{q})$, $W_{\mathrm{str}} = \tilde{W}_{\mathrm{str}}(\boldsymbol{C}, \boldsymbol{F}_{\mathrm{p}}, \mathfrak{q})$, and $W_{\mathrm{Grad}} = \tilde{W}_{\mathrm{Grad}}(\boldsymbol{F}_{\mathrm{p}}, \operatorname{Grad}\mathfrak{q})$. Subsequently, we introduce the Mandel stress tensors

$$\boldsymbol{\Sigma}_{\mathrm{std}} = -\boldsymbol{F}_{\mathrm{p}}^{\mathrm{T}}\frac{\partial\tilde{W}_{\mathrm{std}}}{\partial\boldsymbol{F}_{\mathrm{p}}} = \boldsymbol{C}\left(2\frac{\partial\tilde{W}_{\mathrm{std}}}{\partial\boldsymbol{C}}\right), \tag{3.21a}$$

$$\boldsymbol{\Sigma}_{\mathrm{str}} = -\boldsymbol{F}_{\mathrm{p}}^{\mathrm{T}}\left(\Phi_{1\mathrm{s}\nu}\frac{\partial\tilde{W}_{\mathrm{str}}}{\partial\boldsymbol{F}_{\mathrm{p}}}\right) = \boldsymbol{C}\left(2\Phi_{1\mathrm{s}\nu}\frac{\partial\tilde{W}_{\mathrm{str}}}{\partial\boldsymbol{C}}\right)$$

$$= \left\langle\!\!\left\langle f \mathrm{Dev}\left(\boldsymbol{C}\boldsymbol{F}_{\mathrm{p}}^{-1}\mathfrak{a}\boldsymbol{F}_{\mathrm{p}}^{-\mathrm{T}}\right)\right\rangle\!\!\right\rangle , \tag{3.21b}$$

$$\boldsymbol{\Sigma}_{\mathrm{Grad}} = -\boldsymbol{F}_{\mathrm{p}}^{\mathrm{T}}\left(\Phi_{1\mathrm{s}\nu}\frac{\partial \tilde{W}_{\mathrm{Grad}}}{\partial \boldsymbol{F}_{\mathrm{p}}}\right) = \mathrm{Grad}\,\mathfrak{q} \otimes \left(\Phi_{1\mathrm{s}\nu}\frac{\partial \tilde{W}_{\mathrm{Grad}}}{\partial\,\mathrm{Grad}\,\mathfrak{q}}\right), \tag{3.21c}$$

where the factor f is defined by

$$f = 2\Phi_{1\mathrm{s}\nu}\mathscr{A}_0\mathscr{P}(\mathfrak{q})I_{3\mathrm{e}}^{-1/3}k_2[\bar{I}_{4\mathrm{e}} - 1]\exp\left(k_2[\bar{I}_{4\mathrm{e}} - 1]^2\right)\mathcal{H}(I_{4\mathrm{e}} - 1). \tag{3.22}$$

We highlight that, with the Eqs. (3.21a), (3.21b) and (3.21c) we contribute to answer the research question 3.3.

Hence, we obtain the residual dissipation inequality

$$\begin{aligned}\mathfrak{D}_{\mathrm{res}} = &-\phi_{\mathrm{f}}^{-1}\boldsymbol{\pi}_{\mathrm{fd}}.\boldsymbol{F}\boldsymbol{\mathcal{Q}} + \left\{y^{(0)} - \frac{\partial \tilde{W}_\nu}{\partial \mathfrak{q}}\right\}\dot{\mathfrak{q}} + \left\{\boldsymbol{y}^{(1)} - \frac{\partial \tilde{W}_\nu}{\partial \mathrm{Grad}\mathfrak{q}}\right\}\mathrm{Grad}\dot{\mathfrak{q}} \\ &+ \left\{\boldsymbol{F}_{\mathrm{p}}^{-\mathrm{T}}\left(\boldsymbol{F}_{\mathrm{p}}^{\mathrm{T}}\boldsymbol{Y}_\nu^{\mathrm{int}} + \boldsymbol{\Sigma}_{\mathrm{std}} + \boldsymbol{\Sigma}_{\mathrm{str}} + \boldsymbol{\Sigma}_{\mathrm{Grad}}\right)\boldsymbol{F}_{\mathrm{p}}^{\mathrm{T}}\right\} : \boldsymbol{L}_{\mathrm{p}} \geq 0,\end{aligned} \tag{3.23}$$

where $\boldsymbol{\pi}_{\mathrm{fd}}$ is the force density describing the exchange of linear momentum between the solid and the fluid, and $\boldsymbol{\mathcal{Q}} = J\boldsymbol{F}^{-1}\boldsymbol{q}$ is referred to as *material filtration velocity*, i.e., the backward Piola-transformation of the filtration velocity $\boldsymbol{q} = \phi_{\mathrm{f}}[\boldsymbol{v}_{\mathrm{f}} - \boldsymbol{v}_{\mathrm{s}}]$.

With reference to (3.21a)–(3.21c), $\boldsymbol{\Sigma}_{\mathrm{std}}$ can be found in several theories on remodelling available in the literature (see e.g. [98, 13]); $\boldsymbol{\Sigma}_{\mathrm{str}}$ represents a *structural* generalised force that descends from the coupling between the deformation and the evolution of the fibres accounted for by W_{str}; $\boldsymbol{\Sigma}_{\mathrm{Grad}}$ stems from the coupling of the plastic-like distortions with the evolution of the fibres, and is a direct consequence of the introduction of the free energy density W_{Grad}.

Tensor $\boldsymbol{\Sigma}_{\mathrm{Grad}}$ can be interpreted as a generalisation of the Korteweg stress tensor. Coherently with W_{Grad}, it represents a generalised configurational force that is power-conjugate to $\boldsymbol{L}_{\mathrm{p}} = \dot{\boldsymbol{F}}_{\mathrm{p}}\boldsymbol{F}_{\mathrm{p}}^{-1}$, and that results from the coupling between $\boldsymbol{F}_{\mathrm{p}}$ and $\mathfrak{q}$. We also remark that, since in our model W_{Grad} is independent of $\boldsymbol{C}$, the differentiation of W_{Grad} with respect to $\boldsymbol{C}$ is null, thereby implying that W_{Grad} does not contribute to the second Piola-Kirchhoff stress tensor of the solid. Therefore, $\boldsymbol{\Sigma}_{\mathrm{Grad}}$ cannot possess the same properties as the Mandel stress tensors $\boldsymbol{\Sigma}_{\mathrm{std}}$ and $\boldsymbol{\Sigma}_{\mathrm{str}}$ defined in (3.21a) and (3.21b), respectively. For instance, it cannot be written in terms of the product of $\boldsymbol{C}$ with $(2\Phi_{1\mathrm{s}\nu}\partial\tilde{W}_{\mathrm{Grad}}/\partial\boldsymbol{C})$, and it does not fulfil the symmetry conditions $\boldsymbol{\Sigma}_{\mathrm{std}}\boldsymbol{C} = (\boldsymbol{\Sigma}_{\mathrm{std}}\boldsymbol{C})^{\mathrm{T}}$ and $\boldsymbol{\Sigma}_{\mathrm{str}}\boldsymbol{C} = (\boldsymbol{\Sigma}_{\mathrm{str}}\boldsymbol{C})^{\mathrm{T}}$. These stem from the coupling among $\boldsymbol{F}$, $\boldsymbol{F}_{\mathrm{p}}$, and $\mathfrak{q}$, a coupling that is accounted for by $\tilde{W}_{\mathrm{std}}$ and $\tilde{W}_{\mathrm{str}}$, but not by $\tilde{W}_{\mathrm{Grad}}$. We notice that $\boldsymbol{\Sigma}_{\mathrm{Grad}}$ satisfies the symmetry conditions $\boldsymbol{B}_{\mathrm{p}}\boldsymbol{\Sigma}_{\mathrm{Grad}} = (\boldsymbol{B}_{\mathrm{p}}\boldsymbol{\Sigma}_{\mathrm{Grad}})^{\mathrm{T}}$ [169].

In (3.23), we perform the identification

$$\boldsymbol{y}^{(1)} = \frac{\partial \tilde{W}_\nu}{\partial \mathrm{Grad}\mathfrak{q}} = \Phi_{1\mathrm{s}\nu}D_0\boldsymbol{B}_{\mathrm{p}}\mathrm{Grad}\mathfrak{q}, \tag{3.24}$$

which amounts to require that $\boldsymbol{y}^{(1)}$ has no dissipative contribution, and, by recalling the definition of $\mathscr{R}_\nu^{\mathrm{int}}$ given in (3.5b), we introduce the dissipative parts of the internal generalised forces $\mathscr{R}_\nu^{\mathrm{int}}$ and $\boldsymbol{Y}_\nu^{\mathrm{int}}$:

$$\mathscr{R}_{\nu,\mathrm{d}}^{\mathrm{int}} := y^{(0)} - \frac{\partial \tilde{W}_\nu}{\partial \mathfrak{q}} = \mathscr{R}_\nu^{\mathrm{int}} - \mathscr{E}(\mathfrak{q}, \operatorname{Grad}\mathfrak{q}), \tag{3.25a}$$

$$\boldsymbol{F}_{\mathrm{p}}^{\mathrm{T}}\boldsymbol{Y}_{\nu,\mathrm{d}}^{\mathrm{int}} := \operatorname{dev}(\boldsymbol{F}_{\mathrm{p}}^{\mathrm{T}}\boldsymbol{Y}_{\nu}^{\mathrm{int}}) + \operatorname{dev}(\boldsymbol{\Sigma}_{\mathrm{std}} + \boldsymbol{\Sigma}_{\mathrm{str}} + \boldsymbol{\Sigma}_{\mathrm{Grad}}), \tag{3.25b}$$

where $\mathscr{E}(\mathfrak{q}, \operatorname{Grad}\mathfrak{q})$ is the scalar generalised force given by

$$\mathscr{E}(\mathfrak{q}, \operatorname{Grad}\mathfrak{q}) := \frac{\partial \tilde{W}_\nu}{\partial \mathfrak{q}} - \operatorname{Div}\left(\frac{\partial \tilde{W}_\nu}{\partial \operatorname{Grad}\mathfrak{q}}\right). \tag{3.26}$$

Hence, $\mathfrak{D}_{\mathrm{res}}$ becomes

$$\mathfrak{D}_{\mathrm{res}} = -\,\phi_{\mathrm{f}}^{-1}\boldsymbol{\pi}_{\mathrm{fd}}.\boldsymbol{F}\boldsymbol{Q} + \mathscr{R}_{\nu,\mathrm{d}}^{\mathrm{int}}\dot{\mathfrak{q}} + \boldsymbol{F}_{\mathrm{p}}^{-\mathrm{T}}\left(\boldsymbol{F}_{\mathrm{p}}^{\mathrm{T}}\boldsymbol{Y}_{\nu,\mathrm{d}}^{\mathrm{int}}\right)\boldsymbol{F}_{\mathrm{p}}^{\mathrm{T}} : \boldsymbol{L}_{\mathrm{p}} \geq 0. \tag{3.27}$$

By recalling the force balances (3.2), reformulated for the case of isochoric plastic-like distortions, and (3.6), which allow to substitute $\mathscr{R}_\nu^{\mathrm{int}}$ with $\mathscr{R}_\nu^{\mathrm{ext}}$ in (3.25a) and $\boldsymbol{Y}_\nu^{\mathrm{int}}$ with $\boldsymbol{Y}_\nu^{\mathrm{ext}}$ in (3.25b), we obtain [108, 183, 110]

$$\mathscr{R}_{\nu,\mathrm{d}}^{\mathrm{int}} = \mathscr{R}_\nu^{\mathrm{ext}} - \mathscr{E}(\mathfrak{q}, \operatorname{Grad}\mathfrak{q}), \tag{3.28a}$$

$$\boldsymbol{F}_{\mathrm{p}}^{\mathrm{T}}\boldsymbol{Y}_{\nu,\mathrm{d}}^{\mathrm{int}} = \operatorname{dev}(\boldsymbol{F}_{\mathrm{p}}^{\mathrm{T}}\boldsymbol{Y}_{\nu}^{\mathrm{ext}}) + \operatorname{dev}(\boldsymbol{\Sigma}_{\mathrm{std}} + \boldsymbol{\Sigma}_{\mathrm{str}} + \boldsymbol{\Sigma}_{\mathrm{Grad}}). \tag{3.28b}$$

If $\mathscr{R}_{\nu,\mathrm{d}}^{\mathrm{int}}$ and $\boldsymbol{Y}_{\nu,\mathrm{d}}^{\mathrm{int}}$ can be related constitutively to $\dot{\mathfrak{q}}$ and $\boldsymbol{L}_{\mathrm{p}}$, respectively, (3.28a) and (3.28b) become evolution laws for $\mathfrak{q}$ and $\boldsymbol{F}_{\mathrm{p}}$. For this purpose, we study the dissipation inequality, and we require here each summand of (3.27) to be non-negative independently on the other ones [112], i.e.,

$$\mathfrak{D}_{\mathrm{flow}} = -\phi_{\mathrm{f}}^{-1}\boldsymbol{\pi}_{\mathrm{fd}}.\boldsymbol{F}\boldsymbol{Q} \geq 0, \tag{3.29a}$$

$$\mathfrak{D}_{\mathfrak{q}} = \mathscr{R}_{\nu,\mathrm{d}}^{\mathrm{int}}\dot{\mathfrak{q}} \geq 0, \tag{3.29b}$$

$$\mathfrak{D}_{\mathrm{p}} = \boldsymbol{F}_{\mathrm{p}}^{-\mathrm{T}}\left(\boldsymbol{F}_{\mathrm{p}}^{\mathrm{T}}\boldsymbol{Y}_{\nu,\mathrm{d}}^{\mathrm{int}}\right)\boldsymbol{F}_{\mathrm{p}}^{\mathrm{T}} : \boldsymbol{L}_{\mathrm{p}} \geq 0. \tag{3.29c}$$

First, we consider the inequality $\mathfrak{D}_{\mathrm{flow}} \geq 0$, and, by hypothesising a linear relationship between $\boldsymbol{\pi}_{\mathrm{fd}}$ and $\boldsymbol{Q}$ [132, 27], we obtain Darcy's law, i.e.,

$$\boldsymbol{Q} = -\boldsymbol{K}\operatorname{Grad} p. \tag{3.30}$$

Then, to satisfy $\mathfrak{D}_{\mathfrak{q}} \geq 0$, we assume $\mathscr{R}_{\nu,\mathrm{d}}^{\mathrm{int}} = \Gamma\dot{\mathfrak{q}}$, with Γ being a strictly positive quantity (in general, it suffices that Γ be non-negative).

Finally, we turn to $\mathfrak{D}_{\mathrm{p}}$, and we assume that the plastic-like distortions evolve according to a modified rate-independent formulation of plasticity, compatible with an associative normality rule [124]. Moreover, we hypothesise that $\boldsymbol{Y}_{\nu}^{\mathrm{ext}}$ is identically null [44] and, by performing the change of variable $\boldsymbol{H} = \boldsymbol{F}_{\mathrm{p}}^{-1}$ and setting $\boldsymbol{\Lambda}_{\mathrm{p}} = \dot{\boldsymbol{H}}\boldsymbol{H}^{-1}$, we obtain

$$\boldsymbol{H}^{-\mathrm{T}}\boldsymbol{Y}_{\nu,\mathrm{d}}^{\mathrm{int}} = \mathrm{dev}(\boldsymbol{\Sigma}_{\mathrm{std}} + \boldsymbol{\Sigma}_{\mathrm{str}} + \boldsymbol{\Sigma}_{\mathrm{Grad}}) \equiv \mathrm{dev}\boldsymbol{\Sigma}_{\mathrm{eff}}, \tag{3.31a}$$

$$\mathfrak{D}_{\mathrm{p}} = -\boldsymbol{\Sigma}_{\mathrm{eff}} : \boldsymbol{\Lambda}_{\mathrm{p}} = -(\mathrm{dev}\boldsymbol{\Sigma}_{\mathrm{eff}}) : \boldsymbol{\Lambda}_{\mathrm{p}} \geq 0, \tag{3.31b}$$

where $\boldsymbol{\Sigma}_{\mathrm{eff}}$ is referred to as the *effective* Mandel-like stress tensor and is the sum of $\boldsymbol{\Sigma}_{\mathrm{std}}$, $\boldsymbol{\Sigma}_{\mathrm{str}}$, and $\boldsymbol{\Sigma}_{\mathrm{Grad}}$. We remark that, because of the constraint $\det \boldsymbol{H} = 1$, $\boldsymbol{\Lambda}_{\mathrm{p}}$ is deviatoric and, consequently, it selects only the deviatoric part of $\boldsymbol{\Sigma}_{\mathrm{eff}}$ in $\mathfrak{D}_{\mathrm{p}}$.

Next, we use $\boldsymbol{\Sigma}_{\mathrm{eff}}$ to define the *effective* Cauchy-like stress tensor

$$\boldsymbol{\sigma}_{\mathrm{eff}} := J^{-1}\boldsymbol{g}^{-1}\boldsymbol{F}^{-\mathrm{T}}\boldsymbol{\Sigma}_{\mathrm{eff}}\boldsymbol{F}^{\mathrm{T}}. \tag{3.32}$$

We remark that, because of the presence of $\boldsymbol{\Sigma}_{\mathrm{Grad}}$, $\boldsymbol{\Sigma}_{\mathrm{eff}}$ is *not* a true Mandel stress tensor and, analogously, $\boldsymbol{\sigma}_{\mathrm{eff}}$ is *not* a true Cauchy stress tensor. Rather, $\boldsymbol{\sigma}_{\mathrm{eff}}$ only represents the spatial counterpart of $\boldsymbol{\Sigma}_{\mathrm{eff}}$, constructed as shown in (3.32), but it does not necessarily satisfy the properties that a true Cauchy stress tensor should fulfil. For example, it is not symmetric. Still, we employ $\boldsymbol{\sigma}_{\mathrm{eff}}$ to formulate a yield criterion of the von Mises type. To this end, we introduce the yield function

$$\mathscr{Y} = \|\mathrm{dev}\boldsymbol{\sigma}_{\mathrm{eff}}\|_{\boldsymbol{g}} - \sqrt{(2/3)}\,\sigma_y, \tag{3.33}$$

where σ_y is a strictly positive yield stress, and, to comply with the condition $J_{\mathrm{p}} = 1$, only the deviatoric part of $\boldsymbol{\sigma}_{\mathrm{eff}}$ is considered. We remark that the norm $\|\mathrm{dev}\boldsymbol{\sigma}_{\mathrm{eff}}\|_{\boldsymbol{g}}$ is computed with respect to the spatial metric $\boldsymbol{g}$, i.e.,

$$\|\mathrm{dev}\boldsymbol{\sigma}_{\mathrm{eff}}\|_{\boldsymbol{g}} = \sqrt{\boldsymbol{g} : (\mathrm{dev}\boldsymbol{\sigma}_{\mathrm{eff}})\boldsymbol{g}(\mathrm{dev}\boldsymbol{\sigma}_{\mathrm{eff}})^{\mathrm{T}}}. \tag{3.34}$$

By expressing the norm $\|\mathrm{dev}\boldsymbol{\sigma}_{\mathrm{eff}}\|_{\boldsymbol{g}}$ in terms of $\boldsymbol{\Sigma}_{\mathrm{eff}}$, i.e.,

$$\|\mathrm{dev}\boldsymbol{\sigma}_{\mathrm{eff}}\|_{\boldsymbol{g}} = J^{-1}\|\mathrm{dev}\boldsymbol{\Sigma}_{\mathrm{eff}}\|_{\boldsymbol{C}}, \tag{3.35a}$$

$$\|\mathrm{dev}\boldsymbol{\Sigma}_{\mathrm{eff}}\|_{\boldsymbol{C}} := \sqrt{\boldsymbol{C}^{-1} : (\mathrm{dev}\boldsymbol{\Sigma}_{\mathrm{eff}})\boldsymbol{C}(\mathrm{dev}\boldsymbol{\Sigma}_{\mathrm{eff}})^{\mathrm{T}}}, \tag{3.35b}$$

we rephrase $\mathscr{Y}$ in terms of $\boldsymbol{\Sigma}_{\mathrm{eff}}$ and $\boldsymbol{C}$, thereby obtaining

$$\mathscr{Y} = \hat{\mathscr{Y}}(\boldsymbol{C}, \boldsymbol{\Sigma}_{\mathrm{eff}}) = J^{-1}\|\mathrm{dev}\boldsymbol{\Sigma}_{\mathrm{eff}}\|_{\boldsymbol{C}} - \sqrt{(2/3)}\,\sigma_y. \tag{3.36}$$

We use (3.36) to maximise $\mathfrak{D}_{\mathrm{p}}$ over all the possible stresses [218]. For this purpose, we adopt the Karush-Kuhn-Tucker technique [218], along with the modified dissipation

$$\tilde{\mathfrak{D}}_{\mathrm{p}}(\boldsymbol{C}, \boldsymbol{\Sigma}_{\mathrm{eff}}, \lambda) = -\mathrm{dev}\boldsymbol{\Sigma}_{\mathrm{eff}} : \boldsymbol{\Lambda}_{\mathrm{p}} - \lambda\hat{\mathscr{Y}}(\boldsymbol{C}, \boldsymbol{\Sigma}_{\mathrm{eff}}) \geq 0, \tag{3.37}$$

where λ is a Karush-Kuhn-Tucker (KKT) multiplier, to be determined. The search for maximisers of $\tilde{\mathfrak{D}}_{\mathrm{p}}(\boldsymbol{C}, \boldsymbol{\Sigma}_{\mathrm{eff}}, \lambda)$ is accomplished by differentiating $\tilde{\mathfrak{D}}_{\mathrm{p}}$ with respect to $\boldsymbol{\Sigma}_{\mathrm{eff}}$ and λ, and leads to the Karush-Kuhn-Tucker optimality conditions [218]. Since in this work the yield stress, σ_y, is assumed to be a given model parameter, such optimality conditions read

$$\frac{\partial \tilde{\mathfrak{D}}_{\mathrm{p}}}{\partial \boldsymbol{\Sigma}_{\mathrm{eff}}}(\boldsymbol{C}, \boldsymbol{\Sigma}_{\mathrm{eff}}, \lambda) = -\boldsymbol{\Lambda}_{\mathrm{p}} - \lambda \frac{\partial \hat{\mathscr{Y}}}{\partial \boldsymbol{\Sigma}_{\mathrm{eff}}}(\boldsymbol{C}, \boldsymbol{\Sigma}_{\mathrm{eff}}) = \mathbf{0}, \tag{3.38a}$$

$$\lambda \geq 0, \qquad \hat{\mathscr{Y}}(\boldsymbol{C}, \boldsymbol{\Sigma}_{\mathrm{eff}}) \leq 0, \qquad \lambda \hat{\mathscr{Y}}(\boldsymbol{C}, \boldsymbol{\Sigma}_{\mathrm{eff}}) = 0. \tag{3.38b}$$

3.4.1 Reorientation of the fibres

By substituting $\mathscr{R}^{\mathrm{int}}_{\nu,\mathrm{d}} = \Gamma \dot{\mathfrak{q}}$ into (3.28a), and writing $\mathscr{E}(\mathfrak{q}, \mathrm{Grad}\,\mathfrak{q})$ explicitly, Eq. (3.28a) takes on the form

$$\Gamma \dot{\mathfrak{q}} = \mathrm{Div}\left[\Phi_{1\mathrm{s}\nu} D_0 \boldsymbol{B}_{\mathrm{p}} \mathrm{Grad}\,\mathfrak{q}\right] - \Phi_{1\mathrm{s}\nu} \frac{\partial(\hat{W}_{1\mathrm{a}} + \hat{W}_{\mathrm{str}})}{\partial \mathfrak{q}} + \mathscr{R}^{\mathrm{ext}}_{\nu}. \tag{3.39}$$

The first term on the right-hand-side of (3.39) contributes to the evolution of the fibre mean angle by resolving the spatial variability of $\mathfrak{q}$. The coefficient $\Phi_{1\mathrm{s}\nu} D_0$ multiplies the inverse (plastic) metric tensor $\boldsymbol{B}_{\mathrm{p}}$, thereby leading to the tensorial coefficient $\Phi_{1\mathrm{s}\nu} D_0 \boldsymbol{B}_{\mathrm{p}}$. We notice that, in spite of some formal similarities with a diffusion-reaction equation, (3.39) describes no diffusion, since it is not a mass balance, but the evolution of an order parameter [122].

To solve (3.39), we need to provide $\mathscr{R}^{\mathrm{ext}}_{\nu}$. In two previous papers on this subject [108, 116], one of us reviewed some results presented by other authors, e.g. [127, 183], who defined the external remodelling force $\mathscr{R}^{\mathrm{ext}}_{\nu}$ by introducing the concept of *target angle*, $\mathfrak{q}_T$. The target angle is an angle that defines the direction of space, which we may call *target direction*, along which the fibres "would like to be aligned". By definition, the fibres tend to orient themselves along the target direction and it has been observed that, in a tissue subjected to mechanical stress and deformation, the target angle depends on stress [127, 183] or deformation [64, 21].

Although the issue of the target angle was discussed in [108, 116], the focus in those papers was on the particular situations in which no external force $\mathscr{R}^{\mathrm{ext}}_{\nu}$ was active, i.e., when the condition $\mathscr{R}^{\mathrm{ext}}_{\nu} = 0$ applies in (3.39). In these cases, indeed, a "target angle" may be identified with a stationary solution of (3.39), i.e., a function $\mathfrak{q}_\infty$ satisfying

$$\mathrm{Div}\left[\Phi_{1\mathrm{s}\nu} D_0 \boldsymbol{B}_{\mathrm{p}} \mathrm{Grad}\,\mathfrak{q}\right] - \Phi_{1\mathrm{s}\nu} \frac{\partial(\hat{W}_{1\mathrm{a}} + \hat{W}_{\mathrm{str}})}{\partial \mathfrak{q}} = 0, \tag{3.40}$$

together with time-independent boundary conditions. Since $\partial \hat{W}_{\mathrm{str}}/\partial \mathfrak{q}$ does not vanish when $\boldsymbol{B}_{\mathrm{p}} = \boldsymbol{G}^{-1}$ and the tissue is undeformed, (3.40) admits solutions of sigmoidal shape that interpolate between the zeroes of the double-well potential $\mathscr{P}(\mathsf{q})$, i.e., $\mathsf{q}_0 = 0$ and $\mathsf{q}_1 = \pi/2$. Always in the absence of deformation, such profiles can also be obtained as the stationary solutions of (3.39), when the initial distribution of q is a random function of material points [108].

In the case of vanishing D_0, the energy density W_{Grad} is null, and we end up with a description of remodelling determined by ordinary differential equations. In such situations, and for $\mathscr{R}_\nu^{\mathrm{ext}} = 0$, the search for stationary solutions amounts to seek for the zeros of the equation

$$-\Phi_{1\mathrm{s}\nu} \frac{\partial(\hat{W}_{1\mathrm{a}} + \hat{W}_{\mathrm{str}})}{\partial \mathsf{q}} = 0. \tag{3.41}$$

In general, however, (3.41) may admit either no solutions or multiple solutions, i.e., different target angles. Whereas the existence of multiple stationary solutions to (3.41) can be a normal fact, because the Cauchy problem

$$\Gamma \dot{\mathsf{q}} = -\Phi_{1\mathrm{s}\nu} \frac{\partial(\hat{W}_{1\mathrm{a}} + \hat{W}_{\mathrm{str}})}{\partial \mathsf{q}}, \tag{3.42a}$$

$$\mathsf{q}(X,0) = \mathsf{q}_{\mathrm{in}}(X), \tag{3.42b}$$

if well-posed, selects a unique solution, the case of no stationary solution may be non-physical. Similar circumstances may occur when the right-hand-side of (3.42a) features only $\partial \hat{W}_{1\mathrm{a}} / \partial \mathsf{q}$.

By introducing a non-vanishing $\mathscr{R}_\nu^{\mathrm{ext}}$, relating it to the concept of an *a priori* defined target angle, q_T, and assuming the existence of a stationary limit q_T^∞, the non-physical case of no stationary solutions is eliminated at source. Indeed, it suffices to notice that a stationary angle is attained when the external force $\mathscr{R}_\nu^{\mathrm{ext}}$ balances the internal ones under the condition $\dot{\mathsf{q}} = 0$. This implies that the following equality has to be verified [183]

$$\mathscr{R}_\nu^{\mathrm{ext}} = \Phi_{1\mathrm{s}\nu} \left. \frac{\partial(\hat{W}_{1\mathrm{a}} + \hat{W}_{\mathrm{str}})}{\partial \mathsf{q}} \right|_{\mathsf{q} = \mathsf{q}_T^\infty}. \tag{3.43}$$

This result can also be generalised to the case in which the target angle is not stationary, so that Eq. (3.42a) is rewritten as

$$\Gamma \dot{\mathsf{q}} = -\Phi_{1\mathrm{s}\nu} \frac{\partial(\hat{W}_{1\mathrm{a}} + \hat{W}_{\mathrm{str}})}{\partial \mathsf{q}} + \Phi_{1\mathrm{s}\nu} \left. \frac{\partial(\hat{W}_{1\mathrm{a}} + \hat{W}_{\mathrm{str}})}{\partial \mathsf{q}} \right|_{\mathsf{q} = \mathsf{q}_T}, \tag{3.44}$$

where the term on the right-hand-side is computed for a non-stationary target angle q_T, driven by stress or deformation.

Even more generally, when the remodelling equation is given by (3.39), the external force $\mathscr{R}_\nu^{\mathrm{ext}}$ may be defined as

$$\mathscr{R}_\nu^{\mathrm{ext}} = \mathscr{E}(q_{\mathrm{T}}, \mathrm{Grad}\, \mathsf{q}_T)$$

$$= -\mathrm{Div}\left[\Phi_{1\mathrm{s}\nu} D_0 \boldsymbol{B}_\mathrm{p} \mathrm{Grad}\mathfrak{q}_T\right] + \Phi_{1\mathrm{s}\nu} \left.\frac{\partial(\hat{W}_{1\mathrm{a}} + \hat{W}_{\mathrm{str}})}{\partial \mathfrak{q}}\right|_{\mathfrak{q}=\mathfrak{q}_T}, \tag{3.45}$$

thereby obtaining the following generalisation of [108, 183, 116]:

$$\begin{aligned}\Gamma\dot{\mathfrak{q}} =& \mathrm{Div}\left[\Phi_{1\mathrm{s}\nu} D_0 \boldsymbol{B}_\mathrm{p} \mathrm{Grad}\,\mathfrak{q}\right] - \Phi_{1\mathrm{s}\nu} \frac{\partial(\hat{W}_{1\mathrm{a}} + \hat{W}_{\mathrm{str}})}{\partial \mathfrak{q}} \\ & - \mathrm{Div}\left[\Phi_{1\mathrm{s}\nu} D_0 \boldsymbol{B}_\mathrm{p} \mathrm{Grad}\,\mathfrak{q}_T\right] + \Phi_{1\mathrm{s}\nu} \left.\frac{\partial(\hat{W}_{1\mathrm{a}} + \hat{W}_{\mathrm{str}})}{\partial \mathfrak{q}}\right|_{\mathfrak{q}=\mathfrak{q}_T}. \end{aligned} \tag{3.46}$$

We highlight that, within the above discussion, we contribute to answer the research question 3.3.

3.4.2 Evolution of the plastic-like distortions

The explicit computation of the derivative of $\hat{\mathscr{Y}}$ with respect to $\boldsymbol{\Sigma}_{\mathrm{eff}}$, see (3.36), permits to rewrite (3.38a) as

$$\boldsymbol{\Lambda}_\mathrm{p} = -J^{-1}\lambda \frac{\boldsymbol{C}^{-1}(\mathrm{dev}\boldsymbol{\Sigma}_{\mathrm{eff}})\boldsymbol{C}}{\|\mathrm{dev}\boldsymbol{\Sigma}_{\mathrm{eff}}\|_{\boldsymbol{C}}}, \tag{3.47}$$

which implies $\|\boldsymbol{\Lambda}_\mathrm{p}\|_{\boldsymbol{C}} \equiv \sqrt{\boldsymbol{C} : \boldsymbol{\Lambda}_\mathrm{p}\boldsymbol{C}^{-1}\boldsymbol{\Lambda}_\mathrm{p}^{\mathrm{T}}} = J^{-1}\lambda \geq 0$. Moreover, since $\boldsymbol{\Lambda}_\mathrm{p}$ is given by $\boldsymbol{\Lambda}_\mathrm{p} = \dot{\boldsymbol{H}}\boldsymbol{H}^{-1}$, (3.47) can be recast in the form of an evolution equation for $\boldsymbol{H}$ or, equivalently, for $\boldsymbol{F}_\mathrm{p} = \boldsymbol{H}^{-1}$, i.e.,

$$\dot{\boldsymbol{H}} = \left\{-J^{-1}\lambda \frac{\boldsymbol{C}^{-1}(\mathrm{dev}\boldsymbol{\Sigma}_{\mathrm{eff}})\boldsymbol{C}}{\|\mathrm{dev}\boldsymbol{\Sigma}_{\mathrm{eff}}\|_{\boldsymbol{C}}}\right\}\boldsymbol{H}. \tag{3.48}$$

Within the classical framework of finite Elastoplasticity, the KKT-multiplier λ is determined by enforcing a condition known as "consistency condition" [218], which has to be solved together with the flow rule —represented here by (3.48)— and the other model equations. Very often, the consistency condition is solved algorithmically (see e.g. [218]). In this work, however, we propose a rather different approach, which is motivated by the need of keeping our calculations at a minimum level of complexity. In fact, we prescribe λ from the outset, and, for our purposes, we define it as

$$\lambda = J\zeta_0\phi_\mathrm{s}\left[\|\mathrm{dev}\boldsymbol{\sigma}_{\mathrm{eff}}\|_{\boldsymbol{g}} - \sqrt{(2/3)}\,\sigma_y\right]_+ = \zeta_0\Phi_{\mathrm{s}\nu}\left[J^{-1}\|\mathrm{dev}\boldsymbol{\Sigma}_{\mathrm{eff}}\|_{\boldsymbol{C}} - \sqrt{(2/3)}\,\sigma_y\right]_+, \tag{3.49}$$

where $\zeta_0 > 0$ is a constant model parameter, and $[A]_+ = A$, for $A > 0$, and $[A]_+ = 0$, otherwise. We notice that the equality $\Phi_{\mathrm{s}\nu} = J\phi_\mathrm{s}$ is verified, because it holds that $J = J_\mathrm{e}$, since the condition $J_\mathrm{p} = 1$ applies. Finally, by substituting (3.49) into (3.48), we obtain

$$\dot{\boldsymbol{H}} = -\frac{\zeta_0 \Phi_{\mathrm{s}\nu} \left[J^{-1} \|\mathrm{dev}\boldsymbol{\Sigma}_\mathrm{eff}\|_{\boldsymbol{C}} - \sqrt{(2/3)}\, \sigma_y \right]_+}{J} \frac{\boldsymbol{C}^{-1}(\mathrm{dev}\boldsymbol{\Sigma}_\mathrm{eff})\boldsymbol{C}}{\|\mathrm{dev}\boldsymbol{\Sigma}_\mathrm{eff}\|_{\boldsymbol{C}}} \boldsymbol{H}, \qquad (3.50)$$

i.e., the ordinary differential equation describing the evolution of $\boldsymbol{H}$.

Equation (3.50) looks like an evolution law of the Norton-Hoff type [181] and, with some modifications, might be rated among those. However, compared with that in [181], our (3.50) features three differences: (i) the full tensor $\mathrm{dev}\boldsymbol{\Sigma}_\mathrm{eff}$ is considered in lieu of its symmetric part only (see [181] for some remarks on this issue); (ii) the "transformed" generalised stress $\boldsymbol{C}^{-1}\mathrm{dev}\boldsymbol{\Sigma}_\mathrm{eff}\boldsymbol{C}$, rather than $\mathrm{dev}\boldsymbol{\Sigma}_\mathrm{eff}$, is regarded as the driving force for $\boldsymbol{H}$; (iii) our $\boldsymbol{\Sigma}_\mathrm{eff}$ contains $\boldsymbol{\Sigma}_\mathrm{Grad}$, which is a fundamental character of our framework.

We notice that the coefficient λ in (3.49) has the form of the activation factor featuring in the flow rule of a Perzyna-like model of viscoplasticity [176]. Dimensional analysis shows that the parameter ζ_0 can be expressed as $\zeta_0 = (\tau_\mathrm{c}\sigma_\mathrm{c})^{-1}$, where τ_c is the characteristic relaxation time of $\boldsymbol{H}$, and σ_c is a reference value of stress. The time scale τ_c is available in the literature, and we choose $\tau_\mathrm{c} = 22\,\mathrm{s}$, as suggested in [104], where the inelastic behaviour of cellular aggregates is studied by means of a Perzyna-like flow rule. However, there seems to be some freedom in the choice of the reference stress σ_c. In principle, indeed, σ_c could be taken equal to σ_y, if one wants to normalise λ with the yield stress, or it could be defined by combining the material parameters involved in the definition of $\boldsymbol{\sigma}_\mathrm{eff}$. In the latter case, one should use parameters, such as D_0 and $\mathscr{A}_0$, that, being other than the standard elastic coefficients, are not available in the literature, at least to the best of our knowledge. Thus, we refer here to a value of σ_c that has already been used in [104], within a framework similar to ours. To this end, by comparing (3.49) with the flow rule in [104], we identify σ_c with $\sigma_\mathrm{c} = 2\mu_0\langle\Phi_{\mathrm{s}\nu}\rangle$, where μ_0 is the shear modulus of the matrix, and $\langle\Phi_{\mathrm{s}\nu}\rangle$ is the mean value of the solid phase volumetric ratio. Hence, upon computing $\mu_0 = 2(\alpha_1 + \alpha_2)\alpha_0 \approx 0.222\,\mathrm{MPa}$ [138] and $\langle\Phi_{\mathrm{s}\nu}\rangle = \int_0^1 \Phi_{\mathrm{s}\nu}(\xi)\mathrm{d}\xi = 0.2$ (see Table 3.1), we find $\sigma_\mathrm{c} \approx 0.09\,\mathrm{MPa}$ and $\zeta_0 \approx 0.50\,\mathrm{MPa}^{-1}\mathrm{s}^{-1}$ (cf. Table 3.1). Such σ_c is obtained by considering only the isotropic part of the standard energy of our model, whereas considering also the other terms of the energy would lead to higher values of σ_c and, then, to smaller values of ζ_0. On the other hand, smaller values of σ_c are conceivable, but they could result into too high values of ζ_0 for the problem at hand, thereby leading to non-physical time scales for the evolution of $\boldsymbol{H}$.

3.4.3 Summary of the model equations and technical details

After enforcing the left polar decomposition of $\boldsymbol{H}$, i.e., $\boldsymbol{H} = \boldsymbol{V}.\boldsymbol{R}$ [165], we study only the case in which $\boldsymbol{R}$ reduces to a shifter [165], so that the unknown determining the plastic-like distortions becomes the symmetric, second-order tensor $\boldsymbol{V}$. Even though this choice has the disadvantage of restricting the investigation to the case of no plastic-like rotations, it allows to work with $\boldsymbol{V}$, which, being symmetric, is computationally cheaper. In summary, thus, our mathematical model consists of the following set of four, highly non-linear, coupled equations,

$$\dot{J} - \mathrm{Div}\,(\boldsymbol{K}\mathrm{Grad}\,p) = 0, \tag{3.51a}$$

$$\mathrm{Div}\left(-J\,p\,\boldsymbol{g}^{-1}\boldsymbol{F}^{-\mathrm{T}} + \boldsymbol{P}_{\mathrm{sc}}\right) = \boldsymbol{0}, \tag{3.51b}$$

$$\begin{aligned}\Gamma\dot{\mathfrak{q}} = {} & \mathrm{Div}\,[\Phi_{1\mathrm{s}\nu}D_0\boldsymbol{B}_{\mathrm{p}}\mathrm{Grad}\,\mathfrak{q}] - \Phi_{1\mathrm{s}\nu}\frac{\partial(\hat{W}_{1\mathrm{a}} + \hat{W}_{\mathrm{str}})}{\partial\mathfrak{q}} \\ & - \mathrm{Div}\,[\Phi_{1\mathrm{s}\nu}D_0\boldsymbol{B}_{\mathrm{p}}\mathrm{Grad}\,\mathfrak{q}_T] + \Phi_{1\mathrm{s}\nu}\left.\frac{\partial(\hat{W}_{1\mathrm{a}} + \hat{W}_{\mathrm{str}})}{\partial\mathfrak{q}}\right|_{\mathfrak{q}=\mathfrak{q}_T},\end{aligned} \tag{3.51c}$$

$$\dot{\boldsymbol{V}} = -\mathrm{sym}\left[\left(\frac{\lambda}{J}\,\frac{\boldsymbol{C}^{-1}(\mathrm{dev}\boldsymbol{\Sigma}_{\mathrm{eff}})\boldsymbol{C}}{\|\mathrm{dev}\boldsymbol{\Sigma}_{\mathrm{eff}}\|_{\boldsymbol{C}}}\right)\boldsymbol{V}\right], \tag{3.51d}$$

in the unknowns p, χ, $\mathfrak{q}$, and $\boldsymbol{V}$, respectively. Note that we take the symmetric part of the right-hand-side of (3.51d) in order to ensure that $\dot{\boldsymbol{V}}$, and its time discrete form, be symmetric. Moreover, the material permeability tensor is given by [138, 84, 82, 80]

$$\boldsymbol{K} = k_0\frac{(J-\Phi_{1\mathrm{s}\nu})^2}{J}\boldsymbol{C}^{-1} + k_0\frac{(J-\Phi_{1\mathrm{s}\nu})\Phi_{1\mathrm{s}\nu}}{J}\boldsymbol{H}\left\langle\frac{\mathfrak{a}}{I_{4\mathrm{e}}}\right\rangle\boldsymbol{H}^{\mathrm{T}}, \tag{3.52a}$$

$$k_0 = k_{0\nu}\left[\frac{J-\Phi_{\mathrm{s}\nu}}{1-\Phi_{\mathrm{s}\nu}}\right]^{\kappa_0}\exp\left(\tfrac{1}{2}m_0[J^2-1]\right). \tag{3.52b}$$

The material parameters κ_0 and m_0 are reported in Table 3.1.

We solve Eqs. (3.51a)–(3.51d) for a cylindrical specimen of tissue, of initial height $L = 1\,\mathrm{mm}$ and initial radius $R = 1.5\,\mathrm{mm}$, and whose boundary can be written as $\partial\mathscr{B} = \partial\mathscr{B}_{\mathrm{U}} \sqcup \partial\mathscr{B}_{\mathrm{L}} \sqcup \partial\mathscr{B}_{\ell}$, where the subscripts "U", "L", "ℓ" stand for "upper", "lower" and "lateral", respectively. Then, we complete Eqs. (3.51a)–(3.51d) with the following boundary and initial conditions

$$-(\boldsymbol{K}\,\mathrm{Grad}\,p).\boldsymbol{N} = 0, \qquad \text{on } \partial\mathscr{B}_{\mathrm{U}} \sqcup \partial\mathscr{B}_{\mathrm{L}}, \tag{3.53a}$$

$$p = 0, \qquad \text{on } \partial\mathscr{B}_{\ell}, \tag{3.53b}$$

$$[\chi(X,0) - \chi(X,t)].\boldsymbol{e}_3 = u(t), \qquad \text{on } \partial\mathscr{B}_{\mathrm{U}}, \tag{3.53c}$$

$$\chi(X,t) - \chi(X,0) = \boldsymbol{0}, \qquad \text{on } \partial\mathscr{B}_{\mathrm{L}}, \tag{3.53d}$$

$$\left(-J\,p\,\boldsymbol{g}^{-1}\boldsymbol{F}^{-\mathrm{T}}+\boldsymbol{P}_{\mathrm{sc}}\right).\boldsymbol{N}=\boldsymbol{0}, \qquad \text{on } \partial\mathscr{B}_{\ell}, \tag{3.53e}$$

$$(\Phi_{1\mathrm{s}\nu}D_0\boldsymbol{B}_{\mathrm{p}}\,\mathrm{Grad}\,\mathfrak{q}).\boldsymbol{N}=0, \qquad \text{on } \partial\mathscr{B}_{\mathrm{U}}\sqcup\partial\mathscr{B}_{\ell}, \tag{3.53f}$$

$$\mathfrak{q}(X,t)=0, \qquad \text{on } \partial\mathscr{B}_{\mathrm{L}}, \tag{3.53g}$$

$$\chi(X,0)=\chi_0(X), \qquad \text{in } \mathscr{B}, \tag{3.53h}$$

$$\mathfrak{q}(X,0)=\mathfrak{q}_{\mathrm{hist}}(X), \qquad \text{in } \mathscr{B}, \tag{3.53i}$$

$$\boldsymbol{V}(X,0)=\boldsymbol{G}^{-1}(X), \qquad \text{in } \mathscr{B}. \tag{3.53j}$$

In (3.53a), (3.53e), and (3.53f), $\boldsymbol{N}$ is the field of unit vectors normal to $\partial\mathscr{B}$; in (3.53c), the imposed displacement $u(t)$ is given by

$$u(t)=\frac{u_{\mathrm{max}}\,t}{t_{\mathrm{ramp}}}[\Theta(t)-\Theta(t-t_{\mathrm{ramp}})]+u_{\mathrm{max}}\Theta(t-t_{\mathrm{ramp}}), \tag{3.54}$$

where $\Theta(s)=1$, for $s\geq 0$, and $\Theta(s)=0$, for $s<0$, $u_{\mathrm{max}}=0.20\,\mathrm{mm}$ is the maximum imposed displacement, and $t_{\mathrm{ramp}}=20\,\mathrm{s}$ is the final time of the loading ramp. In the simulated compression test, u_{max} is kept constant until $t_{\mathrm{f}}=120\,\mathrm{s}$. In (3.53h), $\chi_0(X)$ represents the initial placement and, in this work, it returns the points X of the reference configuration $\mathscr{B}$. In (3.53i), $\mathfrak{q}_{\mathrm{hist}}(X)$ denotes the initial distribution of the fibre mean angle, and is taken here to be equal to an experimentally observed "histological" profile [85], given by

$$\mathfrak{q}_{\mathrm{hist}}(X)=\frac{\pi}{2}\left\{1-\cos\left(\frac{\pi}{2}\left[-\frac{2}{3}\left(\frac{X^3}{L}\right)^2+\frac{5}{3}\frac{X^3}{L}\right]\right)\right\}, \tag{3.55}$$

where X^3 is the axial coordinate. Finally, the initial value $\boldsymbol{V}(X,0)$ is taken in (3.53j) equal to the inverse metric tensor associated with $\mathscr{B}$, which means that no inelastic distortions occur before the deformation process commences.

We remark that (3.51a)–(3.51d) are valid in general, in the sense that they apply to the studied system, under all the specified hypotheses, but without any specialisation to a particular benchmark problem. In fact, they can be adopted for a variety of case studies, and to formulate a proof of concept for testing a proposed model. In our work, we employ (3.51a)–(3.51d) for analysing the coupling among fluid flow, deformation and structural reorganisation of the matrix, and fibre reorientation in the tissue under study. For this purpose, we solve numerically a well-documented benchmark test consisting in the unconfined compression of a cylindrical specimen of tissue. The latter is assumed here to be articular cartilage because of the availability of experimental data, but the test can also be performed on other tissues. For the considered test, a sample of tissue is placed between two plates, assumed to be rigid and impermeable (see (3.53a)), as shown in 3.1. The lower plate is fixed and the specimen is clamped to it, so as to simulate the adhesion of the cartilage to bone (see (3.53d)). The upper plate, instead, compresses axially the sample (see (3.53c)), in such a way that the deformation remains axial-symmetric over the

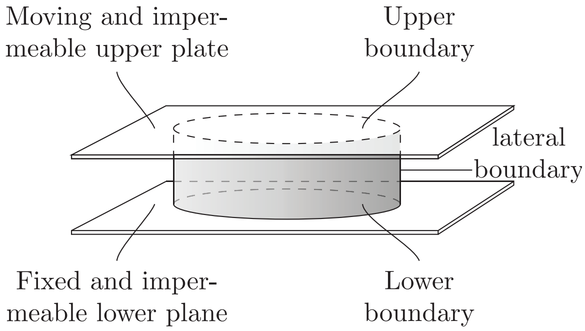

Figure 3.1: Panel describing the considered benchmark test

whole duration of the simulation. The lateral surface of the sample is assumed to constitute a free boundary, which means that both the pressure and the radial stress have to be equal to zero (see (3.53b) and (3.53e)).

We also have to impose boundary conditions on the fibre mean angle, $\mathfrak{q}$. These are specified by (3.53f) and (3.53g). The Dirichlet condition (3.53g) forces the fibres to remain orthogonal to the bone-cartilage interface for the whole duration of the simulation. Due to the geometry of the specimen and the symmetry of the problem, this restriction implies that, on the lower boundary, the fibres are maintained parallel to the specimen's symmetry axis. Furthermore, the Neumann condition (3.53f) requires that the normal component of $\boldsymbol{y}^{(1)} = \Phi_{1\mathrm{s}\nu} D_0 \boldsymbol{B}_{\mathrm{p}} \mathrm{Grad}\mathfrak{q}$ vanishes on the upper and lateral boundary of the sample. We notice that the coupling between $\mathfrak{q}$ and $\boldsymbol{F}_{\mathrm{p}}$, accounted for by $\boldsymbol{B}_{\mathrm{p}} = \boldsymbol{F}_{\mathrm{p}}^{-1}.\boldsymbol{F}_{\mathrm{p}}^{-\mathrm{T}}$, affects the way in which (3.53f) is satisfied and, consequently, the way in which $\mathfrak{q}$ approaches the boundary. Indeed, in the absence of plastic-like distortions, i.e., for $\boldsymbol{B}_{\mathrm{p}} = \boldsymbol{G}^{-1}$, (3.53f) requires that the normal derivative of $\mathfrak{q}$ is zero on $\partial\mathscr{B}_{\mathrm{U}} \sqcup \partial\mathscr{B}_{\ell}$. For $\boldsymbol{B}_{\mathrm{p}} \neq \boldsymbol{G}^{-1}$, this result is no longer true, and the gradient of $\mathfrak{q}$ is no longer orthogonal to $\boldsymbol{N}$.

Remark 3.4.1. To clarify the physical meaning of (3.53f), we recall that, in our model, $\mathfrak{q}$ and $\mathrm{Grad}\mathfrak{q}$ are kinematic descriptors and, consistently with (3.3), the vector $\boldsymbol{y}^{(1)}$ is the internal generalised force conjugated with $\mathrm{Grad}\mathfrak{q}$. Thus, $\boldsymbol{y}^{(1)}$ plays the role of stress and, as anticipated in (3.4b), $\boldsymbol{y}^{(1)}.\boldsymbol{N}$ is the stress component that has to balance the generalised "contact" force $h^{(1)}$, defined on the Neumann boundary of the sample. It follows from these considerations that (3.53f) rephrases (3.4b) in the particular case in which no such forces are active, thereby yielding $\boldsymbol{y}^{(1)}.\boldsymbol{N} = h^{(1)} = 0$. This amounts to say that $\partial\mathscr{B}_{\mathrm{U}} \sqcup \partial\mathscr{B}_{\ell}$ is a free boundary with respect to $\mathfrak{q}$.

3.5 Results

To perform a comparative study of the various phenomena accounted for in our work, we consider four different sub-models, which we denominate M1, M2, M3, and M4.

Model M1 (poroelasticity with $\mathscr{R}_\nu^{\text{ext}} = 0$) As reference case, we consider a deformable porelastic material, in which the evolution of the fibre direction is driven by deformation only. Thus, we solve (3.51a)–(3.51c), along with (3.53a)–(3.53i). In the computations we set $\mathscr{R}_\nu^{\text{ext}}$ equal to zero, which amounts to ignore in (3.51c) all the terms containing the target angle $\mathfrak{q}_T$. We do that with the aim of providing an estimate of the importance of the target angle on the guidance of the fibre evolution. Indeed, even in the absence of $\mathscr{R}_\nu^{\text{ext}}$, the inhomogeneity of the fibre mean angle and the generalised forces $\Phi_{1\text{s}\nu}\partial(\hat{W}_{1\text{a}} + \hat{W}_{\text{str}})/\partial\mathfrak{q}$ are capable of triggering the evolution of the fibres. By dealing with a poroelastic model, $\boldsymbol{V}$ is kept equal to its initial value, $\boldsymbol{G}^{-1}$, thereby switching off the evolution of the plastic-like distortions.

Model M2 (poroelasticity with $\mathscr{R}_\nu^{\text{ext}} \neq 0$) This case is the completion of the model M1, as fibre re-orientation is also driven by the target angle. To this end, we solve the same set of equations and initial and boundary conditions as implemented in M1. In M2, however, all the terms appearing in (3.51c) are activated, and $\mathfrak{q}_T$ is computed as

$$\mathfrak{q}_T = \arctan\left(\frac{1}{C_{\text{e}33}}\left[\frac{1}{2\pi}\int_0^{2\pi} \boldsymbol{C}_\text{e} : \mathfrak{e}_R(\varphi)\otimes\mathfrak{e}_R(\varphi)\,\text{d}\varphi\right]\right) = \arctan\left(\frac{\frac{1}{2}[C_{\text{e}11} + C_{\text{e}22}]}{C_{\text{e}33}}\right), \tag{3.56}$$

where $\mathfrak{e}_R(\varphi) = \cos\varphi\,\mathfrak{e}_1 + \sin\varphi\,\mathfrak{e}_2$ is a unit vector orthogonal to the specimen's symmetry axis, and oriented radially. Note that other definitions are possible. For example, one may define the target angle as a function of stress [64, 21, 127, 183] or as a function of the deformation [21]. The expression of $\mathfrak{q}_T$ given in (3.56) takes inspiration from [64, 21], and assumes that the target angle is entirely determined by $\boldsymbol{C}_\text{e}$. Specifically, the factor $\frac{1}{2}[C_{\text{e}11} + C_{\text{e}22}]$ is the in-plane directional average of the radial component of $\boldsymbol{C}_\text{e}$, while $C_{\text{e}33}$ is the axial component of $\boldsymbol{C}_\text{e}$. Under the considered loading conditions, (3.56) implies that, for increasing radial dilatation and increasing axial contraction, $\frac{1}{2}[C_{\text{e}11} + C_{\text{e}22}]/C_{\text{e}33}$ tends towards infinity, and $\mathfrak{q}_T$ tends towards $\pi/2$. In this limit, the target angle indicates that the fibres should be preferably aligned orthogonally to the specimen's symmetry axis. Clearly, the way in which the fibre mean angle complies with this condition is modulated both by the deformation and the plastic-like distortions. To us, another physically relevant situation occurs in the absence of deformation and elastic distortions, i.e., when

(3.56) prescribes $\mathfrak{q}_T = \pi/4$, and (3.51c) becomes

$$\Gamma\dot{\mathfrak{q}} = \mathrm{Div}[\Phi_{1\mathrm{s}\nu} D_0 \boldsymbol{G}^{-1}\mathrm{Grad}\mathfrak{q}] - \Phi_{1\mathrm{s}\nu}\mathscr{A}_0 \frac{\mathrm{d}\mathscr{P}}{\mathrm{d}\mathfrak{q}}. \tag{3.57}$$

In this case, the concept of target angle $\mathfrak{q}_T$ as manifestation of external force is not explicitly present in (3.57), and the evolution of $\mathfrak{q}$ is self-driven, with the target angles being identified with the stationary solutions of (3.57).

Model M3 (full model, with $\mathscr{R}_\nu^{\mathrm{ext}} = 0$) This case study is complete, since it requires to solve the whole set of the model equations (3.51a)–(3.51d) together with (3.53a)–(3.53g) and (3.53h)–(3.53j). However, as done in M1, in the computations we set $\mathscr{R}_\nu^{\mathrm{ext}}$ equal to zero.

Model M4 (full model) As for M3, also M4 describes the complete model and requires the solution of the same list of equations, with the same boundary and initial conditions. However, in M4 the target angle is accounted for.

Computational aspects To determine the numerical solution of our problem, we perform Finite Element simulations for each of the sub-models M1, M2, M3, and M4. This requires the weak formulation of (3.51a)–(3.51d), the generation of a grid for the discretisation of $\mathscr{B}$ and $\partial\mathscr{B}$, and the selection of a time integration scheme. Since the problem is nonlinear, a linearisation procedure is necessary. In general, the grid is unstructured and the interpolations adopted for p, χ, and $\mathfrak{q}$ are different from each other. Equation (3.51d) is solved only at the integration points of the finite element discretisation, for it does not contain partial derivatives of $\boldsymbol{V}$ with respect to the spatial variables. Hence, we do not provide any weak form for (3.51d), nor do we introduce in this work test functions associated with $\boldsymbol{V}$.

A Backward Euler scheme of the fifth order is used for the integration in time of all the model equations and boundary conditions. Moreover, in each sub-model, the directional averages of the constitutive functions are computed by employing the Spherical Design Algorithm (see e.g. [79, 126]) as implemented in [40], i.e., the integrals over $\mathbb{S}^2\mathscr{B}$ are evaluated for each time step and at each iteration of the Newton method.

In our work, the numerical simulations were performed with the aid of the commercial software COMSOL©v5.3. Details about the algorithms used for the Finite Element solution of a problem involving (3.51a), (3.51b), and an evolution equation similar to (3.51d) can be found in [112, 111].

Comments to figures Within the following discussion, we answer the research questions 3.1 and 3.2.To sample the data, we took four measuring points, located

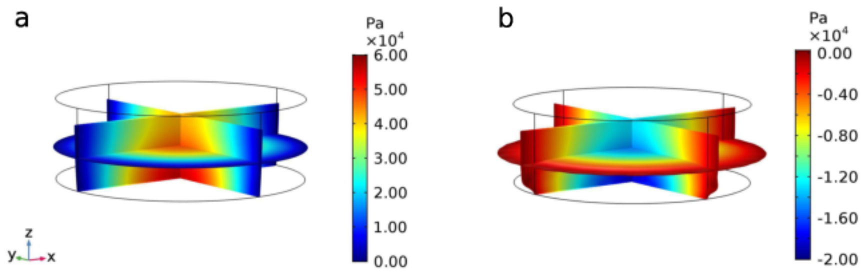

Figure 3.2: Pressure. 3D contour plots of the pressure for the models M2 (panel a) and M4 (panel b), whilst showing the deformation undergone by the tissue. The models M1 and M3 are not reported since they would lead to no observable difference with respect to M2 and M4, respectively.

along the vertical axis, and with Cartesian coordinates $X_L = (0{,}0, L)$, $X_{3L/4} = (0{,}0{,}3L/4)$, $X_{L/4} = (0{,}0, L/4)$, $X_0 = (0{,}0{,}0)$.

First of all, we present a three-dimensional view of the deformed tissue at the end of the loading history. Figure 3.2 depicts the differences in the deformation of the sample and in the pressure distribution for the models M2 and M4. The radial displacement of the tissue appears relatively contained in M2 (Fig. 3.2a), while it is more pronounced in M4, i.e., when plastic distortions are active (Fig. 3.2b). A peculiar characteristic of this case is given by the shape of the profile of the deformed lateral boundary. Indeed, in M2, such profile undergoes a gradual deformation from the bottom to the top, whereas in M4 it experiences an abrupt deformation close to the bottom, while it remains almost parallel to the symmetry axis in the middle and in the upper parts of the sample. A possible explanation of this phenomenon can be outlined through the analysis of the fibre mean angle, as shown in Fig. 3.5.

Another peculiarity of Fig. 3.2 concerns the values attained by the pressure. In contrast to the elastic case, when plastic-like distortions are accounted for, the pressure goes lower than zero, thereby leading to a “syringe effect” [61]. To better describe this phenomenon, Fig. 3.3 presents the time variation of the pressure in X_0. No significant differences can be observed for models M1 and M2, in which, after the increase due to the loading ramp, the pressure monotonically decreases toward zero. On the other hand, for both models accounting for the plastic-like distortions, i.e., M3 and M4, after a first rapid increase at the beginning of the loading experiment, we observed a rather slow increase of the pressure values. Afterwards, when the loading ramp terminates, we assist to an abrupt pressure drop, that leads to negative pressure values. This sudden change is then followed by a slow recovery, that would lead to null pressure in the long term.

A key point of this work is the role played by the fibre mean angle and by the target angle. To analyse their evolution we present Fig. 3.4. The top panels of Fig. 3.4 depict the evolution of the fibre mean angle, $\mathfrak{q}$, along the symmetry axis,

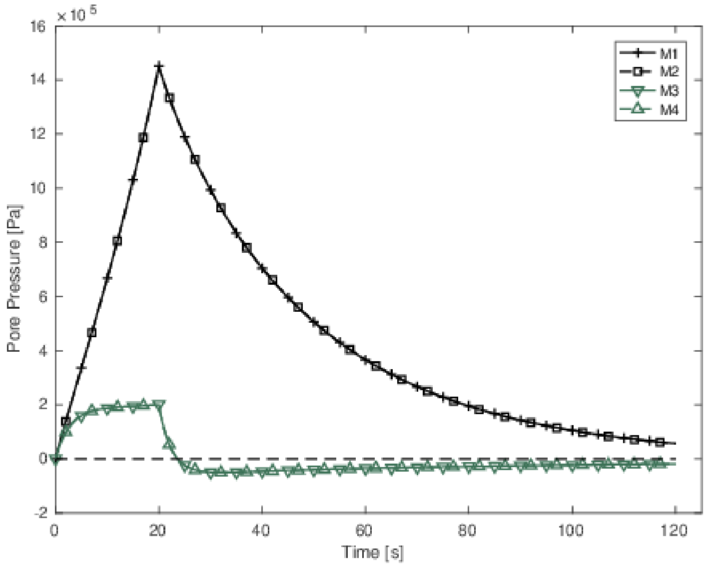

Figure 3.3: Time-evolution of the pore pressure. For all the implemented models, the temporal evolution of the pore pressure is monitored in X_0.

starting from the initial histological profile (3.53i), to the final fibre distribution obtained within M2 (Fig. 3.4a) and M4 (Fig. 3.4b). Note that, thanks to the upper boundary condition (3.53f), the value of $\mathfrak{q}$ corresponding to the upper surface is free to evolve. Interestingly, the greater variations are registered in the plastic case (M4) and, enhanced by the introduction of the gradient term, the variability extends to the tissue beneath. While in the middle-upper portion of the tissue we assist to a smooth change of the fibre mean angle, on the lower part there is quite an abrupt variation from the histological profile. This might be due to the Dirichlet boundary condition on the lower boundary of the specimen.

To understand the role of $\mathfrak{q}_T$ and to further describe the behaviour of $\mathfrak{q}$, the temporal evolution of the fibre mean angle is shown in the lower panels of Fig. 3.4, where the trend of the target angle $\mathfrak{q}_T$ is presented alongside the fibre mean angle, evaluated in two different sampling points. Indeed, by comparing M1 with M2, and M3 with M4, it is evident that the introduction of $\mathfrak{q}_T$ strongly modulates $\mathfrak{q}$ by controlling, and then by reducing, its variation, especially in M2. In particular, looking at Fig. 3.4d, we see how $\mathfrak{q}$ is driven upward by the presence of $\mathfrak{q}_T$ (M2 and M4), especially during the loading ramp.

Comparing Fig. 3.2 with Fig. 3.4c and Fig. 3.4d, we notice that the behaviour of $\mathfrak{q}$ influences the way in which the tissue deforms. Indeed, the more the variation of $\mathfrak{q}$ is contained in time, the less the sample tends to deform radially. This behaviour is model dependent and is more evident for M3 end M4 than it is for M1 and M2.

The analysis of the target angle is worth of a separate discussion. Once again,

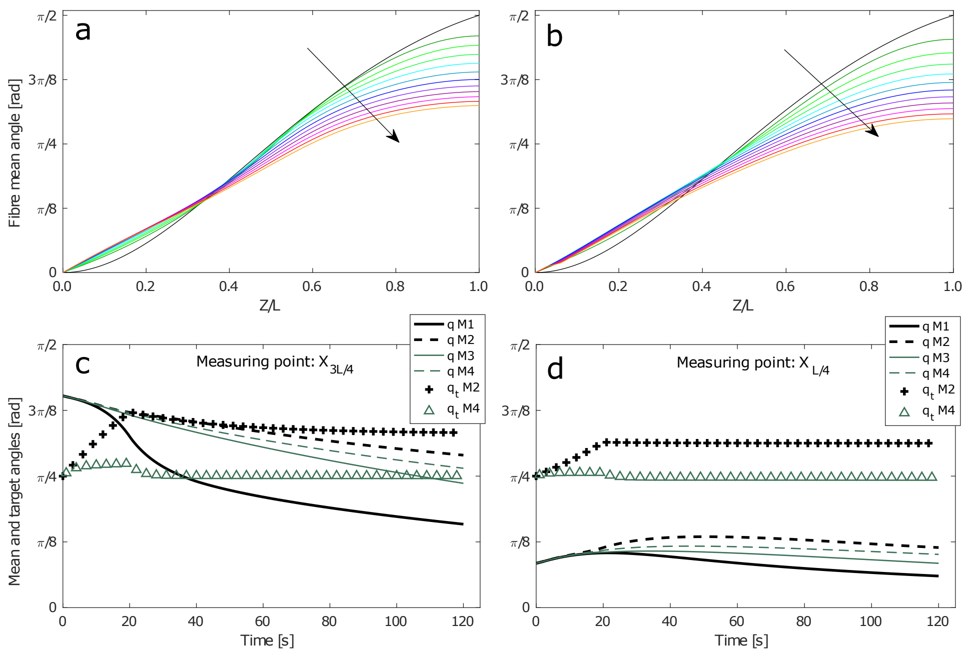

Figure 3.4: Fibre mean angle. In panels a and b, 10 seconds time-laps recording the evolution of the fibre mean angle along the vertical axis, for M2 (a) and M4 (b); arrows indicate the increase of time. In panels c and d, the temporal evolution of both the fibre mean angle and the target angle, observed in $X_{3L/4}$ (c) and $X_{L/4}$ (d), for all the presented models. The target angle is implemented in M2 and M4 only.

by making reference to Fig. 3.4c and Fig. 3.4d there are appreciable differences among the elastic and the plastic case studies, concerning both the evolution and the stationary limit of $\mathfrak{q}_T$. The most relevant variations of $\mathfrak{q}_T$ can be appreciated in M2, in which the relatively high values of the target angle, reached at the end of the loading ramp, seem to affect the stationary limit. In this case, different values of $\mathfrak{q}_T^\infty$ are recovered at a different depth. On the other hand, in M4 elastic distortions fade after the loading ramp, practically leading to the recovery of the stationary value $\pi/4$ throughout the whole tissue.

To complete the analysis, Fig. 3.5 depicts the norm of the deviatoric part of the effective stress tensor, i.e. $\|\mathrm{dev}\boldsymbol{\sigma}_{\mathrm{eff}}\|_{\boldsymbol{g}}$. With the exception of the bottom of the sample (see Fig. 3.5d), where the specimen is tied to the tidemark, $\|\mathrm{dev}\boldsymbol{\sigma}_{\mathrm{eff}}\|_{\boldsymbol{g}}$ reaches its maximum at the end of the loading ramp. The consequent decrease towards a stationary value is monotonic for the elastic cases M1 and M2, while it is not for the plastic models M3 and M4 (see Figs. 3.5a and 3.5c). In the insert of Figs. 3.5a and 3.5b, $\sqrt{2/3}\sigma_y$ is reported to highlight when and where plastic-like distortions are de-activated. In Fig. 3.5a we note that, after approximately 70 s, the effective stress is below the threshold $\sqrt{2/3}\sigma_y$, thereby implying a temporary

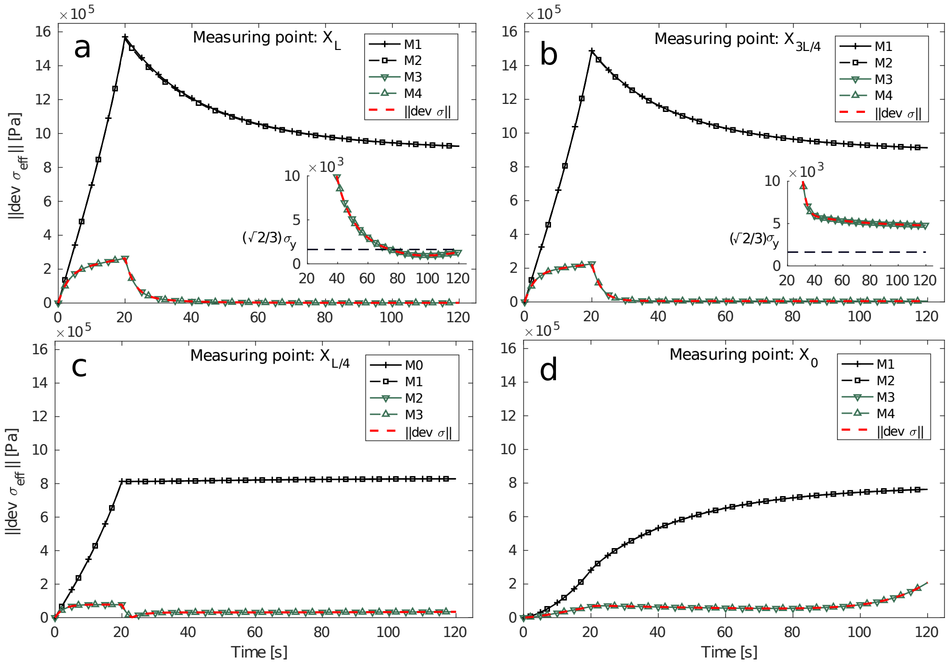

Figure 3.5: Effective stress tensor. For all the presented models, the norm of the effective stress tensor is evaluated in the measuring points X_L (a), $X_{3L/4}$ (b), $X_{L/4}$ (c) and X_0 (d).

switch-off of the plastic-like distortions. Figure 3.5 also reports $\|\mathrm{dev}\boldsymbol{\sigma}\|_{\boldsymbol{g}}$, evaluated for model M4. Although not visible at the length scale selected for our figures, we do measure differences between the effective stress, $\boldsymbol{\sigma}_{\mathrm{eff}}$, and the "standard" Cauchy stress $\boldsymbol{\sigma}$, which does not take into account $\boldsymbol{\Sigma}_{\mathrm{Grad}}$. In turn, $\boldsymbol{\Sigma}_{\mathrm{Grad}}$ is influenced by $\Phi_{1\mathrm{s}\nu}$ and $\boldsymbol{B}_{\mathrm{p}}$, and it vanishes gradually on the way to X_L, because of the Neumann zero boundary condition on $\mathfrak{q}$ on $\partial\mathscr{B}_{\mathrm{U}}$.

3.6 Discussion

The key aspect of our work is the mutual interaction among the motion, χ, the tensor of plastic-like distortions, $\boldsymbol{F}_{\mathrm{p}}$, and the fibre mean angle, $\mathfrak{q}$. Firstly, we notice that $\boldsymbol{F}_{\mathrm{p}}$ and $\mathfrak{q}$ interact with χ through the constitutive law expressing $\boldsymbol{P}_{\mathrm{sc}}$ in (3.51b). Secondly, χ and $\mathfrak{q}$ interact with $\boldsymbol{F}_{\mathrm{p}}$ through the term between parentheses in (3.51d). Such interaction manifests itself through $\boldsymbol{C}$ and $\boldsymbol{\Sigma}_{\mathrm{eff}}$. Thirdly, the interaction of χ and $\boldsymbol{F}_{\mathrm{p}}$ with $\mathfrak{q}$ finds its expression in the generalised forces $\Phi_{1\mathrm{s}\nu}[\partial(\hat{W}_{1\mathrm{a}}+\hat{W}_{\mathrm{str}})/\partial\mathfrak{q}]$. Finally, $\boldsymbol{F}_{\mathrm{p}}$ and $\mathfrak{q}$ interact with each other through $\Phi_{1\mathrm{s}\nu}D_0\boldsymbol{B}_{\mathrm{p}}\mathrm{Grad}\,\mathfrak{q}$, i.e., in such a way that only two players out of three interact.

Role played by the free energy density W_{Grad} In the form given in (3.17), W_{Grad} constitutes the lowest-order approximation of the self-interaction of the scalar field $\mathfrak{q}$. The strength of such self-interaction is measured by D_0. As in [108], we consider the particular case in which $\hat{W}_{\mathrm{Grad}}$ is independent of deformation, but we do allow it to depend on the plastic-like distortions through $\boldsymbol{B}_{\mathrm{p}}$, whose presence generates $\boldsymbol{\Sigma}_{\mathrm{Grad}}$. This tensor is purely configurational, and has no direct geometric counterpart, since it emerges as a consequence of the coupling between the structural degrees of freedom $\mathfrak{q}$ and $\boldsymbol{F}_{\mathrm{p}}$. More importantly, $\boldsymbol{\Sigma}_{\mathrm{Grad}}$ features as a summand of $\boldsymbol{\Sigma}_{\mathrm{eff}}$ among the configurational forces that drive the evolution law of the plastic-like distortions in (3.50). Hence, differently from other models on the subject (see e.g. [183]), in which the configurational stress that triggers remodelling can be obtained from Cauchy stress, in our theory we have the configurational force $\boldsymbol{\Sigma}_{\mathrm{Grad}}$ that exists on its own, and participates to activate the structural reorganisations of the tissue. In fact, it might be interpreted as the contribution to the structural reorganisation given by the reorientation of the fibres, i.e., the output of the interplay between $\boldsymbol{F}_{\mathrm{p}}$ and $\mathfrak{q}$ alone.

Role played by the free energy density W_{str} The energy density W_{str} defined in our model is such that the "structural" contribution to the overall second Piola-Kirchhoff stress tensor, $\boldsymbol{S}_{\mathrm{str}} = 2\Phi_{1\mathrm{s}\nu}(\partial\hat{W}_{\mathrm{str}}/\partial\boldsymbol{C}_{\mathrm{e}})$, and the "structural" contribution to the overall elasticity tensor, $\mathbb{C}_{\mathrm{str}} = 4(\partial^2\hat{W}_{\mathrm{str}}/\partial\boldsymbol{C}_{\mathrm{e}}^2)$ vanishes in the natural state. The function $\mathscr{A}_0\mathscr{P}(\mathfrak{q})$ coincides with the structural energy in the natural state, i.e., $\hat{W}_{\mathrm{str}}^{(0)}(\mathfrak{q}) = \mathscr{A}_0\mathscr{P}(\mathfrak{q})$. We notice that such functional form is adequate for describing large fluctuations of the order parameter $\mathfrak{q}$ from the two reference values $\mathfrak{q}_0 = 0$ and $\mathfrak{q}_1 = \pi/2$, each of which returns the global minimum of $\hat{W}_{\mathrm{str}}^{(0)}$, i.e., $\hat{W}_{\mathrm{str}}^{(0)}(0) = \hat{W}_{\mathrm{str}}^{(0)}(\pi/2) = 0$. As discussed in [108], an example of this behaviour is provided by the articular cartilage used for mechanical tests [85] in which, prior to the application of any loading history, a "histological profile" of the fibre mean angle can be defined [108, 85], which varies throughout the tissue, taking on the values $\mathfrak{q}_0$ and $\mathfrak{q}_1$ at the interface with the bone and at the articular surface, respectively [31].

One may wonder whether the introduction of W_{str} is really necessary and, if it is, why it should have the functional form suggested in this work. To answer these questions, let us first notice that there are studies in which the structural energy is tacitly used. Baaijens et al. [21], for example, prescribe that the fibre mean angle evolves according to the law

$$\dot{\mathfrak{q}} = -\tfrac{1}{\tau}[\mathfrak{q} - \mathfrak{q}_T], \tag{3.58}$$

where τ is a model parameter describing the system's relaxation coefficient, $\mathfrak{q}$ is the angle that the fibres in a blood vessel form with the symmetry axis, and the target angle, $\mathfrak{q}_T$, determines the preferred alignment of the fibres (in the case of a blood vessel, $2\mathfrak{q}$ is the angle between the two families of fibres coiled helically around the vessel). Looking at (3.58), and comparing it with our (3.44), which is obtained in the limit of vanishing D_0, we notice that (3.58) can be recovered from (3.44) by neglecting the force $\Phi_{1s\nu}(\partial \hat{W}_{1a}/\partial\mathfrak{q})$, and retaining only $\Phi_{1s\nu}(\partial \hat{W}_{\text{str}}/\partial\mathfrak{q})$, with the constitutive choice

$$\hat{W}_{\text{str}}(\mathfrak{q}) \equiv \hat{W}_{\text{str}}^{\text{quad}}(\mathfrak{q}) = \tfrac{1}{2}\kappa[\mathfrak{q} - \mathfrak{q}_{\text{ref}}]^2, \tag{3.59}$$

where the superscript "quad" stands for "quadratic", κ is an angular stiffness density (thus, having units of force per unit area), and $\mathfrak{q}_{\text{ref}}$ is a reference angle. Indeed, computing the derivative of $\hat{W}_{\text{str}}^{\text{quad}}$ with respect to $\mathfrak{q}$, and substituting the result into (3.44) yield

$$\Gamma\dot{\mathfrak{q}} = -\Phi_{1s\nu}\kappa[\mathfrak{q} - \mathfrak{q}_T], \tag{3.60}$$

and (3.58) is re-obtained upon identifying $1/\tau = \Phi_{1s\nu}\kappa/\Gamma$.

In the absence of deformation and plastic-like distortions, W_{std} vanishes identically, regardless of the value taken by $\mathfrak{q}$, and the energetic content of the tissue is the integral over $\mathscr{B}$ of the remodelling energy density

$$\hat{W}_{\text{rem}}^{(0)}(\mathfrak{q}, \text{Grad}\mathfrak{q}) = \tfrac{1}{2}\Phi_{1s\nu}D_0\|\text{Grad}\mathfrak{q}\|^2 + \Phi_{1s\nu}\hat{W}_{\text{str}}^{(0)}(\mathfrak{q}), \tag{3.61}$$

which is nonzero for $\mathfrak{q}$ other than the constant values $\mathfrak{q} = \mathfrak{q}_0$ and $\mathfrak{q} = \mathfrak{q}_1$ [108]. Hence, as reported in [108], the "natural state" of the tissue, which corresponds to the state of zero mechanical stress, is not necessarily its *ground state*, which is attained when the residual energy density $\hat{W}_{\text{rem}}^{(0)}$ reaches its global minimum. The ground state, in fact, is individuated by either $\mathfrak{q} = \mathfrak{q}_0$ or $\mathfrak{q} = \mathfrak{q}_1$, for which each term on the right-hand-side of (3.61) is identically null. In our case, the probability density, $\check{\Psi}(\vartheta, \mathfrak{q}_0)$, depicts the situation in which the fibres are most likely oriented along the tissue's symmetry axis, whereas $\check{\Psi}(\vartheta, \mathfrak{q}_1)$ describes the case in which the fibres tend to align themselves perpendicularly to the symmetry axis. Any other distribution of the fibre mean angle corresponds to a deviation from the ground state, and is associated with nontrivial energies. The coefficient $\mathscr{A}_0$ defines the height of the energy barrier that has to be overcome to pass from one ground state configuration, e.g. $\mathfrak{q}_0$, to the other one, $\mathfrak{q}_1$, or vice versa. In our model, such height is assumed to depend only on $\Phi_{1s\nu}$, which is point-dependent. However, when deformation and plastic-like distortions are active, we allow for a modulation of $\mathscr{A}_0$ by means of the terms between brackets in (3.15). Note that, since the directional average in (3.15) depends on $\mathfrak{q}$, the modulation also represents a self-interaction of the fibre-mean angle.

3.7 Conclusions

We proposed two conceptual results that, to the best of our knowledge, might be regarded as novelties: First, our calculations naturally lead to a Mandel-like stress tensor, denoted by $\boldsymbol{\Sigma}_{\mathrm{Grad}}$, which contributes to the onset and evolution of the plastic-like distortions. These, in turn, contribute to the evolution of the fibre mean angle through the term $\Phi_{1\mathrm{s}\nu} D_0 \boldsymbol{B}_{\mathrm{p}} \mathrm{Grad}\mathsf{q}$. Secondly, we define a structural energy that generalises some other choices available in the literature (see e.g. [21]). These results characterise the interplay between the reorientation of fibres and plastic-like distortions.

As anticipated above, our model can be used, with some modifications, for a generic tissue with fibre-reinforcement and evolving internal structure. The major strength of our model is its flexibility, since it establishes the “mathematical infrastructure” for describing transverse isotropy and for resolving interactions that are usually not resolved in more “classical” theories (see e.g. [21, 183, 116]). In turn, its major weakness is that it does not account for growth, which is crucial for tissues like cellular aggregates and tumours.

Describing growth requires to reformulate the present setting to consider different cell populations, include chemical substances, and account for the coupling among stress, structural reorganisation, and variation of mass. These modifications result in the introduction of an evolution equation for the inelastic distortions related to growth, and in one mass balance law for each chemical species and cell population considered in the model. All these equations should be combined with (3.51a)–(3.51d), and new interactions should be resolved. These also call for a review of the constitutive framework.

Another possible specific problem for which our theory could be useful is “inverse poroelasticity” [65]. Finally, the theory presented in this work could be compared with that developed by Capriz in [39], and this is subject of our current investigations.

By summarising the results obtained in this chapter, we answer the research questions 3.1—3.3 in the following way:

- Also in this case, the “syringe effect” is observed, thereby leading to a macroscopic change of the hydraulic properties of the tissue. The evolution of the fibre mean angle produces a contribution in the “effective Cauchy stress tensor”, which, in turns, is no longer monotonic. As a consequence of this behaviour, there exists an instant of time for which the effective stress is below its threshold value, which causes a temporary switch-off of the evolution of the plastic-like distortions.

- The visible deformation of the sample of the tissue is affected by the time and space evolution of the fibre mean angle. Indeed, the magnitude of the radial deformation of the tissue decreases with decreasing amplitude the time variation of $\mathfrak{q}$.

- In the model M2, the stationary limit of the target angle is influenced by the high values attained by the target angle itself when the loading ramp reaches the target displacement. In the model M4, the target angle is capable of recovering the stationary value $\pi/4$ throughout the whole tissue stationary value $\pi/4$ throughout the whole tissue, since the the elastic distortions diminish.

- An *effective Mandel stress tensor* arises from the chosen constitutive framework. In fact, the latter involves the coupling between the variables associated with the anelastic distortions and the gradient of the fibre mean angle (see Eqs. (3.21a), (3.21b) and (3.21c)).

Chapter 4

An Asymptotic Homogenisation Approach to the micro-structural evolution of heterogeneous media

The work reported in this chapter has been previously published in [205].

Note that in this Chapter, and only in this Chapter, we employ the symbol $\boldsymbol{H}$ to denote the "material gradient of the displacement".

4.1 Asymptotic Homogenisation and remodelling

In the present work, we apply the asymptotic homogenisation technique to the equations describing the dynamics of a heterogeneous material with evolving micro-structure, thereby obtaining a set of upscaled, effective equations. We consider the case in which the heterogeneous body comprises two hyperelastic materials and we assume that the evolution of their micro-structure occurs through the development of plastic-like distortions, the latter ones being accounted for by means of the Bilby-Kröner-Lee (BKL) decomposition. The asymptotic homogenisation approach is applied simultaneously to the linear momentum balance law of the body and to the evolution law for the plastic-like distortions. Such evolution law models a stress-driven production of inelastic distortions, and stems from phenomenological observations done on cellular aggregates. The whole study is also framed within the limit of small elastic distortions, and provide a robust framework that can be readily generalized to growth and remodelling of nonlinear composites. Finally, we complete our theoretical model by performing numerical simulations.

The study of material growth, remodelling and ageing is of great importance in Biomechanics, specially when the tissue, in which these processes occur, features a very complex structure, with different scales of observation and various constituents.

In the literature, the study of heterogeneous materials follows several approaches. In this work we focus on the multi-scale asymptotic homogenisation technique [20, 23, 28, 52, 214], which exploits the information available at the smallest scale characterizing the considered medium or phenomenon to obtain an effective description of the medium or phenomenon itself valid at its largest scale. This is achieved by expanding in asymptotic series the equations constituting the mathematical model formulated at the lowest scale. As a result, the coefficients of the effective governing equations encode the information on the other hierarchical levels, as they are to be computed solving micro structural problems at the smaller scales. The multi-scale asymptotic homogenisation approach has been successfully applied to investigate various physical systems due to its potentiality in decreasing the complexity of the problem at hand. Biomechanical applications of asymptotic homogenisation may be found mainly in nanomedicine [223], biomaterials modelling, such as the bone [185, 186], tissue engineering [75], poroelasticity [190], and active elastomers [191]. Most of the literature concerning applications of the asymptotic homogenisation technique focuses on linearised governing equations, as in this case it is possible to obtain, under a number of simplifying assumptions, a full decoupling between scales, which leads to a dramatic reduction in the computational complexity, as also noted for example in [191]. In fact, homogenisation in nonlinear mechanics is usually tackled via average field approaches based on representative volume elements or Eshelby-based techniques (see e.g. [141] for a comparison between the latter and asymptotic homogenisation), as done for example in [43]. These homogenisation approaches are typically well-suited when seeking for suitable bounds for the coefficients of the model, such as the elastic moduli, while asymptotic homogenisation can provide a precise characterization of the coefficients under appropriate regularity assumptions (namely, *local periodicity*).

However, to the best of our knowledge and understanding, there exists only a few examples, e.g. [54, 201, 211, 162], dealing with the asymptotic homogenisation in the case of media undergoing large deformations. In [201], the static micro-structural effects of periodic hyperelastic composites at finite strain are investigated. In [211], the interactions between large deforming solid and fluid media at the microscopic level are described by using the two-scale homogenisation technique and the updated Lagrangian formulation. In [54], the effective equations describing the flow, elastic deformation and transport in an active poroelastic medium were obtained. Therein, the authors considered the spatial homogenisation of a coupled transport and fluid-structure interaction model, incorporating details of the microscopic system and admitting finite growth and deformation at the pore scale. Some works can be also found dealing with homogenisation in the case of elastic perfectly plastic constituents [221, 226].

Here we embrace the asymptotic homogenisation approach and consider a heterogeneous body composed of two hyperelastic solid constituents subjected to the evolution of their internal structure. We refer to this phenomenon as to material remodelling and we interpret it with the production of plastic-like distortions. The wording “material remodelling” is used as a synonym of “evolution of the internal structure” of a tissue, and is intended in the sense of [55], who states that *“biological systems can adapt their structure* [...] *to accommodate a changed mechanical load environment”*. In this case, always in the terminology of [55] and [222], one speaks of *epigenetic* adaptation (or material remodelling). In the framework of the manuscript, such adaptation is assumed to occur through plastic-like distortions that represent processes like the redistribution of the adhesion bonds among the tissue cells.

It is worth to recall in which sense the concept of “plastic distortions”, conceived in the context of the Theory of Plasticity (cf. e.g. [161, 176]), and originally referred to non-living materials such as metals or soils, can be imported to describe the structural evolution of biological tissues. To this end, it is important to emphasize that the wording “plastic distortions” is understood as the result of a complex of transformations that conducts to the reorganization of the internal structure of a material, and that —as anticipated in the Introduction— such reorganization is referred to as “remodelling” in the biomechanical context.

The ways in which the structural transformations may take place in a given material depend on the structural properties of the material itself. For this reason, the plasticity in metals is markedly different from that occurring in amorphic materials. In the case of metals, indeed, for which the internal structure is granular and characterized by the arrangement of the atomic lattice within each grain, plastic distortions are the *macroscopic* manifestation of the formation and evolution of lattice defects. As reported in [176], such defects can be due, for example, to edge dislocations, wedge disclinations, missing atoms at some lattice sites, or to the presence of atoms in the lattice interstices. To describe how the defects evolve, thereby giving rise to the plastic distortions, one should compare the real lattice at the current instant of time with an ideal lattice, and decompose the overall deformation (i.e., shape change *and* structural transformation) into an elastic and an inelastic contribution [176]. The elastic contribution describes the part of deformation that is recoverable by completely relaxing mechanical stress, whereas the inelastic contribution represents the structural variation, which, in general, is of irreversible nature.

Clearly, metals have structural features markedly different from those of living matter. Still, some of the fundamental mechanisms that trigger the reorganization of their internal structure can be adapted to describe the remodelling of biological tissues.

For instance, in the case of bones, plastic-like phenomena are due to the formation of micro cracks that, in turn, favours the gliding of the material along the direction of the opening of the cracks [57]. Lastly, as anticipated above, in the case of biological tissues such as cellular aggregates, the phenomenon analogous to the generation of dislocations is the rearrangement of the adhesion bonds among the cells or the reorganization of the extracellular matrix due to the reorientation of the collagen fibres or their deposition and resorption, as is the case for blood vessels [154]. Also in all these situations, the comparison of the real configuration of the tissue with an "ideal" one, taken as reference, permits the separation of the overall deformation into an elastic part and a structure-related, "plastic-like" part.

Here, taking inspiration from the theory of finite Elastoplasticity [176, 218, 112], we describe the plastic-like distortions by invoking the Bilby-Kröner-Lee (BKL) decomposition of the deformation gradient tensor, and rephrasing it in a scale-dependent fashion. We remark that, at each of the medium's characteristic scales, a tensor of plastic distortions is introduced, which accounts for the fact that the structural variations of the medium cannot be expressed, in general, in terms of compatible deformations. Our study is conducted within a purely mechanical framework and under the assumption of negligible inertial forces. These hypotheses imply that the model equations reduce to a set comprising a scale-dependent, quasi-static law of balance of linear momentum and an evolution law for the tensor of plastic-like distortions. The latter one is assumed to obey a phenomenological flow rule driven by stress.

4.2 Theoretical background

4.2.1 Separation of scales

The homogenisation of a highly heterogeneous medium is only possible when the characteristic length of the the local structure (ℓ_0) and the characteristic length of the material, or of the phenomenon, of interest (L_0) are well separated. This condition of separation of scales can be expressed as

$$\varepsilon_0 := \frac{\ell_0}{L_0} \ll 1. \tag{4.1}$$

There may exist more than two coexisting scales and, if they are well separated from each other, a homogenisation approach is possible. In this case, we then move from the smallest scale to the largest one by homogenisation [4, 28, 163, 224, 207].

Condition (4.1) is taken as a base assumption for all homogenisation processes. The two characteristic length scales ℓ_0 and L_0 introduce two dimensionless spatial variables in the reference configuration, $\tilde{Y} = X/\ell_0$ and $\tilde{X} = X/L_0$, where X is said to be the *physical spatial variable*, whereas $\tilde{Y}$ and $\tilde{X}$ represent the microscopic and the macroscopic non-dimensional spatial variables, respectively. By using (4.1), $\tilde{Y}$ and $\tilde{X}$ can be related through the expression

$$\tilde{Y} = \varepsilon_0^{-1}\tilde{X}. \tag{4.2}$$

Given a field Φ defined over the region of interest of the heterogeneous medium, the separation of scales allows to rephrase the space dependence of Φ as $\Phi(X) =$

$\check{\Phi}(\tilde{X}(X), \tilde{Y}(X))$, and the spatial derivative of Φ takes thus the form

$$\mathrm{Grad}_X \Phi = L_0^{-1} \left(\mathrm{Grad}_{\tilde{X}} \check{\Phi} + \varepsilon_0^{-1} \mathrm{Grad}_{\tilde{Y}} \check{\Phi} \right). \tag{4.3}$$

By following this approach, all equations should be written in non-dimensional form. In the literature, the switch to the auxiliary variables $\tilde{X}$ and $\tilde{Y}$ is often omitted. However, as shown for example in [20], both paths are equivalent, provided that the dimensional formulation of the problem consistently accounts for any asymptotic behaviour of the involved fields and parameters (see e.g. [188] and the discussion therein concerning problems where such a behaviour is actually deduced via a non-dimensional analysis). By exploiting this result, in what follows, our analysis is carried out directly in a system of physical variables X and Y. Moreover, by adopting the approach usually followed in asymptotic multi scale analysis, we assume that each field and each material property characterizing the considered medium are functions of both X and Y, with $Y = \varepsilon_0^{-1} X$. Roughly speaking, the dependence on X captures the behaviour of a given physical quantity over the largest length-scale, while the dependence on Y captures the behaviour over the smallest one. We express this property by introducing the notation $\Phi^{\varepsilon}(X) = \Phi(X, \varepsilon_0^{-1} X) = \Phi(X, Y)$ [192]. Moreover, for a fixed X, we assume that $\Phi(X, Y)$ is periodic with respect to Y.

In the classical theory of two-scale asymptotic homogenisation [23, 28, 52], the small scaling dimensionless parameter ε_0 is constant. However, in the case of a composite material subjected to deformation and change of internal structure (as is the case, for instance, when plastic-like distortions occur), the characteristic macroscopic and microscopic lengths, which refer to the body and to its heterogeneities, respectively, depend on X and t, and should thus be denoted by $\ell(X, t)$ and $L(X, t)$. Therefore, the corresponding scaling parameter, obtained as the ratio $\varepsilon(X, t) = \ell(X, t)/L(X, t)$, is also a function of X and t, which need not be equal to ε_0 in general. This variability notwithstanding, if $\varepsilon(X, t)$ is bounded from above for all X and for all t, and if the upper bound is much smaller than unity, we can indicate such upper bound with ε, and use this constant as a scaling parameter for our asymptotic analysis.

4.2.2 Kinematics

Let us denote by $\mathcal{B}^{\varepsilon}$ a continuum body with periodic micro structure, and by $\mathcal{S}$ the three-dimensional Euclidean space. Furthermore, we denote by $\mathcal{B}_0^{\varepsilon}$ the reference, unloaded configuration of $\mathcal{B}^{\varepsilon}$, in which the body's periodic micro-structure is reproduced. Now, let us assume that $\chi^{\varepsilon} : \mathcal{B}_0^{\varepsilon} \times \mathcal{T} \to \mathcal{S}$ describes the motion of the heterogeneous body, where $\mathcal{T} = [t_0, t_f[$ is an interval of time. Then, the region occupied by the body at time $t \in \mathcal{T}$ is $\mathcal{B}_t^{\varepsilon} := \chi^{\varepsilon}(\mathcal{B}_0^{\varepsilon}, t) \subset \mathcal{S}$ and is said to be its current configuration. Each point $x \in \mathcal{B}_t^{\varepsilon}$ is such that $x = \chi^{\varepsilon}(X, t)$, with $X \in \mathcal{B}_0^{\varepsilon}$ being the point's reference placement. The deformation from $\mathcal{B}_0^{\varepsilon}$ to $\mathcal{B}_t^{\varepsilon}$ is characterized by the deformation gradient, $\boldsymbol{F}^\varepsilon(X,t)$, which is defined as $\boldsymbol{F}^\varepsilon(X,t) = T\chi^\varepsilon(X,t)$ [165], with $T\chi^\varepsilon$ being the tangent map of the motion χ^ε, defined from the tangent space $T_X\mathcal{B}_0^\varepsilon$ into $T_x\mathcal{S}$. In the sequel, however, since our focus is on Homogenisation Theory, we find it convenient to use the less formal definition

$$\boldsymbol{F}^\varepsilon = \boldsymbol{I} + \mathrm{Grad}\boldsymbol{u}^\varepsilon, \tag{4.4}$$

where $\boldsymbol{I}$ is the second-order identity tensor and $\mathrm{Grad}\boldsymbol{u}^\varepsilon$ denotes the gradient operator of the displacement $\boldsymbol{u}^\varepsilon$. The condition $J^\varepsilon = \det\boldsymbol{F}^\varepsilon > 0$ must be satisfied in order for χ^ε to be admissible. The symmetric, positive definite, second-order tensor $\boldsymbol{C}^\varepsilon = (\boldsymbol{F}^\varepsilon)^T\boldsymbol{F}^\varepsilon$ is the right Cauchy-Green deformation tensor induced by $\boldsymbol{F}^\varepsilon$. For our purposes, we partition $\mathcal{B}_0^\varepsilon$ into two sub-domains $\mathcal{B}_0^1$ and $\mathcal{B}_0^2$, such that $\bar{\mathcal{B}}_0^1 \cup \bar{\mathcal{B}}_0^2 = \bar{\mathcal{B}}_0^\varepsilon$ and $\bar{\mathcal{B}}_0^1 \cap \mathcal{B}_0^2 = \mathcal{B}_0^1 \cap \bar{\mathcal{B}}_0^2 = \emptyset$, where the bar over a set denotes its closure. We let Γ_0^ε stand for the interface between $\mathcal{B}_0^1$ and $\mathcal{B}_0^2$. Particularly, $\mathcal{B}_0^1$ denotes the matrix of $\mathcal{B}^\varepsilon$ (also referred to as *host phase*) and $\mathcal{B}_0^2$ a collection of N disjoint inclusions. The periodic cell in the reference configuration is denoted by $\mathcal{Y}_0$. The portion of matrix contained in $\mathcal{Y}_0$ is indicated by $\mathcal{Y}_0^1$, while $\mathcal{Y}_0^2$ is the inclusion in $\mathcal{Y}_0$. In each cell, $\mathcal{Y}_0^1$ and $\mathcal{Y}_0^2$ are such that $\bar{\mathcal{Y}}_0^1 \cup \bar{\mathcal{Y}}_0^2 = \bar{\mathcal{Y}}_0$ and $\bar{\mathcal{Y}}_0^1 \cap \mathcal{Y}_0^2 = \mathcal{Y}_0^1 \cap \bar{\mathcal{Y}}_0^2 = \emptyset$. The symbol Γ_0 indicates the interface between $\mathcal{Y}_0^1$ and $\mathcal{Y}_0^2$. In the present work, we assume that the periodicity of the body's micro-structure is preserved even though the body evolves by both changing its shape and varying its internal structure. In general, however, this is not the case. Clearly, our hypothesis is unrealistic in several circumstances, but it might be helpful to describe those situations in which the breaking of the material symmetries occurs at a scale different from those of interest, as is the case, for instance, when the plastic distortions occur in a tissue with evolving material properties [159], that are not directly related to the change of the tissue's micro-geometry. On the other hand, for nonperiodic media, the macro model is still valid when one assumes local boundedness. In that case, the coefficients are simply to be retrieved experimentally, as the "cell" problem is no longer to be computed on the cell but on the whole micro domain, which would be more complex than the original problem.

Moreover, we define $\chi_1^\varepsilon := \chi^\varepsilon|_{\mathcal{B}_0^1} : \mathcal{B}_0^1 \times \mathcal{T} \to \mathcal{S}$ such that $\mathcal{B}_t^1 := \chi_1^\varepsilon(\mathcal{B}_0^1, t)$ denotes the host phase at the current configuration and $\chi_2^\varepsilon := \chi^\varepsilon|_{\mathcal{B}_0^2} : \mathcal{B}_0^2 \times \mathcal{T} \to \mathcal{S}$, with $\mathcal{B}_t^2 := \chi_2^\varepsilon(\mathcal{B}_0^2, t)$ denoting the inclusions. Specifically, we enforce the condition $\bar{\mathcal{B}}_t^1 \cup \bar{\mathcal{B}}_t^2 = \bar{\mathcal{B}}_t^\varepsilon$, with $\bar{\mathcal{B}}_t^1 \cap \mathcal{B}_t^2 = \mathcal{B}_t^1 \cap \bar{\mathcal{B}}_t^2 = \emptyset$, and denote by Γ_t^ε the interface between $\mathcal{B}_t^1$ and $\mathcal{B}_t^2$. In addition, we let $\mathcal{Y}_t$ indicate the periodic cell in the current configuration, with $\bar{\mathcal{Y}}_t^1 \cup \bar{\mathcal{Y}}_t^2 = \bar{\mathcal{Y}}_t$, $\bar{\mathcal{Y}}_t^1 \cap \mathcal{Y}_t^2 = \mathcal{Y}_t^1 \cap \bar{\mathcal{Y}}_t^2 = \emptyset$, and with Γ_t being the interface between $\mathcal{Y}_t^1$ and $\mathcal{Y}_t^2$ (see Fig. 4.1). We emphasize that $\mathcal{Y}_t^1$ is the portion of matrix and $\mathcal{Y}_t^2$ is the inclusion in $\mathcal{Y}_t$. We note that inside a single cell it can be present also a collection of inclusions and, in such a case, we should consider multiple interface conditions [189].

4.2.3 "Multi scale" BKL decomposition

When the body $\mathcal{B}^\varepsilon$ is subjected to a system of external loads, the change of its shape could be accompanied by a rearrangement of its intrinsic structure. This process is generally inelastic and may not be described just in terms of deformation. Moreover, when mechanical agencies are removed, the body is generally unable to recover the unloaded configuration $\mathcal{B}_0^\varepsilon$, and may occupy a configuration characterized by the presence of residual stresses and strains. To bring the body into a fully relaxed state, an ideal tearing process has to be introduced [176]. More specifically, for each material point $X \in \mathcal{B}^\varepsilon$, we individuate a small neighbourhood of X, referred to as *body element*, we ideally cut it out from the body, and we let it relax until it reaches a stress-free state. Such state is the *ground state* of the relaxed body element and is called *natural state*. This concept, originally used in the theory of elasto-plasticity (see [161, 176]), has been used in the biomechanical context by various authors like, for instance,[72, 210, 106, 96, 95, 145, 183, 60, 176, 112, 61]. Before going further with the use of the BKL decomposition, we mention that, in the literature, there exist other approaches to the issue of residual stresses in biological tissues, which call neither for the multiplicative decomposition of the deformation gradient tensor, nor for the introduction of an "intermediate, relaxed configuration". One recent publication adhering to this philosophy is for example [49], in which the authors warn that the intermediate configuration may *"not exist in physical reality and must be postulated a priori"*. Although we are aware of the fact that a framework based on the BKL-decomposition may lead in some cases to assume unrealistic results —as any other framework would do—, we prefer here to adhere to the BKL approach for consistency with previous works of ours.

By performing the ideal process described above for all the body points, a collection of relaxed body pieces is obtained, in which each piece finds itself in its natural state. We denote such collection by $\mathcal{B}_\nu^\varepsilon$. In the language of continuum mechanics, these physical considerations lead to the BKL decomposition [176, 112]. Although summarizing these theoretical results is useful for sake of completeness, the consequences of the BKL decomposition are well-known, as it is one the pillars of Elastoplasticity. For this reason, we do not fuss over its theoretical justification, and we highlight, rather, the fact that one of the purposes of this work is to investigate the use of a scale-dependent BKL decomposition. In detail, by referring to Figure 4.1, we invoke a multiplicative decomposition of the deformation gradient $\boldsymbol{F}^\varepsilon$ that is parametrized by the scaling ratio ε, i.e.,

$$\boldsymbol{F}^\varepsilon = \boldsymbol{F}_\mathrm{e}^\varepsilon \boldsymbol{F}_\mathrm{p}^\varepsilon, \tag{4.5}$$

where the tensors $\boldsymbol{F}_\mathrm{e}^\varepsilon$ and $\boldsymbol{F}_\mathrm{p}^\varepsilon$ describe, respectively, the elastic and the inelastic distortions contributing to $\boldsymbol{F}^\varepsilon$ Along with (4.5), we also define the determinants $J_\mathrm{e}^\varepsilon = \det \boldsymbol{F}_\mathrm{e}^\varepsilon$ and $J_\mathrm{p}^\varepsilon = \det \boldsymbol{F}_\mathrm{p}^\varepsilon$, which are both strictly positive. Consistently with the notation introduced above, it holds true that $\boldsymbol{F}_\mathrm{e}^\varepsilon(X) = \boldsymbol{F}_\mathrm{e}(X, Y)$, $\boldsymbol{F}_\mathrm{p}^\varepsilon(X) =$

$\boldsymbol{F}_{\mathrm{p}}(X, Y)$, and $\boldsymbol{F}^{\varepsilon}(X) = \boldsymbol{F}(X, Y)$ as well as $J^{\varepsilon}_{\mathrm{e}}(X) = J_{\mathrm{e}}(X, Y)$ and $J^{\varepsilon}_{\mathrm{p}}(X) = J_{\mathrm{p}}(X, Y)$.

In this work, we focus on remodelling, i.e., plastic-like distortions that occur to modify the internal structure of $\mathcal{B}^{\varepsilon}$. Although this phenomenon is not visible, it could lead to the alteration of the mechanical properties of $\mathcal{B}^{\varepsilon}$.

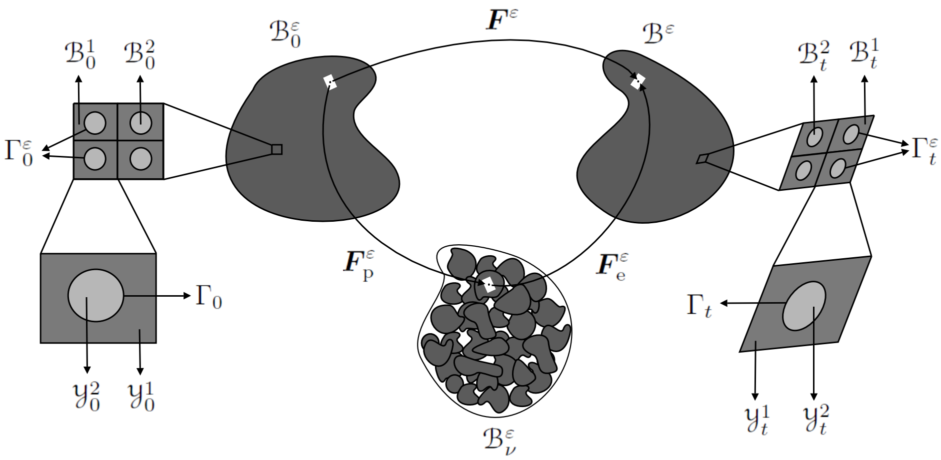

Figure 4.1: Schematic of a composite material with periodic internal micro-structure and subjected to inelastic remodelling distortions. From left to right: Magnification of an excerpt of material and description of its nested, periodic micro-structure. Change of shape of the body from the reference to the current configuration, and definition of the conglomerate of relaxed body pieces, each in its natural state. Magnification of an excerpt of material, taken from the body's current configuration, and description of its deformed, and remodelled, micro-structure.

4.3 Formulation of the problem

We consider a composite material comprising two solid constituents, whose point-wise constitutive response is hyperelastic. Therefore, to model its mechanical behaviour, we introduce the scale-dependent strain energy function, defined per unit volume of the natural state,

$$\check{\psi}_{\nu}(X, t) = \psi^{\varepsilon}_{\nu}(\boldsymbol{F}^{\varepsilon}_{\mathrm{e}}(X, t), i^{\varepsilon}(X, t)) = \psi_{\nu}(\boldsymbol{F}_{\mathrm{e}}(X, Y, t), i(X, Y, t)), \tag{4.6}$$

where i is defined by the expression $i(X, Y, t) = (X, Y)$, i.e., i extracts the spatial pair (X, Y) from the triplet (X, Y, t). From (4.6) we can derive the first Piola-Kirchhoff stress tensor,

$$\boldsymbol{P}^{\varepsilon} = J^{\varepsilon}_{\mathrm{p}} \frac{\partial \psi^{\varepsilon}_{\nu}}{\partial \boldsymbol{F}^{\varepsilon}_{\mathrm{e}}} \left(\boldsymbol{F}^{\varepsilon}_{\mathrm{p}}\right)^{-\mathrm{T}}, \tag{4.7}$$

where $J_{\mathrm{p}}^{\varepsilon} = \det \boldsymbol{F}_{\mathrm{p}}^{\varepsilon}$. In particular, if we neglect body forces and inertial terms, the balance of linear momentum reads,

$$\begin{cases} \operatorname{Div} \boldsymbol{P}^{\varepsilon} = \boldsymbol{0}, & \text{in } \mathcal{B}_0^{\varepsilon} \setminus \Gamma_0^{\varepsilon} \times \mathcal{T}, \\ \boldsymbol{P}^{\varepsilon} \cdot \boldsymbol{N} = \bar{\boldsymbol{P}}, & \text{on } \partial_T \mathcal{B}_0^{\varepsilon} \times \mathcal{T}, \\ \boldsymbol{u}^{\varepsilon} = \bar{\boldsymbol{u}}, & \text{on } \partial_u \mathcal{B}_0^{\varepsilon} \times \mathcal{T}, \end{cases} \tag{4.8}$$

where $\bar{\boldsymbol{P}}$ and $\bar{\boldsymbol{u}}$ are, respectively, the prescribed traction and displacement on the boundary $\partial \mathcal{B}_0^{\varepsilon} = \partial_T \mathcal{B}_0^{\varepsilon} \cup \partial_u \mathcal{B}_0^{\varepsilon}$ with $\overline{\partial_T \mathcal{B}_0^{\varepsilon}} \cap \partial_u \mathcal{B}_0^{\varepsilon} = \partial_T \mathcal{B}_0^{\varepsilon} \cap \overline{\partial_u \mathcal{B}_0^{\varepsilon}} = \emptyset$ and $\boldsymbol{N}$ is the outward unit vector normal to the surface $\partial \mathcal{B}_0^{\varepsilon}$. Continuity conditions for displacement and traction are imposed,

$$[\![\boldsymbol{u}^{\varepsilon}]\!] = \boldsymbol{0} \quad \text{and} \quad [\![\boldsymbol{P}^{\varepsilon} \cdot \boldsymbol{N}_{\mathcal{Y}}]\!] = \boldsymbol{0}, \quad \text{on } \Gamma_0 \times \mathcal{T}, \tag{4.9}$$

where $[\![\bullet]\!]$ denotes the jump across the interface between the two constituents and $\boldsymbol{N}_{\mathcal{Y}}$ defines the unit outward normal to Γ_0. Moreover, problem (4.8) must be supplemented with an appropriate evolution law for $\boldsymbol{F}_{\mathrm{p}}^{\varepsilon}$. It is worth mentioning that the homogenisation process can be performed regardless of the particular choice of *external* boundary conditions (Dirichlet-Neumann in this case). This means that the formulation presented in this work is potentially applicable also to other external boundary conditions, such as e.g. those of Robin-type. This is due to the fact that, as pointed out in [207], also in the present study the homogenisation is applied in regions sufficiently far away from the outer boundary of the considered medium. For problems in which it is necessary to homogenize also close to the outer heterogeneous boundaries, we refer to [28, 184, 152].

Remark 4.3.1. In the present work, we impose conditions (4.9) for displacements and tractions just to exemplify the homogenisation technique applied to heterogeneous media with evolving micro structure. In other words, we assume that the contact interface between the constituents is ideal. This means that the displacements are congruent, and thus continuous, and that linear momentum is conserved across the interface, which in our context, implies the continuity of the tractions. However, the hypothesis of the ideal interface can be relaxed in some biological situations. For instance, in cancerous tissues, there exist cross-links between normal and malignant cells, whose density and strength determine a spring constant that relates the normal stresses on each cell surface, thereby making it non-ideal [153, 125]. Another example of non-ideal interface is the periodontal ligament, which represents the thin layer between the cementum of the tooth to the adjacent alveolar bone [101]. In the context of composite materials, when non-ideal interfaces are accounted for, the interface conditions are suitably reformulated [128, 129, 30, 29]. In particular, the asymptotic homogenisation technique has been applied for linear elastic periodic fibre reinforced composites with imperfect contact between matrix and fibres (see e.g. [121]).

4.4 Asymptotic homogenisation of the balance of linear momentum

A formal two-scale asymptotic expansion is performed for the displacement $\boldsymbol{u}^{\varepsilon}$, which thus reads

$$\boldsymbol{u}^{\varepsilon}(X,t) = \boldsymbol{u}^{(0)}(X,t) + \sum_{k=1}^{+\infty} \boldsymbol{u}^{(k)}(X,Y,t)\varepsilon^{k}, \tag{4.10}$$

where, for all $k \geq 1$, $\boldsymbol{u}^{(k)}$ is periodic with respect to Y. Following [201] we consider the leading order term of the expansion (4.10) to be independent of the fast variable Y. From formula (4.4), the expansion (4.10), and taking into account the property of scale separation, it follows that the deformation gradient tensor can be written as

$$\boldsymbol{F}^{\varepsilon}(X,t) = \sum_{k=0}^{+\infty} \boldsymbol{F}^{(k)}(X,Y,t)\varepsilon^{k}, \tag{4.11}$$

with the notation

$$\boldsymbol{F}^{(0)} := \boldsymbol{I} + \mathrm{Grad}_X \boldsymbol{u}^{(0)} + \mathrm{Grad}_Y \boldsymbol{u}^{(1)}, \tag{4.12a}$$

$$\boldsymbol{F}^{(k)} := \mathrm{Grad}_X \boldsymbol{u}^{(k)} + \mathrm{Grad}_Y \boldsymbol{u}^{(k+1)}, \quad \forall\, k \geq 1, \tag{4.12b}$$

where Grad_X and Grad_Y are the gradient operators with respect to X and Y, respectively. Now, the following two-scale asymptotic expansion is proposed for the first Piola-Kirchhoff stress tensor $\boldsymbol{P}^{\varepsilon}$,

$$\boldsymbol{P}^{\varepsilon}(X,t) = \sum_{k=0}^{+\infty} \boldsymbol{P}^{(k)}(X,Y,t)\varepsilon^{k}, \tag{4.13}$$

where the fields $\boldsymbol{P}^{(k)}$ are periodic with respect to Y. By substituting the power series representation (4.13) into (4.8), using the scale separation condition, and multiplying the result by ε, the following multi-scale system is obtained

$$\mathrm{Div}\, \boldsymbol{P}^{\varepsilon} = \sum_{k=0}^{+\infty} \mathfrak{D}^{(k)}\varepsilon^{k} = \boldsymbol{0}, \tag{4.14}$$

with

$$\mathfrak{D}^{(0)} := \mathrm{Div}_Y \boldsymbol{P}^{(0)}, \tag{4.15a}$$

$$\mathfrak{D}^{(k)} := \mathrm{Div}_X \boldsymbol{P}^{(k-1)} + \mathrm{Div}_Y \boldsymbol{P}^{(k)}, \quad \forall\, k \geq 1. \tag{4.15b}$$

We require that the equilibrium equation (4.14) is satisfied at every ε, which amounts to impose the conditions

$$\mathrm{Div}_Y \boldsymbol{P}^{(0)} = \boldsymbol{0}, \tag{4.16a}$$

$$\mathrm{Div}_X \boldsymbol{P}^{(k-1)} + \mathrm{Div}_Y \boldsymbol{P}^{(k)} = \mathbf{0}, \quad \forall\, k \geq 1. \tag{4.16b}$$

At this point we introduce the average operator over the microscopic cell, i.e.

$$\langle \bullet \rangle = \frac{1}{|\mathcal{Y}_t|} \int_{\mathcal{Y}_t} \bullet \, \mathrm{d}Y, \tag{4.17}$$

where $|\mathcal{Y}_t|$ represents the volume of the periodic cell $\mathcal{Y}_t$ at time t. Indeed, because of the deformations and distortions to which the microscopic, reference periodic cell is subjected, $\mathcal{Y}_t$ is different at every time instant. Averaging (4.16b) over the microscopic cell yields, for $k = 1$,

$$\langle \mathrm{Div}_X \boldsymbol{P}^{(0)} \rangle + \frac{1}{|\mathcal{Y}_t|} \int_{\partial \mathcal{Y}_t} \boldsymbol{P}^{(1)} \cdot \boldsymbol{N} \mathrm{d}Y = \mathbf{0}, \tag{4.18}$$

where, on the left-hand side, we have applied the divergence theorem. Since the contributions on the periodic cell boundary $\partial\mathcal{Y}_t$ cancel due to the Y-periodicity, the integral over $\mathcal{Y}_t$ is equal to zero, and (4.18) becomes

$$\langle \mathrm{Div}_X \boldsymbol{P}^{(0)} \rangle = \mathbf{0}. \tag{4.19}$$

Here, we restrict our analysis to the particular case in which the periodic cell can be uniquely chosen independently of X, which implies that the integration over $\mathcal{Y}_t$ and the computation of the divergence commute. This assumption is also referred to as *macroscopic uniformity*, see also [35, 137, 187] for examples dealing with non-macroscopically uniform media in the context of poroelasticity and diffusion. Therefore, Equation (4.19) can be recast as

$$\mathrm{Div}_X \langle \boldsymbol{P}^{(0)} \rangle = \mathbf{0}. \tag{4.20}$$

Equations (4.16a) and (4.20) represent, respectively, the local and the homogenised equation associated with the original one, stated in (4.8). Both equations still need to be supplemented with the corresponding interface, boundary, and initial conditions. Note that, although both problems feature no time derivative, initial conditions are required because $\boldsymbol{P}^{(0)}$ depends on the variable $\boldsymbol{F}_{\mathrm{p}}^{(0)}$, which satisfies an evolution equation in time.

We remark that the leading term $\boldsymbol{P}^{(0)} = \boldsymbol{P}^{(0)}(X, Y, t)$ of the multi-scale expansion (4.13) is the unknown, both in (4.16a) and in (4.20). To identify $\boldsymbol{P}^{(0)}$, we propose here to expand $\boldsymbol{F}_{\mathrm{p}}^{\varepsilon}$ and ψ_ν^{ε} as

$$\boldsymbol{F}_{\mathrm{p}}^{\varepsilon}(X, t) = \sum_{k=0}^{+\infty} \boldsymbol{F}_{\mathrm{p}}^{(k)}(X, Y, t)\varepsilon^k, \tag{4.21a}$$

$$\psi_\nu^{\varepsilon}(X, t) = \sum_{k=0}^{+\infty} \psi_\nu^{(k)}(\boldsymbol{F}_{\mathrm{e}}(X, Y, t), X, Y)\varepsilon^k, \tag{4.21b}$$

where $\boldsymbol{F}_{\mathrm{p}}^{(k)}$ and $\psi_\nu^{(k)}$ are periodic in Y. By using (4.5), (4.11) and (4.21a), we can deduce a series expansion for $\boldsymbol{F}_{\mathrm{e}}^{\varepsilon}$ in powers of ε, where the leading order term $\boldsymbol{F}_{\mathrm{e}}^{(0)}$ is given by

$$\boldsymbol{F}_{\mathrm{e}}^{(0)} = \boldsymbol{F}^{(0)}(\boldsymbol{F}_{\mathrm{p}}^{(0)})^{-1}. \tag{4.22}$$

Following [54] and [201], $\boldsymbol{P}^{(0)}$ is therefore supplied constitutively as

$$\boldsymbol{P}^{(0)} = J_{\mathrm{p}}^{(0)} \frac{\partial \psi_\nu^{(0)}}{\partial \boldsymbol{F}_{\mathrm{e}}^{(0)}} (\boldsymbol{F}_{\mathrm{p}}^{(0)})^{-\mathrm{T}}, \tag{4.23}$$

with $\psi_\nu^{(0)} = \psi_\nu^{(0)}(\boldsymbol{F}_{\mathrm{e}}^{(0)}(X,Y,t),X,Y)$ and $J_{\mathrm{p}}^{(0)} = \det \boldsymbol{F}_{\mathrm{p}}^{(0)}$. To obtain the *cell problem*, equation (4.14) must be supplemented with the corresponding interface conditions. This is done by substituting the asymptotic expansions of $\boldsymbol{u}^\varepsilon$ and of $\boldsymbol{P}^\varepsilon$ into the interface conditions $[\![\boldsymbol{u}^\varepsilon]\!] = \boldsymbol{0}$ and $[\![\boldsymbol{P}^\varepsilon \cdot \boldsymbol{N}_{\mathcal{Y}}]\!] = \boldsymbol{0}$. Both conditions are satisfied at any order of ε. At the order ε^0, we simply obtain $[\![\boldsymbol{P}^{(0)} \cdot \boldsymbol{N}_{\mathcal{Y}}]\!] = \boldsymbol{0}$ for the stresses, and that the condition $[\![\boldsymbol{u}^{(0)}]\!] = \boldsymbol{0}$ is trivially satisfied, because $\boldsymbol{u}^{(0)}$ depends solely on X and t. Thus, the interface condition on the displacements is written only for $\boldsymbol{u}^{(1)}$ and reads, $[\![\boldsymbol{u}^{(1)}]\!] = \boldsymbol{0}$. By summarizing these results, the cell problem at zero order of the epsilon parameter can be stated as

$$\begin{cases} \mathrm{Div}_Y \boldsymbol{P}^{(0)} = \boldsymbol{0}, & \text{in } \mathcal{Y}_0 \setminus \Gamma_0 \times \mathcal{T}, \\ [\![\boldsymbol{u}^{(1)}]\!] = \boldsymbol{0}, & \text{on } \Gamma_0 \times \mathcal{T}, \\ [\![\boldsymbol{P}^{(0)} \cdot \boldsymbol{N}_{\mathcal{Y}}]\!] = \boldsymbol{0}, & \text{on } \Gamma_0 \times \mathcal{T}. \end{cases} \tag{4.24}$$

Together with the cell problem, we also need to formulate the macro-scopic homogenised problem. To this end, we take equation (4.20) and complete it with a set of boundary conditions. This is done by substituting the asymptotic expansions of $\boldsymbol{P}^\varepsilon$ and $\boldsymbol{u}^\varepsilon$ into the boundary conditions $\boldsymbol{P}^\varepsilon \cdot \boldsymbol{N} = \bar{\boldsymbol{P}}$ and $\boldsymbol{u}^\varepsilon = \bar{\boldsymbol{u}}$, respectively. Thus, equating the coefficients at order ε^0, and averaging the results over the unit cell, we find the *homogenised problem*,

$$\begin{cases} \mathrm{Div}_X \langle \boldsymbol{P}^{(0)} \rangle = \boldsymbol{0}, & \text{in } \mathcal{B}_h \times \mathcal{T}, \\ \langle \boldsymbol{P}^{(0)} \rangle \cdot \boldsymbol{N} = \bar{\boldsymbol{P}}, & \text{on } \partial_T \mathcal{B}_h \times \mathcal{T}, \\ \boldsymbol{u}^{(0)} = \bar{\boldsymbol{u}}, & \text{on } \partial_u \mathcal{B}_h \times \mathcal{T}, \end{cases} \tag{4.25}$$

where $\mathcal{B}_h$ denotes the homogeneous macro-scale domain in which the homogenised equations are defined.

The problem (4.25) has to be solved along with a homogenised evolution equation for $\boldsymbol{F}_{\mathrm{p}}^{(0)}$ and the initial condition associated with it. In addition, we remark that, according to (4.25), the boundary tractions acting on $\partial_T \mathcal{B}_h$ are balanced *only* by the normal component of the average of the leading order stress, $\boldsymbol{P}^{(0)}$, and *only* the leading order displacement, $\boldsymbol{u}^{(0)}$, has to be equal to the displacement $\bar{\boldsymbol{u}}$, imposed on $\partial_u \mathcal{B}_h$.

Remark 4.4.1. In the medical scientific literature, there exist studies that identify the existence of anatomical boundary layers interposed between the brain surface and tumours (see e.g. [208]). Here we do not address boundary layer phenomena, which are usually neglected in the asymptotic homogenisation literature. The homogenisation process described in this work is fine for regions far enough away from the boundary so that its effect is not felt because, close to the boundaries, the material will not behave as an effective material with homogenised coefficients. To properly account for boundary effects, the so-called boundary-layer technique could be used [28, 184].

4.5 Constitutive framework and evolution law

In this section, we prescribe a constitutive equation for the response of the material and, independently, an evolution equation for the tensor of plastic-like distortions.

4.5.1 Constitutive law

In the following, we formulate the local and homogenised problems for a specific constitutive law. In general, this process can be rather cumbersome for complicated strain energy densities, and it becomes even more involved when plastic-like distortions are accounted for. To reduce complexity, we choose a very simple constitutive law for ψ_ν^ε, such as the De Saint-Venant strain energy density,

$$\psi_\nu^\varepsilon = \frac{1}{2}\boldsymbol{E}_{\mathrm{e}}^\varepsilon : \mathscr{C}^\varepsilon : \boldsymbol{E}_{\mathrm{e}}^\varepsilon, \tag{4.26}$$

where $\boldsymbol{E}_{\mathrm{e}}^\varepsilon = \frac{1}{2}\Big((\boldsymbol{F}_{\mathrm{e}}^\varepsilon)^T \boldsymbol{F}_{\mathrm{e}}^\varepsilon - \boldsymbol{I}\Big)$ is the elastic Green-Lagrange strain tensor and $\mathscr{C}^\varepsilon(X) = \mathscr{C}(X, Y)$ is the positive definite fourth-order elasticity tensor, which satisfies both major and minor symmetries, i.e. $\mathscr{C}_{ijkl} = \mathscr{C}_{jikl} = \mathscr{C}_{ijlk} = \mathscr{C}_{klij}$. Particularly, we consider that the constituents of the heterogeneous material are isotropic, and thus

$$\mathscr{C}^\varepsilon = 3\kappa^\varepsilon \mathscr{K} + 2\mu^\varepsilon \mathscr{M}, \tag{4.27}$$

where $\kappa^\varepsilon(X) = \kappa(X, Y)$ is the bulk modulus, $\mu^\varepsilon(X) = \mu(X, Y)$ is the shear modulus, and the fourth-order tensors $\mathscr{K} = \frac{1}{3}(\boldsymbol{I} \otimes \boldsymbol{I})$ and $\mathscr{M} = \mathscr{I} - \mathscr{K}$ extract the spherical and the deviatoric part, respectively, of a symmetric second-order tensor $\boldsymbol{A}$, i.e., $\mathscr{K} : \boldsymbol{A} = \frac{1}{3}\mathrm{tr}(\boldsymbol{A})\boldsymbol{I}$ and $\mathscr{M} : \boldsymbol{A} = \boldsymbol{A} - \frac{1}{3}\mathrm{tr}(\boldsymbol{A})\boldsymbol{I} := \mathrm{dev}(\boldsymbol{A})$ [231, 232]. We remark that the fourth-order identity tensor $\mathscr{I}$ is the identity operator over the linear subspace of symmetric second-order tensors. Indeed, for every $\boldsymbol{A}$ such that $\boldsymbol{A} = \boldsymbol{A}^{\mathrm{T}}$, it holds that $\mathscr{I} : \boldsymbol{A} = \boldsymbol{A}$. In terms of $\boldsymbol{I}$, an explicit expression of $\mathscr{I}$ is given by $\mathscr{I} = \frac{1}{2}\left[\boldsymbol{I}\underline{\otimes}\boldsymbol{I} + \boldsymbol{I}\overline{\otimes}\boldsymbol{I}\right]$ (in components: $\mathscr{I}_{ijkl} = \frac{1}{2}\left[I_{ik}I_{jl} + I_{il}I_{jk}\right]$ [57]).

We can identify the leading order term in the expansion of the constitutive law (4.26), which reads

$$\psi_\nu^{(0)} = \frac{1}{2}\boldsymbol{E}_{\mathrm{e}}^{(0)} : \mathscr{C} : \boldsymbol{E}_{\mathrm{e}}^{(0)}, \tag{4.28}$$

with $\boldsymbol{E}_{\mathrm{e}}^{(0)} = \frac{1}{2}\left((\boldsymbol{F}_{\mathrm{e}}^{(0)})^{\mathrm{T}}\boldsymbol{F}_{\mathrm{e}}^{(0)} - \boldsymbol{I}\right)$. We recall that, although the expression of $\psi_\nu^{(0)}$ in (4.28) depends only on $\boldsymbol{E}_{\mathrm{e}}^{(0)}$, the material coefficient $\mathscr{C}$ is still a two-scale function and should be thus interpreted as $\mathscr{C}(X, Y)$. As a consequence, $\psi_\nu^{(0)}$ is not homogenised yet.

By taking into account the major and minor symmetries of $\mathscr{C}$, we obtain

$$\boldsymbol{S}_\nu^{(0)} = \frac{\partial \psi_\nu^{(0)}}{\partial \boldsymbol{E}_{\mathrm{e}}^{(0)}} = \mathscr{C} : \boldsymbol{E}_{\mathrm{e}}^{(0)} = \lambda \mathrm{tr}(\boldsymbol{E}_{\mathrm{e}}^{(0)})\boldsymbol{I} + 2\mu \boldsymbol{E}_{\mathrm{e}}^{(0)}, \tag{4.29}$$

where $\boldsymbol{S}_\nu^{(0)}$ is the leading order term of the second Piola-Kirchhoff stress tensor written with respect to the natural state, $\lambda = \kappa - \frac{2}{3}\mu$ is Lamé's constant, and $\boldsymbol{E}_{\mathrm{e}}^{(0)}$ is given by

$$\boldsymbol{E}_{\mathrm{e}}^{(0)} = (\boldsymbol{F}_{\mathrm{p}}^{(0)})^{-\mathrm{T}}\left(\boldsymbol{E}^{(0)} - \boldsymbol{E}_{\mathrm{p}}^{(0)}\right)(\boldsymbol{F}_{\mathrm{p}}^{(0)})^{-1}, \tag{4.30}$$

with $\boldsymbol{E}^{(0)} = \frac{1}{2}\left((\boldsymbol{F}^{(0)})^{\mathrm{T}}\boldsymbol{F}^{(0)} - \boldsymbol{I}\right)$ and $\boldsymbol{E}_{\mathrm{p}}^{(0)} = \frac{1}{2}\left((\boldsymbol{F}_{\mathrm{p}}^{(0)})^{\mathrm{T}}\boldsymbol{F}_{\mathrm{p}}^{(0)} - \boldsymbol{I}\right)$.

By pulling $\boldsymbol{S}_\nu^{(0)}$ back to the reference configuration, and recalling that the plastic-like distortions are assumed to be isochoric in our framework, (i.e. $J_{\mathrm{p}}^{\varepsilon} = 1$), we obtain the second Piola-Kirchhoff stress tensor

$$\boldsymbol{S}^{(0)} = \mathscr{C}_{\mathrm{R}} : (\boldsymbol{E}^{(0)} - \boldsymbol{E}_{\mathrm{p}}^{(0)}), \tag{4.31}$$

where

$$\begin{aligned}\mathscr{C}_{\mathrm{R}} &= (\boldsymbol{F}_{\mathrm{p}}^{(0)})^{-1} \underline{\otimes} (\boldsymbol{F}_{\mathrm{p}}^{(0)})^{-1} : \mathscr{C} : (\boldsymbol{F}_{\mathrm{p}}^{(0)})^{-\mathrm{T}} \underline{\otimes} (\boldsymbol{F}_{\mathrm{p}}^{(0)})^{-\mathrm{T}} \\ &= 3\lambda \mathscr{K}_{\mathrm{p}}^{(0)} + 2\mu \mathscr{I}_{\mathrm{p}}^{(0)},\end{aligned} \tag{4.32}$$

is the elasticity tensor pulled-back to the reference configuration through $\boldsymbol{F}_{\mathrm{p}}^{(0)}$, and, upon setting $\boldsymbol{B}_{\mathrm{p}}^{(0)} = (\boldsymbol{F}_{\mathrm{p}}^{(0)})^{-1}(\boldsymbol{F}_{\mathrm{p}}^{(0)})^{-\mathrm{T}}$, we employed the notation

$$\mathscr{K}_{\mathrm{p}}^{(0)} = \tfrac{1}{3}\boldsymbol{B}_{\mathrm{p}}^{(0)} \otimes \boldsymbol{B}_{\mathrm{p}}^{(0)}, \tag{4.33a}$$

$$\mathscr{I}_{\mathrm{p}}^{(0)} = \tfrac{1}{2}\left[\boldsymbol{B}_{\mathrm{p}}^{(0)} \underline{\otimes} \boldsymbol{B}_{\mathrm{p}}^{(0)} + \boldsymbol{B}_{\mathrm{p}}^{(0)} \overline{\otimes} \boldsymbol{B}_{\mathrm{p}}^{(0)}\right]. \tag{4.33b}$$

We remark that $\mathscr{K}_{\mathrm{p}}^{(0)}$ extracts the "volumetric part" of a generic second-order tensor, taken with respect to the inverse plastic metric tensor $\boldsymbol{B}_{\mathrm{p}}^{(0)}$ i.e. for all $\boldsymbol{A} = \boldsymbol{A}^T$, it holds that $\mathscr{K}_{\mathrm{p}}^{(0)} : \boldsymbol{A} = \frac{1}{3}\mathrm{tr}(\boldsymbol{B}_{\mathrm{p}}^{(0)}\boldsymbol{A})\boldsymbol{B}_{\mathrm{p}}^{(0)}$. Furthermore, $\mathscr{I}_{\mathrm{p}}^{(0)}$ transforms

$\boldsymbol{A}$ into $\mathscr{I}_{\mathrm{p}}^{(0)} : \boldsymbol{A} = \boldsymbol{B}_{\mathrm{p}}^{(0)}\boldsymbol{A}\boldsymbol{B}_{\mathrm{p}}^{(0)}$ and $\mathscr{M}_{\mathrm{p}}^{(0)} = \mathscr{I}_{\mathrm{p}}^{(0)} - \mathscr{K}_{\mathrm{p}}^{(0)}$ extracts the "deviatoric part" of $\boldsymbol{A}$ with respect to the metric tensor $\boldsymbol{B}_{\mathrm{p}}^{(0)}$, i.e. $\mathscr{M}_{\mathrm{p}}^{(0)} : \boldsymbol{A} = \boldsymbol{B}_{\mathrm{p}}^{(0)}\boldsymbol{A}\boldsymbol{B}_{\mathrm{p}}^{(0)} - \frac{1}{3}\mathrm{tr}(\boldsymbol{B}_{\mathrm{p}}^{(0)}\boldsymbol{A})\boldsymbol{B}_{\mathrm{p}}^{(0)}$. We note that similar results have been obtained in the case of non-linear elasticity in [77].

Next, we notice that $\boldsymbol{F}^{(0)}$ can be written as

$$\boldsymbol{F}^{(0)} = \boldsymbol{I} + \boldsymbol{H}, \tag{4.34}$$

with $\boldsymbol{H} = \mathrm{Grad}_X \boldsymbol{u}^{(0)} + \mathrm{Grad}_Y \boldsymbol{u}^{(1)}$. Thus, by substituting (4.34) in $\boldsymbol{E}_{\mathrm{e}}^{(0)}$, the result into (4.31), and retaining only the terms linear in $\boldsymbol{H}$, $\boldsymbol{S}^{(0)}$ can be linearised as

$$\boldsymbol{S}_{\mathrm{lin}}^{(0)} = \mathscr{C}_{\mathrm{R}} : (\mathrm{sym}\boldsymbol{H} - \boldsymbol{E}_{\mathrm{p}}^{(0)}). \tag{4.35}$$

We recall now that, at the leading order, the first Piola-Kirchhoff stress tensor reads $\boldsymbol{P}^{(0)} = \boldsymbol{F}^{(0)}\boldsymbol{S}^{(0)}$. Hence, its linearised form is given by

$$\boldsymbol{P}_{\mathrm{lin}}^{(0)} = \mathscr{C}_{\mathrm{R}} : \mathrm{sym}\boldsymbol{H} - (\boldsymbol{I} + \boldsymbol{H})(\mathscr{C}_{\mathrm{R}} : \boldsymbol{E}_{\mathrm{p}}^{(0)}). \tag{4.36}$$

Looking at the definition of $\mathscr{C}_{\mathrm{R}}$ in (4.32), it can be noticed that our model resolves at the macro-scale the structural evolution of the considered medium through the dependence of $\mathscr{C}_{\mathrm{R}}$ on $\boldsymbol{F}_{\mathrm{p}}^{(0)}$, which indeed describes the production of material inhomogeneities [69, 70, 72]. Additionally, our model is also capable of simultaneously resolving the material heterogeneities at both the micro- and macro-scale through the dependence of $\mathscr{C}_{\mathrm{R}}$ on X and Y. The latter dependence in fact, keeps track of the variability of the elastic coefficient at both scales.

Because of Equations (4.33a) and (4.33b), $\mathscr{C}_{\mathrm{R}}$ possesses the same symmetry properties of $\mathscr{C}$, i.e.

$$(\mathscr{C}_{\mathrm{R}})_{IJKL} = (\mathscr{C}_{\mathrm{R}})_{JIKL} = (\mathscr{C}_{\mathrm{R}})_{IJLK} = (\mathscr{C}_{\mathrm{R}})_{KLIJ}, \tag{4.37}$$

and therefore, $\boldsymbol{P}_{\mathrm{lin}}^{(0)}$ can be written as

$$\boldsymbol{P}_{\mathrm{lin}}^{(0)} = \mathscr{C}_{\mathrm{R}} : \boldsymbol{H} - (\boldsymbol{I} + \boldsymbol{H})(\mathscr{C}_{\mathrm{R}} : \boldsymbol{E}_{\mathrm{p}}^{(0)}). \tag{4.38}$$

Local problem Substituting (4.38) in the equation of the local problem (4.24), the linear momentum balance law is rephrased as

$$\mathrm{Div}_Y\Big[\mathscr{C}_{\mathrm{R}} : \boldsymbol{H} - (\boldsymbol{I} + \boldsymbol{H})(\mathscr{C}_{\mathrm{R}} : \boldsymbol{E}_{\mathrm{p}}^{(0)})\Big] = \boldsymbol{0}, \tag{4.39}$$

or, equivalently,

$$\begin{aligned} &\mathrm{Div}_Y\Big[\mathscr{C}_{\mathrm{R}} : \mathrm{Grad}_Y \boldsymbol{u}^{(1)} - \mathrm{Grad}_Y \boldsymbol{u}^{(1)}(\mathscr{C}_{\mathrm{R}} : \boldsymbol{E}_{\mathrm{p}}^{(0)})\Big] = \\ &- \mathrm{Div}_Y\Big[\mathscr{C}_{\mathrm{R}} : \mathrm{Grad}_X \boldsymbol{u}^{(0)} - (\boldsymbol{I} + \mathrm{Grad}_X \boldsymbol{u}^{(0)})(\mathscr{C}_{\mathrm{R}} : \boldsymbol{E}_{\mathrm{p}}^{(0)})\Big]. \end{aligned} \tag{4.40}$$

In the absence of plastic distortions, i.e., when $\boldsymbol{F}_{\mathrm{p}}^{\varepsilon} = \boldsymbol{I}$, Equation (4.40) coincides with the equation of the classical cell problem encountered in the homogenisation of linear elasticity, which is known to admit a unique solution, up to a Y-constant function, if the average over the cell of the right-hand-side vanishes identically (in the jargon of Homogenisation Theory, this condition is referred to as *solvability condition* or *compatibility condition*) [23]. In our case, since the pulled-back elasticity tensor $\mathscr{C}_{\mathrm{R}}$ is periodic in Y, while $\boldsymbol{u}^{(0)}$ is independent of Y, the solvability condition is satisfied, i.e.,

$$\left\langle \mathrm{Div}_Y \Big[\mathscr{C}_{\mathrm{R}} : \mathrm{Grad}_X \boldsymbol{u}^{(0)} - (\boldsymbol{I} + \mathrm{Grad}_X \boldsymbol{u}^{(0)})(\mathscr{C}_{\mathrm{R}} : \boldsymbol{E}_{\mathrm{p}}^{(0)}) \Big] \right\rangle = \boldsymbol{0}. \tag{4.41}$$

Exploiting the linearity of equation (4.40) in $\boldsymbol{u}^{(1)}$, we make the *ansatz*

$$\boldsymbol{u}^{(1)}(X,Y,t) = \boldsymbol{\xi}(X,Y,t) : \mathrm{Grad}_X \boldsymbol{u}^{(0)}(X,t) + \boldsymbol{\omega}(X,Y,t), \tag{4.42}$$

where $\boldsymbol{\xi}$ and $\boldsymbol{\omega}$ are a third-order tensor field and a vector field, both periodic in Y.

We now require that $\boldsymbol{\xi}$ and $\boldsymbol{\omega}$ satisfy two independent cell problems. The cell problem for $\boldsymbol{\xi}$ reads

$$\begin{cases} \mathrm{Div}_Y \Big[\mathscr{C}_{\mathrm{R}} : T\mathrm{Grad}_Y \boldsymbol{\xi} - T\mathrm{Grad}_Y \boldsymbol{\xi} (\mathscr{C}_{\mathrm{R}} : \boldsymbol{E}_{\mathrm{p}}^{(0)}) \Big] & \\ \quad = \mathrm{Div}_Y \Big[-\mathscr{C}_{\mathrm{R}} + \boldsymbol{I} \underline{\otimes} (\mathscr{C}_{\mathrm{R}} : \boldsymbol{E}_{\mathrm{p}}^{(0)}) \Big], & \text{in } \mathcal{Y}_0 \setminus \Gamma_0 \times \mathcal{T}, \\ [\![\boldsymbol{\xi}]\!] = \boldsymbol{0}, & \text{on } \Gamma_0 \times \mathcal{T}, \\ \Big[\!\!\Big[\Big[\mathscr{C}_{\mathrm{R}} : T\mathrm{Grad}_Y \boldsymbol{\xi} - T\mathrm{Grad}_Y \boldsymbol{\xi} (\mathscr{C}_{\mathrm{R}} : \boldsymbol{E}_{\mathrm{p}}^{(0)}) & \\ \quad + \mathscr{C}_{\mathrm{R}} - \boldsymbol{I} \underline{\otimes} (\mathscr{C}_{\mathrm{R}} : \boldsymbol{E}_{\mathrm{p}}^{(0)}) \Big] \cdot \boldsymbol{N}_{\mathcal{Y}} \Big]\!\!\Big] = \boldsymbol{0}, & \text{on } \Gamma_0 \times \mathcal{T}. \end{cases} \tag{4.43}$$

Before going further, some words of explanation on the notation are necessary. First, we notice that $\mathrm{Grad}_Y \boldsymbol{\xi}$ is a fourth-order tensor function, which admits the representation $\mathrm{Grad}_Y \boldsymbol{\xi} = (\partial \xi_{ABC})/(\partial Y_D) \boldsymbol{e}_A \otimes \boldsymbol{e}_B \otimes \boldsymbol{e}_C \otimes \boldsymbol{e}_D$. Then, $T\mathrm{Grad}_Y \boldsymbol{\xi}$ is a fourth-order tensor function obtained by ordering the indices of $\mathrm{Grad}_Y \boldsymbol{\xi}$ in the following fashion

$$\begin{aligned} T\mathrm{Grad}_Y \boldsymbol{\xi} &= (T\mathrm{Grad}_Y \boldsymbol{\xi})_{ABCD} \boldsymbol{e}_A \otimes \boldsymbol{e}_B \otimes \boldsymbol{e}_C \otimes \boldsymbol{e}_D \\ &= (\mathrm{Grad}_Y \boldsymbol{\xi})_{ACDB} \boldsymbol{e}_A \otimes \boldsymbol{e}_B \otimes \boldsymbol{e}_C \otimes \boldsymbol{e}_D \\ &= \frac{\partial \xi_{ACD}}{\partial Y_B} \boldsymbol{e}_A \otimes \boldsymbol{e}_B \otimes \boldsymbol{e}_C \otimes \boldsymbol{e}_D. \end{aligned} \tag{4.44}$$

The cell problem for $\boldsymbol{\omega}$ is given by

$$\begin{cases} \mathrm{Div}_Y \Big[\mathscr{C}_{\mathrm{R}} : \mathrm{Grad}_Y \boldsymbol{\omega} - \mathrm{Grad}_Y \boldsymbol{\omega} (\mathscr{C}_{\mathrm{R}} : \boldsymbol{E}_{\mathrm{p}}^{(0)}) \Big] & \\ \quad = \mathrm{Div}_Y \Big[\mathscr{C}_{\mathrm{R}} : \boldsymbol{E}_{\mathrm{p}}^{(0)} \Big], & \text{in } \mathcal{Y}_0 \setminus \Gamma_0 \times \mathcal{T}, \\ [\![\boldsymbol{\omega}]\!] = \boldsymbol{0}, & \text{on } \Gamma_0 \times \mathcal{T}, \\ \Big[\!\!\Big[\Big(\mathscr{C}_{\mathrm{R}} : \mathrm{Grad}_Y \boldsymbol{\omega} - \mathrm{Grad}_Y \boldsymbol{\omega} (\mathscr{C}_{\mathrm{R}} : \boldsymbol{E}_{\mathrm{p}}^{(0)}) & \\ \quad - \mathscr{C}_{\mathrm{R}} : \boldsymbol{E}_{\mathrm{p}}^{(0)} \Big) \cdot \boldsymbol{N}_{\mathcal{Y}} \Big]\!\!\Big] = \boldsymbol{0}, & \text{on } \Gamma_0 \times \mathcal{T}. \end{cases} \tag{4.45}$$

By virtue of the linearisation process, we obtain two auxiliary cell problems where the macroscopic term $\mathrm{Grad}_X\boldsymbol{u}^{(0)}$ is not explicitly present. Indeed, this is in general possible only when accounting for the linearised deformations' regime, see also [54]. Then, the dependence of the macro-scale variable is given through the tensor $\boldsymbol{F}_{\mathrm{p}}^{(0)}$, which describes the plastic-like distortions. Moreover, if $\boldsymbol{F}_{\mathrm{p}}^{(0)}$ only depends on time, as is the case in [10], the cell problems are also decoupled in the spatial micro- and macro-variables provided that the elasticity tensor solely depends on the micro scale variable. The cell problems are in any case time-dependent, as they encode the evolution of the material response and its link with the plastic-like distortions. This section answers to the research question 4.1.

Homogenized problem From (4.36) and (4.42), the homogenised problem rewrites

$$\begin{cases} \mathrm{Div}_X\Big[\hat{\mathscr{C}}_{\mathrm{R}} : \mathrm{Grad}_X\boldsymbol{u}^{(0)}\Big] = -\mathrm{Div}_X\Big[\hat{\boldsymbol{D}}_{\mathrm{R}}\Big], & \text{in } \mathcal{B}_h \times \mathcal{T}, \\ (\hat{\mathscr{C}}_{\mathrm{R}} : \mathrm{Grad}_X\boldsymbol{u}^{(0)}) \cdot \boldsymbol{N} + \hat{\boldsymbol{D}}_{\mathrm{R}} \cdot \boldsymbol{N} = \bar{\boldsymbol{P}}, & \text{on } \partial_T\mathcal{B}_h \times \mathcal{T}, \\ \boldsymbol{u}^{(0)} = \bar{\boldsymbol{u}}, & \text{on } \partial_u\mathcal{B}_h \times \mathcal{T}, \end{cases} \tag{4.46}$$

where

$$\hat{\mathscr{C}}_{\mathrm{R}} = \Big\langle \mathscr{C}_{\mathrm{R}} + \mathscr{C}_{\mathrm{R}} : T\mathrm{Grad}_Y\boldsymbol{\xi} - T\mathrm{Grad}_Y\boldsymbol{\xi}(\mathscr{C}_{\mathrm{R}} : \boldsymbol{E}_{\mathrm{p}}^{(0)}) - \boldsymbol{I}\underline{\otimes}(\mathscr{C}_{\mathrm{R}} : \boldsymbol{E}_{\mathrm{p}}^{(0)})\Big\rangle, \tag{4.47a}$$

$$\hat{\boldsymbol{D}}_{\mathrm{R}} = \Big\langle \mathscr{C}_{\mathrm{R}} : \mathrm{Grad}_Y\boldsymbol{\omega} - \mathrm{Grad}_Y\boldsymbol{\omega}(\mathscr{C}_{\mathrm{R}} : \boldsymbol{E}_{\mathrm{p}}^{(0)}) - \mathscr{C}_{\mathrm{R}} : \boldsymbol{E}_{\mathrm{p}}^{(0)}\Big\rangle. \tag{4.47b}$$

Remark 4.5.1. In the absence of distortions, that is for $\boldsymbol{F}_{\mathrm{p}}^{\varepsilon} = \boldsymbol{I}$, the cell problems (4.43) and (4.45) reduce to one single cell problem,

$$\begin{cases} \mathrm{Div}_Y[\mathscr{C} + \mathscr{C} : T\mathrm{Grad}_Y\boldsymbol{\xi}] = \boldsymbol{0}, & \text{in } \mathcal{Y}_0 \setminus \Gamma_0 \times \mathcal{T}, \\ [\![\boldsymbol{\xi}]\!] = \boldsymbol{0}, & \text{on } \Gamma_0 \times \mathcal{T}, \\ [\![(\mathscr{C} + \mathscr{C} : T\mathrm{Grad}_Y\boldsymbol{\xi}) \cdot \boldsymbol{N}_{\mathcal{Y}}]\!] = \boldsymbol{0}, & \text{on } \Gamma_0 \times \mathcal{T}. \end{cases} \tag{4.48}$$

This is due to the fact that the symmetric tensor $\boldsymbol{E}_{\mathrm{p}}^{(0)}$ appearing in (4.40) is equal to zero. On the other hand, the homogenised problem is rewritten as follows,

$$\begin{cases} \mathrm{Div}_X[\hat{\mathscr{C}} : \mathrm{Grad}_X\boldsymbol{u}^{(0)}] = \boldsymbol{0}, & \text{in } \mathcal{B}_h \times \mathcal{T}, \\ (\hat{\mathscr{C}} : \mathrm{Grad}_X\boldsymbol{u}^{(0)}) \cdot \boldsymbol{N} = \bar{\boldsymbol{P}}, & \text{on } \partial_T\mathcal{B}_h \times \mathcal{T}, \\ \boldsymbol{u}^{(0)} = \bar{\boldsymbol{u}}, & \text{on } \partial_u\mathcal{B}_h \times \mathcal{T}, \end{cases} \tag{4.49}$$

where $\hat{\mathscr{C}} = \langle \mathscr{C} + \mathscr{C} : T\mathrm{Grad}_Y\boldsymbol{\xi}\rangle$ is the effective elasticity tensor. Formulations (4.48) and (4.49) are the counterparts of (4.24) and (4.25), respectively, when plastic-like distortions are neglected and a linearised approach for the deformations is considered. Particularly, (4.48) and (4.49) identify identically with classical results in the asymptotic homogenisation literature [23, 214].

4.5.2 Evolution law

Several procedures can be adopted to establish a proper evolution law for the inelastic distortions. One choice is to follow a phenomenological approach, which should be based on experimental evidences and comply with suitable constitutive requirements [104]. On the other hand, one could invoke some general principles, such as the invariance of the evolution law with respect to a class of transformations and thermodynamic constraints [69, 70, 72]. Within the latter approach, and adapting the theoretical framework explored in [69, 70, 72, 104], an evolution equation for the inelastic distortions has been studied in [61]. Therein, the plastic-like distortions describe a remodelling process with the following assumptions: (*i*) $\boldsymbol{F}_{\mathrm{p}}$ is restricted by the constraint $J_{\mathrm{p}} = 1$, (*ii*) the solid phase exhibits hyperelastic behaviour, and (*iii*) the considered system remodels when the stress induced by external loading exceeds a characteristic threshold. An evolution law for $\boldsymbol{F}_{\mathrm{p}}$ satisfying these conditions, and compatible with the Dissipation inequality [44, 107, 110, 112], is given by

$$\operatorname{sym}\left(\boldsymbol{C}\boldsymbol{F}_{\mathrm{p}}^{-1}\dot{\boldsymbol{F}}_{\mathrm{p}}\right) = \gamma\left[\|\operatorname{dev}\boldsymbol{\sigma}\| - \sqrt{\tfrac{2}{3}}\sigma_y\right]_+ \frac{\operatorname{dev}(\boldsymbol{\Sigma})\boldsymbol{C}}{\|\operatorname{dev}\boldsymbol{\sigma}\|}, \tag{4.50}$$

where $\boldsymbol{\sigma}$ is the Cauchy stress tensor, $\operatorname{dev}(\boldsymbol{\Sigma}) = \boldsymbol{\Sigma} - \frac{1}{3}\operatorname{tr}(\boldsymbol{\Sigma})\boldsymbol{I}$, is the deviatoric part of the Mandel stress tensor $\boldsymbol{\Sigma} = \boldsymbol{C}\boldsymbol{S}$ being the Mandel stress tensor, and $\boldsymbol{S} = \boldsymbol{F}^{-1}\boldsymbol{P}$ the second Piola-Kirchhoff stress tensor. Moreover, γ is a strictly positive model parameter, $\sigma_y > 0$ is the yield, or threshold, stress, and the operator $[A]_+$ is such that, for any real number A, $[A]_+ = A$, if $A > 0$, and $[A]_+ = 0$ otherwise. As anticipated in the Introduction, in the present context the physical meaning of the plastic-like distortions, represented by $\boldsymbol{F}_{\mathrm{p}}$, is that of structural reorganization, i.e. remodelling, as is the case in biological tissues when the adhesion bonds among cells or the structure of the ECM reorganize themselves.

Although Equation (4.50) has been successfully used to describe some biological situations in which the onset of remodelling is subordinated to the excess of the yield stress σ_y, the homogenisation of the evolution law (4.50) is too complicated. For this reason, in this work, we replace (4.50) with a much easier law of the type

$$\operatorname{sym}\left(\boldsymbol{C}(\boldsymbol{F}_{\mathrm{p}})^{-1}\dot{\boldsymbol{F}}_{\mathrm{p}}\right) = \gamma\operatorname{dev}(\boldsymbol{\Sigma})\boldsymbol{C}, \tag{4.51}$$

according to which no stress-activation criterion is supplied. Clearly, this choice may turn out to be unrealistic in many circumstances, but it can still be useful to understand the essence of some stress-driven remodelling processes.

We need to clarify that, although in some sentences of this work we mentioned growth, our model focuses on *pure* remodelling. This is reflected by the condition $\det\boldsymbol{F}_{\mathrm{p}} = 1$, and, more importantly, by the fact that the evolution laws (4.50) and (4.51) are triggered and controlled exclusively by mechanical factors. On the one hand, the requirement $\det\boldsymbol{F}_{\mathrm{p}} = 1$ means that the plastic-like distortions are isochoric and, thus, unable to describe volumetric growth. On the other hand, the evolution laws for $\boldsymbol{F}_{\mathrm{p}}$, i.e., Eqs. (4.50) or (4.51), imply that remodelling is viewed as a consequence of the mechanical environment only: When mechanical stress exceeds a given threshold (see also [104, 112]), the internal structure of the tissue starts to vary. In other words, in the present framework, no biochemical phenomena are accounted for as possible activators of remodelling. This is a remarkable difference with growth, which, in contrast, occurs only when the concentration of nutrients is above a certain threshold value [10, 38, 5, 96, 166]. Our results do not apply to growth as they stand, nonetheless, the theory can be adapted to model growth by doing some necessary modifications. This is the reason why in the abstract we stated that our study offers *"a robust framework that can be readily generalized to growth and remodelling of nonlinear composites"*.

To homogenize (4.51), the first step is to rewrite it as

$$\operatorname{sym}\Big(\boldsymbol{C}^{\varepsilon}(\boldsymbol{F}_{\mathrm{p}}^{\varepsilon})^{-1}\dot{\boldsymbol{F}}_{\mathrm{p}}^{\varepsilon}\Big) = \gamma^{\varepsilon}\operatorname{dev}(\boldsymbol{\Sigma}^{\varepsilon})\boldsymbol{C}^{\varepsilon}, \tag{4.52}$$

by admitting that $\gamma^{\varepsilon}(X) = \gamma(X, Y)$ is a rapidly oscillating strictly positive function. Moreover, by performing the power expansion for $\boldsymbol{\Sigma}^{\varepsilon}$,

$$\boldsymbol{\Sigma}^{\varepsilon}(X, t) = \sum_{k=0}^{+\infty} \boldsymbol{\Sigma}^{(k)}(X, Y, t)\varepsilon^{k}\,, \tag{4.53}$$

and using (4.31), the leading order term of $\boldsymbol{\Sigma}^{\varepsilon}$ is

$$\boldsymbol{\Sigma}^{(0)} = \boldsymbol{C}^{(0)}\Big[\mathscr{C}_{\mathrm{R}} : (\boldsymbol{E}^{(0)} - \boldsymbol{E}_{\mathrm{p}}^{(0)})\Big]. \tag{4.54}$$

In the limit of small elastic deformations, in (4.54) we must neglect non-linear terms in $\boldsymbol{H}$. Therefore, $\boldsymbol{\Sigma}^{(0)}$ is approximated with

$$\boldsymbol{\Sigma}_{\mathrm{lin}}^{(0)} = \mathscr{C}_{\mathrm{R}} : \operatorname{sym}\boldsymbol{H} - \Big(\boldsymbol{I} + 2\operatorname{sym}\boldsymbol{H}\Big)\Big(\mathscr{C}_{\mathrm{R}} : \boldsymbol{E}_{\mathrm{p}}^{(0)}\Big).$$

By virtue of (4.12a), $\operatorname{sym}\boldsymbol{H}$ splits additively as the sum of

$$\operatorname{sym}\boldsymbol{H} = \boldsymbol{E}_{X}^{(0)} + \boldsymbol{E}_{Y}^{(1)}, \tag{4.55}$$

where, for $k = 0{,}1$, and $j_k = X, Y$,

$$\boldsymbol{E}_{j_k}^{(k)} = \tfrac{1}{2}\Big[\mathrm{Grad}_{j_k}\boldsymbol{u}^{(k)} + (\mathrm{Grad}_{j_k}\boldsymbol{u}^{(k)})^{T}\Big]. \tag{4.56}$$

By using (4.55) and (4.42), we can now rewrite $\boldsymbol{\Sigma}_{\mathrm{lin}}^{(0)}$ as

$$\boldsymbol{\Sigma}_{\mathrm{lin}}^{(0)} = \mathscr{A}_{\mathrm{R}} : \mathrm{Grad}_{X}\boldsymbol{u}^{(0)} + \mathscr{B}_{\mathrm{R}} : \mathrm{Grad}_{Y}\boldsymbol{\omega} - \mathscr{C}_{\mathrm{R}} : \boldsymbol{E}_{\mathrm{p}}^{(0)}, \tag{4.57}$$

with

$$\begin{aligned}
\mathscr{A}_{\mathrm{R}} &= \mathscr{C}_{\mathrm{R}} + \mathscr{C}_{\mathrm{R}} : T\mathrm{Grad}_Y\boldsymbol{\xi} - \boldsymbol{I}\overline{\underline{\otimes}}(\mathscr{C}_{\mathrm{R}} : \boldsymbol{E}_{\mathrm{p}}^{(0)}) \\
&\quad + \Big[\boldsymbol{I}\underline{\otimes}(\mathscr{C}_{\mathrm{R}} : \boldsymbol{E}_{\mathrm{p}}^{(0)})\Big] : \Big[T\mathrm{Grad}_Y\boldsymbol{\xi} + {}^{t}(T\mathrm{Grad}_Y\boldsymbol{\xi})\Big], && (4.58a)\\
\mathscr{B}_{\mathrm{R}} &= \mathscr{C}_{\mathrm{R}} + \boldsymbol{I}\overline{\underline{\otimes}}(\mathscr{C}_{\mathrm{R}} : \boldsymbol{E}_{\mathrm{p}}^{(0)}). && (4.58b)
\end{aligned}$$

In Equation (4.58a), the symbol ${}^{t}(\bullet)$ transposes the fourth-order tensor to which it is applied by exchanging the order of its first pair of indices only, i.e., given an arbitrary fourth-order tensor $\mathscr{T} = \mathscr{T}_{ABCD}\boldsymbol{e}_A \otimes \boldsymbol{e}_B \otimes \boldsymbol{e}_C \otimes \boldsymbol{e}_D$, ${}^{t}\mathscr{T}$ reads

$$ {}^{t}\mathscr{T} = \mathscr{T}_{BACD}\boldsymbol{e}_A \otimes \boldsymbol{e}_B \otimes \boldsymbol{e}_C \otimes \boldsymbol{e}_D. \tag{4.59}$$

Note that in the calculations performed to obtain $\mathscr{A}_{\mathrm{R}}$ and $\mathscr{B}_{\mathrm{R}}$ in (4.57), we employed the following properties: given two second-order tensors $\boldsymbol{A}$ and $\boldsymbol{U}$, with $\boldsymbol{A}$ being symmetric, it holds that

$$\begin{aligned}
\boldsymbol{U}\boldsymbol{A} &= (\boldsymbol{I}\underline{\otimes}\boldsymbol{A}) : \boldsymbol{U}, && (4.60a)\\
\boldsymbol{U}^T\boldsymbol{A} &= (\boldsymbol{I}\overline{\underline{\otimes}}\boldsymbol{A}) : \boldsymbol{U}. && (4.60b)
\end{aligned}$$

Finally, by substituting the expansions of $\boldsymbol{\Sigma}^{\varepsilon}$ and $\boldsymbol{F}_{\mathrm{p}}^{\varepsilon}$ in (4.52), equating the leading order terms, excluding non-linear terms of $\boldsymbol{H}$ and averaging, the homogenised evolution law for the plastic-like distortions is

$$\mathrm{sym}\Big[\langle \boldsymbol{C}_{\mathrm{lin}}^{(0)}(\boldsymbol{F}_{\mathrm{p}}^{(0)})^{-1}\dot{\overline{\boldsymbol{F}_{\mathrm{p}}^{(0)}}}\rangle\Big] = -\Big\langle \gamma\,\mathrm{dev}(\boldsymbol{\Sigma}_{\mathrm{lin}}^{(0)})\Big\rangle - \Big\langle \gamma(\mathscr{C}_{\mathrm{R}} : \boldsymbol{E}_{\mathrm{p}}^{(0)})(\boldsymbol{C}_{\mathrm{lin}}^{(0)} - \boldsymbol{I})\Big\rangle, \tag{4.61}$$

where $\boldsymbol{\Sigma}_{\mathrm{lin}}^{(0)}$ is given in (4.57) and

$$\begin{aligned}
\boldsymbol{C}_{\mathrm{lin}}^{(0)} &= \boldsymbol{I} + 2\mathrm{sym}\boldsymbol{H} \\
&= \boldsymbol{I} + 2(\mathscr{I} + \mathscr{I} : T\mathrm{Grad}_Y\boldsymbol{\xi}) : \mathrm{Grad}_X\boldsymbol{u}^{(0)} + 2\mathscr{I} : \mathrm{Grad}_Y\boldsymbol{\omega}. && (4.62)
\end{aligned}$$

We note that, to compute $\boldsymbol{C}_{\mathrm{lin}}^{(0)}$, we must first determine $\boldsymbol{\xi}$ and $\boldsymbol{\omega}$, which is done by solving the local problems (4.43) and (4.45). Furthermore, Equation (4.61) needs to be supplemented with an initial condition for $\boldsymbol{F}_{\mathrm{p}}^{(0)}$. We highlight that, with the formulation of Eq. (4.61), we answer the research question 4.2.

Remark 4.5.2. In the linearised theory of elasticity, even when the individual constituents of a given composite material are isotropic, the effective elastic coefficients may turn out to be anisotropic, depending on the geometric properties of the microstructure. In fact, when the Homogenisation Theory is applied, the anisotropy arises quite naturally due to the solution of the local cell problems [23, 28]. In fact, the homogenised material is anisotropic also in the case of rather simple cells, see for instance [190], where an explicit deviation-from- isotropy function is introduced in the context of cubic symmetric elasticity tensors arising from asymptotic homogenisation. This has noticeable repercussions also on the evolution law that should be chosen for a correct description of remodelling. To see this, we first notice that, for an isotropic medium, the evolution law of the plastic-like distortions can be formulated in terms of tensor $\boldsymbol{B}_{\mathrm{p}}$, since the constitutive framework is such that $\boldsymbol{F}_{\mathrm{p}}$ does not feature explicitly in any constitutive function (see e.g. [218]). In such cases, a possible evolution law for $\boldsymbol{B}_{\mathrm{p}}$ may be given in the form

$$\dot{\boldsymbol{B}}_{\mathrm{p}} = \gamma \boldsymbol{B}_{\mathrm{p}} \mathrm{dev}(\boldsymbol{\Sigma}). \tag{4.63}$$

Equation (4.63) is, in fact, in harmony with the symmetry properties of the material Mandel stress tensor, $\boldsymbol{\Sigma}$, i.e., $\boldsymbol{B}_{\mathrm{p}}\boldsymbol{\Sigma} = (\boldsymbol{B}_{\mathrm{p}}\boldsymbol{\Sigma})^{\mathrm{T}}$ [169]. However, if one writes an equation of the same type as (4.63) at the scale of a cell problem (which seems to be a justified choice, because the material is isotropic at that scale), and then homogenizes, one ends up with a material for which the Mandel stress tensor $\boldsymbol{\Sigma}$ no longer obeys the symmetry condition $\boldsymbol{B}_{\mathrm{p}}\boldsymbol{\Sigma} = (\boldsymbol{B}_{\mathrm{p}}\boldsymbol{\Sigma})^{\mathrm{T}}$. This is because the material is not isotropic at the macro scale and, thus, the description of remodelling based on $\boldsymbol{B}_{\mathrm{p}}$ becomes inadequate. Therefore, if one wants to homogenize, one should start with evolution laws at the micro scale, which have to be suitable to account for anisotropy, even though the single constituents are isotropic at that scale. These considerations lead us to Equation (4.52), as suggested in [70, 72], and subsequently employed in [61].

Remark 4.5.3. Equations (4.50) and (4.51) can be obtained by adhering to the philosophy presented in [44, 60], and subsequently adopted, for example, in [5] for growth, in [183] for growth and remodelling, and in [116, 107] for remodelling only. Accordingly, $\boldsymbol{F}_{\mathrm{p}}$ is regarded as the kinematic descriptor of the structural degrees of freedom of the medium, and $\dot{\boldsymbol{F}}_{\mathrm{p}}$ as the generalized velocity with which the structural changes occur. Within this setting, it can be proven that for growth and remodelling problems, the dissipation inequality reads

$$\mathcal{D} = \boldsymbol{Y}_{\nu} : \boldsymbol{L}_{\mathrm{p}} + \mathcal{D}_{\mathrm{nc}} \geq 0, \tag{4.64}$$

where $\mathcal{D}_{\mathrm{mech}} := \boldsymbol{Y}_{\nu} : \boldsymbol{L}_{\mathrm{p}}$ is the *mechanical contribution* to dissipation, with $\boldsymbol{Y}_{\nu}$ being the dissipative part of a generalized internal force, dual to $\boldsymbol{L}_{\mathrm{p}}$. In our work, however, $\boldsymbol{Y}_{\nu}$ can be identified with the tensor $\boldsymbol{Y}_{\nu} \equiv J_{\mathrm{p}}^{-1}\boldsymbol{F}_{\mathrm{p}}^{-\mathrm{T}}\boldsymbol{\Sigma}\boldsymbol{F}_{\mathrm{p}}^{\mathrm{T}}$, so that $\mathcal{D}_{\mathrm{mech}}$ coincides with the mechanical dissipation encountered in the standard formulation of Elastoplasticity, i.e., $\mathcal{D}_{\mathrm{mech}} = J_{\mathrm{p}}^{-1}\boldsymbol{F}_{\mathrm{p}}^{-\mathrm{T}}\boldsymbol{\Sigma}\boldsymbol{F}_{\mathrm{p}}^{\mathrm{T}} : \boldsymbol{L}_{\mathrm{p}} = J_{\mathrm{p}}^{-1}\boldsymbol{\Sigma} : \boldsymbol{F}_{\mathrm{p}}^{-1}\dot{\boldsymbol{F}}_{\mathrm{p}}$.

In the terminology of [149, 106], $\mathcal{D}_{\mathrm{nc}}$ is referred to as "*non-compliant*" contribution to the overall dissipation. Physically, it summarizes a class of phenomena that are not —or cannot be— resolved in terms of mechanical power at the scale at which the dissipation inequality is written. For instance, in the case of growth, $\mathcal{D}_{\mathrm{nc}}$ may represent biochemical effects contributing to the overall dissipation.

The inequality (4.64) can be studied in several ways, depending on the problem at hand. First, we consider a growth problem. To this end, we assume that $\mathcal{D}_{\mathrm{nc}}$ can be written as $\mathcal{D}_{\rm nc} = r\mathcal{A}$, where r is the rate at which mass is added or depleted from the system (its units are given by the reciprocal of time), and $\mathcal{A}$ is the energy density (per unit volume) associated with the introduction or uptake of mass. In this setting, it is possible to conceive a particular state of the system in which the *mechanical* stress is null, i.e., $\boldsymbol{\Sigma} = \mathbf{0}$, while r and $\mathcal{A}$ are generally nonzero. When this occurs, the system grows without mechanical dissipation, i.e., $\mathcal{D}_{\rm mech} = 0$, whereas the overall dissipation of the system reduces to the non-compliant one:

$$\mathcal{D} \equiv \mathcal{D}_{\rm nc} = r\mathcal{A} \geq 0. \tag{4.65}$$

The second case addresses the situation of pure remodelling, for which we set $\mathcal{D}_{\rm nc} = 0$, so that the dissipation inequality (4.64) becomes

$$\mathcal{D} = \mathcal{D}_{\rm mech} = \boldsymbol{Y}_\nu : \boldsymbol{L}_{\rm p} = J_{\rm p}^{-1}\boldsymbol{\Sigma} : \boldsymbol{F}_{\rm p}^{-1}\dot{\boldsymbol{F}}_{\rm p} \geq 0. \tag{4.66}$$

It is possible to show that the evolution laws (4.50) and (4.51) are in harmony with (4.66).

4.6 A computational scheme for small deformations

The macro-scale model given by the problems (4.46) and (4.61), together with the auxiliary cell problems (4.43) and (4.45), requires dedicated numerical schemes which are subject of our current investigations. The main computational challenge is due to the fact that the local problems depend on the macro-scale in a time-dependent way. Therefore, at each time, there is a different cell problem at each macroscopic point $X \in \mathcal{B}_h$. Moreover, one has to transfer the information (represented by the geometry, material coefficients, and unknowns of the problem) from the cell problems to the homogenised problem in the domain $\mathcal{B}_h$, and vice versa.

Here, as a first step towards the numerical study of this kind of problems, we propose an algorithm adapted from [116] that could be useful in our case. In [116] it is introduced a computational algorithm, named Generalised Plasticity Algorithm (GPA), to study the mechanical response of a biological tissue that undergoes large deformations and remodelling of its internal structure. Following [116], the discrete and linearised version of the problem constituted by Equations (4.43), (4.45), (4.46) and (4.61) is formulated in three steps.

First step The weak form of the cell problems (4.43) and (4.45), and of the homogenised problem (4.46) can be *formally* rewritten as

$$\mathcal{L}_1^w(\boldsymbol{\xi}, \boldsymbol{F}_{\rm p}^{(0)}, \tilde{\boldsymbol{\xi}}) = 0, \tag{4.67a}$$

$$\mathcal{L}_2^w(\boldsymbol{\omega}, \boldsymbol{F}_{\rm p}^{(0)}, \tilde{\boldsymbol{\omega}}) = 0, \tag{4.67b}$$

$$\mathcal{H}_1^w(\boldsymbol{u}^{(0)}, \boldsymbol{F}_{\mathrm{p}}^{(0)}, \tilde{\boldsymbol{u}}^{(0)}) = 0, \tag{4.67c}$$

where $\tilde{\boldsymbol{\xi}}$, $\tilde{\boldsymbol{\omega}}$ and $\tilde{\boldsymbol{u}}^{(0)}$ are test functions defined in certain Sobolev spaces, and $\mathcal{L}_1^w$, $\mathcal{L}_2^w$ and $\mathcal{H}_1^w$ are suitable integral operators. Together with (4.67a)-(4.67c), we rewrite in operatorial form also the homogenised problem (4.61) as

$$\mathcal{H}_2(\boldsymbol{\xi}, \boldsymbol{\omega}, \boldsymbol{u}^{(0)}, \boldsymbol{F}_{\mathrm{p}}^{(0)}) = \boldsymbol{0}. \tag{4.68}$$

Note that (4.68) is not a weak form because the corresponding equation does not involved spatial derivatives of $\boldsymbol{F}_{\mathrm{p}}^{(0)}$.

Second step We perform a backward Euler method [218] for discretising the evolution law for $\boldsymbol{F}_{\mathrm{p}}^{(0)}$ given by (4.68), thereby ending up with the following system of time-discrete equations,

$$\mathcal{L}_{1[n]}^w(\boldsymbol{\xi}_{[n]}, \boldsymbol{F}_{\mathrm{p}[n]}^{(0)}, \tilde{\boldsymbol{\xi}}) = 0, \tag{4.69a}$$

$$\mathcal{L}_{2[n]}^w(\boldsymbol{\omega}_{[n]}, \boldsymbol{F}_{\mathrm{p}[n]}^{(0)}, \tilde{\boldsymbol{\omega}}) = 0, \tag{4.69b}$$

$$\mathcal{H}_{1[n]}^w(\boldsymbol{u}_{[n]}^{(0)}, \boldsymbol{F}_{\mathrm{p}[n]}^{(0)}, \tilde{\boldsymbol{u}}^{(0)}) = 0, \tag{4.69c}$$

$$\mathcal{H}_{2[n]}(\boldsymbol{\xi}_{[n]}, \boldsymbol{\omega}_{[n]}, \boldsymbol{u}_{[n]}^{(0)}, \boldsymbol{F}_{\mathrm{p}[n]}^{(0)}) = \boldsymbol{0}, \tag{4.69d}$$

where $n = 1, \dots, N$ enumerates the nodes of a suitable time grid. We notice that an explicit time discrete method could be also used. However, when dealing with problems in Elastoplasticity, this election could lead to a less accurate solution.

Third step The operators $\mathcal{L}_{1[n]}^w$, $\mathcal{L}_{2[n]}^w$, $\mathcal{H}_{1[n]}^w$ and $\mathcal{H}_{2[n]}$, are linear in $\boldsymbol{\xi}_{[n]}$, $\boldsymbol{\omega}_{[n]}$ and $\boldsymbol{u}_{[n]}^{(0)}$, respectively, but they are nonlinear in $\boldsymbol{F}_{\mathrm{p}[n]}^{(0)}$. Thus, to search the solution to (4.69a)-(4.69d), we linearise at each time step according to Newton's method (with a linesearch). Therefore, at the kth iteration, $k \in \mathbb{N}$, $k \geq 1$, $\boldsymbol{F}_{\mathrm{p}[n,k]}^{(0)}$ is written as

$$\boldsymbol{F}_{\mathrm{p}[n,k]}^{(0)} = \boldsymbol{F}_{\mathrm{p}[n,k-1]}^{(0)} + \boldsymbol{\Psi}_{[n,k]}, \tag{4.70}$$

where $\boldsymbol{F}_{\mathrm{p}[n,k-1]}^{(0)}$ is known and $\boldsymbol{\Psi}_{[n,k]}$ represents the unknown increment. We introduce the notation

$$\mathcal{L}_{1[n,k-1]}^w(\boldsymbol{\xi}_{[n]}, \tilde{\boldsymbol{\xi}}) = \mathcal{L}_{1[n]}^w(\boldsymbol{\xi}_{[n]}, \boldsymbol{F}_{\mathrm{p}[n,k-1]}^{(0)}, \tilde{\boldsymbol{\xi}}), \tag{4.71a}$$

$$\mathcal{L}_{2[n,k-1]}^w(\boldsymbol{\omega}_{[n]}, \tilde{\boldsymbol{\omega}}) = \mathcal{L}_{2[n]}^w(\boldsymbol{\omega}_{[n]}, \boldsymbol{F}_{\mathrm{p}[n,k-1]}^{(0)}, \tilde{\boldsymbol{\omega}}), \tag{4.71b}$$

$$\mathcal{H}_{1[n,k-1]}^w(\boldsymbol{u}_{[n]}^{(0)}, \tilde{\boldsymbol{u}}_{[n]}^{(0)}) = \mathcal{H}_{1[n]}^w(\boldsymbol{u}_{[n]}^{(0)}, \boldsymbol{F}_{\mathrm{p}[n,k-1]}^{(0)}, \tilde{\boldsymbol{u}}_{[n]}^{(0)}). \tag{4.71c}$$

Now, for each time step, and at the kth iteration, we solve

$$\mathcal{L}_{1[n,k-1]}^w(\boldsymbol{\xi}_{[n]}, \tilde{\boldsymbol{\xi}}) = 0, \tag{4.72a}$$

$$\mathcal{L}^{w}_{2[n,k-1]}(\boldsymbol{\omega}_{[n]}, \tilde{\boldsymbol{\omega}}) = 0, \tag{4.72b}$$

$$\mathcal{H}^{w}_{1[n,k-1]}(\boldsymbol{u}^{(0)}_{[n]}, \tilde{\boldsymbol{u}}^{(0)}) = 0, \tag{4.72c}$$

and obtain the "temporary" solutions $\boldsymbol{\xi}_{[n,k-1]}$, $\boldsymbol{\omega}_{[n,k-1]}$, and $\boldsymbol{u}^{(0)}_{[n,k-1]}$, respectively. Then, upon setting

$$\mathcal{H}_{2[n,k-1]} = \mathcal{H}_{2[n]}(\boldsymbol{\xi}_{[n,k-1]}, \boldsymbol{\omega}_{[n,k-1]}, \boldsymbol{u}^{(0)}_{[n,k-1]}, \boldsymbol{F}^{(0)}_{\mathrm{p}[n,k-1]}), \tag{4.73a}$$

$$\mathscr{H}_{[n,k-1]} = \mathscr{H}_{[n]}(\boldsymbol{\xi}_{[n,k-1]}, \boldsymbol{\omega}_{[n,k-1]}, \boldsymbol{u}^{(0)}_{[n,k-1]}, \boldsymbol{F}^{(0)}_{\mathrm{p}[n,k-1]}), \tag{4.73b}$$

we linearise (4.69d), i.e.,

$$\mathcal{H}_{2[n,k-1]} + \mathscr{H}_{[n,k-1]} : \boldsymbol{\Psi}_{[n,k]} = \boldsymbol{0}, \tag{4.74}$$

where $\mathscr{H}_{[n,k-1]}$ is a fourth-order tensor given by the Gâteaux derivative of $\mathcal{H}_{2[n]}$, computed with respect to its fourth argument, and evaluated in $\boldsymbol{F}^{(0)}_{\mathrm{p}[n,k-1]}$.

If the residuum $\boldsymbol{F}^{(0)}_{\mathrm{p}[n,k]}$ for k greater than, or equal to, a certain k_* is less than a tolerance $\delta > 0$, then we set $\boldsymbol{F}^{(0)}_{\mathrm{p}[n]} \equiv \boldsymbol{F}^{(0)}_{\mathrm{p}[n,k_*]} = \boldsymbol{F}^{(0)}_{\mathrm{p}[n,k_*-1]} + \boldsymbol{\Psi}_{[n,k_*]}$ and we regard it as the solution of Newton's method. Thus, we compute $\boldsymbol{\xi}_{[n]}$, $\boldsymbol{\omega}_{[n]}$ and $\boldsymbol{u}^{(0)}_{[n]}$.

These three steps are summarized in the algorithm 1.

Algorithm 1

```
1: procedure
2:   for n = 1, ..., N do
3:     State k = 1
4:     while e > δ do (Known F^(0)_p[n,k-1])
5:       Solve L^w_1[n,k-1] and L^w_2[n,k-1] (To find ξ_[n,k-1] and ω_[n,k-1])
6:       Solve H^w_1[n,k-1] (To find u^(0)_[n,k-1])
7:       Solve H^w_1[n,k-1] (To find Ψ_[n,k])
8:       F^(0)_p[n,k-1] ← F^(0)_p[n,k-1] + Ψ_[n,k]
9:       Compute e
10:      k = k + 1
11:    end while
12:    F^(0)_p[n] = F^(0)_p[n,k-1] + Ψ_[n,k]
13:    Solve L^w_1[n] and L^w_2[n] (To find ξ_[n] and ω_[n])
14:    Solve H^w_1[n] (To find u^(0)_[n])
15:    Update micro and macro geometries
16:  end for
17: end procedure
```

We highlight that this section answers the research question 4.3.

4.7 Numerical results

In this section, the potentiality of our model, which is given by Equations (4.43), (4.45), (4.46) and (4.61), is shown by performing numerical simulations. In particular, we make the following considerations.

(i) Geometry We consider the composite body $\mathscr{B}^\varepsilon$ to have a layered three-dimensional structure, and we assume that the layers are orthogonal to the direction $\boldsymbol{\mathcal{E}}_3$, where $\{\boldsymbol{\mathcal{E}}_A\}_{A=1}^3$ is an orthonormal basis of a system of Cartesian coordinates $\{X_A\}_{A=1}^3$. In this particular case, the material properties of the heterogeneous body only change along the $\boldsymbol{\mathcal{E}}_3$ direction and, thus, they depend solely on the coordinate X_3. Consequently, the benchmark test at hand can be recast into a one dimensional problem, that is, the reference configuration of the periodic cell and the body are considered to be the unidimensional domains $\mathcal{Y}_0 = [0, \ell]$ and $\mathcal{B}_h = [0, L]$, respectively. We denote with ℓ and L, respectively, the dimension of the periodic cell and the body along the direction $\boldsymbol{\mathcal{E}}_3$. Moreover, we suppose that the interface Γ_0 is the middle point $\ell/2$, so that, each material under consideration has the same volume in the microscopic cell $\mathcal{Y}_0$.

(ii) Material properties We prescribe the elasticity tensor $\mathscr{C}^\varepsilon$ to be independent on the macro scale variable X_3, i.e. $\mathscr{C}^\varepsilon(X_3) = \mathscr{C}(X_3, Y_3) \equiv \mathscr{C}(Y_3)$, where $\{Y_A\}_{A=1}^3$ is a system of micro scale Cartesian coordinates. In addition, as stated above, we consider that the constituents of the heterogeneous material are isotropic, which implies that the non zero components of the 6×6 symmetric matrix representation of $\mathscr{C}$ are given by

$$[\mathscr{C}]_{11} = [\mathscr{C}]_{22} = [\mathscr{C}]_{33} = \lambda + 2\mu, \tag{4.75a}$$

$$[\mathscr{C}]_{12} = [\mathscr{C}]_{13} = [\mathscr{C}]_{23} = \lambda, \tag{4.75b}$$

$$[\mathscr{C}]_{44} = [\mathscr{C}]_{55} = [\mathscr{C}]_{66} = \tfrac{1}{2}([\mathscr{C}]_{11} - [\mathscr{C}]_{12}) = \mu, \tag{4.75c}$$

where λ and μ are Lamé's parameters. We suppose that $\mathscr{C}$ is piece-wise constant, which means that λ and μ are defined as

$$\lambda(Y_3) = \begin{cases} \lambda_1, & \text{in } \mathcal{Y}_0^1 \\ \lambda_2, & \text{in } \mathcal{Y}_0^2 \end{cases} \quad \text{and} \quad \mu(Y_3) = \begin{cases} \mu_1, & \text{in } \mathcal{Y}_0^1 \\ \mu_2, & \text{in } \mathcal{Y}_0^2 \end{cases}. \tag{4.76}$$

Furthermore, we consider that γ has the same value in both constituents, which means that it is already averaged.

(iii) Plastic-like distortions We assume that the matrix representation of the tensor $\boldsymbol{F}_{\mathrm{p}}^{(0)}$ is diagonal with non-zero components $[\boldsymbol{F}_{\mathrm{p}}^{(0)}]_{11} = \frac{1}{\sqrt{p}}$, $[\boldsymbol{F}_{\mathrm{p}}^{(0)}]_{22} = \frac{1}{\sqrt{p}}$ and $[\boldsymbol{F}_{\mathrm{p}}^{(0)}]_{33} = p$, where p is defined as the remodelling parameter. Furthermore, we restrict our investigation to the simpler case of $\boldsymbol{F}_{\mathrm{p}}^{(0)}$ depending solely on X_3. This means that, the plastic-like distortions of order ε^0 are, in a sense, already averaged, and thus variable from one cell to the other, not inside them. In other words, we are interested in the production of distortions in the tissue starting from the cell scale, rather than from the cell's micro structure. This, of course, does not mean that the cell's micro structure does not change.

Together the with assumption (ii), we find that the 6×6 matrix representation of the elasticity tensor, pulled-backed to the reference configuration, is symmetric, and its non-zero components are given by

$$[\mathscr{C}_{\mathrm{R}}]_{11} = [\mathscr{C}_{\mathrm{R}}]_{22} = (\lambda + 2\mu)p^2, \qquad [\mathscr{C}_{\mathrm{R}}]_{33} = (\lambda + 2\mu)p^{-4}, \tag{4.77a}$$

$$[\mathscr{C}_{\mathrm{R}}]_{12} = \lambda p^2, \qquad [\mathscr{C}_{\mathrm{R}}]_{44} = [\mathscr{C}_{\mathrm{R}}]_{55} = \mu p^{-1}, \tag{4.77b}$$

$$[\mathscr{C}_{\mathrm{R}}]_{13} = [\mathscr{C}_{\mathrm{R}}]_{23} = \lambda p^{-1}, \qquad [\mathscr{C}_{\mathrm{R}}]_{66} = \mu p^2. \tag{4.77c}$$

We remark that $\mathscr{C}_{\mathrm{R}}$ depends on X_3 and time through p, whereas it inherits the dependence of $\mathscr{C}$ on the micro-scale variable, Y_3.

(iv) Initial and boundary conditions In the present context, we impose Dirichlet conditions for $\boldsymbol{u}^{(0)}$ on the whole boundary $\partial\mathcal{B}_h$, i.e. we do not consider a Neumann condition and therefore, $\partial_u\mathcal{B}_h \equiv \partial\mathcal{B}_h$. We note that, although the homogenisation process was developed for mixed boundary conditions, the whole procedure stands, since the type of boundary conditions does not play a role in the derivation of the homogenised model. In particular, we set $[\boldsymbol{u}^{(0)}]_3 = 0$ at $X_3 = 0$, and $[\boldsymbol{u}^{(0)}]_3 = \frac{u_L t}{t_f}$ at $X_3 = L$, where u_L is a target value for the displacement in the direction $\boldsymbol{\mathcal{E}}_3$. Moreover, we enforce an initial spatial distribution for the remodelling parameter p as $p_{\mathrm{in}}(X_3) = \alpha + \beta\cos(\frac{\pi}{L}X_3)$, where α and β are constants, such that $p_{\mathrm{in}}(X_3)$ is always strictly positive.

4.7.1 Discussion of the numerical results

Given the above considerations, we solve the following homogenised equations for $\boldsymbol{u}^{(0)}$ and p,

$$-\frac{\partial}{\partial X_3}([\hat{\mathscr{C}}_{\mathrm{R}}]_{i3n3}\frac{\partial[\boldsymbol{u}^{(0)}]_n}{\partial X_3}) = \frac{\partial[\hat{\boldsymbol{D}}_R]_{i3}}{\partial X_3}, \quad \text{for } i = 1,2,3, \tag{4.78a}$$

$$\langle[\boldsymbol{C}^{(0)}_{\mathrm{lin}}]_{33}\rangle\frac{\partial p}{\partial t} = \frac{\gamma}{3}\langle\mathrm{dev}(\boldsymbol{\Sigma}^{(0)}_{\mathrm{lin}})\rangle p - \gamma\langle[\mathscr{C}_{\mathrm{R}}]_{33nn}[\boldsymbol{E}_{\mathrm{p}}]_{nn}([\boldsymbol{C}^{(0)}_{\mathrm{lin}}]_{33} - 1)\rangle p, \tag{4.78b}$$

The coefficients $[\hat{\mathscr{C}}_{\mathrm{R}}]_{ijkl}$, $[\hat{\boldsymbol{D}}_R]_{ij}$ and $[\boldsymbol{C}^{(0)}_{\mathrm{lin}}]_{ij}$ are given by Equations (4.47a), (4.47b) and (4.62), respectively, and are to be found by solving the auxiliary cell problems for $\boldsymbol{\xi}$ and $\boldsymbol{\omega}$, given by

$$-\frac{\partial}{\partial Y_3}([\mathscr{Q}]_{i3i3}\frac{\partial[\boldsymbol{\xi}]_{ik3}}{\partial Y_3}) = \frac{\partial[\mathscr{Q}]_{i3i3}}{\partial Y_3}\delta_{ik}, \quad \text{for } i,k = 1,2,3, \tag{4.79a}$$

$$-\frac{\partial}{\partial Y_3}([\mathscr{Q}]_{i3i3}\frac{\partial[\boldsymbol{\omega}]_i}{\partial Y_3}) = -\frac{\partial[\boldsymbol{Q}]_{33}}{\partial Y_3}\delta_{i3}, \quad \text{for } i = 1,2,3, \tag{4.79b}$$

with

$$[\mathscr{Q}]_{i3i3} = [\mathscr{C}_{\mathrm{R}}]_{i3i3} - [\boldsymbol{Q}]_{33}, \quad [\boldsymbol{Q}]_{33} = [\mathscr{C}_{\mathrm{R}}]_{33nn}[\boldsymbol{E}_{\mathrm{p}}]_{nn}. \tag{4.80a}$$

In this work, we are not interested to address a real world situation. Our aim is, instead, to show how the present theoretical framework can be numerically simulated. For this reason, the parameters used in our computations are arbitrarily chosen (see Table 4.1).

Parameter	Unit	Value	Parameter	Unit	Value
L	[cm]	28.000	λ_1	[Pa]	1.00
u_L	[cm]	1.0000	λ_2	[Pa]	2.00
γ	[1/s]	1.0000	μ_1	[Pa]	0.10
α	[–]	1.0035	μ_2	[Pa]	0.06
β	[–]	−0.0035	t_0	[s]	0.00
N	[–]	4.0000	t_f	[s]	10.0

Table 4.1: Parameters used in the numerical simulations.

In Fig. 4.2, it is plotted the time evolution of the remodelling parameter p at two different points of the macroscopic domain, that is at $X_3 = 7\,\text{cm}$ and $X_3 = 21\,\text{cm}$. We observe that the evolution of p is quite different at these two points. Indeed, at $X_3 = 21\,\text{cm}$, p increases and it is always greater than one. On the contrary, at $X_3 = 7\,\text{cm}$, it is monotonically decreasing and tends to be lower than one. In Fig. 4.3, we show the spatial profile of the effective coefficients $[\hat{\mathscr{C}}]_{33}$, $[\hat{\mathscr{C}}_{\mathrm{R}}]_{33}$ and $[\hat{\boldsymbol{D}}_{\mathrm{R}}]_{33}$. The effective coefficient $[\hat{\mathscr{C}}]_{33}$ (see Remark 4.5.1) can be computed by using the analytical formula (see e.g. [177, 207]),

$$[\hat{\mathscr{C}}]_{ijkl} = \langle [\mathscr{C}]_{ijkl} - [\mathscr{C}]_{ijp3}([\mathscr{C}]_{p3s3})^{-1}[\mathscr{C}]_{s3kl}\rangle \\ + \langle [\mathscr{C}]_{ijp3}([\mathscr{C}]_{p3s3})^{-1}\rangle \langle ([\mathscr{C}]_{s3t3})^{-1}\rangle^{-1} \langle ([\mathscr{C}]_{t3m3})^{-1}[\mathscr{C}]_{m3kl}\rangle. \tag{4.81}$$

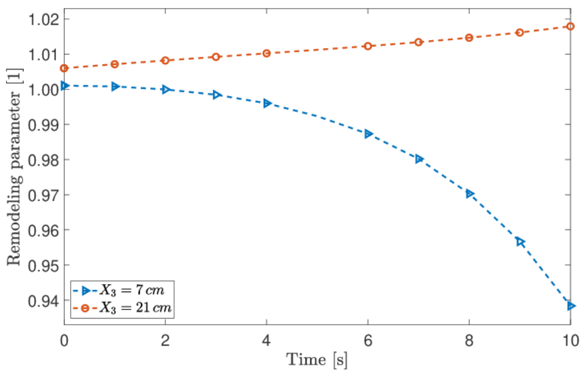

Figure 4.2: Evolution of the remodelling parameter p at two different points ($X_3 = 7\,\text{cm}$ and $X_3 = 21\,\text{cm}$) of the macroscopic domain.

We observe that even if a loading ramp condition has been imposed on $\boldsymbol{u}^{(0)}$ at the border $X_3 = L$, the effective coefficient $[\hat{\mathscr{C}}]_{33}$ does not vary on time. This is because, in contrast to the case in which the plastic-like distortions are accounted for, the cell and homogenised problems (cf. (4.48) and (4.49)) are decoupled. On the other hand, the pulled-back effective coefficients $[\hat{\mathscr{C}}_{\mathrm{R}}]_{33}$ and $[\hat{\boldsymbol{D}}_{\mathrm{R}}]_{33}$, given by Equations (4.47a) and (4.47b), respectively, do change in time since their equations are coupled with an evolution one and, as it can be observed, they are strongly influenced by the initial distribution of p. In fact, at the spatial point $X_3 = 21\,\mathrm{cm}$, that is, when $p > 1$, $[\hat{\mathscr{C}}_{\mathrm{R}}]_{33}$ decreases and $[\hat{\boldsymbol{D}}_{\mathrm{R}}]_{33}$ increases with time. The contrary occurs at $X_3 = 7\,\mathrm{cm}$, i.e. when $p < 1$.

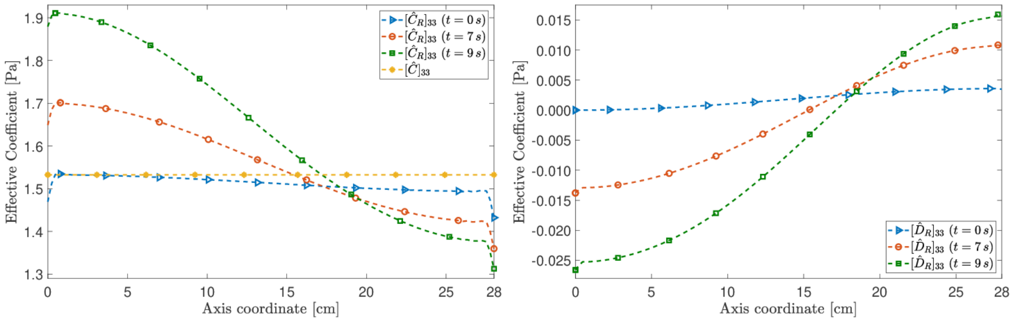

Figure 4.3: Spatial distribution of the effective coefficients $[\hat{\mathscr{C}}]_{33}$, $[\hat{\mathscr{C}}_{\mathrm{R}}]_{33}$ and $[\hat{\boldsymbol{D}}_{\mathrm{R}}]_{33}$ at different time instants.

Additionally, in Fig. 4.4 it is illustrated the third component of the macroscopic leading order term of the displacement $\boldsymbol{u}^{\varepsilon}$ at three different time instants. Particularly, we plot the numerical solution of the homogenised problems (4.46) and (4.49), represented with $[\boldsymbol{u}_{\mathrm{R}}^{(0)}]_3$ and $[\boldsymbol{u}^{(0)}]_3$, respectively. We note that, as expected from our election of the boundary condition, the displacement component increases monotonically in time. However, we notice that the introduction of the plastic-like distortions has a direct impact on the displacement distribution in the interior macroscopic points. Specifically, in these points the displacement has a higher magnitude.

The situation described in our numerical simulations, although simplified, could be a good starting point in the study of the remodelling of biological tissues. For example, the geometrical properties of bone's osteons permit to model them as layered composites (see e.g. [205]).

4.8 Concluding remarks

In the present work, we studied the dynamics of a heterogeneous material, constituted by two hyperelastic media with evolving micro-structure, by the application of the asymptotic homogenisation technique. The evolution of the micro-structure of the composite media was characterized through the development of plastic-like distortions, which were described by means of the BKL decomposition.

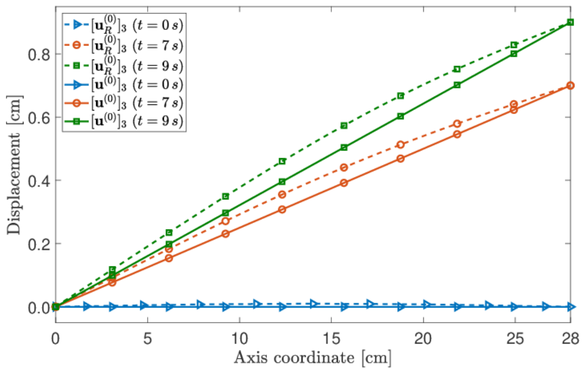

Figure 4.4: Spatial distribution of the macroscopic leading order term of the displacement with remodelling ($[\boldsymbol{u}_{\mathrm{R}}^{(0)}]_3$) and without remodelling ($[\boldsymbol{u}^{(0)}]_3$).

The asymptotic homogenisation method was applied to a set of problems comprising a scale-dependent, quasi-static law of balance of linear momentum and an evolution law for the tensor of plastic-like distortions. After obtaining the local and homogenised problems, we rewrote them by considering the De Saint-Venant strain energy density within the limit of small deformations. Although the selection of the strain energy density was due to its simplicity, it is helpful for the description of remodelling processes undergoing small deformations. For instance, this could be the case for describing bone ageing. Then, the theoretical setting developed in the present work is applicable (Elastoplasticity is actually quite appropriate to model the bone [209]). In such a case, appropriate constitutive laws describing the progression of the material properties should be found based on experimental literature (e.g. [118]). Nevertheless, for studying a larger range of problems, we need to select nonlinear constitutive laws and write the corresponding cell and homogenised problems.

As a consequence of the introduction of the tensor of plastic distortions, two independent cell problems were inferred, which reduce to the classical cell problems encountered in the homogenisation of linear problems in Elastostatics. Moreover, we proposed an evolution equation for the inelastic distortions describing a remodelling process. Such evolution law models a stress-driven production of inelastic distortions, as the one that is often encountered in studies of inelastic processes constructed on the decomposition given by (4.5) [218]. The evolution law is suitable for the case of finite strain Elastoplasticity, and for the case of remodelling of biological tissues. Finally, we outlined a computational procedure in order to solve the up-scaled problems and we performed numerical simulations for a particular case of a layered composite body. Besides, we assumed that the leading order term of the asymptotic expansion of the tensor of plastic distortions, $\boldsymbol{F}_{\mathrm{p}}^{(0)}$, depends only on the macro-scale variable X. This consideration, however, might be relaxed by allowing $\boldsymbol{F}_{\mathrm{p}}^{(0)}$ to take into account the heterogeneities of the composite material through the microscopic spatial variable Y. The numerical results showed the influence of the plastic-like distortions on both the effective coefficients and the macroscopic leading order term of the displacement.

As future work, we intend to deal with the resolution of a particular problem, like for instance the modelling of bones [159], tumour growth [200, 10, 144, 166, 204, 206], or tissue ageing [68]. A further step could be the study, with the aid of the Homogenisation Theory, of the coupling between the results presented in this work and the fluid flow in a hydrated tissue, or in the case of wavy laminar structures.

In summary, we answer the research questions 4.1—4.3 in the following way

- The macro-scale model and the auxiliary cell problems derived in this chapter require specific methods to be numerically solved. In particular an algorithm taken from the literature proved to be useful of our scopes. Such a computational algorithm, named *Generalised Plasticity Algorithm* (GPA) is introduced in [116] to study the remodelling occurring biological tissues.

- We obtain two auxiliary cell problems and a homogenised problem, which are coupled with each other, thereby establishing a major difference with the standard problems solve by means of the Asymptotic Homogenisation Technique. Such a coupling is determined by the presence of the remodelling tensor and its dependence on the macro-scale variable. Note that, in the simpler case in which $\boldsymbol{F}_{\mathrm{p}}^{(0)}$ is a function of time only, it is possible to decouple the cell problems from the homogenised one. Also in this situation, the problems at hand are time dependent, because of the time evolution of $\boldsymbol{F}_{\mathrm{p}}^{(0)}$, prescribed by an evolution law.

- Even when the individual constituents of a given composite material are isotropic, the effective elastic coefficients may turn out to be anisotropic, depending on the geometric properties of the micro-structure. This has noticeable repercussions also on the evolution law that should be chosen for a correct description of remodelling. In this sense, the evolution law should comply with such an effective anisotropy. An example of an evolution of this kind is given in Eq. (4.52), whose homogenised version in given in Eq. (4.61).

Chapter 5

Self-influenced growth through evolving material inhomogeneities

The work reported in this chapter has been previously published in [62].

5.1 Growth-induced inhomogeneities

We reformulate a model of avascular tumour growth in which the tumour tissue is studied as a biphasic medium featuring an interstitial fluid and a solid phase. The description of growth relies on two fundamental features: One of those is given by the mass transfer among the constituents of the phases, which is taken into account through source and sink terms; the other one is the multiplicative decomposition of the deformation gradient tensor of the solid phase, with the introduction of a *growth tensor*, which represents the growth-induced structural changes of the tumour.In general, such tensor is non-integrable, and it may allow to define a Levi-Civita connection with non-trivial curvature.Moreover, its evolution is related to the source and sink of mass of the solid phase through an evolution equation. Our goal is to study how growth can be influenced by the inhomogeneity of the growth tensor. To this end, we study the evolution of the latter, as predicted by two different models. In the first one, the dependence of the growth tensor on the tumour's material points is not explicitly considered in the evolution equation. In the second model, instead, the inhomogeneity of the growth tensor is resolved explicitly by introducing the curvature associated with it into the evolution equation. Through numerical simulations, we compare the results produced by these two models, and we evaluate a possible role of the material inhomogeneities on growth.

Because of its repercussion on public health, the study of tumour growth is a very active research field, to which mathematical modelling can give an important contribution [16, 2, 94]. A rather standard approach is to answer specific questions at each scale of interest by formulating dedicated models. These can be based on

Statistical Mechanics [119], Kinetic Theories [26, 36, 37, 164, 212], and Continuum Mechanics [13, 142] (and references therein), depending on whether the given problem involves the molecular, cellular, or the tissue scale. One of the main challenges, however, is to understand the complexes of phenomena that contribute to initiate the sprouting of a tumour, and to bridge across the physical scales at which they occur. The difficulty arises, for instance, when different types of models, conceived for different scales and disciplines, have to be combined efficiently, and solved simultaneously.

Within the framework of Continuum Mechanics, the search for the multi-scale and interdisciplinary approach outlined above is put into action by formulating multiphasic models of tumour growth (see e.g. [38, 200, 11, 110, 18, 182]). In such models, growth is described as the mass variation of the solid phase of the tumour at the expenses of its fluid constituents, and the mass variation is often viewed as the result of the cooperation of both chemical ad mechanical factors [14].

As long as tumour growth is concerned, the hypothesis is often made that the growth tensor is a pure dilatation [230, 180], thereby depending on one parameter only, denoted by γ and referred to as "growth parameter" in the sequel. In such cases, one has to supply an evolution law for γ (see e.g. (5.11b) below), which translates the mass balance law for the tissue's solid phase into a kinematic constraint on γ itself [166, 10, 8, 105]. When this line of thought is followed, the evolution of the growth tensor is entirely dictated by the law describing the variation of mass of the tissue, denoted by r_{s} in our notation.

Since r_{s} is related to the rate of change of γ, the problem arises to determine a generalised force that is conjugate to the variation of γ and that, thus, triggers growth. However, since r_{s} is almost always assigned on the basis of biological observations (see e.g. [10, 8]), which may be phenomenological or "*micro-mechanically motivated*" [13], it may not be possible to identify mechanical stress with the "driving force" that moves the growth-related distortions (i.e., the inhomogeneities, in the jargon of [72, 66]). This is, in fact, a relevant difference with elastoplasticity, in general, and with the models put forward in [72, 183], in which stress plays a central role. Indeed, it should be emphasised that the growth of a tumour may occur also in the absence of stress, whereas it strongly depends on the presence of nutrients, and may result in a loss of mass when these are unavailable. Still, stress may contribute to modulate the way in which the mass change takes place [166, 135]. Perhaps, we might say that, whereas stress is the "starring character" of pure remodelling (be it growth-induced or not), as it can be the trigger of the changes of the tissue's structure, it is somehow "downgraded" to a modulating factor in the case of pure growth.

A rather different approach is suggested in [66], where the concept of "*self-driven*" inhomogeneities is introduced. The underlying idea, framed within the theory of defects in solids, could be rephrased as follows. Assume to have an inhomogeneous solid medium with a non-uniform distribution of defects, which can be modelled as incompatible distortions, and thus associated with $\boldsymbol{F}_\gamma$. Assume, in addition, that the defects interact with each other, and that the strength of their mutual interaction is accounted for by the variability of $\boldsymbol{F}_\gamma$ (i.e., the more $\boldsymbol{F}_\gamma$ varies, the stronger the interaction is). Then, to adhere to Epstein's statement [66]:

> "*The evolution is* intrinsic *or* self-driven *if* [...] *the inhomogeneity moves just by virtue of its being there, perhaps in its effort to relax itself*"

we claim that the spatial variability of $\boldsymbol{F}_\gamma$ is sufficient to initiate a spontaneous evolution of $\boldsymbol{F}_\gamma$ in time.

In our work, we formulate a model of tumour growth based on the theory presented in [66, 166]. We are interested in quantifying how, and to what extent, the inhomogeneities produced by growth influence the spatio-temporal evolution of γ. For this purpose, we propose a model that merges the quasi-phenomenological definition of r_s supplied in [166] with the concept of "*self-driven*" distortions put forward in [66]. The underlying idea is that the functional form of the source/sink of mass r_s should be modified by introducing a term that takes explicitly into account the scalar curvature, κ_γ, associated with $\boldsymbol{\mathcal{R}}$. Our motivation for undertaking this task, inspired by [66], is to give a possible answer to the following question:

> Let us "prepare" the tissue in some grown configuration, with initial distribution of γ, γ_in, corresponding to nonzero curvature, $\kappa_{\gamma\mathrm{in}}$. Then, giving for granted that growth produces inhomogeneities [72, 66], what is the impact of the initial inhomogeneities on the growth of the tissue in the subsequent instants of time?

5.2 A model of tumour growth

5.2.1 Growth and curvature

In this work, $\boldsymbol{F}_\gamma$ is assumed to induce the Riemannian metric tensor

$$\boldsymbol{C}_\gamma = \boldsymbol{F}_\gamma^\mathrm{T}.\boldsymbol{F}_\gamma, \tag{5.1}$$

with is said to be the *growth metric tensor*. As pointed out in [197], $\boldsymbol{C}_\gamma$ induces a Levi-Civita connection with non-trivial curvature [235, 236]. To see this, we first construct the Christoffel symbols of the connection, which, for a given coordinate system, are given by [165]

$$\Gamma^A{}_{MN} = \frac{1}{2}(\boldsymbol{C}_\gamma^{-1})^{AB}\left[\frac{\partial(\boldsymbol{C}_\gamma)_{BN}}{\partial X^M} + \frac{\partial(\boldsymbol{C}_\gamma)_{BM}}{\partial X^N} - \frac{\partial(\boldsymbol{C}_\gamma)_{MN}}{\partial X^B}\right], \tag{5.2}$$

and are symmetric in the lower indices, thereby implying the vanishing of the torsion [165], i.e.,

$$\mathbf{Tor} = (\Gamma^{A}{}_{MN} - \Gamma^{A}{}_{NM})\boldsymbol{E}_A \otimes \boldsymbol{E}^M \otimes \boldsymbol{E}^N = \mathbf{0}. \tag{5.3}$$

Then, we compute the fourth-order curvature tensor generated by $\boldsymbol{C}_\gamma$, i.e., $\boldsymbol{\mathcal{R}} = \mathcal{R}^{A}{}_{BMN}\boldsymbol{E}_A \otimes \boldsymbol{E}^B \otimes \boldsymbol{E}^M \otimes \boldsymbol{E}^N$, whose components read [235, 236, 165]

$$\mathcal{R}^{A}{}_{BMN} = \frac{\partial \Gamma^{A}{}_{BN}}{\partial X^M} - \frac{\partial \Gamma^{A}{}_{BM}}{\partial X^N} + \Gamma^{A}{}_{MD}\Gamma^{D}{}_{BN} - \Gamma^{A}{}_{ND}\Gamma^{D}{}_{BM}. \tag{5.4}$$

Moreover, by contracting the first and the third index of $\boldsymbol{\mathcal{R}}$, we obtain the Ricci curvature tensor,

$$\boldsymbol{R} = R_{BN}\boldsymbol{E}^B \otimes \boldsymbol{E}^N = \mathcal{R}^{D}{}_{BDN}\boldsymbol{E}^B \otimes \boldsymbol{E}^N, \tag{5.5}$$

and, by double-contracting $\boldsymbol{R}$ with $\boldsymbol{C}_\gamma^{-1}$, we determine the scalar curvature associated with growth, i.e.,

$$\kappa_\gamma = \boldsymbol{R} : \boldsymbol{C}_\gamma^{-1}. \tag{5.6}$$

5.3 A model of tumour growth

We report on a mathematical model of tumour growth that, in spite of two important differences, largely follows the path designated in [166]. The first difference concerns the benchmark problem that we solve, whose geometry is much simpler than the one used therein. This choice is due to the fact that we are interested here in purely modelling issues The second difference concerns the definition of the source/sink term r_s.

5.3.1 Growth and balance laws

By adhering to the model of tumour growth developed in [166], we describe a tumour in avascular stage as a biphasic medium comprising a solid and a fluid phase. At each point of the tissue, the amount of solid is measured by means of the apparent mass density $\varphi_\mathrm{s}\varrho_\mathrm{s}$, where φ_s and ϱ_s are said to be solid volumetric fraction and true mass density, respectively. Analogously, the amount of fluid is determined by the apparent density $\varphi_\mathrm{f}\varrho_\mathrm{f}$, with φ_f and ϱ_f being the volumetric fraction and true mass density, respectively. We recall that the *true* mass density of one of the phases constituting a mixture is the *intrinsic* mass density of the considered phase. In other words, it is the density that the phase would have if it were present in the mixture with unitary volumetric fraction. For this reason, the true mass density of a phase expresses its mass per unit volume of the phase itself, whereas the apparent mass density expresses the phase mass per unit volume of the mixture as a whole.

Within our biphasic model, the tumour represents a saturated porous medium, so that the condition $\varphi_{\rm f} = 1 - \varphi_{\rm s}$ applies. Moreover, the fluid is assumed to feature only two constituents: nutrients, with mass fraction $\omega_{\rm N}$, and "water", with mass fraction $\omega_{\rm w} = 1 - \omega_{\rm N}$. We hypothesise that $\omega_{\rm N}$ is very small, so that the mass density of the fluid, $\varrho_{\rm f}$, can be regarded as constant, and approximately equal to the mass density of water. What we call "water" here is, in fact, a fluid comprising several substances, among which the constituents of the dead cells that return to the fluid in order to be expelled.

For simplicity, we prescribe that the solid phase consists of two types of cells only: the proliferating cells, with mass fraction $\omega_{\rm p}$, and the necrotic cells, with mass fraction $\omega_{\rm n} = 1 - \omega_{\rm p}$. The former ones describe the gain of mass of the tissue in response to the consumption of the nutrients. However, they become necrotic when the nutrients fall below a given threshold. The necrotic cells, in turn, are absorbed by the fluid, thereby accounting for the tissue's loss of mass due to cell death. In our model, the transition of a cell from the proliferating to the necrotic stage preserves the mass density of the cells. Hence, $\varrho_{\rm s}$ is independent of the composition of the solid phase, and may be regarded as constant, in spite of the fact that the mass fractions of the solid constituents may change in space and time [38, 166, 105].

To account for the gain and loss of mass pertaining to the proliferating and necrotic cells, we introduce their mass balance laws, which we write under the hypothesis that both types of cells move with the same velocity $\boldsymbol{v}_{\rm s}$, i.e., the solid phase velocity. By extending the model developed in [166], we write such balance laws as

$$\partial_t(\varphi_{\rm s}\varrho_{\rm s}\omega_{\rm p}) + {\rm div}(\varphi_{\rm s}\varrho_{\rm s}\omega_{\rm p}\boldsymbol{v}_{\rm s}) = r_{\rm pn} + r_{\rm fp} + r_{{\rm p}\gamma}, \tag{5.7a}$$

$$\partial_t(\varphi_{\rm s}\varrho_{\rm s}\omega_{\rm n}) + {\rm div}(\varphi_{\rm s}\varrho_{\rm s}\omega_{\rm n}\boldsymbol{v}_{\rm s}) = r_{\rm np} + r_{\rm nf} + r_{{\rm n}\gamma}, \tag{5.7b}$$

where $r_{\rm pn}$, $r_{\rm fp}$, $r_{\rm np}$, $r_{\rm nf}$, $r_{{\rm p}\gamma}$, and $r_{{\rm n}\gamma}$ denote the rates of mass uptake or depletion for the solid constituents. In particular, $r_{\rm pn}$ describes the portion of proliferating cells that, per unit volume and unit time, is converted into necrotic cells. In turn, $r_{\rm np}$ is the rate at which the necrotic cells are generated at the expenses of the proliferating ones, so that the condition $r_{\rm pn} + r_{\rm np} = 0$ is respected. Moreover, $r_{\rm fp}$ measures the growth of the proliferating cells due to the presence of nutrients, while $r_{\rm nf}$ represents the depletion of the necrotic cells in the fluid. We remark that $r_{\rm pn}$, $r_{\rm fp}$, $r_{\rm np}$, and $r_{\rm nf}$ address processes that are at the basis of tumour evolution and, in this respect, their physical interpretation is rather intuitive. On the contrary, $r_{{\rm p}\gamma}$ and $r_{{\rm n}\gamma}$ are introduced to investigate possible consequences of the properties of $\boldsymbol{F}_\gamma$ on growth itself. In other words, their task is to establish a feed-back loop among growth, the distortions that it generates, i.e., $\boldsymbol{F}_\gamma$, and the influence of those on the mass exchange terms. To the best of our knowledge, the presence of $r_{{\rm p}\gamma}$ and $r_{{\rm n}\gamma}$ in (5.7a) and (5.7b) is a novelty in the framework of mathematical modelling of tumour growth.

Since the mass fraction of the necrotic cells can be written as $\omega_{\mathrm{n}} = 1 - \omega_{\mathrm{p}}$, Equation (5.7b) can be replaced by the mass balance law of the solid phase as a whole. Indeed, by adding together (5.7a) and (5.7b), we obtain [166]

$$\partial_t(\varphi_{\mathrm{s}}\varrho_{\mathrm{s}}\omega_{\mathrm{p}}) + \mathrm{div}(\varphi_{\mathrm{s}}\varrho_{\mathrm{s}}\omega_{\mathrm{p}}\boldsymbol{v}_{\mathrm{s}}) = r_{\mathrm{pn}} + r_{\mathrm{fp}} + r_{\mathrm{p}\gamma}, \tag{5.8a}$$

$$\partial_t(\varphi_{\mathrm{s}}\varrho_{\mathrm{s}}) + \mathrm{div}(\varphi_{\mathrm{s}}\varrho_{\mathrm{s}}\boldsymbol{v}_{\mathrm{s}}) = r_{\mathrm{s}}, \tag{5.8b}$$

where $r_{\mathrm{s}} = r_{\mathrm{fp}} + r_{\mathrm{nf}} + r_{\mathrm{p}\gamma} + r_{\mathrm{n}\gamma}$ is the overall source/sink of mass for the solid phase. In general, this term can be diverted into changes either of density or of volume. In this work, since ϱ_{s} is constant, r_{s} is diverted into changes of volume. To show this, we perform the backward Piola transformation of (5.8a) and (5.8b) by multiplying both equations by $J = \det \boldsymbol{F}$. Then, by splitting J as $J = J_{\mathrm{e}}J_\gamma$, with $J_{\mathrm{e}} = \det \boldsymbol{F}_{\mathrm{e}}$ and $J_\gamma = \det \boldsymbol{F}_\gamma$, we obtain

$$J_\gamma \Phi_{\mathrm{s}\nu}\varrho_{\mathrm{s}}\dot{\omega}_{\mathrm{p}} = J[r_{\mathrm{pn}} + r_{\mathrm{fp}}\ r_{\mathrm{p}\gamma} - \omega_{\mathrm{p}} r_{\mathrm{s}}], \tag{5.9a}$$

$$\dot{\overline{(J_\gamma \Phi_{\mathrm{s}\nu}\varrho_{\mathrm{s}})}} = J r_{\mathrm{s}} = J[r_{\mathrm{fp}} + r_{\mathrm{nf}} + r_{\mathrm{p}\gamma} + r_{\mathrm{n}\gamma}], \tag{5.9b}$$

where $\Phi_{\mathrm{s}\nu} := J_{\mathrm{e}}\varphi_{\mathrm{s}}$ is the volumetric fraction of the solid phase expressed per unit volume of the intermediate, stress-free configuration. We require now that $\Phi_{\mathrm{s}\nu}$ is constant in time. Since ϱ_{s} is constant too, the left-hand-side of (5.9b) is proportional to $\dot{J}_\gamma = J_\gamma \mathrm{tr}[\dot{\boldsymbol{F}}_\gamma \boldsymbol{F}_\gamma^{-1}]$. Hence, (5.9a) and (5.9b) become

$$\dot{\omega}_{\mathrm{p}} = \frac{J[r_{\mathrm{pn}} + r_{\mathrm{fp}} + r_{\mathrm{p}\gamma} - \omega_{\mathrm{p}} r_{\mathrm{s}}]}{J_\gamma \Phi_{\mathrm{s}\nu}\varrho_{\mathrm{s}}}, \tag{5.10a}$$

$$\mathrm{tr}[\dot{\boldsymbol{F}}_\gamma \boldsymbol{F}_\gamma^{-1}] = \frac{J[r_{\mathrm{fp}} + r_{\mathrm{nf}} + r_{\mathrm{p}\gamma} + r_{\mathrm{n}\gamma}]}{\Phi_{\mathrm{s}\nu}\varrho_{\mathrm{s}} J_\gamma}. \tag{5.10b}$$

In general, besides varying the mass of a tissue, growth may also induce isochoric distortions. Accordingly, $\boldsymbol{F}_\gamma$ can be written as $\boldsymbol{F}_\gamma = [\det \boldsymbol{F}_\gamma]^{1/3}\bar{\boldsymbol{F}}_\gamma$, where $[\det \boldsymbol{F}_\gamma]^{1/3}$ measures the tissue's volume changes, and $\bar{\boldsymbol{F}}_\gamma$ is a volume-preserving tensor field that keeps track of the tissue's remodelling at constant mass. Thus, by adopting the notation $\gamma \equiv [\det \boldsymbol{F}_\gamma]^{1/3}$, we obtain [166]

$$\dot{\omega}_{\mathrm{p}} = \frac{J[r_{\mathrm{pn}} + r_{\mathrm{fp}} + r_{\mathrm{p}\gamma} - \omega_{\mathrm{p}} r_{\mathrm{s}}]}{J_\gamma \Phi_{\mathrm{s}\nu}\varrho_{\mathrm{s}}}, \tag{5.11a}$$

$$\frac{\dot{\gamma}}{\gamma} = \frac{J[r_{\mathrm{fp}} + r_{\mathrm{nf}} + r_{\mathrm{p}\gamma} + r_{\mathrm{n}\gamma}]}{3\Phi_{\mathrm{s}\nu}\varrho_{\mathrm{s}} J_\gamma}. \tag{5.11b}$$

Remark 5.3.1. The hypothesis of constant true mass density of the solid phase is due to the fact that such phase is considered to be a representation of the tissue's cells. These, in turn, are essentially made of water, whose mass density is constant in the biophysical range relevant to our work. It follows, thus, that also ϱ_{s} can be safely assumed to be constant. However, if this assumption is relaxed, Eq. (5.8b) can be recast in the form

$$\overline{\varphi_{\rm s}\varrho_{\rm s}}^{\boldsymbol{\cdot}} + \varphi_{\rm s}\varrho_{\rm s}{\rm div}\boldsymbol{v}_{\rm s} = r_{\rm s}, \tag{5.12}$$

and, by exploiting the identity $\dot{J} = J({\rm div}\boldsymbol{v}_{\rm s})$, one can write

$$J\dot{\varphi}_{\rm s}\varrho_{\rm s} + J\varphi_{\rm s}\dot{\varrho}_{\rm s} + \dot{J}\varphi_{\rm s}\varrho_{\rm s} = Jr_{\rm s}. \tag{5.13}$$

Since it holds that $\dot{J} = \dot{J}_{\rm e}J_{\rm g} + J_{\rm e}\dot{J}_\gamma = J{\rm tr}[\boldsymbol{L}_{\rm e}] + J{\rm tr}[\boldsymbol{L}_\gamma]$, with $\boldsymbol{L}_{\rm e} = \dot{\boldsymbol{F}}_{\rm e}\boldsymbol{F}_{\rm e}^{-1}$ and $\boldsymbol{L}_\gamma = \dot{\boldsymbol{F}}_\gamma\boldsymbol{F}_\gamma^{-1}$, one obtains

$$J\dot{\varphi}_{\rm s}\varrho_{\rm s} + J\varphi_{\rm s}\dot{\varrho}_{\rm s} + J\varphi_{\rm s}\varrho_{\rm s}{\rm tr}[\boldsymbol{L}_{\rm e}] + J\varphi_{\rm s}\varrho_{\rm s}{\rm tr}[\boldsymbol{L}_\gamma] = Jr_{\rm s}. \tag{5.14}$$

Moreover, we require ${\rm tr}[\boldsymbol{L}_\gamma] = r_{\rm s}/(\varphi_{\rm s}\varrho_{\rm s})$, so that (5.14) becomes

$$\dot{\varphi}_{\rm s}\varrho_{\rm s} + \varphi_{\rm s}\dot{\varrho}_{\rm s} + \varphi_{\rm s}\varrho_{\rm s}{\rm tr}[\boldsymbol{L}_{\rm e}] = 0, \tag{5.15}$$

which can be equivalently rearranged as $\overline{J_{\rm e}\varphi_{\rm s}\varrho_{\rm s}}^{\boldsymbol{\cdot}} = 0$. Thus, only the product $\varphi_{\rm s}\varrho_{\rm s}$, which individuates the mass density of the solid phase, is constant in time. Without loss of generality, it can be expressed with respect to the natural state, i.e., for $J_{\rm e} = 1$, as

$$J_{\rm e}\varphi_{\rm s}\varrho_{\rm s} = \Phi_{{\rm s}\nu}\varrho_{\rm s0}, \tag{5.16}$$

where $\Phi_{{\rm s}\nu}$ is the volumetric fraction in the natural state, and $\varrho_{\rm s0}$ denotes a constant reference value of the solid phase mass density. Equation (5.16) implies that $\varphi_{\rm s}\varrho_{\rm s}$ is a function of the elastic part of the overall deformation gradient tensor through $J_{\rm e}$. In this case, $\varrho_{\rm s}$ can be either treated as an independent variable of the theory or specified through a state law. If the first option is chosen, the model necessitates an additional equation determining the volumetric fraction (cf. e.g. [27, 215, 217]). If, instead, the second choice is made, and one assumes that $\varrho_{\rm s}$ is a constitutive function e.g. of the composition of the solid phase, one obtains

$$\varphi_{\rm s} = \frac{\Phi_{{\rm s}\nu}\hat{\varrho}_{\rm s}(\omega_{\rm p0})}{J_{\rm e}\hat{\varrho}_{\rm s}(\omega_{\rm p})} = \frac{J_\gamma\Phi_{{\rm s}\nu}\hat{\varrho}_{\rm s}(\omega_{\rm p0})}{J\hat{\varrho}_{\rm s}(\omega_{\rm p})}. \tag{5.17}$$

Here, $\hat{\varrho}_{\rm s}(\omega_{\rm p})$ is the constitutive representation of the true mass density of the solid phase. As anticipated above, it is specified as a function of the composition of the solid phase, which, within our model, is determined by the amount of proliferant and necrotic cells. Since it holds that $\omega_{\rm p} + \omega_{\rm n} = 1$, it suffices to use only one of the two mass fractions $\omega_{\rm p}$ and $\omega_{\rm n}$ to characterise the composition. Upon choosing $\omega_{\rm p}$, we let $\hat{\varrho}_{\rm s}$ depend on $\omega_{\rm p}$ only, and we take $\omega_{\rm p0}$ as a reference value for $\omega_{\rm p}$.

In conjunction with (5.11a) and (5.11b), also the mass balance laws of the nutrients and the fluid phase as a whole need to be studied

$$\partial_t(\varphi_\mathrm{f}\varrho_\mathrm{f}\omega_\mathrm{N}) + \mathrm{div}(\varphi_\mathrm{f}\varrho_\mathrm{f}\omega_\mathrm{N}\boldsymbol{v}_\mathrm{f} + \boldsymbol{y}_\mathrm{N}) = r_\mathrm{Np}, \tag{5.18a}$$

$$\partial_t(\varphi_\mathrm{f}\varrho_\mathrm{f}) + \mathrm{div}(\varphi_\mathrm{f}\varrho_\mathrm{f}\boldsymbol{v}_\mathrm{f}) = -r_\mathrm{s}. \tag{5.18b}$$

In (5.18a) and (5.18b), $\boldsymbol{v}_\mathrm{f}$ is the velocity of the fluid, $\boldsymbol{y}_\mathrm{N}$ is the mass flux vector associated with the motion of the nutrients relative to the fluid phase, and r_Np is the rate at which the nutrients are "eaten" by the proliferating cells. We remark that, to ensure the conservation of the mass of the biphasic medium under study, the right-hand-side of (5.18b) is taken equal to the negative of r_s.

After some calculations, (5.18a) and (5.18b) can be rephrased as

$$\varphi_\mathrm{f}\varrho_\mathrm{f}\dot{\omega}_\mathrm{N} + \varrho_\mathrm{f}\boldsymbol{q}\,\mathrm{grad}\omega_\mathrm{N} + \mathrm{div}\boldsymbol{y}_\mathrm{N} = r_\mathrm{Np} + \omega_\mathrm{N}r_\mathrm{s}, \tag{5.19a}$$

$$\mathrm{div}\,\boldsymbol{q} + \mathrm{div}\,\boldsymbol{v}_\mathrm{s} = \left(\frac{1}{\varrho_\mathrm{s}} - \frac{1}{\varrho_\mathrm{f}}\right) r_\mathrm{s}, \tag{5.19b}$$

where $\boldsymbol{q} = \varphi_\mathrm{f}[\boldsymbol{v}_\mathrm{f} - \boldsymbol{v}_\mathrm{s}]$ is said to be filtration velocity. Finally, (5.19a) and (5.19b) can be pulled-back to the reference configuration, thereby obtaining

$$(J - J_\mathrm{g}\Phi_{\mathrm{s}\nu})\varrho_\mathrm{f}\dot{\omega}_\mathrm{N} + \varrho_\mathrm{f}\boldsymbol{Q}\,\mathrm{Grad}\,\omega_\mathrm{N} + \mathrm{Div}\boldsymbol{Y}_\mathrm{N} = J[r_\mathrm{Np} + \omega_\mathrm{N}r_\mathrm{s}], \tag{5.20a}$$

$$\mathrm{Div}\,\boldsymbol{Q} + \dot{J} = \left(\frac{1}{\varrho_\mathrm{s}} - \frac{1}{\varrho_\mathrm{f}}\right) Jr_\mathrm{s}, \tag{5.20b}$$

where $\boldsymbol{Q} = J\boldsymbol{F}^{-1}\boldsymbol{q}$ is the material filtration velocity, and $\boldsymbol{Y}_\mathrm{N} = J\boldsymbol{F}^{-1}\boldsymbol{y}_\mathrm{N}$ is the material mass flux vector of the nutrients. Under the hypothesis of validity of Darcy's law for the fluid, and of Fick's law for the nutrients, $\boldsymbol{Q}$ and $\boldsymbol{Y}_\mathrm{N}$ read $\boldsymbol{Q} = -\boldsymbol{K}\mathrm{Grad}\,p$ and $\boldsymbol{Y}_\mathrm{N} = -\varrho_\mathrm{f}\boldsymbol{D}\mathrm{Grad}\,\omega_\mathrm{N}$, with $\boldsymbol{K} = J\boldsymbol{F}^{-1}\boldsymbol{k}\boldsymbol{F}^{-\mathrm{T}}$ being the material permeability, p the pore pressure, and $\boldsymbol{D} = J\boldsymbol{F}^{-1}\boldsymbol{d}\boldsymbol{F}^{-\mathrm{T}}$ the material diffusivity tensor of the nutrients in water. The tensors $\boldsymbol{K}$ and $\boldsymbol{D}$ are the backward Piola transforms of the spatial permeability, $\boldsymbol{k}$, and of the spatial diffusivity, $\boldsymbol{d}$, respectively.

To conclude, we introduce the momentum balance law for the biphasic medium as a whole, which we write directly in material form (see [166] for details), i.e.,

$$\mathrm{Div}\left(-Jp\,\boldsymbol{g}^{-1}\boldsymbol{F}^{-\mathrm{T}} + \boldsymbol{P}_\mathrm{sc}\right) = \boldsymbol{0}, \tag{5.21}$$

where $\boldsymbol{P}_\mathrm{sc}$ is referred to as the constitutive part of the first Piola-Kirchhoff stress tensor of the solid phase.

5.3.2 Constitutive laws

In this work, the tumour tissue is assumed to be isotropic, and, for simplicity, $\boldsymbol{k}$ and $\boldsymbol{d}$ are taken "*unconditionally isotropic*" [19], which means that they are both proportional to the inverse metric tensor $\boldsymbol{g}^{-1}$. Hence, we write $\boldsymbol{k} = k_0\boldsymbol{g}^{-1}$ and $\boldsymbol{d} = d_0\boldsymbol{g}^{-1}$, where k_0 is given in the form of the Holmes-Mow scalar permeability [19, 138], and d_0 is defined as a function of J and J_γ through the fluid phase volumetric fraction, i.e.,

$$\begin{aligned} k_0 &= k_{0\mathrm{R}} \left[\frac{\Phi_{\mathrm{s}\nu}\varphi_{\mathrm{f}}}{\varphi_{\mathrm{f}0}\varphi_{\mathrm{s}}}\right]^{m_0} \exp\left(\frac{m_1}{2}\left[\frac{J^2 - J_\gamma^2}{J_\gamma^2}\right]\right) \\ &= k_{0\mathrm{R}} \left[\frac{J - J_\gamma\Phi_{\mathrm{s}\nu}}{J_\gamma\varphi_{\mathrm{f}0}}\right]^{m_0} \exp\left(\frac{m_1}{2}\left[\frac{J^2 - J_\gamma^2}{J_\gamma^2}\right]\right), \end{aligned} \tag{5.22a}$$

$$d_0 = \varphi_{\mathrm{f}} d_{0\mathrm{R}} = \frac{J - J_\gamma\Phi_{\mathrm{s}\nu}}{J} d_{0\mathrm{R}}. \tag{5.22b}$$

In (5.22a), $\varphi_{\mathrm{f}0} = 1 - \Phi_{\mathrm{s}\nu}$ is a reference value of the fluid phase volumetric fraction, m_0 and m_1 are constant material coefficients, and $k_{0\mathrm{R}}$ is said to be the reference permeability of the medium. This quantity is assumed to be a constant in this work, even though it should be defined as a function of material points in a more general setting. The factor $d_{0\mathrm{R}}$ in (5.22b) is the reference diffusivity, which, for simplicity, is assumed here to be constant. This condition, in fact, may be violated when the nutrient mass fraction, ω_{N}, is sufficiently greater than zero, in which case $d_{0\mathrm{R}}$ should be defined as a function of ω_{N}.

By substituting (5.22a) and (5.22b) into the definitions of $\boldsymbol{k}$ and $\boldsymbol{d}$, and the corresponding results into the expressions of the material permeability and diffusivity, we find

$$\boldsymbol{K} = Jk_0\boldsymbol{C}^{-1}, \tag{5.23a}$$

$$\boldsymbol{D} = (J - J_\gamma\Phi_{\mathrm{s}\nu})d_{0\mathrm{R}}\boldsymbol{C}^{-1}. \tag{5.23b}$$

Besides being isotropic, the solid phase of the tissue is assumed to be hyperelastic. Hence, its mechanical behaviour can be described by means of a strain energy density function, $\mathcal{W}$, which we express per unit volume of the reference configuration. To account for the variation of internal structure induced by growth, $\mathcal{W}$ is given in terms of a constitutive function, $\tilde{\mathcal{W}}$, of $\boldsymbol{F}$, $\boldsymbol{F}_\gamma$, and material points, X. The purely elastic contribution of the material to the overall energy can be measured by introducing the energy density $\mathcal{W}_\nu$, defined per unit volume of the stress-free configuration, whose associated constitutive representation, $\tilde{\mathcal{W}}_\nu$, depends on $\boldsymbol{F}$ and $\boldsymbol{F}_\gamma$ exclusively through $\boldsymbol{F}_{\mathrm{e}}$. Hence, we write [72] (see also [53] for details)

$$\mathcal{W} = J_\gamma\mathcal{W}_\nu, \quad \tilde{\mathcal{W}}(\boldsymbol{F}, \boldsymbol{F}_\gamma, X) = J_\gamma\tilde{\mathcal{W}}_\nu(\boldsymbol{F}_{\mathrm{e}}). \tag{5.24}$$

For $\tilde{\mathcal{W}}_\nu(\boldsymbol{F}_{\mathrm{e}})$, we choose a constitutive law of the Holmes-Mow type [138], i.e.,

$$\begin{aligned} \tilde{\mathcal{W}}_\nu(\boldsymbol{F}_{\mathrm{e}}) &= \hat{\mathcal{W}}_\nu(\boldsymbol{C}_{\mathrm{e}}) = \check{\mathcal{W}}_\nu(\hat{I}_1(\boldsymbol{C}_{\mathrm{e}}), \hat{I}_2(\boldsymbol{C}_{\mathrm{e}}), \hat{I}_3(\boldsymbol{C}_{\mathrm{e}})) \\ &= \alpha_0\left\{\exp(\hat{\Psi}(\boldsymbol{C}_{\mathrm{e}})) - 1\right\}, \end{aligned} \tag{5.25a}$$

$$\begin{aligned}\hat{\Psi}(\boldsymbol{C}_{\rm e}) &= \check{\Psi}(\hat{I}_1(\boldsymbol{C}_{\rm e}), \hat{I}_2(\boldsymbol{C}_{\rm e}), \hat{I}_3(\boldsymbol{C}_{\rm e})) \\ &= \alpha_1[\hat{I}_1(\boldsymbol{C}_{\rm e}) - 3] + \alpha_2[\hat{I}_2(\boldsymbol{C}_{\rm e}) - 3] - \alpha_3 \ln\Big(\hat{I}_3(\boldsymbol{C}_{\rm e})\Big)\,, \end{aligned} \tag{5.25b}$$

where $\boldsymbol{C}_{\rm e} = \boldsymbol{F}_{\rm e}^{\rm T}.\boldsymbol{F}_{\rm e}$ is the elastic Cauchy-Green deformation tensor, $\hat{\mathcal{W}}_\nu(\boldsymbol{C}_{\rm e})$ is introduced to comply with objectivity, and, to account for isotropy, the dependence of $\check{\mathcal{W}}_\nu$ on $\boldsymbol{C}_{\rm e}$ is expressed through the principal invariants

$$I_1 = \hat{I}_1(\boldsymbol{C}_{\rm e}) = \mathrm{tr}\left(\boldsymbol{\eta}^{-1}\boldsymbol{C}_{\rm e}\right), \tag{5.26a}$$

$$I_2 = \hat{I}_2(\boldsymbol{C}_{\rm e}) = \tfrac{1}{2}\{[\hat{I}_1(\boldsymbol{C}_{\rm e})]^2 - \mathrm{tr}[(\boldsymbol{\eta}^{-1}\boldsymbol{C}_{\rm e})^2]\}, \tag{5.26b}$$

$$I_3 = \hat{I}_3(\boldsymbol{C}_{\rm e}) = \det \boldsymbol{C}_{\rm e}. \tag{5.26c}$$

Here, $\boldsymbol{\eta}$ is the metric tensor of the "intermediate configuration" and, by using the equality $\boldsymbol{C}_{\rm e} = \boldsymbol{F}_\gamma^{-\rm T}\boldsymbol{C}\boldsymbol{F}_\gamma^{-1}$, it can be eliminated from (5.26a)–(5.26c), so that the invariants can be rephrased as functions of $\boldsymbol{C}$ and $\boldsymbol{C}_\gamma$. Finally, in (5.25b), the material coefficients α_0, α_1, α_2, and α_3 are functions of Lamé's elastic parameters [225] (in particular, as in [138], we set $\alpha_3 = 1$), i.e.,

$$\alpha_0 = \frac{2\mu+\lambda}{4\alpha_3}, \quad \alpha_1 = \alpha_3\frac{2\mu-\lambda}{2\mu+\lambda}, \quad \alpha_2 = \alpha_3\frac{\lambda}{2\mu+\lambda}, \quad \alpha_3 = \alpha_1 + 2\alpha_2. \tag{5.27}$$

Equations (5.24), (5.25a), (5.25b), and (5.26a)–(5.26c) permit to calculate the constitutive part of the second Piola-Kirchhoff stress tensor of the solid phase:

$$\begin{aligned}\boldsymbol{S}_{\rm sc} = \hat{\boldsymbol{S}}_{\rm sc}(\boldsymbol{C}, \boldsymbol{C}_\gamma) &= \left[J_\gamma \boldsymbol{F}_\gamma^{-1}\left(2\frac{\partial\hat{\mathcal{W}}_\nu}{\partial \boldsymbol{C}_{\rm e}}(\boldsymbol{C}_{\rm e})\right)\boldsymbol{F}_\gamma^{-\rm T}\right] \\ &= 2J_\gamma b_1 \boldsymbol{C}_\gamma^{-1} + 2J_\gamma b_2[I_1\boldsymbol{C}_\gamma^{-1} - \boldsymbol{C}_\gamma^{-1}\boldsymbol{C}\boldsymbol{C}_\gamma^{-1}] + 2J_\gamma b_3 I_3 \boldsymbol{C}^{-1}, \end{aligned} \tag{5.28}$$

with $b_i = \partial\check{\mathcal{W}}_\nu/\partial I_i$, $i \in \{1,2,3\}$. Consequently, the first Piola-Kirchhoff stress tensor $\boldsymbol{P}_{\rm sc}$ can be expressed constitutively as

$$\boldsymbol{P}_{\rm sc} = \hat{\boldsymbol{P}}_{\rm sc}(\boldsymbol{F}, \boldsymbol{C}_\gamma) = \boldsymbol{F}\hat{\boldsymbol{S}}_{\rm sc}(\boldsymbol{C}, \boldsymbol{C}_\gamma), \tag{5.29}$$

and, thus, the constitutive part of the Cauchy stress tensor reads

$$\begin{aligned}\boldsymbol{\sigma}_{\rm sc} = \hat{\boldsymbol{\sigma}}_{\rm sc}(\boldsymbol{F}, \boldsymbol{C}_\gamma) &= J^{-1}\hat{\boldsymbol{P}}_{\rm sc}(\boldsymbol{F}, \boldsymbol{C}_\gamma)\boldsymbol{F}^{\rm T} \\ &= \frac{J_\gamma}{J}\left\{2b_1\boldsymbol{b}_{\rm e} + 2b_2[I_1\boldsymbol{b}_{\rm e} - \boldsymbol{b}_{\rm e}.\boldsymbol{b}_{\rm e}] + 2b_3 I_3 \boldsymbol{g}^{-1}\right\}, \end{aligned} \tag{5.30}$$

where $\boldsymbol{b}_{\rm e} = \boldsymbol{F}\boldsymbol{C}_\gamma^{-1}\boldsymbol{F}^{\rm T}$ is the elastic right Cauchy-Green deformation tensor.

5.3.3 Sources and sinks of mass

To model growth, it is necessary to describe the mass exchanges among the constituents of the system under study. In our framework, this requires to provide mathematical expressions for r_{fp}, r_{pn}, r_{nf}, and r_{Np}, and to relate each of these quantities with the appropriate set of chemo-mechanical variables. For r_{pn}, r_{nf}, r_{Np} and r_{fp}, we adopt the phenomenological expressions suggested in [166], which we report here with slight changes of notation, i.e.,

$$r_{\mathrm{pn}} = -\zeta_{\mathrm{pn}} \left\langle 1 - \frac{\omega_{\mathrm{N}}}{\omega_{\mathrm{Ncr}}} \right\rangle_+ \varphi_{\mathrm{s}}\omega_{\mathrm{p}} = -\zeta_{\mathrm{pn}} \left\langle 1 - \frac{\omega_{\mathrm{N}}}{\omega_{\mathrm{Ncr}}} \right\rangle_+ \frac{J_\gamma \Phi_{\mathrm{s}\nu}}{J}\omega_{\mathrm{p}}, \tag{5.31a}$$

$$r_{\mathrm{nf}} = -\zeta_{\mathrm{nf}}\varphi_{\mathrm{s}}[1-\omega_{\mathrm{p}}] = -\zeta_{\mathrm{nf}}\frac{J_\gamma \Phi_{\mathrm{s}\nu}}{J}[1-\omega_{\mathrm{p}}], \tag{5.31b}$$

$$r_{\mathrm{Np}} = -\zeta_{\mathrm{Np}}\frac{\omega_{\mathrm{N}}}{\omega_{\mathrm{N}}+\omega_{\mathrm{N0}}}\varphi_{\mathrm{s}}\omega_{\mathrm{p}} = -\zeta_{\mathrm{Np}}\frac{\omega_{\mathrm{N}}}{\omega_{\mathrm{N}}+\omega_{\mathrm{N0}}}\frac{J_\gamma \Phi_{\mathrm{s}\nu}}{J}\omega_{\mathrm{p}}, \tag{5.31c}$$

$$\begin{aligned} r_{\mathrm{fp}} &= \zeta_{\mathrm{fp}} \left\langle \frac{\omega_{\mathrm{N}} - \omega_{\mathrm{Ncr}}}{\omega_{\mathrm{Nenv}} - \omega_{\mathrm{Ncr}}} \right\rangle_+ \left[1 - \frac{\delta_1 \langle \bar{\sigma} \rangle_+}{\delta_2 + \langle \bar{\sigma} \rangle_+}\right] \frac{\varphi_{\mathrm{f}}\varphi_{\mathrm{s}}}{\varphi_{\mathrm{f0}}}\omega_{\mathrm{p}} \\ &= \zeta_{\mathrm{fp}} \left\langle \frac{\omega_{\mathrm{N}} - \omega_{\mathrm{Ncr}}}{\omega_{\mathrm{Nenv}} - \omega_{\mathrm{Ncr}}} \right\rangle_+ \left[1 - \frac{\delta_1 \langle \bar{\sigma} \rangle_+}{\delta_2 + \langle \bar{\sigma} \rangle_+}\right] \frac{J - J_\gamma \Phi_{\mathrm{s}\nu}}{J\varphi_{\mathrm{f0}}}\frac{J_\gamma \Phi_{\mathrm{s}\nu}}{J}\omega_{\mathrm{p}}. \end{aligned} \tag{5.31d}$$

The terms r_{pn}, r_{nf}, and r_{Np} are sinks of mass for the constituents to which they refer. In particular, r_{pn} represents the loss of mass of the proliferant cells that become necrotic. The term r_{fp}, instead, is a source of mass for the proliferant cells, and represents the mass gained by this population of cells at the expenses of the fluid. We need to emphasise that both r_{pn} and r_{fp} represent processes whose occurrence is strongly controlled by the availability of the nutrients in the tissue. To describe mathematically the concept of “availability of the nutrients”, we introduce a critical value of the nutrient mass fraction, $\omega_{\mathrm{Ncr}} \in]0,1[$, and we model the transfers of mass associated with r_{pn} and r_{fp} as threshold processes. Accordingly, when it holds that $\omega_{\mathrm{N}} \leq \omega_{\mathrm{Ncr}}$, the proliferant cells die, which means that r_{pn} is active, while r_{fp} is switched off. On the contrary, for $\omega_{\mathrm{N}} > \omega_{\mathrm{Ncr}}$, r_{pn} must vanish identically, whereas r_{fp} is switched on. Such activation and deactivation of r_{pn} and r_{fp} is formulated by means of the operator $\langle \cdot \rangle_+$, which returns the argument to which it is applied, when the argument is greater than zero, and zero otherwise. Thus, it is introduced to switch off cell death when the mass fraction of the nutrients, ω_{N}, is above, or equal to, the threshold level $\omega_{\mathrm{Ncr}} \in]0,1[$, which is assumed to be a constant of the model.

In our model, the coefficients ζ_{pn}, ζ_{nf}, ζ_{Np} and ζ_{fp} are constants, and can be related to the characteristic time scales with which, respectively, the proliferating cells die, the necrotic cells are converted into fluid, the nutrients are consumed and the interstitial fluid becomes a tumour due to cell growth.

We notice that the sinks defined in (5.31a)–(5.31d) depend on the solid phase volumetric fraction, $\varphi_{\mathrm{s}} = (J_\gamma \Phi_{\mathrm{s}\nu})/J$, in such a way that they vanish for vanishing

$\varphi_{\rm s}$. For the same reason, $r_{\rm pn}$ must be zero for zero $\omega_{\rm p}$, $r_{\rm Np}$ must be zero when $\omega_{\rm p}$ or $\omega_{\rm N}$ is zero, and $r_{\rm nf}$ must be zero for unitary $\omega_{\rm p}$, i.e., for zero $\omega_{\rm n}$ (indeed, $\omega_{\rm n} = 1 - \omega_{\rm p}$). We remark, in addition, that the dependence of $r_{\rm Np}$ on $\omega_{\rm N}$ is taken from Population Dynamics [24], with the constant $\omega_{\rm N0} \in]0,1]$ being a reference value of the nutrient concentration, introduced to modulate the rate at which their uptake occurs. The dependence of $r_{\rm fp}$ on $\varphi_{\rm s}$ and $\varphi_{\rm f} = 1 - \varphi_{\rm s}$ guarantees that growth ceases in the limit of compaction, i.e., when all the fluid flows away, and the porous medium features no voids, or when the solid disappears, which means that $\varphi_{\rm s}$ becomes zero. Besides, $r_{\rm fp}$ vanishes for vanishing $\omega_{\rm p}$, and is modulated by stress through the term $\langle \bar{\sigma} \rangle_+$, where $\bar{\sigma}$ is defined as

$$\bar{\sigma} = -\tfrac{1}{3}(\boldsymbol{g} : \boldsymbol{\sigma}_{\rm sc}) = -\frac{\frac{2}{3}\sum_{i=1}^{3} i\, b_i I_i}{J_{\rm e}}. \tag{5.32}$$

We reserve now a separate treatment for the non-standard terms $r_{{\rm p}\gamma}$ and $r_{{\rm n}\gamma}$. In particular, for the sake of simplicity, we set $r_{{\rm n}\gamma} = 0$ and we prescribe $r_{{\rm p}\gamma}$ as

$$r_{{\rm p}\gamma} = c\left[\zeta_{\rm fp}\frac{\omega_{\rm N}}{\omega_{\rm Ncr}}\frac{\varphi_{\rm f}\varphi_{\rm s}}{\varphi_{\rm f0}}\omega_{\rm p}\right]\kappa_\gamma = c\left[\zeta_{\rm fp}\frac{\omega_{\rm N}}{\omega_{\rm Ncr}}\frac{J - J_\gamma\Phi_{{\rm s}\nu}}{J\varphi_{\rm f0}}\frac{J_\gamma\Phi_{{\rm s}\nu}}{J}\omega_{\rm p}\right]\kappa_\gamma. \tag{5.33}$$

With the formulation of $r_{{\rm p}\gamma}$ given in (5.33), we assume that $r_{{\rm p}\gamma}$ is proportional to κ_γ through the factor $c\,\zeta_{\rm fp}(\omega_{\rm N}/\omega_{\rm Ncr})(\varphi_{\rm f}\varrho_{\rm s})/\varphi_{\rm f0}$. In this work, the product $c\,\zeta_{\rm fp}$ is assumed to be constant and it represents, with respect to a suitable time scale, the way in which the inhomogeneities induced by growth evolve in the tissue. Moreover, as explained above for the standard terms (5.31a)–(5.31d), we need to account for the limit cases in which compaction occurs ($\varphi_{\rm f} = 0$) or the solid phase is locally absent ($\varphi_{\rm s} = 0$). In fact, we ensure that $r_{{\rm p}\gamma}$ vanishes when $\varphi_{\rm f}$ or $\varphi_{\rm s}$ vanish. Finally, we relate the availability of nutrients to growth. In fact, we prescribe that growth does not take place if $\omega_{\rm N} = 0$, and we modulate the growth rate through the reference value $\omega_{\rm Ncr}$. This factor, indeed, is introduced to re-scale the current mass fraction of the nutrients, $\omega_{\rm N}$. In particular, the effect of κ_γ is amplified for $\omega_{\rm N} > \omega_{\rm Ncr}$, and reduced for $\omega_{\rm N} \leq \omega_{\rm Ncr}$.

For the sake of a lighter exposition, in the present work we suppress the rotations related to growth, so that $\boldsymbol{R}_\gamma$ reduces to a shifter [165] from $T\mathscr{B}$ to $T\mathscr{N}_t$, and we assume that $\boldsymbol{U}_\gamma$ represents a pure dilatation, i.e., we set $\boldsymbol{U}_\gamma = \gamma\boldsymbol{I}$. This form of $\boldsymbol{U}_\gamma$ also implies $J_\gamma = \gamma^3$ and $\boldsymbol{C}_\gamma = \gamma^2\boldsymbol{G}$, so that the material metric, $\boldsymbol{G}$, is rescaled by γ^2. Hence, no remodelling is considered in this work, and growth is entirely expressed in terms of an evolution law for γ, which, for given $r_{\rm fp}$ and $r_{\rm nf}$, coincides with (5.11b).

We emphasise that the introduction of κ_γ in our model of tumour growth is the major novelty of our work, and it constitutes the principal difference with respect to the model developed in [166]. The difference is in the fact that, while (5.11b) is an ordinary differential equation in [166], it is a partial differential equation in our model. This feature of our approach allows for an explicit resolution of the spatial variability of γ and, more importantly, it permits to estimate to what extent such variability influences growth. In fact, going through the calculations leading to (5.6), we notice that κ_γ features the derivatives of γ up to the second order. Hence, by introducing $r_{\mathrm{p}\gamma}$ into (5.11b), we obtain a nonlinear diffusion-reaction like equation in the unknown γ. Solving this equation shows how the resolved spatial variability of γ influences the evolution of the other model descriptors, i.e., the mass fraction of the proliferating cells, the mass fraction of the nutrients, the motion, and pressure.

Looking at (5.11b), and combining it with the definitions (5.31b), (5.31d), and (5.33), we notice that, when the mass fraction of the nutrients, ω_{N}, is below the threshold ω_{Ncr} (so that $r_{\mathrm{fp}} = 0$), we obtain

$$\frac{\dot{\gamma}}{\gamma} = c\left[\frac{\zeta_{\mathrm{fp}}}{3\varrho_{\mathrm{s}}}\frac{\omega_{\mathrm{N}}}{\omega_{\mathrm{Ncr}}}\frac{\varphi_{\mathrm{f}}}{\varphi_{\mathrm{f0}}}\omega_{\mathrm{p}}\right]\kappa_\gamma - \frac{\zeta_{\mathrm{nf}}}{3\varrho_{\mathrm{s}}}[1-\omega_{\mathrm{p}}]. \tag{5.34}$$

In (5.34), indeed, the evolution of γ is governed by an affine function of κ_γ, and is modulated by the mass fractions ω_{p} and ω_{N}. More generally, instead, when ω_{N} is above ω_{Ncr}, Equation (5.34) becomes:

$$\begin{aligned}\frac{\dot{\gamma}}{\gamma} =& c\left[\frac{\zeta_{\mathrm{fp}}}{3\varrho_{\mathrm{s}}}\frac{\omega_{\mathrm{N}}}{\omega_{\mathrm{Ncr}}}\frac{\varphi_{\mathrm{f}}}{\varphi_{\mathrm{f0}}}\omega_{\mathrm{p}}\right]\kappa_\gamma - \frac{\zeta_{\mathrm{nf}}}{3\varrho_{\mathrm{s}}}[1-\omega_{\mathrm{p}}] \\ &+ \frac{\zeta_{\mathrm{fp}}}{3\varrho_{\mathrm{s}}}\left\langle\frac{\omega_{\mathrm{N}}-\omega_{\mathrm{Ncr}}}{\omega_{\mathrm{Nenv}}-\omega_{\mathrm{Ncr}}}\right\rangle_+\left[1-\frac{\delta_1\langle\bar{\sigma}\rangle_+}{\delta_2+\langle\bar{\sigma}\rangle_+}\right]\frac{\varphi_{\mathrm{f}}}{\varphi_{\mathrm{f0}}}\omega_{\mathrm{p}}.\end{aligned} \tag{5.35}$$

Equation (5.35) combines two models: The first two terms on the right-hand-side of (5.35) are an adaptation of the model by Epstein [66] to our biphasic problem, which requires the introduction of the mass fraction of nutrients and proliferating cells as well as the volumetric fraction of the fluid phase. The last term, instead, is taken from the model by Mascheroni et al. [166] and has phenomenological nature in order to account for the fact that growth occurs when the mass fraction of the nutrients, ω_{N}, is greater than ω_{Ncr}, and it is modulated by stress.

Remark 5.3.2. Following [66], one could formulate a more general model, without the *a priori* assumptions of no growth-induced rotations and $\boldsymbol{U}_\gamma = \gamma\boldsymbol{I}$. In this case, a possible evolution law for $\boldsymbol{F}_\gamma$ could be obtained by relating $\dot{\boldsymbol{F}}_\gamma$ to a known function of $\boldsymbol{\mathcal{R}}$ and Grad$\boldsymbol{\mathcal{R}}$ [66]. Such an evolution law, however, is out of the scope of this work. Therefore, for the moment, we simply neglect Grad$\boldsymbol{\mathcal{R}}$ in the evolution law for $\boldsymbol{F}_\gamma$, thereby keeping only its derivatives up to the second order. Moreover, since in our framework it holds that $\boldsymbol{U}_\gamma = \gamma\boldsymbol{I}$, we end up with model in which the evolution of γ is a function of the scalar curvature, κ_γ, whereas it does not depend on the spatial derivatives of γ of order higher than the second.

5.4 Solution of a benchmark problem

5.4.1 Summary of the model

Before addressing the details of the considered benchmark problem, we summarise the model equations, and declare the unknowns to be determined. In doing this, we perform the following simplifications: (a) since the cells consist mainly of water, the mass densities ϱ_{s} and ϱ_{f} are regarded as equal to each other, so that the right-hand-side of (5.20a) is zero; (b) the advective term $\boldsymbol{Q}\,\mathrm{Grad}\,\omega_{\mathrm{N}}$ is considered to be negligible with respect to the other terms of (5.20a). In conclusion, the model equations are given by (5.11a), (5.11b), (5.20a), (5.20b), and (5.21), which we rewrite as

$$\mathrm{Div}\left[-Jp\boldsymbol{g}^{-1}\boldsymbol{F}^{-\mathrm{T}} + \boldsymbol{P}_{\mathrm{sc}}\right] = \boldsymbol{0}, \tag{5.36a}$$

$$\dot{J} - \mathrm{Div}\left[\boldsymbol{K}\mathrm{Grad}\,p\right] = 0, \tag{5.36b}$$

$$(J - \gamma^3\Phi_{\mathrm{s}\nu})\dot{\omega}_{\mathrm{N}} - \mathrm{Div}\left[\boldsymbol{D}\mathrm{Grad}\,\omega_{\mathrm{N}}\right] = J\left(\frac{r_{\mathrm{Np}}}{\varrho_{\mathrm{f}}} + \frac{3\gamma^3\,\Phi_{\mathrm{s}\nu}\,\omega_{\mathrm{N}}}{J}\frac{\dot{\gamma}}{\gamma}\right), \tag{5.36c}$$

$$\dot{\omega}_{\mathrm{p}} = -\frac{\zeta_{\mathrm{pn}}}{\varrho_{\mathrm{s}}}\left\langle 1 - \frac{\omega_{\mathrm{N}}}{\omega_{\mathrm{Ncr}}}\right\rangle_{+}\omega_{\mathrm{p}} + \frac{\zeta_{\mathrm{nf}}}{\varrho_{\mathrm{s}}}[1-\omega_{\mathrm{p}}] + 3[1-\omega_{\mathrm{p}}]\frac{\dot{\gamma}}{\gamma}, \tag{5.36d}$$

$$\frac{\dot{\gamma}}{\gamma} = c\left[\frac{\zeta_{\mathrm{fp}}}{3\varrho_{\mathrm{s}}}\frac{\omega_{\mathrm{N}}}{\omega_{\mathrm{Ncr}}}\frac{J-\gamma^3\Phi_{\mathrm{s}\nu}}{J - J\Phi_{\mathrm{s}\nu}}\omega_{\mathrm{p}}\right]\kappa_{\gamma} + \frac{J[r_{\mathrm{fp}} + r_{\mathrm{nf}}]}{3\gamma^3\Phi_{\mathrm{s}\nu}\varrho_{\mathrm{s}}}, \tag{5.36e}$$

where r_{nf}, r_{Np}, and r_{fp} are defined in (5.31b), (5.31c), and (5.31d). Consistently with (5.36a)–(5.36e), the unknown of the models are the motion of the solid phase, χ, the pressure, p, the nutrient mass fraction, ω_{N}, the growth parameter, γ, and the mass fraction of the proliferating cells, ω_{p}. Finally, $\boldsymbol{K}$, $\boldsymbol{D}$, and $\boldsymbol{P}_{\mathrm{sc}}$ are specified in (5.23a), (5.23b), and (5.29), and all the material parameters are reported in Table 5.1 and in Table 5.2.

5.4.2 Description of the benchmark test

As a proof of concept, we specialise now Equations (5.36a)–(5.36e) to a benchmark problem taken from the literature. For our purposes, we select the problem of "*isotropic and homogeneous growth inside a rigid cylinder*", formulated in [10] for the case of mono-phasic growing medium, and we adapt it to our scopes.

Also in our formulation, the growth is isotropic, i.e., $\boldsymbol{U}_{\gamma} = \gamma\boldsymbol{I}$, and takes place inside a tissue specimen of cylindrical shape, with undeformable curved surface. Hence, both the reference and the current configurations of the tissue have cylindrical shapes, with equal radius and different lengths. We indicate by R_{in} and L the initial radius and the initial length of the cylinder, respectively. Moreover, the reference configuration is covered with a system of cylindrical coordinates

$\hat{X} = (R, \Theta, Z)$, where R, Θ, and Z are the radial, circumferential, and axial coordinate, respectively. Analogously, the generic current configuration of the tissue is covered with the system of cylindrical coordinates $\hat{x} = (r, \vartheta, z)$. Any rigid rotation of the specimen about the axis of the cylinder is suppressed from the outset.

The restrictions imposed on χ imply that only the axial component of the momentum balance law (5.36a) has to be solved, and that the sole unknown component of the motion is the axial one, χ^z, while the radial and circumferential ones, χ^r and χ^ϑ, return the radial and the angular coordinate, respectively.

The growth cannot be assumed to be homogeneous in our framework, as the scalar curvature, κ_γ, would then be trivially zero, and our model would boil down to a simple biphasic rephrasing of the model presented in [10]. On the contrary, to highlight the role of κ_γ, we prescribe initial distributions of γ with a strong gradient.

In [10], the two extremities of the considered cylinder are free of applied forces, so that the axial component of stress is zero both at two outermost sections of the cylinder and, because of homogeneity, everywhere else inside it. In our setting, however, we may only conclude that the overall axial Cauchy stress, $\sigma^{zz} = -p + \sigma^{zz}_{\mathrm{sc}}$ is zero, whereas the pressure, p, and the constitutive Cauchy stress, $\sigma^{zz}_{\mathrm{sc}}$, cannot be individually zero because of the point-dependent distribution of γ. In fact, they can be such only in the limit in which the initial inhomogeneities relax, and the conditions $p = 0$ and $\sigma^{zz}_{\mathrm{sc}} = 0$ are the unique, stationary solutions to (5.36a) and (5.36b). Further differences with [10] are due to the different constitutive relations which we work with, and to the fact that our solid phase consists of two types of cells.

To solve (5.36a)–(5.36e) compatibly with the descriptions given so far, we prescribe the reference configuration of the tissue, $\mathscr{B}$, to be of cylindrical shape, and we assign the following set of boundary conditions, which apply for all times:

$$\chi^r = R_{\mathrm{in}}, \qquad \text{on } (\partial\mathscr{B})_{\mathrm{C}}, \tag{5.37a}$$

$$\chi^\vartheta = \Theta, \qquad \text{on } (\partial\mathscr{B})_{\mathrm{C}}, \tag{5.37b}$$

$$(-Jp\boldsymbol{g}^{-1}\boldsymbol{F}^{-\mathrm{T}} + \boldsymbol{P}_{\mathrm{sc}}).\boldsymbol{N}_{\mathrm{A}} = \boldsymbol{0}, \qquad \text{on } (\partial\mathscr{B})_{\mathrm{Left}} \text{ and } (\partial\mathscr{B})_{\mathrm{Right}}, \tag{5.37c}$$

$$(-\boldsymbol{K}\,\mathrm{Grad}\,p).\boldsymbol{N}_{\mathrm{C}} = 0, \qquad \text{on } (\partial\mathscr{B})_{\mathrm{C}}, \tag{5.37d}$$

$$p = 0, \qquad \text{on } (\partial\mathscr{B})_{\mathrm{Left}} \text{ and } (\partial\mathscr{B})_{\mathrm{Right}}, \tag{5.37e}$$

$$(-\varrho_{\mathrm{f}}\boldsymbol{D}\mathrm{Grad}\,\omega_{\mathrm{N}}).\boldsymbol{N}_{\mathrm{C}} = 0, \qquad \text{on } (\partial\mathscr{B})_{\mathrm{C}}, \tag{5.37f}$$

$$\omega_{\mathrm{N}} = \omega_{\mathrm{Nenv}}, \qquad \text{on } (\partial\mathscr{B})_{\mathrm{Left}} \text{ and } (\partial\mathscr{B})_{\mathrm{Right}}, \tag{5.37g}$$

$$(\mathrm{Grad}\gamma)\boldsymbol{N} = 0, \qquad \text{on } \partial\mathscr{B}. \tag{5.37h}$$

In (5.37a)–(5.37g), $(\partial\mathscr{B})_{\mathrm{C}}$ is the lateral boundary of the cylinder specimen, whereas $(\partial\mathscr{B})_{\mathrm{Left}}$ and $(\partial\mathscr{B})_{\mathrm{Right}}$ are the left and the right surfaces at the extremities of $\mathscr{B}$, respectively, $\boldsymbol{N}_{\mathrm{A}}$ is the unit vector field normal to $(\partial\mathscr{B})_{\mathrm{Left}}$ and $(\partial\mathscr{B})_{\mathrm{Right}}$, $\boldsymbol{N}_{\mathrm{C}}$ is the unit vector field oriented normal to $(\partial\mathscr{B})_{\mathrm{C}}$, and R_{in} is the initial radius of the cylinder. Furthermore, it holds that $\partial\mathscr{B} = (\partial\mathscr{B})_{\mathrm{Left}} \cup (\partial\mathscr{B})_{\mathrm{Right}} \cup (\partial\mathscr{B})_{\mathrm{C}}$, and that $\boldsymbol{N}$ is the unit vector field normal to $\partial\mathscr{B}$.

Before going further, we remark that the boundary conditions (5.37d) and (5.37f) describe the situation in which $(\partial\mathscr{B})_{\mathrm{C}}$, besides being undeformable, is also impermeable to the fluid and to the nutrients. Finally, the Dirichlet condition (5.37g), with ω_{Nenv} kept constant in all calculations, means that the tissue specimen finds itself in a "bath" of nutrients, which can flow through the boundary surfaces $(\partial\mathscr{B})_{\mathrm{Left}}$ and $(\partial\mathscr{B})_{\mathrm{Right}}$.

Together with (5.37a)–(5.37g), we enforce the initial conditions:

$$\chi^r(R,\Theta,Z,0) = R, \quad \chi^\vartheta(R,\Theta,Z,0) = \Theta, \tag{5.38a}$$

$$\chi^z(R,\Theta,Z,0) = Z + u_{\mathrm{in}}(Z), \tag{5.38b}$$

$$p(R,\Theta,Z,0) = 0, \tag{5.38c}$$

$$\omega_{\mathrm{N}}(R,\Theta,Z,0) = \omega_{\mathrm{Nenv}}, \tag{5.38d}$$

$$\gamma(R,\Theta,Z,0) = \gamma_{\mathrm{in}}(Z), \tag{5.38e}$$

$$\omega_{\mathrm{p}}(R,\Theta,Z,0) = 1, \tag{5.38f}$$

which apply at all inner points of $\mathscr{B}$. The way in which the problem is formulated allows to infer that the deformation gradient tensor takes on the form $\boldsymbol{F} = \boldsymbol{e}_r \otimes \boldsymbol{E}^R + \boldsymbol{e}_\vartheta \otimes \boldsymbol{E}^\Theta + (1+u')\boldsymbol{e}_z \otimes \boldsymbol{E}^Z$, where u is the axial displacement, the prime indicates partial differentiation in the axial direction (i.e., $u' \equiv \partial u/\partial Z$), while $\{\boldsymbol{e}_r, \boldsymbol{e}_\vartheta, \boldsymbol{e}_z\}$ and $\{\boldsymbol{E}^R, \boldsymbol{E}^\Theta, \boldsymbol{E}^Z\}$ are the vector basis and the co-vector basis generated by the coordinate systems $\hat{x} = (r,\vartheta,z)$ and $\hat{X} = (R,\Theta,Z)$, respectively. It is understood that $R \in [0, R_{\mathrm{in}}]$, $\Theta \in [0,2\pi[$, and $Z \in \left[-\frac{1}{2}L, \frac{1}{2}L\right]$.

As a further simplification, we require that all the physical quantities involved in the model are point-independent on each cross-section of the specimen, whereas they *do* vary along the axis of the cylinder, i.e., they are point-dependent only through the axial coordinate, Z. Therefore, the scalar curvature reads

$$\kappa_\gamma = \frac{2(\gamma')^2 - 4\gamma\gamma''}{\gamma^4} = \frac{6(\gamma')^2 - (4\gamma\gamma')'}{\gamma^4}, \tag{5.39}$$

and the model equations simplify as reported below:

$$[(\boldsymbol{P}_{\mathrm{sc}})^{zZ}]' = p', \tag{5.40a}$$

$$\dot{\overline{1+u'}} = \left[\frac{k_0}{1+u'}p'\right]', \tag{5.40b}$$

$$\begin{aligned}[(1+u') - \gamma^3\Phi_{\mathrm{s}\nu}]\dot{\omega}_{\mathrm{N}} = {} & \left[\left(\frac{(1+u') - \gamma^3\Phi_{\mathrm{s}\nu}}{(1+u')^2}d_{0\mathrm{R}}\right)\omega_{\mathrm{N}}'\right]' \\ & + \gamma^3\Phi_{\mathrm{s}\nu}\left[3\frac{\dot{\gamma}}{\gamma}\omega_{\mathrm{N}} - \frac{\zeta_{\mathrm{Np}}}{\varrho_{\mathrm{f}}}\frac{\omega_{\mathrm{N}}}{\omega_{\mathrm{N}} + \omega_{\mathrm{N0}}}\omega_{\mathrm{p}}\right],\end{aligned} \tag{5.40c}$$

$$\dot{\omega}_{\mathrm{p}} = -\frac{\zeta_{\mathrm{pn}}}{\varrho_{\mathrm{s}}}\left\langle 1 - \frac{\omega_{\mathrm{N}}}{\omega_{\mathrm{Ncr}}}\right\rangle_{+}\omega_{\mathrm{p}} + \frac{\zeta_{\mathrm{nf}}}{\varrho_{\mathrm{s}}}[1-\omega_{\mathrm{p}}] + 3[1-\omega_{\mathrm{p}}]\frac{\dot{\gamma}}{\gamma}, \tag{5.40d}$$

$$\begin{aligned}\frac{\dot{\gamma}}{\gamma} = {} & |c|\left[\frac{\zeta_{\mathrm{fp}}}{3\varrho_{\mathrm{s}}}\frac{\omega_{\mathrm{N}}}{\omega_{\mathrm{Ncr}}}\frac{(1+u') - \gamma^3\Phi_{\mathrm{s}\nu}}{(1+u')(1-\Phi_{\mathrm{s}\nu})}\omega_{\mathrm{p}}\right]\frac{4\gamma\gamma'' - 2(\gamma')^2}{\gamma^4} \\ & + \frac{\zeta_{\mathrm{fp}}}{3\varrho_{\mathrm{s}}}\left\langle\frac{\omega_{\mathrm{N}} - \omega_{\mathrm{Ncr}}}{\omega_{\mathrm{Nenv}} - \omega_{\mathrm{Ncr}}}\right\rangle_{+}\left[1 - \frac{\delta_1\langle\bar{\sigma}\rangle_{+}}{\delta_2 + \langle\bar{\sigma}\rangle_{+}}\right]\frac{(1+u') - \gamma^3\Phi_{\mathrm{s}\nu}}{(1+u')(1-\Phi_{\mathrm{s}\nu})}\omega_{\mathrm{p}} \\ & - \frac{\zeta_{\mathrm{nf}}}{3\varrho_{\mathrm{s}}}[1-\omega_{\mathrm{p}}],\end{aligned} \tag{5.40e}$$

where we have set $J = 1+u'$, and k_0 is defined in (5.22a). Equations (5.40a)–(5.40d) are now put in weak form, and solved by employing the Finite Element Method. To eliminate rigid motions along the axial direction, we introduce a Dirichlet point for u at $Z = 0$, where we prescribe $u(0,t) = 0$ for all t. Finally, we assign the initial conditions $\gamma_{\mathrm{in}}(Z)$ and $u_{\mathrm{in}}(Z)$ in such a way that the problem results to be symmetric with respect to $Z = 0$.

Parameter	Unit	Value	Equation	Reference
L	[cm]	1.000	Initial length	—
R_{in}	[cm]	$1.000 \cdot 10^{-2}$	Initial radius	—
λ	[Pa]	$1.333 \cdot 10^4$	(5.27)	[220]
μ	[Pa]	$1.999 \cdot 10^4$	(5.27)	[220]
k_0	[mm^4/(N s)]	0.4875	(5.22a), (5.23a),	[138]
m_0	[–]	0.0848	(5.22a)	[138]
m_1	[–]	4.638	(5.22a)	[138]
$d_{0\mathrm{R}}$	[m^2/s]	$3.200 \cdot 10^{-9}$	(5.22b), (5.40c)	[216]

Table 5.1: Parameters used in the definitions of the energy density, permeability and diffusivity. The mass fraction of the solid phase in the natural state is $\Phi_{\mathrm{s}\nu} = 0.8$. The solid and fluid phase densities are $\varrho_{\mathrm{s}} = \varrho_{\mathrm{f}} = 1000$ kg/m^3.

5.5 Results

To evaluate the impact of the scalar curvature, κ_γ, on the evolution of the system under study, we solve (5.40a)–(5.40e) twice: First, we set $c = 0$ in (5.40e), thereby switching off the term with κ_γ (this first model is denominated M1). Then, we set $c \neq 0$, and solve (5.40a)–(5.40e), paying particular attention to the effect of κ_γ (this second model is referred to as M2).

For our purposes, we prepare a protocol of numerical experiments in which the initial distribution of the growth-related distortions, $\gamma_{\mathrm{in}}(Z)$, has strong gradients

Parameter	Unit	Value	Description	Reference
$\zeta_{\rm fp}$	$[{\rm kg}/({\rm m}^3\,{\rm s})]$	$1.343\cdot 10^{-3}$	(5.31d),(5.33),(5.42)	[45]
$\zeta_{\rm pn}$	$[{\rm kg}/({\rm m}^3\,{\rm s})]$	$1.500\cdot 10^{-3}$	(5.31a)	[45]
$\zeta_{\rm nf}$	$[{\rm kg}/({\rm m}^3\,{\rm s})]$	$1.150\cdot 10^{-5}$	(5.31b)	[45]
$\zeta_{\rm Np}$	$[{\rm kg}/({\rm m}^3\,{\rm s})]$	$3.000\cdot 10^{-4}$	(5.31c)	[41, 42]
c	$[{\rm m}^2]$	$\{0,-10^{-6}\}$	(5.33)	—
g_0	$[-]$	$0.125\cdot 10^{-1}$	(5.41a)	—
f_0	$[-]$	$1+g_0$	(5.41a)	—
h_0	$[1/{\rm cm}]$	$8\,\pi$	(5.41a)	—
a_0	$[-]$	1.020	(5.41b)	—
b_0	$[-]$	0.010	(5.41b)	—
r_0	$[1/{\rm cm}]$	$50\,\pi$	(5.41b)	—
$\omega_{\rm Ncr}$	$[-]$	$1.000\cdot 10^{-3}$	(5.31d), (5.33),(5.42)	—
$\omega_{\rm Nenv}$	$[-]$	$7.000\cdot 10^{-3}$	(5.31d),(5.42)	—
$\omega_{\rm N0}$	$[-]$	$1.480\cdot 10^{-4}$	(5.31c)	—
δ_1	$[-]$	$7.138\cdot 10^{-1}$	(5.31d),(5.42)	[167]
δ_2	$[{\rm Pa}]$	$1.541\cdot 10^{3}$	(5.31d),(5.42)	[167]

Table 5.2: Parameters used in the definitions of the system's geometry, in the definitions of the sources and sinks of mass, and in the initial conditions for γ.

and non-vanishing curvatures. Specifically, we consider two types of $\gamma_{\rm in}(Z)$, i.e.,

$$\gamma_{\rm osc}(Z) = f_0 + g_0\cos(h_0 Z), \tag{5.41a}$$

$$\gamma_{\rm atan}(Z) = \begin{cases} a_0 - b_0\,{\rm atan}\Big(r_0\left(Z+\frac{1}{4}L\right)\Big), & Z\in\left[-\frac{1}{2}L,0\right], \\ a_0 + b_0\,{\rm atan}\Big(r_0\left(Z-\frac{1}{4}L\right)\Big), & Z\in\left]0,\frac{1}{2}L\right], \end{cases} \tag{5.41b}$$

both defining even functions with respect to $Z=0$, and representing a grown configuration of the tumour characterised by strong inhomogeneities. All the parameters featuring in (5.41a) and (5.41b) are reported in Table 5.2. The models 'M1' and 'M2' are further specialised in 'M1(a)' and 'M2(a)', for $\gamma_{\rm in}=\gamma_{\rm osc}$, and 'M1(b)' and 'M2(b)', for $\gamma_{\rm in}=\gamma_{\rm atan}$.

5.5.1 Formulation of specialised sub-models

Models M1(a) and M1(b) [no spatial resolution of the inhomogeneities]
We solve (5.40a)–(5.40e) with $c=0$, thereby switching off the curvature in the simulations. Hence, (5.40e) reduces to the ordinary differential equation

$$\frac{\dot{\gamma}}{\gamma} = \frac{\zeta_{\rm fp}}{3\varrho_{\rm s}}\left\langle\frac{\omega_{\rm N}-\omega_{\rm Ncr}}{\omega_{\rm Nenv}-\omega_{\rm Ncr}}\right\rangle_+\left[1-\frac{\delta_1\langle\bar{\sigma}\rangle_+}{\delta_2+\langle\bar{\sigma}\rangle_+}\right]\frac{(1+u')-\gamma^3\Phi_{{\rm s}\nu}}{(1+u')(1-\Phi_{{\rm s}\nu})}\omega_{\rm p} - \frac{\zeta_{\rm nf}}{3\varrho_{\rm s}}[1-\omega_{\rm p}], \tag{5.42}$$

and the boundary condition (5.37h) is no longer necessary. Therefore, together with (5.40a)–(5.40d) and (5.42), only the boundary conditions (5.37a)–(5.37g) and the initial conditions (5.38a)–(5.38f) have to be accounted for.

Although the spatial variability of γ does not play a direct role on (5.42), the initial distribution of the growth-related distortions *does* influence the evolution of γ.

Models M2(a) and M2(b) [spatial resolution of the inhomogeneities] We solve (5.40a)–(5.40e) with $c \neq 0$, and we enforce the complete set of boundary and initial conditions, i.e., (5.37a)–(5.37h) and (5.38a)-(5.38f), respectively. In this case, the scalar curvature, κ_γ, *does* contribute to drive the evolution of γ, through the first term on the right-hand-side of (5.40e).

5.5.2 Numerical results

In this section, with the description of the obtained numerical results and the role played by the scalar curvature associated with the growth, we answer to the research question (5.1). In Fig. 5.1, we report the displacement of the tumour in the axial direction of the specimen, evaluated at the cross section of the cylinder $Z = L/2$, i.e., $u(L/2,t) = \chi^z(L/2,t) - \chi^z(L/2,0)$. As expected, in all the considered cases, the results of our simulations show that $u(L/2,t)$ increases monotonically with time. By comparing M1(a) with M2(a), and M1(b) with M2(b), we note that the curvature seems to play a significant role in the evolution of the tumour displacement. In fact, the inclusion of the curvature augments the steepness of the displacement from the beginning of the simulation, and, from the 3rd day onward, it increases its magnitude appreciably. This result suggests, in addition, that the initial curvature relaxes, and that the system, at the end of the simulation, finds itself in a less curved configuration.These deductions are confirmed by Fig. 5.2 and Fig. 5.3, in which the spatial distribution of the scalar curvature κ_γ, at the initial and final instants of time, is presented.

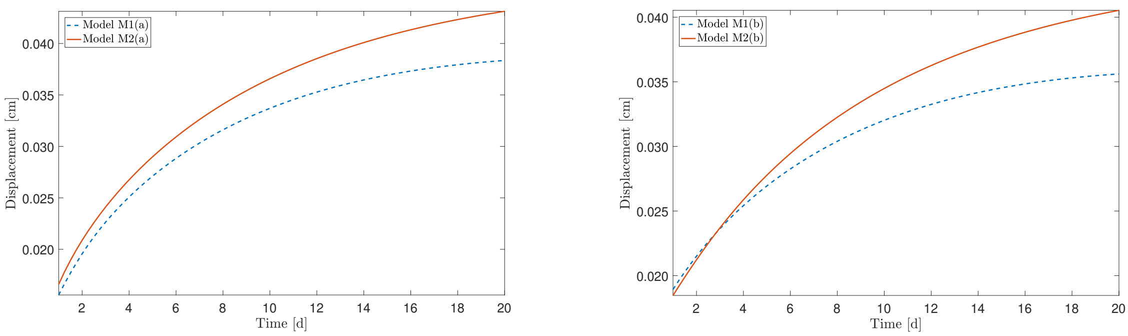

Figure 5.1: Evolution of the tumour in the axial direction, evaluated at the cross section $Z = L/2$. Panel on the left: comparison between M1(a) and M2(a), for which $\gamma_{\text{in}} = \gamma_{\text{osc}}$. Panel on the right: comparison between M1(b) and M2(b), for which $\gamma_{\text{in}} = \gamma_{\text{atan}}$.

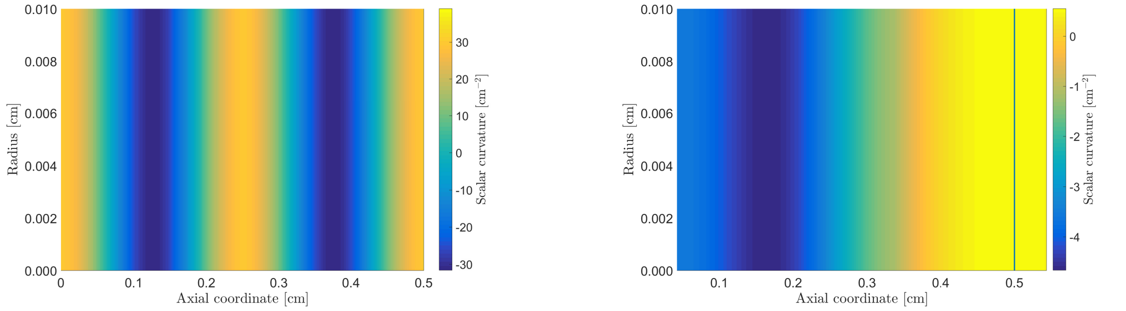

Figure 5.2: Spatial distribution of the scalar curvature κ_γ evaluated on the meridian section of the specimen, in the case of $\gamma_{\text{in}} = \gamma_{\text{osc}}$. Panel on the left: initial instant of time. Panel on the right: final instant of time.

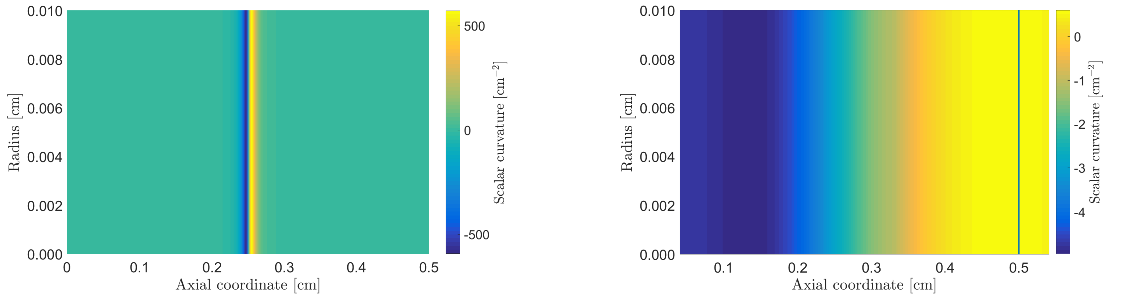

Figure 5.3: Spatial distribution of the scalar curvature κ_γ evaluated on the meridian section of the specimen, in the case of $\gamma_{\text{in}} = \gamma_{\text{atan}}$. Panel on the left: initial instant of time. Panel on the right: final instant of time.

Starting from Fig. 5.2, we note that the oscillating behaviour of the scalar curvature κ_γ, which reflects the trend of the initial distribution of the inhomogeneities $\gamma_{\text{in}} = \gamma_{\text{osc}}$, results strongly mitigated at the end of the simulation. In fact, oscillations are appeased in this case, and κ_γ is closer to zero than the initial case, which means that tissue is evolving towards a configuration with reduced curvature. Analogously, in Fig. 5.3, the concentration of the gradient, which characterizes the scalar curvature for the model with $\gamma_{\text{in}} = \gamma_{\text{osc}}$, relaxes at the end of the simulation. Also in this case, the tissue attains a final configuration in which the inhomogeneities are appreciably redistributed. The presence of the curvature κ_γ in the model and its relaxation, influences the spatial trend of the growth. In this sense, looking at Fig. 5.4, we notice that marked qualitative differences emerge among the spatial profiles of γ computed with M1(a) and M2(a), or M1(b) and M2(b). Still, if we neglect the embodiment of the curvature, the curves are qualitatively similar, with the magnitude increasing as time goes by. In particular, no peculiarity of the initial data seems to be found in the computed curves: The presence of oscillations in the case for which $\gamma_{\text{in}} = \gamma_{\text{osc}}$ (left), or the steep change in concavity, for the other

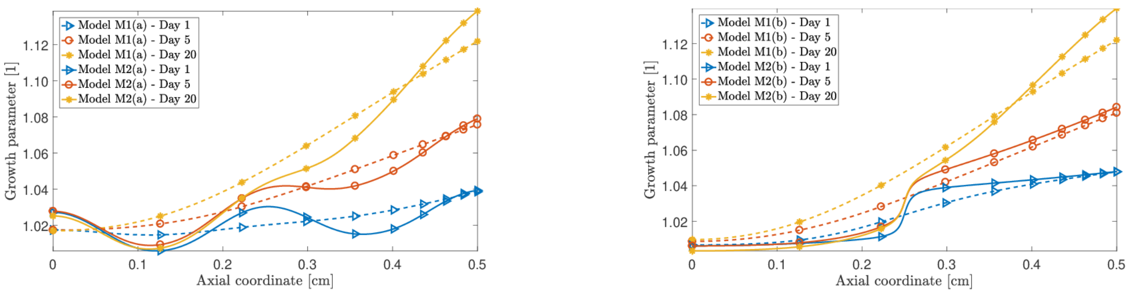

Figure 5.4: Spatial profile of the growth parameter γ for the models with $\gamma_{\text{in}} = \gamma_{\text{osc}}$ (panel on the left) and $\gamma_{\text{in}} = \gamma_{\text{atan}}$ (panel on the right). Since the problem is symmetric, only the half $[0, L/2]$ of the domain is shown.

choice of γ_{in}, i.e. $\gamma_{\text{in}} = \gamma_{\text{atan}}$ (right). On the other hand, when the curvature is explicitly considered, the spatial distribution of the growth is strongly influenced by the initial conditions. In detail, depending on time, the oscillations (left) and the rapid change in concavity (right), characterizing the two chosen initial distribution of inhomogeneities, are mitigated, but still present, until the end of the simulations. Although the differences outlined above, and independently on the initial condition γ_{in}, all the considered models lead to a final spatial behaviour of γ, in which the inhomogeneities are present.

Another point to put in evidence concerns Fig. 5.4 (left). The sub-system corresponding to the interval $[0, L/2]$ is initially symmetric with respect to $Z = L/4$. Yet, this further symmetry is lost in the course of time, as visible from the the spatial profile of γ. This peculiarity of the results could be explained by referring to biological motivations, rather than geometric ones. To specify this aspect, let us focus on Fig. 5.5, which reports the trend of the nutrient mass fraction. We note, indeed, that the nutrients tend to diffuse from the boundaries $(\partial\mathscr{B})_{\text{Left}}$ and $(\partial\mathscr{B})_{\text{Right}}$ towards the centre of the specimen, along its axial direction. In the course of this process, there exists an instant of time after which the mass fraction of the nutrients becomes smaller than the critical value ω_{Ncr} in the interior of the tumour. Hence, while the growth of the tumour is inhibited in its centre, it is active close to the free boundaries, where the mass fraction of the nutrients is still higher than the critical threshold.

A relevant result concerns the dynamics of the proliferating cells, as shown in Fig. 5.6. Their mass fraction, ω_{p}, remains close to unity in the proximity of the boundary $(\partial\mathscr{B})_{\text{Right}}$, where the level of nutrients is still high, while it diminishes in the centre of the tumour, where nutrients tend to become unavailable (this means that the proliferating cells are "converted" into necrotic ones). This phenomenon is influenced by the explicit resolution of the curvature in the model. Indeed, when the curvature is explicitly considered, the conversion process of proliferating cells into necrotic ones is accelerated in the first days, and slowed down towards the end

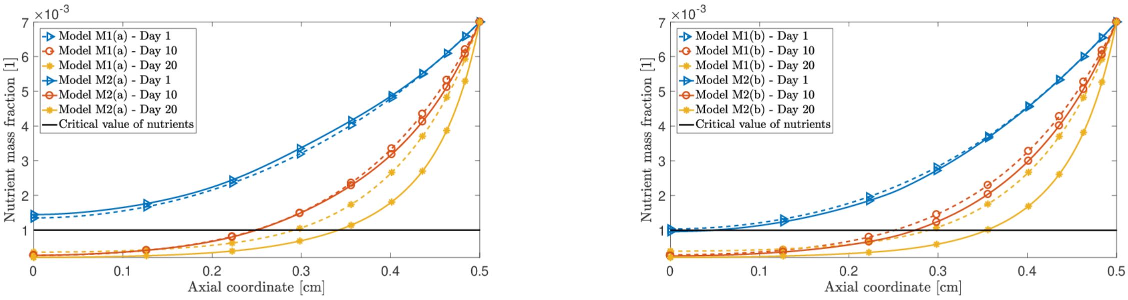

Figure 5.5: Spatial profile of the nutrient mass fraction ω_N for the models with $\gamma_{in} = \gamma_{osc}$ (panel on the left) and $\gamma_{in} = \gamma_{atan}$ (panel on the right). Since the problem is symmetric, only the half $[0, L/2]$ of the domain is shown.

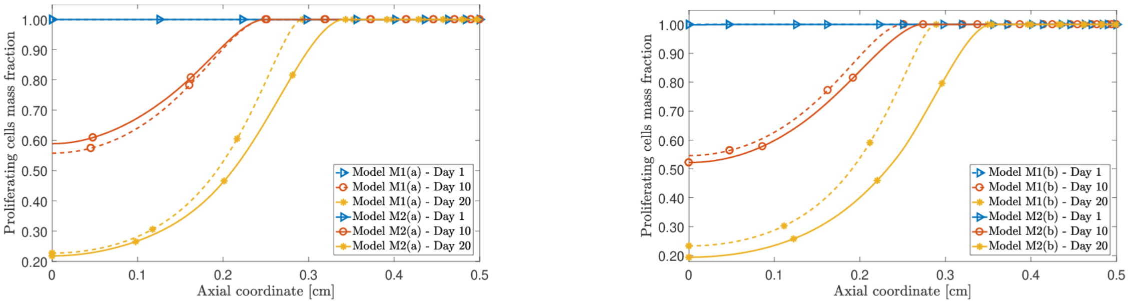

Figure 5.6: Spatial profile of the proliferating cells mass fraction ω_P for the models with $\gamma_{in} = \gamma_{osc}$ (panel on the left) and $\gamma_{in} = \gamma_{atan}$ (panel on the right). Since the problem is symmetric, only the half $[0, L/2]$ of the domain is shown.

of the simulations. This behaviour occurs for both choices of γ_{in}, but appears to be slightly more pronounced for $\gamma_{in} = \gamma_{atan}$.

To proceed with our analysis, we refer to Fig. 5.7, where we plot the behaviour of the pressure, p. When the tumour grows, the interstitial fluid flows towards the centre of the tumour, and p decreases from the free boundary (where the condition $p = 0$ applies) to the tumour's interior, where it takes on negative values. However, when the system goes towards the end of the simulations, p tends to become positive in the cases in which the curvature is explicitly accounted for, while it tends to zero from below otherwise.

Finally, in Fig. 5.8, we display the effective stress $\bar{\sigma}$. First, we notice that the tumour is subjected to a compressive stress, since $\bar{\sigma}$ is positive. Apart from this result, which is common to all the studied cases, we report that the curvature modifies the qualitative behaviour of $\bar{\sigma}$. As final remark, we note how the spatial evolution of the stress in the specimen, independently of the model, is strongly affected by the initial distribution of the inhomogeneities.

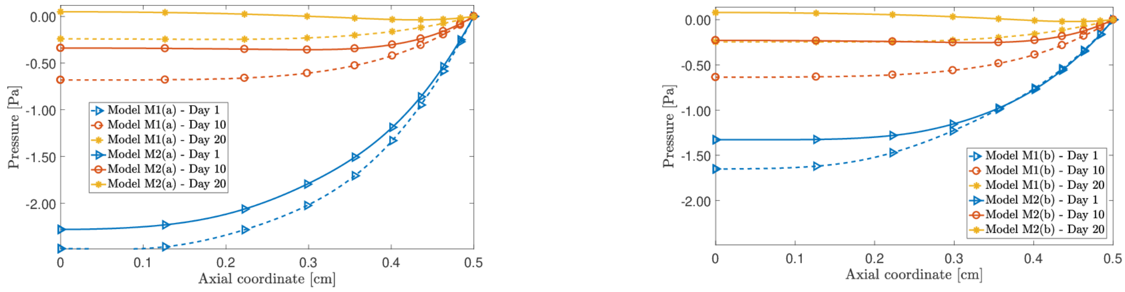

Figure 5.7: Spatial profile of the pore pressure p for the models with $\gamma_{\rm in} = \gamma_{\rm osc}$ (panel on the left) and $\gamma_{\rm in} = \gamma_{\rm atan}$ (panel on the right). Since the problem is symmetric, only the half $[0, L/2]$ of the domain is shown.

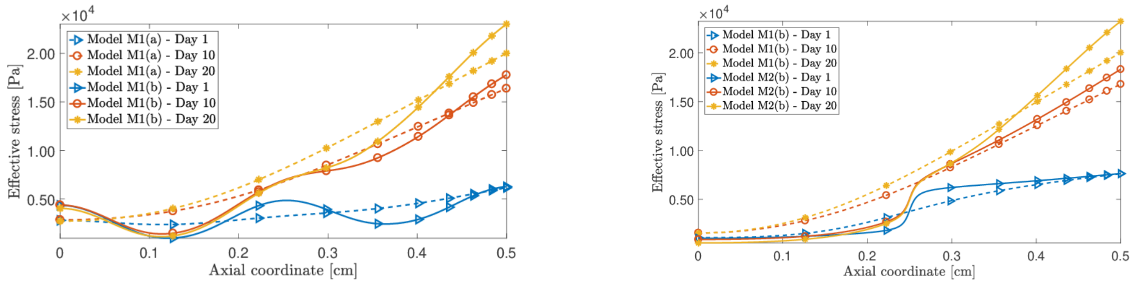

Figure 5.8: Spatial profile of the effective stress $\bar{\sigma}$ for the models with $\gamma_{\rm in} = \gamma_{\rm osc}$ (panel on the left) and $\gamma_{\rm in} = \gamma_{\rm atan}$ (panel on the right). Since the problem is symmetric, only the half $[0, L/2]$ of the domain is shown.

5.6 Conclusion

In this work, a mathematical model addressing tumour growth has been presented. The mechanical framework has been developed by regarding the tumour as a multi-constituent, biphasic medium, and by enforcing the BKL-decomposition of the deformation gradient tensor. The growth of the tumour is influenced by both mechanical stimuli and biological factors, such as the nutrients transported by the interstitial fluid, and the interactions among proliferating and necrotic cells.

The principal novelty of our approach consists of a partial reformulation of the balance laws for the constituents of the solid phase, in such a way that it is introduced an explicitly dependence on the scalar curvature, κ_γ, generated by the growth tensor $\boldsymbol{U}_\gamma = \gamma \boldsymbol{I}$ through the Riemannian, growth-related metric tensor $\boldsymbol{C}_\gamma = \gamma^2 \boldsymbol{G}$.

The introduction of κ_γ amounts to express the evolution law for γ as a partial differential equation, with the purpose of obtaining a better resolution of the material inhomogeneities, and an estimate of their influence on growth. To accomplish this task, we prescribe two types of initial conditions for γ, both characterised by strong gradient and nonzero initial curvature, $\kappa_{\gamma\rm in}$.

Two more thoughts about our results may be worth to be mentioned. The first one concerns the physical interpretation of the evolution of the initial inhomogeneities accompanying $\gamma_{\rm in}$. Indeed, since γ evolves according to a generalised diffusion-reaction like equation, one may say that, in our model, the material inhomogeneities brought about by growth "dissipate" towards a configuration in which they are redistributed over the tissue. This discussion answers the research question 5.2. The second thought pertains to the structure of the evolution equation (5.40e), and is also related to the first one. Indeed, in the case in which the initial inhomogeneities relax, the system tends to pass from a configuration in which it is not invariant under material translations to a homogeneous configuration in which it is translational invariant, thereby restoring the symmetry that is initially broken by $\gamma_{\rm in}$. This discussion answers the research question 5.3.

One limitation of our study is related to the fact that, in this work, we have just relied on a phenomenological model in which κ_γ appears without a strong theoretical justification. We have not built a systematic constitutive framework, in which, for example, the strain energy density of our material depends on γ *and* on κ_γ, nor have we conducted any study of the dissipation inequality of the system at hand. Yet, confident in the intuitions that have led to the model presented in [66], we hope that our results could provide a basis for further investigations.

In our work, we concentrated on an academic benchmark problem in order to compare our results with those of other Authors and, in particular, with those of Ambrosi and Mollica [10]. For this reason, our general setting is *as* simple *as* the setting of the problems taken as reference, expect for the fact that we deal with a biphasic system featuring two cell populations and for the fact that we account for the role of inhomogeneities through the introduction of the term $r_{\rm p\gamma}$ in the mass balance law of the proliferant cells. Clearly, our model can be further generalised and, in our opinion, this could be done in several steps. Here, we give some indications on how the formulation of our problem should look like if such generalisations were done.

First, one could consider exactly the same framework and geometry as the ones presented here, while relaxing the hypothesis of axial symmetry of the problem. In this case, the initial inhomogeneities may vary not only in the axial direction, but also radially or circumferentially, and the scalar curvature κ_γ must be computed according to its own definition (5.6), since it is no longer represented by (5.39). This requires the computation of all the partial derivatives necessary to determine the Christoffel symbols as well as the fourth-order curvature tensor specified in (5.4) and (5.5), respectively.

A second option could be to formulate an evolution law for γ in which the evolution is driven by the full curvature tensor $\boldsymbol{\mathcal{R}}$ and its gradient $\mathrm{Grad}\boldsymbol{\mathcal{R}}$, rather than by the scalar curvature only. In this case, the definitions of $r_{\rm p\gamma}$ and $r_{\rm n\gamma}$ should be further generalised, thereby implying a rewriting of the mass balance laws of the proliferant and necrotic cells.

A further extension of the model could be the formulation of an evolution law for the whole growth tensor $\boldsymbol{F}_\gamma$, with a restriction on $\mathrm{tr}[\dot{\boldsymbol{F}}_\gamma \boldsymbol{F}_\gamma^{-1}]$, as done in (5.10b). A model of this type extends the concept of growth presented in this work and further rephrases the theory proposed in [66].

Another step is to specialise our model to problems with more realistic geometries, which may arise from two- and three-dimensional studies. For a given study, this means that the boundary value problem formulated in our work has to be modified, and the Finite Element scheme adopted to solve it has to be extended accordingly. In particular, the use of new computational schemes may not be needed to resolve physical phenomena that could not be captured otherwise, as is the case, for example, when the growth of a tumour in the present of a host tissue and is studied [166].

Finally, although in the present work we dispensed with remodelling from the outset, we are aware of the fact that such process accompanies growth. In fact, it plays an important role in the redistribution of the mechanical stress within the tissue and, thus, on the modulating effect of the latter on the growth of a tumour. One possible way for studying remodelling is to use the decompositions $\boldsymbol{F} = \boldsymbol{F}_\mathrm{e}\boldsymbol{F}_\mathrm{r}\boldsymbol{F}_\gamma$ or as $\boldsymbol{F} = \boldsymbol{F}_\mathrm{e}\boldsymbol{F}_\gamma\boldsymbol{F}_\mathrm{r}$, where $\boldsymbol{F}_\mathrm{r}$ represents the distortion tensor describing the remodelling process, and to study the dynamics of $\boldsymbol{F}_\mathrm{r}$ in relationship with all the other model variables. In the literature, $\boldsymbol{F}_\mathrm{r}$ is often assumed to describe a plastic-like phenomenon and is thus treated accordingly. Within the context of tumour growth, $\boldsymbol{F}_\mathrm{r}$ accounts for the structural transformations of a tissue at the cellular level. Its introduction requires to elaborate numerical schemes capable of capturing the interplay between the growth and the structural evolution of a tissue, even when these phenomena exhibit rather separated time scales. Finally, at the pore scale, the effect of inhomogeneities could be studied by introducing a kinematic descriptor, called "*intrinsic volume ratio*" [217].

We summarise the answers to the research questions 5.1—5.3 in the following way:

- In general, we note that the scalar curvature associated with the growth tensor plays a significant role, both qualitatively and quantitatively, on the evolution of the main quantities of interest related to the growth of a tumour in the avascular stage (we recall, however, that these results are not ready to be used for clinical purposes).

- The growth in the regions close to the ends of the specimen is more pronounced than in the case in which the scalar curvature associated with γ is not considered.

- The growth parameter evolves in such a way that, in the model M2(a), its initial oscillations tend to disappear and its profile tends to become more straight, and, in the model M2(b), the material gradient of γ, initially concentrated at $Z = L/4$, tends to spread over the tumour's domain. In the model M2(a), the symmetry of the initial distribution of the growth parameter tends to be lost. Indeed, we start with a discrete symmetry, given by the period of the oscillations and, as time goes by, the curves tend to acquire a more uniform gradient. In the model M2(b), the distribution of the growth parameter is such that the tumour is materially homogeneous before and after the kink of $\gamma_{\mathrm{atan}}(Z = L/4)$ at early times and become increasingly inhomogeneous as time goes by.

Chapter 6

Growth and remodelling through strain-gradient plasticity.

The work reported in this chapter has been previously published in [114].

6.1 Strain gradient theories for remodelling and growth

Motivated by the increasing interest of the biomechanical community towards the employment of strain-gradient theories for solving biological problems, we study the growth and remodelling of a biological tissue on the basis of a strain-gradient formulation of remodelling. Our scope is to evaluate the impact of such an approach on the principal physical quantities that determine the growth of the tissue. For our purposes, we assume that remodelling is characterised by a coarse and a fine length scale and, taking inspiration from a work by L. Anand, O. Aslan, and S.A. Chester, we introduce a kinematic variable that resolves the fine scale inhomogeneities induced by remodelling. With respect to this variable, a strain-gradient framework of remodelling is developed. We adopt this formulation in order to investigate how a tumour tissue grows *and* how it remodels *in response* to growth. In particular, we focus on a type of remodelling that manifests itself in two different, but complementary, ways: on the one hand, it finds its expression in a stress-induced reorganisation of the adhesion bonds among the tumour cells, and, on the other hand, it leads to a change of shape of the cells and of the tissue, which is generally not recovered when external loads are removed. To address this situation, we resort to a generalised Bilby-Kröner-Lee decomposition of the deformation gradient tensor. We test our model on a benchmark problem taken from the literature, which we rephrase in two ways: micro-scale remodelling is disregarded in the first case, and accounted for in the second one. Finally, we compare and discuss the obtained numerical results.

To further clarify the type of remodelling addressed in this work, and to contextualise the wording "plastic-like distortions", we provide an explicit example of the inelastic rearrangement of the cells of a tissue. For this purpose, we discuss the results of an experiment commented in [86]. In Figure 6.1 (which corresponds to Figure 7 of [86]), Forgacs et al. [86] show three different stages of a cellular aggregate subjected to a loading history referred to as *"centrifugation"* [86]. The first column of Figure 6.1 reports the configuration of the aggregate *"before centrifugation"*[86], when the cells are *"isodiametric"* and the aggregate is spherical. The second column, instead, shows the aggregate after a 5 minute centrifugation: at this stage, the aggregate is no longer spherical, the cells have changed their shape and are said to be in a *"rapidly relaxing, more elastic phase"* [86]. Finally, the third column depicts the configuration of the aggregate after 36 hour centrifugation. In this configuration, the aggregate is believed to have reached a new state of equilibrium, and its cells seem to have attained a state free of stress. Most importantly, the cells seem to have changed their positions and to have redistributed their shape and orientation in a permanent manner, so that the aggregate does not spontaneously tend to recover its original configuration, regardless of the absence of external loads. Forgacs et al. [86] use the theory of viscoelasticity to model the experiment described so far. To us, however, the inelastic behaviour of the cellular aggregate may also suggest interpretations other than, and perhaps complementary to, viscoelasticity. Indeed, looking at the third column of Figure 6.1, one observes that the internal structure of the aggregate has changed, and this change seems to be due to the fact that the cells, relaxed or not, have modified their shape and arrangement inside the tissue. Therefore, at least in our opinion, viscoelasticity alone may be insufficient to accurately account for the irreversible deformations (distortions) of the tissue. Rather, the interpretation of the just discussed phenomenology may necessitate concepts borrowed from the theories of plasticity or viscoplasticity, since these are able to describe the tissue's internal kinematics in a way that is similar to the motion of the defects in solids. This view seems to be corroborated also by other experiments conducted on tumour spheroids (see e.g. [219] and references therein). In such experiments, a spheroid is allowed to grow and, after growth has occurred, it is cut radially for a length of about the 80% of its diameter: what is observed is a relaxation of the stresses, resulting in the opening of the spheroid, with the edges of the cut drifting away from one another (see Figure 6.1d). This behaviour, in fact, suggests the existence of an incompatible, stress-free state of the tumour, which is consistent with the description of the tumour as an elasto-plastic material. To us, this observation justifies the approach followed in our work, although it does not exclude visco-plastic effects. While bearing this in mind, for simplicity we restrict here our investigations to the case of plasticity alone, and we adopt this approach to model the internal rearrangement, i.e., the remodelling, of the tissues studied in our work. The above discussion answers the research question 6.3.

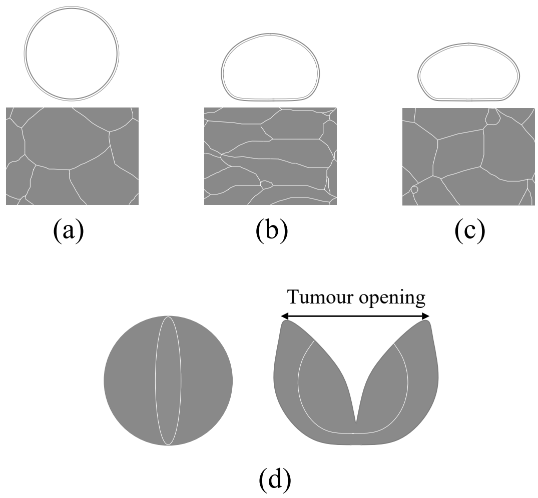

Figure 6.1: First row (redrawn and adapted from Forgacs et al. [86]): Schematic representation of the cells rearrangement in an spherical aggregate (a) before centrifugation, (b) after a 5 minute centrifugation, and (c) after 36 hour centrifugation. Second row (redrawn and adapted from Stylianopoulos et al. [219]): Stress relaxation of a tumour spheroid after a radial cut is performed.

6.2 Kinematics

6.2.1 Kinematical descriptors

To account for the growth and structural reorganisation of the tissue, we have recourse to the multiplicative decomposition of the deformation gradient tensor, which we propose in the form [9, 144, 105]

$$\boldsymbol{F} = \boldsymbol{F}_{\rm e}\boldsymbol{F}_{\rm p}\boldsymbol{F}_{\gamma}. \tag{6.1}$$

In (6.1), $\boldsymbol{F}_{\gamma}$, $\boldsymbol{F}_{\rm p}$, and $\boldsymbol{F}_{\rm e}$ describe the distortions associated with the uptake or loss of mass, the distortions accompanying the plastic-like rearrangement of the tissue's internal structure, and the distortions due to the elastic accommodation of the tissue, respectively. In the sequel, $\boldsymbol{F}_{\rm p}$ and $\boldsymbol{F}_{\gamma}$ will also be referred to as *remodelling tensor*[1] and *growth tensor*, respectively. We notice that, whereas it is rather standard to consider $\boldsymbol{F}_{\rm e}$ as the first factor of the right-hand-side of (6.1), the order of appearance of $\boldsymbol{F}_{\rm p}$ and $\boldsymbol{F}_{\gamma}$ is not standard at all. Indeed, it is conceivable to formulate a decomposition of $\boldsymbol{F}$ in which the inelastic contributions to the overall

[1]We use the subscript "p" to emphasise the fact that the distortions associated with remodelling are plastic-like. In this respect, we could have also referred to $\boldsymbol{F}_{\rm p}$ as "plasticity tensor". However, we prefer to speak here of "remodelling tensor", because the concept of remodelling is more specific for the addressed biological materials.

deformation appear in reverse order. In addition, there exist also cases in which the accommodating part of the deformation is put at the end of the decomposition [46]. We adopt the order shown above because, in the present work, we have in mind a tissue that grows *and* that remodels its internal structure *in response* to growth. This statement notwithstanding, we regard growth and structural reorganisation as independent, yet mutually interacting processes. Consequently, we consider $\boldsymbol{F}_\mathrm{p}$ and $\boldsymbol{F}_\gamma$ as independent kinematic (tensor) variables and, following the same philosophy outlined by some previous publications [44, 60, 183, 110, 62, 56], we associate each of them with degrees of freedom having the same "dignity" as those related to the other kinematic descriptors, i.e., $\boldsymbol{V}_\mathrm{s}$ and $\boldsymbol{V}_\mathrm{f}$. Finally, we emphasise that the decomposition (6.1) is a generalised Bilby-Kröner-Lee decomposition (see e.g. [176] for similar decompositions in the case of damage or other inelastic processes). Since we have recently discussed the decomposition (6.1) in [62] for the case of growth, here we do not fuss over the physics behind it, and we suggest the reviews [176, 213] and Chapter 5 for details. However, we recall that, for every $X \in \mathscr{B}$ and $t \in \mathscr{I}$, the product $\boldsymbol{F}_\mathrm{p}(X,t)\boldsymbol{F}_\gamma(X,t)$ maps vectors of the tangent space $T_X\mathscr{B}$ into vectors of the image vector space $\mathscr{N}_X(t)$, attached at X. By ideally performing such transformation for all $X \in \mathscr{B}$, the solid phase is brought into a relaxed state at time t, the latter being characterised by the absence of *any* stresses, including the residual ones. Such state is also referred to as *natural state* [176, 106].

Differentiation of $\boldsymbol{F}$ with respect to time and left-multiplication by $\boldsymbol{F}^{-1} = \boldsymbol{F}_\gamma^{-1}\boldsymbol{F}_\mathrm{p}^{-1}\boldsymbol{F}_\mathrm{e}^{-1}$ yield

$$\dot{\boldsymbol{F}}\boldsymbol{F}^{-1} = \dot{\boldsymbol{F}}_\mathrm{e}\boldsymbol{F}_\mathrm{e}^{-1} + \boldsymbol{F}_\mathrm{e}\boldsymbol{L}_\mathrm{p}\boldsymbol{F}_\mathrm{e}^{-1} + \boldsymbol{F}_\mathrm{e}\boldsymbol{F}_\mathrm{p}\boldsymbol{L}_\gamma\boldsymbol{F}_\mathrm{p}^{-1}\boldsymbol{F}_\mathrm{e}^{-1}, \tag{6.2}$$

where we introduced the tensor of *rate of remodelling-induced distortions*, $\boldsymbol{L}_\mathrm{p} \equiv \dot{\boldsymbol{F}}_\mathrm{p}\boldsymbol{F}_\mathrm{p}^{-1}$, and the tensor of *rate of growth-induced distortions*, $\boldsymbol{L}_\gamma \equiv \dot{\boldsymbol{F}}_\gamma\boldsymbol{F}_\gamma^{-1}$. In compliance with (6.1), the *volume ratio* $J \equiv \det\boldsymbol{F}$ can be rewritten as $J = J_\mathrm{e}J_\mathrm{p}J_\gamma$, where $J_\mathrm{e} \equiv \det\boldsymbol{F}_\mathrm{e}$, $J_\mathrm{p} \equiv \det\boldsymbol{F}_\mathrm{p}$, and $J_\gamma \equiv \det\boldsymbol{F}_\gamma$ denote, respectively, the volumetric distortions associated with the elastic, remodelling, and growth part of the deformation gradient tensor. We use these definitions to perform the Piola transformations of the mass balance laws (5.10a), (5.10b), (5.20a) and (5.20b) thereby obtaining

$$\rho_{\mathrm{s}0}\Phi_\mathrm{s}\dot{\omega}_\mathrm{p} = R_\mathrm{pn} + R_\mathrm{fp} - R_\mathrm{s}\omega_\mathrm{p}, \tag{6.3a}$$

$$\rho_{\mathrm{s}0}\dot{\Phi}_\mathrm{s} = R_\mathrm{s}, \tag{6.3b}$$

$$\rho_{\mathrm{f}0}\Phi_\mathrm{f}\dot{\omega}_\mathrm{N} + \rho_{\mathrm{f}0}\boldsymbol{Q}\,\mathrm{Grad}\,\omega_\mathrm{N} + \mathrm{Div}\boldsymbol{Y}_\mathrm{N} = R_\mathrm{Np} + R_\mathrm{s}\omega_\mathrm{N}, \tag{6.3c}$$

$$\dot{J} + \mathrm{Div}\,\boldsymbol{Q} = \left(\frac{1}{\rho_{\mathrm{s}0}} - \frac{1}{\rho_{\mathrm{f}0}}\right)R_\mathrm{s}, \tag{6.3d}$$

where, for every $X \in \mathscr{B}$ and $t \in \mathscr{I}$, we denote by

$$\Phi_\alpha(X,t) = J(X,t)\varphi_\alpha(\chi(X,t),t), \qquad \alpha \in \{\mathrm{f},\mathrm{s}\}, \tag{6.4a}$$

$$R_\beta(X,t) = J(X,t) r_\beta(\chi(X,t),t), \qquad \beta \in \{\mathrm{pn}, \mathrm{fp}, \mathrm{s}, \mathrm{Np}\}, \tag{6.4b}$$

$$\omega_\upsilon(X,t) = c_\upsilon(\chi(X,t),t), \qquad \upsilon \in \{\mathrm{p}, \mathrm{N}\}, \tag{6.4c}$$

the material volumetric fractions, the material sources/sinks of mass, and the mass fractions expressed as functions of X and time, respectively. We recall that, in (6.4c), c_p and c_N are the spatial volumetric fraction of the proliferating cells and of the nutrients, respectively [114]. Moreover, we introduced the material flux vectors associated with the filtration velocity $\varphi_\mathrm{f}\boldsymbol{w}$ and with the nutrients' mass flux vector $\boldsymbol{y}_\mathrm{N}$, respectively, i.e.,

$$\boldsymbol{Q}(X,t) = \Phi_\mathrm{f}(X,t)\boldsymbol{w}(\chi(X,t),t)\boldsymbol{F}^{-\mathrm{T}}(X,t), \tag{6.5a}$$

$$\boldsymbol{Y}_\mathrm{N}(X,t) = J(X,t)[\boldsymbol{y}_\mathrm{N}(\chi(X,t),t)]\boldsymbol{F}^{-\mathrm{T}}(X,t). \tag{6.5b}$$

In particular, $\boldsymbol{Q}$ will also be referred to as *material filtration velocity* in the sequel.

The kinematic picture of the problem under study is completed with a scalar descriptor, denoted by $\mathrm{e}_\mathrm{p} : \mathscr{B}(t) \times \mathscr{I} \to \mathbb{R}$. This quantity and its gradient, $\nabla \mathrm{e}_\mathrm{p}$, have been introduced in [15] with the purpose of constructing indicators of the inelastic transformations occurring in the body at the scale of its micro-structure. More precisely, in [15] the Authors speak of e_p in terms of a *"measure of the inhomogeneity of the microscale plasticity"*. In our framework, it is more appropriate to interpret e_p as a variable defined to resolve explicitly the inhomogeneities induced by the remodelling of the tissue. To this end, we define the "Lagrangian field" $\mathfrak{e}_\mathrm{p}$, such that $\mathfrak{e}_\mathrm{p}(X,t) = \mathrm{e}_\mathrm{p}(\chi(X,t),t)$, and the material gradient $\mathrm{Grad}\mathfrak{e}_\mathrm{p}(X,t) = [\nabla \mathrm{e}_\mathrm{p}(\chi(X,t),t)]\boldsymbol{F}(X,t)$.

6.2.2 Constraints on the kinematic variables

By virtue of the presence of growth in our model, the study conducted in this work may be thought of as a slight generalisation of the framework depicted by Anand et al. [15], where the Authors develop a scalar theory of strain-gradient plasticity based on several *ab initio* restrictions on the kinematic variables of their problem. Such restrictions are expressed in terms of the generalised velocities of the proposed theory, and are thus cast in non-holonomic form. To highlight their role on the overall dynamics of the system under investigation, we specify the imposed constraints, and we discuss in detail their impact on the kinematic descriptors that they involve.

For the sake of clarity, we start with rephrasing, in our formalism, the constraints on $\boldsymbol{F}_\mathrm{p}$ and $\dot{\boldsymbol{F}}_\mathrm{p}$ introduced by Anand et al. [15]. On the top of those, we exploit the mass balance laws in order to extract pieces of information that can be interpreted as constraints on the growth tensor, $\boldsymbol{F}_\gamma$, and on its rate $\boldsymbol{L}_\gamma$.

If $\boldsymbol{L}_\mathrm{p}$ is assigned, $\boldsymbol{F}_\mathrm{p}$ can be computed by integrating the ordinary differential equation $\dot{\boldsymbol{F}}_\mathrm{p} = \boldsymbol{L}_\mathrm{p}\boldsymbol{F}_\mathrm{p}$, which can be rewritten as

$$\dot{\boldsymbol{F}}_\mathrm{p} = \left(\boldsymbol{\eta}^{-1}\boldsymbol{D}_\mathrm{p} + \boldsymbol{\eta}^{-1}\boldsymbol{W}_\mathrm{p}\right)\boldsymbol{F}_\mathrm{p}, \tag{6.6}$$

where $\boldsymbol{\eta}$ is the metric tensor associated with the tissue's natural state, while $\boldsymbol{D}_{\mathrm{p}}$ and $\boldsymbol{W}_{\mathrm{p}}$ are the symmetric part and the skew-symmetric part of $\boldsymbol{L}_{\mathrm{p}}$, respectively, i.e.,

$$\boldsymbol{D}_{\mathrm{p}} = \mathrm{sym}(\boldsymbol{\eta}\boldsymbol{L}_{\mathrm{p}}) = \tfrac{1}{2}\left(\boldsymbol{\eta}\boldsymbol{L}_{\mathrm{p}} + \boldsymbol{L}_{\mathrm{p}}^{\mathrm{T}}\boldsymbol{\eta}\right), \tag{6.7a}$$

$$\boldsymbol{W}_{\mathrm{p}} = \mathrm{skew}(\boldsymbol{\eta}\boldsymbol{L}_{\mathrm{p}}) = \tfrac{1}{2}\left(\boldsymbol{\eta}\boldsymbol{L}_{\mathrm{p}} - \boldsymbol{L}_{\mathrm{p}}^{\mathrm{T}}\boldsymbol{\eta}\right). \tag{6.7b}$$

Following the theory of [15], the *first constraint* on $\boldsymbol{F}_{\mathrm{p}}$ is supplied by requiring from the outset that the *"plastic" spin tensor*, $\boldsymbol{W}_{\mathrm{p}}$ vanishes identically, i.e., $\boldsymbol{W}_{\mathrm{p}} = \boldsymbol{0}$. Hence, we obtain the identity $\boldsymbol{L}_{\mathrm{p}} = \boldsymbol{\eta}^{-1}\boldsymbol{D}_{\mathrm{p}}$, and, consequently, Equation (6.6) becomes

$$\dot{\boldsymbol{F}}_{\mathrm{p}} = \boldsymbol{\eta}^{-1}\boldsymbol{D}_{\mathrm{p}}\boldsymbol{F}_{\mathrm{p}}. \tag{6.8}$$

The *second constraint* on $\boldsymbol{F}_{\mathrm{p}}$ stems from the hypothesis of isochoric remodelling distortions, i.e., $J_{\mathrm{p}} = \det \boldsymbol{F}_{\mathrm{p}} = 1$. This relation, in turn, can be put in differential form, i.e., $\dot{J}_{\mathrm{p}} = J_{\mathrm{p}}\mathrm{tr}[\dot{\boldsymbol{F}}_{\mathrm{p}}\boldsymbol{F}_{\mathrm{p}}^{-1}] = 0$, and implies $\mathrm{tr}[\boldsymbol{\eta}^{-1}\boldsymbol{D}_{\mathrm{p}}] = 0$, as can be deduced by right-multiplying Equation (6.8) by $\boldsymbol{F}_{\mathrm{p}}^{-1}$ and taking the trace of the resulting expression. Accordingly, only the deviatoric part of $\boldsymbol{D}_{\mathrm{p}}$, i.e., $\tilde{\boldsymbol{D}}_{\mathrm{p}} = \boldsymbol{D}_{\mathrm{p}} - \frac{1}{3}\mathrm{tr}[\boldsymbol{\eta}^{-1}\boldsymbol{D}_{\mathrm{p}}]\boldsymbol{\eta}$, is involved in (6.8), which reduces to

$$\dot{\boldsymbol{F}}_{\mathrm{p}} = \boldsymbol{\eta}^{-1}\tilde{\boldsymbol{D}}_{\mathrm{p}}\boldsymbol{F}_{\mathrm{p}}. \tag{6.9}$$

In analogy with [15], we base our model on the further hypothesis that $\tilde{\boldsymbol{D}}_{\mathrm{p}}$ is *co-directional* with a tensor $\boldsymbol{N}_{\nu}$, associated with the tissue's natural state, and obtained by normalising a symmetric tensorial measure of stress, which will be specified later. In formulae, by indicating with $\boldsymbol{\Sigma}_{\nu}$ such measure of stress, we define $\boldsymbol{N}_{\nu}$ as

$$\boldsymbol{N}_{\nu} \equiv \frac{\boldsymbol{\eta}\tilde{\boldsymbol{\Sigma}}_{\nu}\boldsymbol{\eta}}{\|\tilde{\boldsymbol{\Sigma}}_{\nu}\|_{\boldsymbol{\eta}}}, \tag{6.10}$$

where $\tilde{\boldsymbol{\Sigma}}_{\nu} \equiv \boldsymbol{\Sigma}_{\nu} - \frac{1}{3}\mathrm{tr}[\boldsymbol{\eta}\boldsymbol{\Sigma}_{\nu}]\boldsymbol{\eta}^{-1}$ is the deviatoric part of $\boldsymbol{\Sigma}_{\nu}$, and $\boldsymbol{\eta}\tilde{\boldsymbol{\Sigma}}_{\nu}\boldsymbol{\eta}$ is the covariant representation of $\tilde{\boldsymbol{\Sigma}}_{\nu}$, and we enforce the co-directionality condition as the *third constraint* on $\boldsymbol{F}_{\mathrm{p}}$, i.e.,

$$\tilde{\boldsymbol{D}}_{\mathrm{p}} = \|\tilde{\boldsymbol{D}}_{\mathrm{p}}\|_{\boldsymbol{\eta}^{-1}}\boldsymbol{N}_{\nu}. \tag{6.11}$$

Equation (6.11) follows from the hypothesis that the distortions associated with remodelling obey an evolution law of the same type as the normality rule of isotropic, associative, finite-strain plasticity. For this reason, the physical quantity that represents them, i.e., $\tilde{\boldsymbol{D}}_{\mathrm{p}}$, has to be co-directional with $\tilde{\boldsymbol{\Sigma}}_{\nu}$ (see Sections 95.5 and 98 of Gurtin et al. [124]). In turn, this condition is automatically satisfied by introducing the direction tensor $\boldsymbol{N}_\nu$ and requiring $\tilde{\boldsymbol{D}}_\mathrm{p}$ to be proportional to $\boldsymbol{N}_\nu$. Clearly, this identifies the corresponding proportionality factor with the norm of $\tilde{\boldsymbol{D}}_\mathrm{p}$.

In (6.10) and (6.11), the norms $\|\tilde{\boldsymbol{\Sigma}}_\nu\|_{\boldsymbol{\eta}}$ and $\|\tilde{\boldsymbol{D}}_\mathrm{p}\|_{\boldsymbol{\eta}^{-1}}$ are defined by

$$\|\tilde{\boldsymbol{\Sigma}}_\nu\|_{\boldsymbol{\eta}} = \sqrt{\mathrm{tr}\left[\left(\boldsymbol{\eta}\tilde{\boldsymbol{\Sigma}}_\nu\boldsymbol{\eta}\right)^\mathrm{T}\tilde{\boldsymbol{\Sigma}}_\nu\right]}, \tag{6.12a}$$

$$\|\tilde{\boldsymbol{D}}_\mathrm{p}\|_{\boldsymbol{\eta}^{-1}} = \sqrt{\mathrm{tr}\left[\boldsymbol{\eta}^{-1}\tilde{\boldsymbol{D}}_\mathrm{p}\boldsymbol{\eta}^{-1}\tilde{\boldsymbol{D}}_\mathrm{p}\right]}, \tag{6.12b}$$

and their product coincides with the double contraction $\tilde{\boldsymbol{\Sigma}}_\nu : \tilde{\boldsymbol{D}}_\mathrm{p} = \|\tilde{\boldsymbol{\Sigma}}_\nu\|_{\boldsymbol{\eta}}\|\tilde{\boldsymbol{D}}_\mathrm{p}\|_{\boldsymbol{\eta}^{-1}}$. Moreover, to simplify the notation, we invoke the definition of *accumulated plastic strain*[15, 176], ε_p, i.e.,

$$\varepsilon_\mathrm{p}(X,t) \equiv \sqrt{\tfrac{2}{3}}\int_0^t \|\tilde{\boldsymbol{D}}_\mathrm{p}(X,\tau)\|_{\boldsymbol{\eta}^{-1}}\mathrm{d}\tau \quad \Rightarrow \quad \dot{\varepsilon}_\mathrm{p}(X,t) = \sqrt{\tfrac{2}{3}}\,\|\tilde{\boldsymbol{D}}_\mathrm{p}(X,t)\|_{\boldsymbol{\eta}^{-1}}, \tag{6.13}$$

so that Equation (6.11) becomes

$$\tilde{\boldsymbol{D}}_\mathrm{p} = \sqrt{\tfrac{3}{2}}\,\dot{\varepsilon}_\mathrm{p}\boldsymbol{N}_\nu. \tag{6.14}$$

Finally, by substituting (6.14) into (6.9), we obtain

$$\dot{\boldsymbol{F}}_\mathrm{p} = \left(\sqrt{\tfrac{3}{2}}\,\dot{\varepsilon}_\mathrm{p}\boldsymbol{\eta}^{-1}\boldsymbol{N}_\nu\right)\boldsymbol{F}_\mathrm{p} \quad \Rightarrow \quad \boldsymbol{L}_\mathrm{p} = \sqrt{\tfrac{3}{2}}\,\dot{\varepsilon}_\mathrm{p}\boldsymbol{\eta}^{-1}\boldsymbol{N}_\nu. \tag{6.15}$$

Equation (6.15) implies that, once $\boldsymbol{N}_\nu$ is assigned, $\boldsymbol{L}_\mathrm{p}$ has only one independent coefficient, given by $\dot{\varepsilon}_\mathrm{p}$. The important consequence of this result is that the body's structural degrees of freedom, originally represented by the tensorial quantity $\boldsymbol{F}_\mathrm{p}$, condense into the scalar variable ε_p.

Remark 6.2.1 (Descriptive adequacy of ε_p). According to Equation (6.13), $\varepsilon_\mathrm{p}(X,t)$ is well-defined for all the tensor fields $\tilde{\boldsymbol{D}}_\mathrm{p}$ such that the norm $\|\tilde{\boldsymbol{D}}_\mathrm{p}(X,\cdot)\|_{\boldsymbol{\eta}^{-1}}$ is an integrable function of time over $[0,t]$, for every $X \in \mathscr{B}$ and $t \in [0,+\infty[$. Coherently with this definition, $\varepsilon_\mathrm{p}(X,t)$ keeps track of all the magnitudes of the rates of inelastic distortions, $\tilde{\boldsymbol{D}}_\mathrm{p}(X,\tau)$, which have occurred in a given material over $[0,t]$. For this reason, ε_p is a suitable descriptor of the mechanical response of materials that are capable of "perfectly memorising" inelastic distortions, as is the case for metals exhibiting rate-independent plasticity [133]. Biological tissues, on the contrary, are often modelled as viscoelastic materials [87, 86], and show fading memory effects. Nonetheless, as discussed in the Introduction, the experiments on cellular aggregates reported in [86, 219] seem to suggest the existence of inelastic distortions that do not fade away in time, unless some active process restores the original configuration of the aggregates. For these reasons, ε_p can be regarded as appropriate for describing the inelastic distortions accumulated in a tissue from the beginning of its loading history. Should the active processes be considered, they could be accounted for by introducing another factor, denoted e.g. by $\boldsymbol{F}_\mathrm{a}$, and representing the active part of the tissue's deformation [193].

We switch now to the constraints placed on $\boldsymbol{F}_\gamma$, and we analyse their impact on the way in which the mass balance law (6.3b) can be reformulated. Upon using the decomposition $J = J_{\mathrm{e}} J_{\mathrm{p}} J_\gamma$, and recalling the condition $J_{\mathrm{p}} = 1$, we rewrite Φ_{s} as $\Phi_{\mathrm{s}} = J_\gamma \Phi_{\mathrm{s}\nu}$, where $\Phi_{\mathrm{s}\nu}$ is such that $\Phi_{\mathrm{s}\nu}(X,t) = J_{\mathrm{e}}(X,t)\varphi_{\mathrm{s}}(\chi(X,t),t)$, and indicates, thus, the solid phase volumetric fraction with respect to the volume measure of the *natural state*. Hence, Equation (6.3b) becomes

$$\rho_{\mathrm{s}0} \dot{J}_\gamma \Phi_{\mathrm{s}\nu} + \rho_{\mathrm{s}0} J_\gamma \dot{\Phi}_{\mathrm{s}\nu} = R_{\mathrm{s}}. \tag{6.16}$$

A rather standard hypothesis in the mechanics of growth, see e.g. [72, 10, 160, 157], is to choose $\boldsymbol{F}_\gamma$ in such a way that the time derivative of its determinant, $\dot{J}_\gamma$, compensates for the mass source R_{s}. In other words, by exploiting the identity $\dot{J}_\gamma = J_\gamma \mathrm{tr}[\dot{\boldsymbol{F}}_\gamma \boldsymbol{F}_\gamma^{-1}] = J_\gamma \mathrm{tr}[\boldsymbol{L}_\gamma]$, we require the fulfilment of the auxiliary condition

$$\rho_{\mathrm{s}0} J_\gamma \Phi_{\mathrm{s}\nu} \mathrm{tr}[\boldsymbol{L}_\gamma] = R_{\mathrm{s}} \quad \Rightarrow \quad \mathrm{tr}[\boldsymbol{L}_\gamma] = \frac{R_{\mathrm{s}}}{\rho_{\mathrm{s}0}\Phi_{\mathrm{s}\nu} J_\gamma}, \tag{6.17}$$

which constitutes the *first constraint* on $\boldsymbol{F}_\gamma$. Such constraint has, in fact, non-holonomic nature, since it is defined through a non-homogeneous algebraic condition on the generalised (tensorial) velocity $\boldsymbol{L}_\gamma$. Plugging (6.17) into (6.16) yields $\rho_{\mathrm{s}0} J_\gamma \dot{\Phi}_{\mathrm{s}\nu} = 0$, thereby implying that the volumetric fraction $\Phi_{\mathrm{s}\nu}$ is necessarily independent of time.

The *second constraint* on $\boldsymbol{F}_\gamma$ is provided by the phenomenological evidence according to which, for the class of problems under study, growth occurs isotropically [9]. The consequences of this fact on the admissible choices of the growth tensor can be deduced by looking at the polar decompositions of $\boldsymbol{F}_\gamma$. Indeed, by considering for instance the right decomposition, $\boldsymbol{F}_\gamma = \boldsymbol{\mathcal{R}}_\gamma \boldsymbol{U}_\gamma$, where $\boldsymbol{\mathcal{R}}_\gamma$ is the rotation tensor and $\boldsymbol{U}_\gamma$ is the stretch tensor associated with $\boldsymbol{F}_\gamma$, the isotropy of growth translates to the kinematic restrictions $\boldsymbol{\mathcal{R}}_\gamma = \boldsymbol{I}$ and $\boldsymbol{U}_\gamma = \gamma \boldsymbol{I}$, where $\boldsymbol{I}$ is the identity tensor. Therefore, it holds that $\boldsymbol{F}_\gamma = \gamma \boldsymbol{I}$ and (6.17) can be rephrased as

$$\frac{\dot{\gamma}}{\gamma} = \frac{R_{\mathrm{s}}}{3\rho_{\mathrm{s}0}\Phi_{\mathrm{s}\nu} J_\gamma} \quad \Rightarrow \quad \dot{\gamma} = \frac{R_{\mathrm{s}}}{3\rho_{\mathrm{s}0}\Phi_{\mathrm{s}\nu}\gamma^2}. \tag{6.18}$$

Finally, we notice that Equation (6.3d) can be regarded as a constraint on the material filtration velocity, $\boldsymbol{Q}$, expressed through a restriction on its divergence.

6.3 Principle of Virtual Powers

After laying down the kinematic picture that describes the problem under investigation, we select the generalised velocities upon which the system's mechanical power is defined. Summarising the discussion reported above, such velocities may be enlisted in the following collection of fields

$$\mathcal{V} = (\boldsymbol{v}_{\mathrm{s}}, \nabla \boldsymbol{v}_{\mathrm{s}}, \mathrm{D}_{\mathrm{s}}\varepsilon_{\mathrm{p}}, \mathrm{D}_{\mathrm{s}}\mathrm{e}_{\mathrm{p}}, \nabla(\mathrm{D}_{\mathrm{s}}\mathrm{e}_{\mathrm{p}}) \,|\, \boldsymbol{v}_{\mathrm{f}}, \nabla \boldsymbol{v}_{\mathrm{f}}), \tag{6.19}$$

which will be employed to define the internal and the external mechanical powers. We remark that, whereas the fluid phase requires only $\boldsymbol{v}_{\mathrm{f}}$ and $\nabla\boldsymbol{v}_{\mathrm{f}}$ for the characterisation of the system's internal power, the solid phase necessitates both *standard* and *non-standard* descriptors. The standard ones, i.e., $\boldsymbol{v}_{\mathrm{s}}$ and $\nabla\boldsymbol{v}_{\mathrm{s}}$, account only for the *"visible"* changes of shape of the system (here, the word *"visible"* is meant in the sense of DiCarlo and Quiligotti [60]), while the non-standard terms are the generalised velocities $\mathrm{D_s}\varepsilon_{\mathrm{p}}$, $\mathrm{D_s e_p}$, and $\nabla(\mathrm{D_s e_p})$, introduced to define the power expended to accomplish the structural changes of the system. As anticipated in the Introduction, the main motivation for taking the approach of Anand et al. [15] and specialising it to our problem is that it allows to develop a strain-gradient formulation of remodelling based on the scalar variable $\mathrm{e_p}$. The latter is defined as the micro-scale counterpart of the accumulated remodelling strain, ε_{p}, and, as such, it is assumed to "condense" in itself all the information about the inelastic processes that determine the micro-scale remodelling of the tissue under study. Moreover, since it is an "effective" representative of these processes, it prevents from the introduction of a micro-scale, second-order remodelling tensor, which would render the theoretical and numerical analysis of the problem at hand much more complicated. Accordingly, the generalised velocities associated with $\mathrm{e_p}$, i.e., $\mathrm{D_s e_p}$ and $\nabla(\mathrm{D_s e_p})$, are a scalar and a co-vector field, rather than being a second-order and a third-order tensor field, respectively. It follows from these considerations that an inelastic model built on ε_{p} and $\mathrm{e_p}$ has the right to stand on its own, independently on any numerical issue, even though Anand et al. [15] have originally introduced $\mathrm{e_p}$ for numerical purposes. Clearly, such a model represents the limit case of more elaborated theories that involve tensor fields, rather than scalar ones.

Coherently with (6.19), we introduce the collection of virtual velocities

$$\mathcal{V}_{\mathrm{v}} = (\boldsymbol{u}_{\mathrm{s}}, \nabla\boldsymbol{u}_{\mathrm{s}}, u_{\varepsilon}, u_{\mathrm{p}}, \nabla u_{\mathrm{p}} |\, \boldsymbol{u}_{\mathrm{f}}, \nabla\boldsymbol{u}_{\mathrm{f}}) \in \mathscr{V}_{\mathrm{v}}, \tag{6.20}$$

where $\mathscr{V}_{\mathrm{v}}$ is referred to as the set of all virtual velocities. The elements $\boldsymbol{u}_{\mathrm{s}}$, $\nabla\boldsymbol{u}_{\mathrm{s}}$, $\boldsymbol{u}_{\mathrm{f}}$, and $\nabla\boldsymbol{u}_{\mathrm{f}}$ are the virtual counterparts of $\boldsymbol{v}_{\mathrm{s}}$, $\nabla\boldsymbol{v}_{\mathrm{s}}$, $\boldsymbol{v}_{\mathrm{f}}$, and $\nabla\boldsymbol{v}_{\mathrm{f}}$, respectively, and the non-standard fields u_{ε}, u_{p}, and ∇u_{p} denote the virtual velocities corresponding to the rates $\mathrm{D_s}\varepsilon_{\mathrm{p}}$, $\mathrm{D_s e_p}$, and $\nabla(\mathrm{D_s e_p})$, respectively.

Once the virtual velocities of the model are identified, it is possible to write the internal and the external virtual powers of the system. These two linear and continuous functionals are defined over $\mathscr{V}_{\mathrm{v}}$, and are specified through the expressions

$$\mathcal{W}_{\mathrm{v}}^{(\mathrm{i})}(\mathcal{V}_{\mathrm{v}}) \equiv \int_{\mathscr{B}(t)} \{\boldsymbol{\sigma}_{\mathrm{s}} : \boldsymbol{g}\nabla\boldsymbol{u}_{\mathrm{s}} + \boldsymbol{m}_{\mathrm{s}}.\boldsymbol{u}_{\mathrm{s}} + \boldsymbol{\sigma}_{\mathrm{f}} : \boldsymbol{g}\nabla\boldsymbol{u}_{\mathrm{f}} + \boldsymbol{m}_{\mathrm{f}}.\boldsymbol{u}_{\mathrm{f}} + h_{\varepsilon}^{(\mathrm{i})} u_{\varepsilon} + h_{\mathrm{p}}^{(\mathrm{i})} u_{\mathrm{p}} + \boldsymbol{\xi}_{\mathrm{p}} \nabla u_{\mathrm{p}}\}, \tag{6.21a}$$

$$\mathcal{W}_{\mathrm{v}}^{(\mathrm{e})}(\mathcal{V}_{\mathrm{v}}) \equiv \int_{\Gamma_t^N} \{\boldsymbol{\tau}_{\mathrm{s}}.\boldsymbol{u}_{\mathrm{s}} + \boldsymbol{\tau}_{\mathrm{f}}.\boldsymbol{u}_{\mathrm{f}} + \zeta_{\mathrm{p}} u_{\mathrm{p}}\} + \int_{\mathscr{B}(t)} \left\{h_{\varepsilon}^{(\mathrm{e})} u_{\varepsilon} + h_{\mathrm{p}}^{(\mathrm{e})} u_{\mathrm{p}}\right\}, \tag{6.21b}$$

By requiring the internal virtual power, $\mathcal{W}_{\mathrm{v}}^{(\mathrm{i})}(\mathcal{V}_{\mathrm{v}})$, to be invariant under the superposition of arbitrary rigid motions, we deduce the symmetry of the total stress tensor, $\boldsymbol{\sigma} = \boldsymbol{\sigma}_{\mathrm{s}} + \boldsymbol{\sigma}_{\mathrm{f}}$, and that the sum of the internal forces $\boldsymbol{m}_{\mathrm{s}}$ and $\boldsymbol{m}_{\mathrm{f}}$ must vanish identically, i.e., we obtain the condition $\boldsymbol{m}_{\mathrm{s}} + \boldsymbol{m}_{\mathrm{f}} = \mathbf{0}$ [202]. Consistently with the *a priori* exclusion of all inertial terms from our model, this last result constitutes an approximation of the more general balance of internal forces that, for a biphasic medium with mass exchange between the phases, is given by $\boldsymbol{m}_{\mathrm{s}} + r_{\mathrm{s}}\boldsymbol{v}_{\mathrm{s}} + \boldsymbol{m}_{\mathrm{f}} - r_{\mathrm{s}}\boldsymbol{v}_{\mathrm{f}} = \mathbf{0}$. In fact, the approximation consists of dropping the term $r_{\mathrm{s}}\boldsymbol{v}_{\mathrm{s}} - r_{\mathrm{s}}\boldsymbol{v}_{\mathrm{f}} = -r_{\mathrm{s}}\boldsymbol{w}$, and is based on the argument that the interphase mass transfer, r_{s}, depends on the micro-scale velocity with which the mass passes from the fluid to the solid, and vice versa. Such velocity, multiplied by the relative macro-scale velocity $\boldsymbol{w}$, is assumed to produce a rate of momentum exchange that weighs much less than $\boldsymbol{m}_{\mathrm{s}}$ and $\boldsymbol{m}_{\mathrm{f}}$, thereby leading to the desired approximation.

We emphasise that, in writing the expressions of $\mathcal{W}_{\mathrm{v}}^{(\mathrm{i})}(\mathcal{V}_{\mathrm{v}})$ and $\mathcal{W}_{\mathrm{v}}^{(\mathrm{e})}(\mathcal{V}_{\mathrm{v}})$, we have omitted *all* inertial and long-range (e.g. gravity) forces, which we regard as negligible from the outset. Moreover, the nature of the forces $h_{\mathrm{p}}^{(\mathrm{i})}$ and $\boldsymbol{\xi}_{\mathrm{p}}$ is necessarily coherent with the hypothesis that the kinematics of the solid phase micro-structure is represented by e_{p} and $\nabla\mathrm{e}_{\mathrm{p}}$. In this sense, the model features some important similarities with Gurtin's approach to the derivation of the generalised Allen-Cahn equation [122], in which the scalar field describing the micro-structural kinematics of the considered medium is regarded as an order parameter.

Looking at (6.21a) and (6.21b), we also notice that, in principle, also the velocity and the velocity gradient of the nutrients should be considered, along with their virtual counterparts, in (6.19) and (6.20). However, in view of a comprehensive formulation of the Principle of Virtual Powers, this would call for the definition of the generalised forces expending power on them, and, above all, for the introduction of surface tractions, acting on Γ_t^N. Individuating a physically sound way for expressing such contact forces is not easy and taking them into account leads unavoidably to both theoretical and computational complications (see, e.g., Grillo et al. [110] for an attempt of including these forces, based on a work by Sciarra et al. [215]). For these reasons, we present here a simplified framework in which we account for the nutrients through the balance law (5.20a), while we omit to study their kinematics and dynamics in detail. In other words, due to their tantamount importance for activating growth, we do include them in our model, but we do not treat them systematically. Hence, we do not consider any force balance associated with the nutrients, nor do we investigate their contribution to the dissipation inequality. Rather, we "guess" that the mass flux vector, $\boldsymbol{y}_{\mathrm{N}}$, obeys a diffusion dynamics of Fickean type, so that it is prescribed to have the form $\boldsymbol{y}_{\mathrm{N}} = -\rho_{\mathrm{f0}}\boldsymbol{d}\nabla c_{\mathrm{N}}$ in the Eulerian description and $\boldsymbol{Y}_{\mathrm{N}} = -\rho_{\mathrm{f0}}\boldsymbol{D}\,\mathrm{Grad}\,\omega_{\mathrm{N}}$ in material formalism, with $\boldsymbol{d}$ being the diffusivity tensor and $\boldsymbol{D}$ its material counterpart. Note that the latter is related to $\boldsymbol{d}$ through the backward Piola transformation $\boldsymbol{D}(X,t) = J(X,t)\boldsymbol{F}^{-1}(\chi(X,t),t)\boldsymbol{d}(\chi(X,t),t)\boldsymbol{F}^{-\mathrm{T}}(X,t)$.

By invoking the Principle of Virtual Powers, we enforce the condition $\mathcal{W}_{\mathrm{v}}^{(\mathrm{i})}(\mathcal{V}_{\mathrm{v}}) = \mathcal{W}_{\mathrm{v}}^{(\mathrm{e})}(\mathcal{V}_{\mathrm{v}})$, which is required to be fulfilled for any admissible set of generalised velocities $\mathcal{V}_{\rm v}$, thereby leading to

$$\begin{aligned}
&\int_{\mathscr{B}(t)} \{[-\mathrm{div}\boldsymbol{\sigma}_{\rm s} + \boldsymbol{m}_{\rm s}].\boldsymbol{u}_{\rm s} + [-\mathrm{div}\boldsymbol{\sigma}_{\rm f} + \boldsymbol{m}_{\rm f}].\boldsymbol{u}_{\rm f}\} \\
&+ \int_{\mathscr{B}(t)} \left\{[h_\varepsilon^{(\rm i)} - h_\varepsilon^{(\rm e)}]u_\varepsilon + [h_{\rm p}^{(\rm i)} - \mathrm{div}\boldsymbol{\xi}_{\rm p} - h_{\rm p}^{(\rm e)}]u_{\rm p}\right\} \\
&+ \int_{\Gamma_t^N} \left\{[\boldsymbol{\sigma}_{\rm s}.\boldsymbol{n} - \boldsymbol{\tau}_{\rm s}].\boldsymbol{u}_{\rm s} + [\boldsymbol{\sigma}_{\rm f}.\boldsymbol{n} - \boldsymbol{\tau}_{\rm f}].\boldsymbol{u}_{\rm f} + [\boldsymbol{\xi}_{\rm p}.\boldsymbol{n} - \zeta_{\rm p}]u_{\rm p}\right\} = 0.
\end{aligned} \tag{6.22}$$

By adopting the usual localisation procedure that extracts the local form of the equations of motion from the Principle of Virtual Powers, Equation (6.22) yields the following balances of generalised forces

$$\boldsymbol{m}_{\rm s} - \mathrm{div}\boldsymbol{\sigma}_{\rm s} = \boldsymbol{0}, \tag{6.23a}$$
$$\boldsymbol{m}_{\rm f} - \mathrm{div}\boldsymbol{\sigma}_{\rm f} = \boldsymbol{0}, \tag{6.23b}$$
$$h_\varepsilon^{(\rm i)} - h_\varepsilon^{(\rm e)} = 0, \tag{6.23c}$$
$$h_{\rm p}^{(\rm i)} - \mathrm{div}\boldsymbol{\xi}_{\rm p} - h_{\rm p}^{(\rm e)} = 0, \tag{6.23d}$$

which hold in $\mathscr{B}(t)$, and the balances of contact forces on Γ_t^N

$$\boldsymbol{\sigma}_{\rm s}.\boldsymbol{n} - \boldsymbol{\tau}_{\rm s} = \boldsymbol{0}, \tag{6.24a}$$
$$\boldsymbol{\sigma}_{\rm f}.\boldsymbol{n} - \boldsymbol{\tau}_{\rm f} = \boldsymbol{0}, \tag{6.24b}$$
$$\boldsymbol{\xi}_{\rm p}.\boldsymbol{n} - \zeta_{\rm p} = 0. \tag{6.24c}$$

It is worthwhile to mention that, in general, upon defining the field of *total* contact forces $\boldsymbol{\tau} = \boldsymbol{\tau}_{\rm s} + \boldsymbol{\tau}_{\rm f}$, and the *total* Cauchy stress tensor $\boldsymbol{\sigma} = \boldsymbol{\sigma}_{\rm s} + \boldsymbol{\sigma}_{\rm f}$, it is rather natural to provide on Γ_t^N boundary conditions of the kind $\boldsymbol{\sigma}.\boldsymbol{n} = \boldsymbol{\tau}$ (see [215] for details). Nevertheless, even in that case, the boundary conditions (6.24a) and (6.24b) can be recovered under the assumption that $\boldsymbol{\tau}_{\rm s}$ and $\boldsymbol{\tau}_{\rm f}$ are obtained by partitioning $\boldsymbol{\tau}$ as $\boldsymbol{\tau}_{\rm s} = (\rho_{\rm s0}\varphi_{\rm s}/\rho)\boldsymbol{\tau}$ and $\boldsymbol{\tau}_{\rm f} = (\rho_{\rm f0}\varphi_{\rm f}/\rho)\boldsymbol{\tau}$, respectively.

6.4 Dissipation and Dynamic Equations

To extract constitutive information on the internal forces presented so far, we study the dissipation inequality of the system. For this purpose, we enrich the picture proposed in Grillo et al. [110], which, in turn, was inspired by Hassanizadeh [132] and Benethum et al. [27]. This is done by framing the formulation of Anand et al. [15] in the context of biphasic media and, above all, by rephrasing it in order to account for growth. The first step in this direction is to introduce the dissipation density, $\mathcal{D}$, measured per unit volume of the current configuration of the medium, and defining the dissipation associated with an open subset $\Omega_t \subset \mathscr{B}(t)$ as

$$\int_{\Omega_t} \mathcal{D} = -\int_{\Omega_t} \{r_{\rm s}(\psi_{\rm s} - \psi_{\rm f}) + \rho_{\rm s0}\varphi_{\rm s}\mathrm{D}_{\rm s}\psi_{\rm s} + \rho_{\rm f0}\varphi_{\rm f}\mathrm{D}_{\rm s}\psi_{\rm f} + (\rho_{\rm f0}\varphi_{\rm f}\nabla\psi_{\rm f})\boldsymbol{w}\}$$

$$+\int_{\partial\Omega_t}\Big\{(\boldsymbol{\sigma}_{\rm s}.\boldsymbol{n}).\boldsymbol{v}_{\rm s}+(\boldsymbol{\sigma}_{\rm f}.\boldsymbol{n}).\boldsymbol{v}_{\rm f}+(\boldsymbol{\xi}_{\rm p}.\boldsymbol{n})\mathrm{D_s e_p}\Big\}$$
$$+\int_{\Omega_t}\Big\{h_\varepsilon^{(\rm e)}\mathrm{D_s}\varepsilon_{\rm p}+h_{\rm p}^{(\rm e)}\mathrm{D_s e_p}\Big\}+\int_{\Omega_t}\mathcal{D}_\gamma\geq 0. \tag{6.25}$$

As shown in (6.25), the dissipation can be written as the sum of four different contributions: with reference to the first integral of the sum defining $\int_{\Omega_t}\mathcal{D}$, we recognise that, by indicating with $\psi_{\rm s}$ and $\psi_{\rm f}$ the Helmholtz free energies per unit mass of the solid and of the fluid, the term $r_{\rm s}(\psi_{\rm s}-\psi_{\rm f})$ expresses the rate of change of the free energy densities, $\rho_{\rm s0}\varphi_{\rm s}\psi_{\rm s}$ and $\rho_{\rm f0}\varphi_{\rm f}\psi_{\rm f}$, due to the mass exchange between the phases. Moreover, $\rho_{\rm s0}\varphi_{\rm s}\mathrm{D_s}\psi_{\rm s}$ and $\rho_{\rm f0}\varphi_{\rm f}\mathrm{D_s}\psi_{\rm f}$ are the rates of change of the Helmholtz free energy densities measured with respect to the solid phase motion, and $(\nabla\psi_{\rm f})\boldsymbol{w}$ describes how $\psi_{\rm f}$ is transported due to the motion of the fluid relative to the solid. The terms in the surface integral denote the contributions to the net power expended on Ω_t due to the contact forces with the surrounding medium, while the terms in the third integral represent the part of net power ascribable to the non-standard forces $h_\varepsilon^{(\rm e)}$ and $h_{\rm p}^{(\rm e)}$. Finally, $\mathcal{D}_\gamma$ is a dissipation density introduced to account for the fact that the medium experiences growth (see e.g. [106] for a discussion on this issue).

By applying Gauss Theorem to the surface integral of Equation (6.25), and using the balance laws (6.23a)–(6.23d) and (6.24a)–(6.24c), the dissipation inequality becomes

$$\int_{\Omega_t}\mathcal{D}=-\int_{\Omega_t}\{r_{\rm s}(\psi_{\rm s}-\psi_{\rm f})+\rho_{\rm s0}\varphi_{\rm s}\mathrm{D_s}\psi_{\rm s}+\rho_{\rm f0}\varphi_{\rm f}\mathrm{D_s}\psi_{\rm f}+(\rho_{\rm f0}\varphi_{\rm f}\nabla\psi_{\rm f})\boldsymbol{w}\}$$
$$+\int_{\Omega_t}\{\boldsymbol{m}_{\rm s}.\boldsymbol{v}_{\rm s}+\boldsymbol{\sigma}_{\rm s}:\boldsymbol{g}\nabla\boldsymbol{v}_{\rm s}+\boldsymbol{m}_{\rm f}.\boldsymbol{v}_{\rm f}+\boldsymbol{\sigma}_{\rm f}:\boldsymbol{g}\nabla\boldsymbol{v}_{\rm f}\}$$
$$+\int_{\Omega_t}\Big\{h_{\rm p}^{(\rm i)}\mathrm{D_s e_p}+\boldsymbol{\xi}_{\rm p}\nabla(\mathrm{D_s e_p})+h_\varepsilon^{(\rm i)}\mathrm{D_s}\varepsilon_{\rm p}\Big\}+\int_{\Omega_t}\mathcal{D}_\gamma\geq 0. \tag{6.26}$$

By localising Equation (6.26) and invoking the condition $\boldsymbol{m}_{\rm s}+\boldsymbol{m}_{\rm f}=\boldsymbol{0}$, we obtain

$$\mathcal{D}=r_{\rm s}(\psi_{\rm f}-\psi_{\rm s})-\rho_{\rm s0}\varphi_{\rm s}\mathrm{D_s}\psi_{\rm s}-\rho_{\rm f0}\varphi_{\rm f}\mathrm{D_s}\psi_{\rm f}+[\boldsymbol{m}_{\rm f}-\boldsymbol{g}^{-1}(\rho_{\rm f0}\varphi_{\rm f}\nabla\psi_{\rm f})].\boldsymbol{w}$$
$$+\boldsymbol{\sigma}_{\rm s}:\boldsymbol{g}\nabla\boldsymbol{v}_{\rm s}+\boldsymbol{\sigma}_{\rm f}:\boldsymbol{g}\nabla\boldsymbol{v}_{\rm f}+h_{\rm p}^{(\rm i)}\mathrm{D_s e_p}+\boldsymbol{\xi}_{\rm p}\nabla(\mathrm{D_s e_p})+h_\varepsilon^{(\rm i)}\mathrm{D_s}\varepsilon_{\rm p}+\mathcal{D}_\gamma\geq 0. \tag{6.27}$$

As a simplifying assumption, we approximate the Helmholtz free energy density of the fluid, $\psi_{\rm f}$, with a constant, so that $\rho_{\rm f0}\varphi_{\rm f}\mathrm{D_s}\psi_{\rm f}$ and $\nabla\psi_{\rm f}$ are negligible with respect to all the other terms featuring in the dissipation inequality. Such situation occurs, for instance, when the state variables characterising $\psi_{\rm f}$ are, at the most, the temperature and the mass fraction of the nutrients dissolved in the fluid, and the latter is so low that $\psi_{\rm f}$ can be safely set equal to the (constant) Helmholtz free energy density of water at constant temperature. Under these hypotheses, Equation (6.27) becomes

$$\mathcal{D}=r_{\rm s}(\psi_{\rm f}-\psi_{\rm s})-\rho_{\rm s0}\varphi_{\rm s}\mathrm{D_s}\psi_{\rm s}+\boldsymbol{m}_{\rm f}.\boldsymbol{w}+\boldsymbol{\sigma}_{\rm s}:\boldsymbol{g}\nabla\boldsymbol{v}_{\rm s}+\boldsymbol{\sigma}_{\rm f}:\boldsymbol{g}\nabla\boldsymbol{v}_{\rm f}$$

$$+ h_{\mathrm{p}}^{(\mathrm{i})}\mathrm{D}_{\mathrm{s}}\mathrm{e}_{\mathrm{p}} + \boldsymbol{\xi}_{\mathrm{p}}\nabla(\mathrm{D}_{\mathrm{s}}\mathrm{e}_{\mathrm{p}}) + h_{\varepsilon}^{(\mathrm{i})}\mathrm{D}_{\mathrm{s}}\varepsilon_{\mathrm{p}} + \mathcal{D}_{\gamma} \geq 0. \tag{6.28}$$

It is convenient to rewrite the dissipation inequality per unit volume of $\mathscr{B}$. To do this, we perform a Piola transformation of (6.28), which yields

$$\begin{aligned}\mathcal{D}_{\mathrm{R}} = R_{\mathrm{s}}(\Psi_{\mathrm{f}} - \Psi_{\mathrm{s}}) - \rho_{\mathrm{s}0}J_{\gamma}\Phi_{\mathrm{s}\nu}\dot{\Psi}_{\mathrm{s}} + \Phi_{\mathrm{f}}^{-1}\boldsymbol{Q}\boldsymbol{M}_{\mathrm{f}} + \boldsymbol{P}_{\mathrm{s}}:\boldsymbol{g}\dot{\boldsymbol{F}} + \boldsymbol{P}_{\mathrm{f}}:\boldsymbol{g}\mathrm{Grad}\boldsymbol{V}_{\mathrm{f}}\\ + H_{\mathrm{p}}^{(\mathrm{i})}\dot{\mathfrak{e}}_{\mathrm{p}} + \boldsymbol{\Xi}_{\mathrm{p}}\mathrm{Grad}\dot{\mathfrak{e}}_{\mathrm{p}} + H_{\varepsilon}^{(\mathrm{i})}\dot{\varepsilon}_{\mathrm{p}} + J\mathcal{D}_{\gamma} \geq 0,\end{aligned} \tag{6.29}$$

where, as anticipated above, $R_{\mathrm{s}}(X,t) = J(X,t)r_{\mathrm{s}}(\chi(X,t),t)$ is the material form of the source/sink of mass for the solid phase as a whole, and we introduced the notation

$$\Psi_{\alpha}(X,t) = \psi_{\alpha}(\chi(X,t),t), \qquad \alpha \in \{\mathrm{f},\mathrm{s}\}, \tag{6.30a}$$
$$\boldsymbol{P}_{\alpha}(X,t) = J(X,t)\boldsymbol{\sigma}_{\alpha}(\chi(X,t),t)\boldsymbol{F}^{-\mathrm{T}}(X,t), \qquad \alpha \in \{\mathrm{f},\mathrm{s}\}, \tag{6.30b}$$
$$H_{\beta}^{(\mathrm{i})}(X,t) = J(X,t)h_{\beta}^{(\mathrm{i})}(\chi(X,t),t), \qquad \beta \in \{\mathrm{p},\varepsilon\}, \tag{6.30c}$$
$$\boldsymbol{\Xi}_{\mathrm{p}}(X,t) = J(X,t)\boldsymbol{\xi}_{\mathrm{p}}(\chi(X,t),t)\boldsymbol{F}^{-\mathrm{T}}(X,t), \tag{6.30d}$$
$$\boldsymbol{M}_{\mathrm{f}}(X,t) = J(X,t)[\boldsymbol{g}(\chi(X,t))\boldsymbol{m}_{\mathrm{f}}(\chi(X,t),t)]\boldsymbol{F}(X,t). \tag{6.30e}$$

Here, $\boldsymbol{P}_{\mathrm{f}}$ and $\boldsymbol{P}_{\mathrm{s}}$ indicate the first Piola-Kirchhoff stress tensors of the fluid and the solid phase, $H_{\mathrm{p}}^{(\mathrm{i})}$ and $H_{\varepsilon}^{(\mathrm{i})}$ express, in material form, the internal generalised forces dual to $\dot{\mathfrak{e}}_{\mathrm{p}}$ and $\dot{\varepsilon}_{\mathrm{p}}$, respectively, $\boldsymbol{\Xi}_{\mathrm{p}}$ is the material representation of the stress-like generalised force, $\boldsymbol{\xi}_{\mathrm{p}}$, and is thus dual to $\mathrm{Grad}\dot{\mathfrak{e}}_{\mathrm{p}}$, and $\boldsymbol{M}_{\mathrm{f}}$ is the material counterpart of the momentum exchange rate $\boldsymbol{m}_{\mathrm{f}}$.

Finally, by generalising the Helmholtz free energy density proposed in [15], we prescribe Ψ_{s} to be given by the sum of three terms, i.e.,

$$\begin{aligned}\hat{\Psi}_{\mathrm{s}}(\boldsymbol{F},\boldsymbol{F}_{\mathrm{p}},\boldsymbol{F}_{\gamma},\varepsilon_{\mathrm{p}},\mathfrak{e}_{\mathrm{p}},\mathrm{Grad}\mathfrak{e}_{\mathrm{p}}) = \hat{\Psi}_{\mathrm{s}}^{(\mathrm{st})}(\boldsymbol{F}\boldsymbol{F}_{\gamma}^{-1}\boldsymbol{F}_{\mathrm{p}}^{-1}) + \tfrac{1}{2}a_0[\varepsilon_{\mathrm{p}} - \mathfrak{e}_{\mathrm{p}}]^2\\ + \tfrac{1}{2}b_0\boldsymbol{F}_{\gamma}^{-1}\boldsymbol{B}_{\mathrm{p}}\boldsymbol{F}_{\gamma}^{-\mathrm{T}} : \mathrm{Grad}\mathfrak{e}_{\mathrm{p}} \otimes \mathrm{Grad}\mathfrak{e}_{\mathrm{p}},\end{aligned} \tag{6.31}$$

with $\boldsymbol{B}_{\mathrm{p}} = \boldsymbol{F}_{\mathrm{p}}^{-1}.\boldsymbol{F}_{\mathrm{p}}^{-\mathrm{T}}$, so that the time derivative of Ψ_{s} reads

$$\begin{aligned}\dot{\Psi}_{\mathrm{s}} = &\left(\frac{\partial\hat{\Psi}_{\mathrm{s}}^{(\mathrm{st})}}{\partial\boldsymbol{F}_{\mathrm{e}}}\boldsymbol{F}_{\mathrm{p}}^{-\mathrm{T}}\boldsymbol{F}_{\gamma}^{-\mathrm{T}}\right):\dot{\boldsymbol{F}} - \frac{1}{3}\frac{\mathrm{tr}(\boldsymbol{\eta}\,\boldsymbol{\Sigma}_{\nu})}{\rho_{\mathrm{s}0}\Phi_{\mathrm{s}\nu}}\frac{R_{\mathrm{s}}}{\rho_{\mathrm{s}0}\Phi_{\mathrm{s}\nu}J_{\gamma}}\\ &- \frac{1}{\rho_{\mathrm{s}0}\Phi_{\mathrm{s}\nu}}\left\{\sqrt{\tfrac{3}{2}}\|\tilde{\boldsymbol{\Sigma}}_{\nu}\|_{\boldsymbol{\eta}} - A_{\nu}[\varepsilon_{\mathrm{p}} - \mathfrak{e}_{\mathrm{p}}]\right\}\dot{\varepsilon}_{\mathrm{p}}\\ &- \frac{A_{\nu}}{\rho_{\mathrm{s}0}\Phi_{\mathrm{s}\nu}}[\varepsilon_{\mathrm{p}} - \mathfrak{e}_{\mathrm{p}}]\dot{\mathfrak{e}}_{\mathrm{p}} + \frac{B_{\nu}}{\rho_{\mathrm{s}0}\Phi_{\mathrm{s}\nu}}\left[\left(\boldsymbol{F}_{\gamma}^{-1}\boldsymbol{B}_{\mathrm{p}}\boldsymbol{F}_{\gamma}^{-\mathrm{T}}\right)\mathrm{Grad}\mathfrak{e}_{\mathrm{p}}\right]\overline{\mathrm{Grad}\mathfrak{e}_{\mathrm{p}}}^{\boldsymbol{\cdot}},\end{aligned} \tag{6.32}$$

where $\hat{\Psi}_{\mathrm{s}}^{(\mathrm{st})}$ is differentiated with respect to $\boldsymbol{F}_{\mathrm{e}} = \boldsymbol{F}\boldsymbol{F}_{\gamma}^{-1}\boldsymbol{F}_{\mathrm{p}}^{-1}$. In (6.32), we introduced the notation

$$\boldsymbol{\Sigma}_{\nu} = \boldsymbol{\eta}^{-1}\boldsymbol{F}_{\mathrm{e}}^{\mathrm{T}}\left(\rho_{\mathrm{s}0}\Phi_{\mathrm{s}\nu}\frac{\partial\hat{\Psi}_{\mathrm{s}}^{(\mathrm{st})}}{\partial\boldsymbol{F}_{\mathrm{e}}}\right)$$

$$+ B_\nu \left[\boldsymbol{\eta}^{-1} \boldsymbol{F}_\mathrm{p}^{-\mathrm{T}} \boldsymbol{F}_\gamma^{-\mathrm{T}} \left(\mathrm{Grad}\mathfrak{e}_\mathrm{p} \otimes \mathrm{Grad}\mathfrak{e}_\mathrm{p} \right) \boldsymbol{F}_\gamma^{-1} \boldsymbol{F}_\mathrm{p}^{-1} \boldsymbol{\eta}^{-1} \right], \tag{6.33a}$$

$$\tilde{\boldsymbol{\Sigma}}_\nu = \boldsymbol{\Sigma}_\nu - \tfrac{1}{3} \mathrm{tr}[\boldsymbol{\eta} \boldsymbol{\Sigma}_\nu] \boldsymbol{\eta}^{-1}, \tag{6.33b}$$

$$A_\nu = \rho_{\mathrm{s}0} \Phi_{\mathrm{s}\nu} a_0, \tag{6.33c}$$

$$B_\nu = \rho_{\mathrm{s}0} \Phi_{\mathrm{s}\nu} b_0, \tag{6.33d}$$

where A_ν and B_ν are the counterparts of the strictly positive constants a_0 and b_0, expressed per unit volume of the tissue's natural state, and $\boldsymbol{\Sigma}_\nu$ is a generalised Mandel stress tensor that comprises both the standard definition of the Mandel stress tensor, i.e.,

$$\boldsymbol{\Sigma}_\nu^{(\mathrm{st})} = \boldsymbol{\eta}^{-1} \boldsymbol{F}_\mathrm{e}^\mathrm{T} \left(\rho_{\mathrm{s}0} \Phi_{\mathrm{s}\nu} \frac{\partial \hat{\Psi}_\mathrm{s}^{(\mathrm{st})}}{\partial \boldsymbol{F}_\mathrm{e}} \right), \tag{6.34}$$

and the non-standard stress-like contribution

$$\boldsymbol{\Sigma}_\nu^{(\text{n-st})} = B_\nu \left[\boldsymbol{\eta}^{-1} \boldsymbol{F}_\mathrm{p}^{-\mathrm{T}} \boldsymbol{F}_\gamma^{-\mathrm{T}} \left(\mathrm{Grad}\mathfrak{e}_\mathrm{p} \otimes \mathrm{Grad}\mathfrak{e}_\mathrm{p} \right) \boldsymbol{F}_\gamma^{-1} \boldsymbol{F}_\mathrm{p}^{-1} \boldsymbol{\eta}^{-1} \right]. \tag{6.35}$$

We remark that $\boldsymbol{\Sigma}_\nu^{(\text{n-st})}$ is purely configurational, and it descends from the introduction of the micro-scale plasticity variable $\mathfrak{e}_\mathrm{p}$. Moreover, $\boldsymbol{\Sigma}_\nu^{(\text{n-st})}$ is independent of deformation, whereas it does depend on the growth and remodelling distortions, $\boldsymbol{F}_\gamma$ and $\boldsymbol{F}_\mathrm{p}$.

Remark 6.4.1 (Tensor $\boldsymbol{\Sigma}_\nu$ and co-directionality). In our work, the deviatoric part of the generalised Mandel stress tensor, $\tilde{\boldsymbol{\Sigma}}_\nu$, is the stress tensor used to define $\boldsymbol{N}_\nu$ in (6.10). Therefore, it is the tensor with which the rate of plastic distortions, $\tilde{\boldsymbol{D}}_\mathrm{p}$, is co-directional. By virtue of the definition of $\boldsymbol{N}_\nu$, the direction of $\tilde{\boldsymbol{D}}_\mathrm{p}$ in the space of the symmetric second-order tensors is determined, partially, by the deviatoric part of the standard Mandel stress tensor, $\tilde{\boldsymbol{\Sigma}}_\nu^{(\mathrm{st})}$, and partially by $\tilde{\boldsymbol{\Sigma}}_\nu^{(\text{n-st})}$, which includes the contributions of the micro-scale "plasticity", through $\mathrm{Grad}\mathfrak{e}_\mathrm{p}$, and of the growth and remodelling distortions through $\boldsymbol{F}_\gamma$ and $\boldsymbol{F}_\mathrm{p}$, respectively. In the work of Anand et al. [15], instead, $\boldsymbol{N}_\nu$ is determined by $\boldsymbol{\Sigma}_\nu^{(\mathrm{st})}$ only.

$$\begin{aligned}
\mathcal{D}_\mathrm{R} = & \left\{ -J_\gamma \left(\rho_{\mathrm{s}0} \Phi_{\mathrm{s}\nu} \frac{\partial \hat{\Psi}_\mathrm{s}^{(\mathrm{st})}}{\partial \boldsymbol{F}_\mathrm{e}} \boldsymbol{F}_\mathrm{p}^{-\mathrm{T}} \boldsymbol{F}_\gamma^{-\mathrm{T}} \right) + \boldsymbol{g} \boldsymbol{P}_\mathrm{s} \right\} : \dot{\boldsymbol{F}} \\
& + \left\{ \Psi_\mathrm{f} - \Psi_\mathrm{s} + \frac{1}{3} \frac{\mathrm{tr}\left(\boldsymbol{\eta} \, \boldsymbol{\Sigma}_\nu \right)}{\rho_{\mathrm{s}0} \Phi_{\mathrm{s}\nu}} \right\} R_\mathrm{s} + \left\{ H_\varepsilon^{(\mathrm{i})} + J_\gamma \sqrt{\tfrac{3}{2}} \|\tilde{\boldsymbol{\Sigma}}_\nu\|_{\boldsymbol{\eta}} - J_\gamma A_\nu [\varepsilon_\mathrm{p} - \mathfrak{e}_\mathrm{p}] \right\} \dot{\varepsilon}_\mathrm{p} \\
& + \left\{ H_\mathrm{p}^{(\mathrm{i})} + J_\gamma A_\nu [\varepsilon_\mathrm{p} - \mathfrak{e}_\mathrm{p}] \right\} \dot{\mathfrak{e}}_\mathrm{p} \\
& + \left\{ \Xi_\mathrm{p} - J_\gamma B_\nu \left[\left(\boldsymbol{F}_\gamma^{-1} \boldsymbol{B}_\mathrm{p} \boldsymbol{F}_\gamma^{-\mathrm{T}} \right) \mathrm{Grad}\mathfrak{e}_\mathrm{p} \right] \right\} \overline{\mathrm{Grad}\mathfrak{e}_\mathrm{p}}^{\,\cdot} \\
& + \Phi_\mathrm{f}^{-1} \boldsymbol{Q} \boldsymbol{M}_\mathrm{f} + \boldsymbol{P}_\mathrm{f} : \boldsymbol{g} \mathrm{Grad} \boldsymbol{V}_\mathrm{f} + J \mathcal{D}_\gamma \geq 0 \,.
\end{aligned} \tag{6.36}$$

We study the dissipation inequality (6.36) by regarding the mass balance law (5.20b) as a constraint [156, 27], and appending it to $\mathcal{D}_{\mathrm{R}}$. To this end, we perform the Piola transformation of (5.20b), thereby obtaining (see e.g. [27, 110])

$$\begin{aligned}\mathcal{C}_{\mathrm{R}} \equiv{}& \Phi_{\mathrm{s}}\boldsymbol{F}^{-\mathrm{T}}:\dot{\boldsymbol{F}} + \Phi_{\mathrm{f}}\boldsymbol{F}^{-\mathrm{T}}:\mathrm{Grad}\boldsymbol{V}_{\mathrm{f}} \\ &+ \Phi_{\mathrm{f}}^{-1}\boldsymbol{Q}\,\mathrm{Grad}(J^{-1}\Phi_{\mathrm{f}}) - \left(\frac{1}{\rho_{\mathrm{s}0}} - \frac{1}{\rho_{\mathrm{f}0}}\right)R_{\mathrm{s}} = 0,\end{aligned} \tag{6.37}$$

where $\mathcal{C}_{\mathrm{R}}$ stands for "constraint". Then, we multiply (6.37) by a Lagrange multiplier, p, which plays the role of hydrostatic pressure, and we attach the resulting expression to (6.36). This leads to a "new" dissipation function, $\mathcal{D}_{\mathrm{R}}^{\mathrm{new}} \equiv \mathcal{D}_{\mathrm{R}} + p\mathcal{C}_{\mathrm{R}}$, that is equal to $\mathcal{D}_{\mathrm{R}}$, but is put in the form

$$\begin{aligned}\mathcal{D}_{\mathrm{R}}^{\mathrm{new}} ={}& \left\{-J_\gamma\left(\rho_{\mathrm{s}0}\Phi_{\mathrm{s}\nu}\frac{\partial\hat{\Psi}_{\mathrm{s}}^{(\mathrm{st})}}{\partial\boldsymbol{F}_{\mathrm{e}}}\boldsymbol{F}_{\mathrm{p}}^{-\mathrm{T}}\boldsymbol{F}_{\gamma}^{-\mathrm{T}}\right) + p\,\Phi_{\mathrm{s}}\boldsymbol{F}^{-\mathrm{T}} + \boldsymbol{g}\boldsymbol{P}_{\mathrm{s}}\right\} : \dot{\boldsymbol{F}} \\ &+ \left\{p\,\Phi_{\mathrm{f}}\boldsymbol{F}^{-\mathrm{T}} + \boldsymbol{g}\boldsymbol{P}_{\mathrm{f}}\right\}:\mathrm{Grad}\boldsymbol{V}_{\mathrm{f}} + \Phi_{\mathrm{f}}^{-1}\boldsymbol{Q}\left\{\boldsymbol{M}_{\mathrm{f}} + Jp\,\mathrm{Grad}(J^{-1}\Phi_{\mathrm{f}})\right\} \\ &+ \left\{\left(\Psi_{\mathrm{f}} + \frac{p}{\rho_{\mathrm{f}0}}\right) - \left(\Psi_{\mathrm{s}} + \frac{p}{\rho_{\mathrm{s}0}}\right) + \frac{1}{3}\frac{\mathrm{tr}\,(\boldsymbol{\eta}\,\boldsymbol{\Sigma}_\nu)}{\rho_{\mathrm{s}0}\Phi_{\mathrm{s}\nu}}\right\}R_{\mathrm{s}} + J\mathcal{D}_\gamma \\ &+ \left\{H_\varepsilon^{(\mathrm{i})} + J_\gamma\sqrt{\tfrac{3}{2}}\,\|\tilde{\boldsymbol{\Sigma}}_\nu\|_{\boldsymbol{\eta}} - J_\gamma A_\nu[\varepsilon_{\mathrm{p}} - \mathfrak{e}_{\mathrm{p}}]\right\}\dot{\varepsilon}_{\mathrm{p}} + \left\{H_{\mathrm{p}}^{(\mathrm{i})} + J_\gamma A_\nu[\varepsilon_{\mathrm{p}} - \mathfrak{e}_{\mathrm{p}}]\right\}\dot{\mathfrak{e}}_{\mathrm{p}} \\ &+ \left\{\Xi_{\mathrm{p}} - J_\gamma B_\nu\left[\left(\boldsymbol{F}_\gamma^{-1}\boldsymbol{B}_{\mathrm{p}}\boldsymbol{F}_\gamma^{-\mathrm{T}}\right)\mathrm{Grad}\mathfrak{e}_{\mathrm{p}}\right]\right\}\dot{\overline{\mathrm{Grad}\mathfrak{e}_{\mathrm{p}}}} \geq 0.\end{aligned} \tag{6.38}$$

6.4.1 Constitutive Laws

We require that the inequality (6.38) be valid for arbitrary values of $\dot{\boldsymbol{F}}$, $\mathrm{Grad}\boldsymbol{V}_{\mathrm{f}}$, $\dot{\mathfrak{e}}_{\mathrm{p}}$, and $\dot{\overline{\mathrm{Grad}\mathfrak{e}_{\mathrm{p}}}}$. Hence, the Coleman-Noll method implies the following identifications

$$\boldsymbol{P}_{\mathrm{s}} = -\Phi_{\mathrm{s}}p\,\boldsymbol{g}^{-1}\boldsymbol{F}^{-\mathrm{T}} + J_\gamma\left(\rho_{\mathrm{s}0}\Phi_{\mathrm{s}\nu}\boldsymbol{g}^{-1}\frac{\partial\hat{\Psi}_{\mathrm{s}}^{(\mathrm{st})}}{\partial\boldsymbol{F}_{\mathrm{e}}}\boldsymbol{F}_{\mathrm{p}}^{-\mathrm{T}}\boldsymbol{F}_\gamma^{-\mathrm{T}}\right), \tag{6.39a}$$

$$\boldsymbol{P}_{\mathrm{f}} = -\Phi_{\mathrm{f}}p\,\boldsymbol{g}^{-1}\boldsymbol{F}^{-\mathrm{T}}, \tag{6.39b}$$

$$H_{\mathrm{p}}^{(\mathrm{i})} = -J_\gamma A_\nu[\varepsilon_{\mathrm{p}} - \mathfrak{e}_{\mathrm{p}}], \tag{6.39c}$$

$$\Xi_{\mathrm{p}} = J_\gamma B_\nu\left[\boldsymbol{F}_\gamma^{-1}\boldsymbol{B}_{\mathrm{p}}\boldsymbol{F}_\gamma^{-\mathrm{T}}\right]\mathrm{Grad}\mathfrak{e}_{\mathrm{p}}. \tag{6.39d}$$

In (6.39a), and in the sequel, the standard part of the solid phase Helmholtz free energy density, $\hat{\Psi}_{\mathrm{s}}^{(\mathrm{st})}$, is assumed to be of the Holmes-Mow type [138], i.e.,

$$\hat{\Psi}_{\mathrm{s}}^{(\mathrm{st})}(\boldsymbol{F}_{\mathrm{e}}) = \frac{\alpha_0}{\rho_{\mathrm{s}0}\Phi_{\mathrm{s}\nu}}\left\{\exp\left(\hat{f}(\boldsymbol{C}_{\mathrm{e}})\right) - 1\right\}, \tag{6.40}$$

where $\boldsymbol{C}_{\rm e} = \boldsymbol{F}_{\rm e}^{\rm T}.\boldsymbol{F}_{\rm e}$ is the elastic Cauchy-Green deformation tensor, α_0 is a material coefficient having physical units of energy per unit volume, and the function $\hat{f}$ is given by

$$
\begin{aligned}
\hat{f}(\boldsymbol{C}_{\rm e}) &= \check{f}(\hat{I}_1(\boldsymbol{C}_{\rm e}), \hat{I}_2(\boldsymbol{C}_{\rm e}), \hat{I}_3(\boldsymbol{C}_{\rm e})) \\
&= \alpha_1[\hat{I}_1(\boldsymbol{C}_{\rm e}) - 3] + \alpha_2[\hat{I}_2(\boldsymbol{C}_{\rm e}) - 3] - \alpha_3 \ln\left(\hat{I}_3(\boldsymbol{C}_{\rm e})\right), \qquad (6.41)
\end{aligned}
$$

with $\hat{I}_1(\boldsymbol{C}_{\rm e})$, $\hat{I}_2(\boldsymbol{C}_{\rm e})$, and $\hat{I}_3(\boldsymbol{C}_{\rm e})$ denoting the first three principal invariants of $\boldsymbol{C}_{\rm e}$. The material parameters α_1, α_2, and α_3 are all assumed to be constant in this work. Moreover, it holds that $\alpha_1 + 2\alpha_2 = \alpha_3$ [138], and the following relations connect α_0, α_1, α_2, and α_3 with Lamé's elastic parameters of the material (see e.g. [225]):

$$
\alpha_0 = \frac{2\mu + \lambda}{4\alpha_3}, \quad \alpha_1 = \alpha_3 \frac{2\mu - \lambda}{2\mu + \lambda}, \quad \alpha_2 = \alpha_3 \frac{\lambda}{2\mu + \lambda}. \qquad (6.42)
$$

In the forthcoming calculations, we set $\alpha_3 = 1$, and we give μ and λ the values reported in Table 6.1.

We recognise the dissipative parts of $\boldsymbol{M}_{\rm f}$ and $H_\varepsilon^{(\rm i)}$, which we identify with the following quantities

$$
\begin{aligned}
\boldsymbol{M}_{\rm f}^{(\rm d)} &= \boldsymbol{M}_{\rm f} + Jp\,\mathrm{Grad}(J^{-1}\Phi_{\rm f}), && (6.43\text{a}) \\
H_\varepsilon^{(\rm i,d)} &= H_\varepsilon^{(\rm i)} + J_\gamma \sqrt{\tfrac{3}{2}}\, \|\tilde{\boldsymbol{\Sigma}}_\nu\|_{\boldsymbol{\eta}} - J_\gamma A_\nu[\varepsilon_{\rm p} - \mathfrak{e}_{\rm p}], && (6.43\text{b})
\end{aligned}
$$

and the dissipation inequality becomes

$$
\begin{aligned}
\mathcal{D}_{\rm R} &= \Phi_{\rm f}^{-1}\boldsymbol{Q}\boldsymbol{M}_{\rm f}^{(\rm d)} + H_\varepsilon^{(\rm i,d)}\dot{\varepsilon}_{\rm p} \\
&+ \left\{\left(\Psi_{\rm f} + \frac{p}{\rho_{\rm f0}}\right) - \left(\Psi_{\rm s} + \frac{p}{\rho_{\rm s0}}\right) + \frac{1}{3}\frac{\mathrm{tr}\,(\boldsymbol{\eta}\,\boldsymbol{\Sigma}_\nu)}{\rho_{\rm s0}\Phi_{{\rm s}\nu}}\right\} R_{\rm s} + J\mathcal{D}_\gamma \geq 0. \qquad (6.44)
\end{aligned}
$$

We notice that, in (6.43b), growth influences the expression of $H_\varepsilon^{(\rm i,d)}$ through the determinant J_γ in the term $J_\gamma A_\nu[\varepsilon_{\rm p} - \mathfrak{e}_{\rm p}]$.

According to (6.44), our model predicts that the system under study features three independent dissipative processes. The first one is due to the power loss associated with the resistance to the fluid flow and, under the hypothesis of negligible inertial forces, it leads to Darcy's law, i.e.,

$$
\boldsymbol{M}_{\rm f}^{(\rm d)} = \Phi_{\rm f}\boldsymbol{K}^{-1}\boldsymbol{Q}. \qquad (6.45)
$$

Equation (6.45) represents the material form of Darcy's law and, accordingly, the tensor $\boldsymbol{K}$ is the *material* permeability tensor of the medium, defined by

$$
\boldsymbol{K}(X,t) = J(X,t)\boldsymbol{F}^{-1}(X,t)\boldsymbol{k}(\chi(X,t),t)\boldsymbol{F}^{-\rm T}(X,t), \qquad (6.46)
$$

with $\boldsymbol{k}$ being the spatial permeability tensor. Finally, we remark that, in deriving (6.45), we have tacitly assumed that $\boldsymbol{K}$ is invertible, whereas sometimes this may not be necessarily the case. By substituting (6.45) into the first term on the right-hand-side of (6.44), we obtain that the dissipation due to fluid flow is always non-negative, i.e., for all $\boldsymbol{Q}$, it holds that $\Phi_{\mathrm{f}}^{-1}\boldsymbol{Q}\boldsymbol{M}_{\mathrm{f}}^{(\mathrm{d})} = \boldsymbol{K}^{-1} : (\boldsymbol{Q} \otimes \boldsymbol{Q}) \geq 0$, as long as $\boldsymbol{K}$ is positive-definite. Note that, by putting together the results (6.43a) and (6.45), $\boldsymbol{M}_{\mathrm{f}}$ is determined constitutively as

$$\boldsymbol{M}_{\mathrm{f}} = \Phi_{\mathrm{f}}\boldsymbol{K}^{-1}\boldsymbol{Q} - Jp\,\mathrm{Grad}(J^{-1}\Phi_{\mathrm{f}}). \tag{6.47}$$

The second process contributing to the dissipation, $\mathcal{D}_{\mathrm{R}}$, is given by $H_{\varepsilon}^{(\mathrm{i,d})}\dot{\varepsilon}_{\mathrm{p}}$, which represents the power that the solid phase expends in order to remodel its internal structure by accumulating plastic strain ε_{p}. We assume that $H_{\varepsilon}^{(\mathrm{i,d})}\dot{\varepsilon}_{\mathrm{p}}$ is non-negative for all $\dot{\varepsilon}_{\mathrm{p}}$ and, since $\dot{\varepsilon}_{\mathrm{p}}$ is always non-negative by virtue of its own definition (see (6.13)), we conclude that $H_{\varepsilon}^{(\mathrm{i,d})}$ has to be non-negative too. In our work, we hypothesise that the tissue remodels in a rate-dependent way and, in particular, we assign $H_{\varepsilon}^{(\mathrm{i,d})}$ as

$$H_{\varepsilon}^{(\mathrm{i,d})} = J\tau_{\mathrm{p}}\dot{\varepsilon}_{\mathrm{p}}, \tag{6.48}$$

where τ_{p} is here taken as a strictly positive coefficient with the physical units of a generalised viscosity. By plugging (6.48) into (6.43b), we determine $H_{\varepsilon}^{(\mathrm{i})}$ through the constitutive law

$$H_{\varepsilon}^{(\mathrm{i})} = J\tau_{\mathrm{p}}\dot{\varepsilon}_{\mathrm{p}} - J_{\gamma}\sqrt{\tfrac{3}{2}}\,\|\tilde{\boldsymbol{\Sigma}}_{\nu}\|_{\boldsymbol{\eta}} + J_{\gamma}A_{\nu}[\varepsilon_{\mathrm{p}} - \mathfrak{e}_{\mathrm{p}}]. \tag{6.49}$$

The third dissipative phenomenon is given by growth, and is represented by the last two summands on the right-hand-side of (6.44), which we denote by $\mathcal{D}_{\mathrm{g}}$ and refer to as the "growth part of $\mathcal{D}_{\mathrm{R}}$". In contrast to what we have done for the other dissipative processes, and even though the terms between braces in (6.44) may be understood as the generalised force power-conjugate to $\dot{\gamma}/\gamma$ through R_{s}, we do not try to look for information on R_{s} from the requirement that $\mathcal{D}_{\mathrm{g}}$ has to be non-negative. Rather, following [10, 9, 38, 104, 105, 166, 62], we enforce a phenomenological law for R_{s}, which is translated into the kinematic constraint (6.18) on $\dot{\gamma}/\gamma$, and we use $\mathcal{D}_{\gamma}$ to adjust $\mathcal{D}_{\mathrm{g}}$ and guarantee that it remains non-negative. We emphasise that, although this path may seem artificial, it can be justified by noticing that $\mathcal{D}_{\gamma}$ represents processes, related to growth, that are not resolved explicitly by our model but that are necessary for growth to occur. In fact, a motivation for introducing a term like $\mathcal{D}_{\gamma}$ in the dissipation inequality of a growth problem can be found in [106].

6.4.2 Dynamic Equations

By adopting the material form of the momentum balance laws (6.23a) and (6.23b), and by invoking the force balance $\boldsymbol{m}_{\rm s} + \boldsymbol{m}_{\rm f} = \boldsymbol{0}$, we obtain

$$-\boldsymbol{g}^{-1}\boldsymbol{F}^{-\rm T}\boldsymbol{M}_{\rm f} - {\rm Div}\boldsymbol{P}_{\rm s} = \boldsymbol{0}, \tag{6.50a}$$

$$\boldsymbol{g}^{-1}\boldsymbol{F}^{-\rm T}\boldsymbol{M}_{\rm f} - {\rm Div}\boldsymbol{P}_{\rm f} = \boldsymbol{0}, \tag{6.50b}$$

where the constitutive expressions of $\boldsymbol{P}_{\rm s}$, $\boldsymbol{P}_{\rm f}$, and $\boldsymbol{M}_{\rm f}$ are given in (6.39a), (6.39b), and (6.47), respectively. Furthermore, by adding together (6.50a) with (6.50b), and using the explicit expression for $\boldsymbol{M}_{\rm f}$ in (6.50b), we find

$${\rm Div}(\boldsymbol{P}_{\rm s} + \boldsymbol{P}_{\rm f}) = \boldsymbol{0}, \tag{6.51a}$$

$$\boldsymbol{K}^{-1}\boldsymbol{Q} + {\rm Grad}\, p = \boldsymbol{0}. \tag{6.51b}$$

We exploit now the generalised force balance (6.23c), which becomes $H_\varepsilon^{(\rm i)} = H_\varepsilon^{(\rm e)}$ in material form and, by replacing $H_\varepsilon^{(\rm i)}$ with the right-hand-side of (6.49), we determine an evolution law for $\varepsilon_{\rm p}$, i.e.,

$$J\tau_{\rm p}\dot{\varepsilon}_{\rm p} - J_\gamma\sqrt{\tfrac{3}{2}}\,\|\tilde{\boldsymbol{\Sigma}}_\nu\|_{\boldsymbol{\eta}} + J_\gamma A_\nu[\varepsilon_{\rm p} - \mathfrak{e}_{\rm p}] = H_\varepsilon^{(\rm e)}. \tag{6.52}$$

To close this equation, we prescribe $H_\varepsilon^{(\rm e)}$ as

$$H_\varepsilon^{(\rm e)} = -\left[J\sigma_{\rm th} + J_\gamma Z_\nu[\varepsilon_{\rm p} - \mathfrak{e}_{\rm p}]\right], \tag{6.53}$$

where $\sigma_{\rm th}$ is a threshold stress, and Z_ν is a material parameter [15]. Hence, setting $\lambda_{\rm p} = 1/\tau_{\rm p}$, Equation (6.52) takes on the form

$$\dot{\varepsilon}_{\rm p} = \frac{\lambda_{\rm p}}{J}\left\{\left(J_\gamma\sqrt{\tfrac{3}{2}}\,\|\tilde{\boldsymbol{\Sigma}}_\nu\|_{\boldsymbol{\eta}} - J\sigma_{\rm th}\right) - J_\gamma(A_\nu + Z_\nu)[\varepsilon_{\rm p} - \mathfrak{e}_{\rm p}]\right\}. \tag{6.54}$$

The last dynamic equation is supplied by (6.23d). Recalling that, in the present framework, the external force $h_{\rm p}^{(\rm e)}$ is zero, the material form of (6.23d) reads

$$H_{\rm p}^{(\rm i)} - {\rm Div}\,\boldsymbol{\Xi}_{\rm p} = 0. \tag{6.55}$$

Hence, by substituting (6.39c) and (6.39d) into (6.55), we obtain

$$-J_\gamma A_\nu[\varepsilon_{\rm p} - \mathfrak{e}_{\rm p}] - {\rm Div}\left(J_\gamma B_\nu\left[\boldsymbol{F}_\gamma^{-1}\boldsymbol{B}_{\rm p}\boldsymbol{F}_\gamma^{-\rm T}\right]{\rm Grad}\mathfrak{e}_{\rm p}\right) = 0. \tag{6.56}$$

In particular, since we take $\boldsymbol{F}_\gamma$ as $\boldsymbol{F}_\gamma = \gamma\boldsymbol{I}$, (6.56) acquires the equivalent form

$$-\gamma^3 A_\nu[\varepsilon_{\rm p} - \mathfrak{e}_{\rm p}] - {\rm Div}\left(\gamma B_\nu\boldsymbol{B}_{\rm p}{\rm Grad}\mathfrak{e}_{\rm p}\right) = 0. \tag{6.57}$$

Remark 6.4.2 (The equation for $\mathfrak{e}_{\mathrm{p}}$). The result (6.57) is our generalisation to Equation (4.40) of Anand et al. [15], which, in our notation, and assuming constant values for A_ν and B_ν, would read

$$-A_\nu[\varepsilon_{\mathrm{p}} - \mathfrak{e}_{\mathrm{p}}] - B_\nu \Delta \mathfrak{e}_{\mathrm{p}} = 0 \quad \Rightarrow \quad \mathfrak{e}_{\mathrm{p}} - l_\nu^2 \Delta \mathfrak{e}_{\mathrm{p}} = \varepsilon_{\mathrm{p}}, \quad l_\nu = \sqrt{B_\nu / A_\nu}, \qquad \text{(A)}$$

with Δ being the Laplace operator, and l_ν the characteristic length scale associated with the micro-scale plasticity variable, $\mathfrak{e}_{\mathrm{p}}$. For a given distribution of ε_{p}, Equation (A) returns a "regularised" version of ε_{p}. In particular, since $\mathfrak{e}_{\mathrm{p}}$ is required to satisfy Neumann-zero boundary conditions, if ε_{p} is constant in $\mathscr{B}$, then the unique solution to (A) is the constant solution $\mathfrak{e}_{\mathrm{p}} = \varepsilon_{\mathrm{p}}$. However, when ε_{p} is strongly localised, the output of (A), i.e., $\mathfrak{e}_{\mathrm{p}}$, tends to be a lot more homogeneous, the more l_ν increases.

Our generalisation to (A) is twofold: first, the plastic-like distortions determine the evolution of $\mathfrak{e}_{\mathrm{p}}$ both through ε_{p} and through the second-order tensor $\boldsymbol{B}_{\mathrm{p}} = \boldsymbol{F}_{\mathrm{p}}^{-1}.\boldsymbol{F}_{\mathrm{p}}^{-\mathrm{T}}$. While ε_{p} is an input for (A), $\boldsymbol{B}_{\mathrm{p}}$ modulates, together with the growth parameter γ, the non-locality of $\mathfrak{e}_{\mathrm{p}}$, which is thus measured by the tensorial coefficient $\gamma B_\nu \boldsymbol{B}_{\mathrm{p}}$. We notice that the occurrence of this coefficient is due to the last term in the definition of $\hat{\Psi}_{\mathrm{s}}$ given in (6.31). Switching to the Eulerian formalism, and using the identity $\mathrm{Grad}\mathfrak{e}_{\mathrm{p}}(X,t) = (\nabla \mathrm{e}_{\mathrm{p}}(\chi(X,t),t)\boldsymbol{F}(X,t)$, this term reads

$$\tfrac{1}{2} b_0 \boldsymbol{b}_{\mathrm{e}} : \nabla \mathrm{e}_{\mathrm{p}} \otimes \nabla \mathrm{e}_{\mathrm{p}},$$

thereby meaning that, in the spatial description, the non-locality of the micro-"plastic" variable, e_{p}, is modulated by the elastic left Cauchy-Green deformation tensor, $\boldsymbol{b}_{\mathrm{e}} = \boldsymbol{F}_{\mathrm{e}}.\boldsymbol{F}_{\mathrm{e}}^{\mathrm{T}}$. To eliminate $\boldsymbol{B}_{\mathrm{p}}$ from (6.57), and obtain a model closer to that of Anand et al. [15], we should substitute $\boldsymbol{b}_{\mathrm{e}}$ with the left Cauchy-Green deformation tensor $\boldsymbol{b} = \boldsymbol{F}.\boldsymbol{F}^{\mathrm{T}}$. Such a choice would lead to replace the last term of (6.31) with

$$\tfrac{1}{2} b_0 \boldsymbol{G}^{-1} : \mathrm{Grad}\mathfrak{e}_{\mathrm{p}} \otimes \mathrm{Grad}\mathfrak{e}_{\mathrm{p}},$$

and would have the consequence of defining the unit tensor $\boldsymbol{N}_\nu$ just in terms of the standard Mandel stress tensor, $\boldsymbol{\Sigma}_\nu^{(\mathrm{st})}$ (see Remark 6.4.1). We recall that $\boldsymbol{G}$ denotes here the natural material metric tensor associated with $\mathscr{B}$.

The second aspect of our generalisation is related to the fact that, in our model, the evolution of $\mathfrak{e}_{\mathrm{p}}$ is influenced by the growth parameter, γ, which couples with the coefficients A_ν and B_ν, thereby rescaling the characteristic length scale associated with $\mathfrak{e}_{\mathrm{p}}$ in a generally inhomogeneous way, i.e., as $l_\nu \to l = l_\nu \|\boldsymbol{B}_{\mathrm{p}}\|_{\boldsymbol{G}}^{1/2}/\gamma$, so that, for a given l_ν, the condition $\gamma > 1$ tends to reduce the length scale associated with $\mathfrak{e}_{\mathrm{p}}$. Note that $\|\boldsymbol{B}_{\mathrm{p}}\|_{\boldsymbol{G}} = [\mathrm{tr}(\boldsymbol{G}\boldsymbol{B}_{\mathrm{p}}\boldsymbol{G}\boldsymbol{B}_{\mathrm{p}})]^{1/2}$.

Remark 6.4.3 (Choice of $H_\varepsilon^{(\mathrm{e})}$). In the literature on remodelling (see e.g. [183, 127, 56]), when an external force, like $H_\varepsilon^{(\mathrm{e})}$, is taken into account, it is often chosen in such a way that a homeostatic state exists for the system under study. If we had followed such philosophy, we should have admitted homeostatic terms for ε_{p} and $\mathfrak{e}_{\mathrm{p}}$, denoted by $\varepsilon_{\mathrm{p}}^{(\mathrm{h})}$ and $\mathfrak{e}_{\mathrm{p}}^{(\mathrm{h})}$, and we should have expressed $H_{\varepsilon}^{(\mathrm{e})}$ as

$$H_{\varepsilon}^{(\mathrm{e})} = -J_{\gamma}\sqrt{\tfrac{3}{2}}\,\|\tilde{\boldsymbol{\Sigma}}_{\nu}^{(\mathrm{h})}\|_{\boldsymbol{\eta}} + J_{\gamma}A_{\nu}[\varepsilon_{\mathrm{p}}^{(\mathrm{h})} - \mathfrak{e}_{\mathrm{p}}^{(\mathrm{h})}], \tag{6.58}$$

where $\tilde{\boldsymbol{\Sigma}}_{\nu}^{(\mathrm{h})}$ is the Mandel-like stress tensor in homeostatic conditions (that is, when its arguments attain the homeostatic state). This consideration notwithstanding, in our work we opted for the expression (6.53) because, in order to formulate a proof of concept for our problem, we needed to remain as close as possible to the framework supplied by [15].

Remark 6.4.4 (Evolution law for ε_{p}). Equation (6.53) represents an essential difference with respect to the evolution law for ε_{p} given by [15]. Indeed, Anand et al. [15] set $H_{\varepsilon}^{(\mathrm{i})} = H_{\varepsilon}^{(\mathrm{e})} = 0$, and assign $H_{\varepsilon}^{(\mathrm{i,d})}$ constitutively as a law that plays the role of an *effective yield stress*, i.e., $H_{\varepsilon}^{(\mathrm{i,d})} = J\sigma_{\mathrm{th}} + J_{\gamma}Z_{\nu}[\varepsilon_{\mathrm{p}} - \mathfrak{e}_{\mathrm{p}}]$, where $\sigma_{\mathrm{th}} > 0$ plays the role of the *"conventional yield stress"* [15][2], while $Z_{\nu} > 0$ is a model parameter defining the purely dissipative part of $H_{\varepsilon}^{(\mathrm{i,d})}$. By doing this, the Authors rewrite the balance equation $H_{\varepsilon}^{(\mathrm{i})} = H_{\varepsilon}^{(\mathrm{e})}$ in terms of a yield function of the type $\mathfrak{f} = J_{\gamma}\sqrt{\tfrac{3}{2}}\|\tilde{\boldsymbol{\Sigma}}_{\nu}\|_{\boldsymbol{\eta}} - (J\sigma_{\mathrm{th}} + J_{\gamma}(A_{\nu} + Z_{\nu})[\varepsilon_{\mathrm{p}} - \mathfrak{e}_{\mathrm{p}}])$. In particular, according to the theory of Anand et al. [15], it occurs that $\dot{\varepsilon}_{\mathrm{p}} = 0$, if $\mathfrak{f} < 0$, and $\dot{\varepsilon}_{\mathrm{p}} > 0$, if $\mathfrak{f} = 0$. This approach is equivalent to the elasto-plastic problem in the Karush-Kuhn-Tucker form, i.e.,

$$\mathfrak{f} \leq 0, \qquad \dot{\varepsilon}_{\mathrm{p}} \geq 0, \qquad \mathfrak{f}\,\dot{\varepsilon}_{\mathrm{p}} = 0, \tag{6.59}$$

where $\dot{\varepsilon}_{\mathrm{p}}$ is determined by means of the consistency condition $\dot{\varepsilon}_{\mathrm{p}}\dot{\mathfrak{f}} = 0$, when $\mathfrak{f} = 0$. If, in our work, we had followed the approach outlined by Anand et al. [15], we would have found a very complicated evolution law for ε_{p}, especially from the computational point of view. To circumvent this technical difficulty, we have proposed a modification to the model, i.e., we have assumed $H_{\varepsilon}^{(\mathrm{i})} = H_{\varepsilon}^{(\mathrm{e})} \neq 0$ and, in order to obtain an evolution law for ε_{p} of the type $J\tau_{\mathrm{p}}\dot{\varepsilon}_{\mathrm{p}} = \mathfrak{f}$ (cf. Equation (6.52)), with $\mathfrak{f}$ defined as done by Anand et al. [15], we have exploited the "freedom" we have to express $H_{\varepsilon}^{(\mathrm{e})}$ as in (6.53). A last comment pertains to the terms λ_{p}/J and $J\sigma_{\mathrm{th}}$ featuring in Equation (6.54): if λ_{p} and σ_{th} are such that $\lambda_{\mathrm{p}}/J_{\mathrm{e}} \equiv \Lambda_{\mathrm{p}}$ and $J_{\mathrm{e}}\sigma_{\mathrm{th}} \equiv \Sigma_{\mathrm{th}}$ are constants, then it holds that $\lambda_{\mathrm{p}}/J = \Lambda_{\mathrm{p}}/J_{\gamma}$ and $J\sigma_{\mathrm{th}} = J_{\gamma}\Sigma_{\mathrm{th}}$. In this case, J_{γ} does not feature explicitly in Equation (6.54), which becomes $\dot{\varepsilon}_{\mathrm{p}} = \Lambda_{\mathrm{p}}\tilde{\mathfrak{f}}$, where we have set $\tilde{\mathfrak{f}} \equiv \mathfrak{f}/J_{\gamma}$. In this case, Σ_{th} acquires the meaning of the yield stress that

[2] Note that, differently from what is assumed here, Anand et al. [15] hypothesise that the conventional yield stress is a monotonically decreasing function of ε_{p}, because they are interested in studying the phenomenon of *strain-softening*.

is used in the yield criteria formulated in terms of the norm of the Mandel stress tensor (see e.g. [124]). We remark, however, that solving $\dot{\varepsilon}_{\rm p} = \Lambda_{\rm p}\tilde{\mathfrak{f}}$ in lieu of (6.54) leads, in our work, to no appreciable differences in the simulation results.

6.5 Model Equations and benchmark test

In this section, we summarise all the model equations and their corresponding unknowns, we highlight the fundamental hypotheses adopted to simplify our simulations, and we describe the benchmark problem used for testing our model.

6.5.1 Summary of the model equations

The first equation of the problem is given by (6.51a), i.e., the momentum balance law for the mixture as a whole, and its associated unknown is given by the solid phase motion, χ. The second equation determines the pressure, p, and is supplied by the mass balance law (6.3d), in which, coherently with (6.51b), $\boldsymbol{Q}$ is expressed as $\boldsymbol{Q} = -\boldsymbol{K}\,\mathrm{Grad}p$. The right-hand-side of (6.3d) is set equal to zero on the basis of the assumption that, in tumours, the mass densities $\rho_{\rm s0}$ and $\rho_{\rm f0}$ are approximately the same. The third equation is the mass balance of the proliferating cells (6.3a), and its corresponding unknown is the mass fraction $\omega_{\rm p}$. The fourth equation is in the mass fraction of the nutrients, $\omega_{\rm N}$, and is obtained from (6.3c) by using the identities $\Phi_{\rm f} = J - J_\gamma \Phi_{\rm s\nu}$ and $\boldsymbol{Y}_{\rm N} = -\rho_{\rm f0}\boldsymbol{D}\,\mathrm{Grad}\,\omega_{\rm N}$. The fifth equation descends for the mass balance law of the solid phase and, by assigning the mass source $R_{\rm s}$ phenomenologically, it puts a constraint on the growth parameter, γ, which is thus bound to comply with (6.18). Except for the sources and sinks of mass, which are defined in a slightly different way in our work, the five equations mentioned so far are the same as those studied by Mascheroni et al. [166] and Di Stefano et al. [62].

The evolution of the plastic distortions is described by the dynamic equation (6.54), which determines $\varepsilon_{\rm p}$, and by the constraint on $\boldsymbol{F}_{\rm p}$ placed by (6.15). These add two more equations to the previous five. Finally, the equation for the micro-scale "plasticity" variable, $\mathfrak{e}_{\rm p}$, is supplied by (6.57).

In conclusion, by putting together all the laws enumerated up to now, we obtain

$$\mathrm{Div}(\boldsymbol{P}_{\rm f} + \boldsymbol{P}_{\rm s}) = \boldsymbol{0}, \tag{6.60a}$$

$$\mathrm{Div}\,(\boldsymbol{K}\mathrm{Grad}p) = \dot{J}, \tag{6.60b}$$

$$\rho_{\rm s0} J_\gamma \Phi_{\rm s\nu}\dot{\omega}_{\rm p} = R_{\rm pn} + R_{\rm fp} - R_{\rm s}\omega_{\rm p}, \tag{6.60c}$$

$$\rho_{\rm f0}[J - J_\gamma \Phi_{\rm s\nu}]\dot{\omega}_{\rm N} + \rho_{\rm f0}\boldsymbol{Q}\,\mathrm{Grad}\omega_{\rm N} = \mathrm{Div}\,(\rho_{\rm f0}\boldsymbol{D}\,\mathrm{Grad}\,\omega_{\rm N}) + R_{\rm Np} + R_{\rm s}\omega_{\rm N}, \tag{6.60d}$$

$$\dot{\gamma} = \frac{R_{\rm s}}{3\rho_{\rm s0}\Phi_{\rm s\nu}\gamma^2}, \tag{6.60e}$$

$$\dot{\varepsilon}_\mathrm{p} = \frac{\lambda_\mathrm{p}}{J}\left\{\left(J_\gamma\sqrt{\tfrac{3}{2}}\|\tilde{\boldsymbol{\Sigma}}_\nu\|_{\boldsymbol{\eta}} - J\sigma_\mathrm{th}\right) - J_\gamma(A_\nu + Z_\nu)[\varepsilon_\mathrm{p} - \mathfrak{e}_\mathrm{p}]\right\}, \tag{6.60f}$$

$$\dot{\boldsymbol{F}}_\mathrm{p} = \left(\sqrt{\tfrac{3}{2}}\,\dot{\varepsilon}_\mathrm{p}\boldsymbol{\eta}^{-1}\boldsymbol{N}_\nu\right)\boldsymbol{F}_\mathrm{p}, \tag{6.60g}$$

$$\mathrm{Div}\,(\gamma B_\nu \boldsymbol{B}_\mathrm{p}\mathrm{Grad}\mathfrak{e}_\mathrm{p}) - \gamma^3 A_\nu \mathfrak{e}_\mathrm{p} = -\gamma^3 A_\nu \varepsilon_\mathrm{p}, \tag{6.60h}$$

which constitutes a system of 18 scalar equations in the 18 unknowns

$$\mathscr{U} = \{\chi, p, \omega_\mathrm{p}, \omega_\mathrm{N}, \gamma, \varepsilon_\mathrm{p}, \boldsymbol{F}_\mathrm{p}, \mathfrak{e}_\mathrm{p}\}. \tag{6.61}$$

For ensuring the non-negativity of $\dot{\varepsilon}_\mathrm{p}$ at all times and at all points, we solve (6.60f) numerically by taking the positive part of its right-hand-side. Moreover, to close the problem, we prescribe the permeability tensor and the diffusion tensor [138, 19, 62, 80],

$$\boldsymbol{K} = Jk_0\boldsymbol{C}^{-1}, \quad k_0 = k_{0\mathrm{R}}\left[\frac{J - J_\gamma\Phi_{\mathrm{s}\nu}}{J_\gamma\varphi_{\mathrm{f}0}}\right]^{m_0}\exp\left(\frac{m_1}{2}\left[\frac{J^2 - J_\gamma^2}{J_\gamma^2}\right]\right), \tag{6.62a}$$

$$\boldsymbol{D} = Jd_0\boldsymbol{C}^{-1}, \quad d_0 = \frac{J - J_\gamma\Phi_{\mathrm{s}\nu}}{J}d_{0\mathrm{R}}, \tag{6.62b}$$

as well as the sources and sinks of mass [166, 62], i.e.,

$$R_\mathrm{pn} = -J\zeta_\mathrm{pn}\left\langle 1 - \frac{\omega_\mathrm{N}}{\omega_\mathrm{Ncr}}\right\rangle_+ \frac{J_\gamma\Phi_{\mathrm{s}\nu}}{J}\omega_\mathrm{p}, \tag{6.63a}$$

$$R_\mathrm{fp} = J\zeta_\mathrm{fp}\left\langle \frac{\omega_\mathrm{N} - \omega_\mathrm{Ncr}}{\omega_\mathrm{Nenv} - \omega_\mathrm{Ncr}}\right\rangle_+ \left[1 - \frac{\delta_1\langle\wp\rangle_+}{\delta_2 + \langle\wp\rangle_+}\right]\frac{J - J_\gamma\Phi_{\mathrm{s}\nu}}{J\varphi_{\mathrm{f}0}}\frac{J_\gamma\Phi_{\mathrm{s}\nu}}{J}\omega_\mathrm{p}, \tag{6.63b}$$

$$R_\mathrm{s} = R_\mathrm{fp} + R_\mathrm{nf}, \tag{6.63c}$$

$$R_\mathrm{nf} = -J\zeta_\mathrm{nf}[1 - \omega_\mathrm{p}]\frac{J_\gamma\Phi_{\mathrm{s}\nu}}{J}, \tag{6.63d}$$

$$R_\mathrm{Np} = -J\zeta_\mathrm{Np}\frac{\omega_\mathrm{N}}{\omega_\mathrm{N} + \omega_\mathrm{N0}}\frac{J_\gamma\Phi_{\mathrm{s}\nu}}{J}\omega_\mathrm{p}. \tag{6.63e}$$

Since the expressions of R_pn, R_fp, R_nf, and R_Np have been already commented in previous works [166, 62], we do not spend any more words here on their derivation. We recall, however, that the operator $\langle\,\cdot\,\rangle_+$ returns the positive part of its argument, and that ω_Ncr denotes a critical value of the mass fraction of the nutrients, below which the proliferating cells tend to be necrotic (that is, $R_\mathrm{pn} < 0$), whereas ω_Nenv represents the mass fraction of the nutrients in the "environment". Both ω_Nenv and ω_Ncr are regarded as constant parameters in our work, and it is assumed that the condition $\omega_\mathrm{Nenv} > \omega_\mathrm{Ncr}$ is always respected, so that also R_fp is deactivated, i.e., $R_\mathrm{fp} = 0$, for $\omega_\mathrm{N} < \omega_\mathrm{Ncr}$. Moreover, looking at the definition of R_fp, and bearing in mind that, for $\omega_\mathrm{N} > \omega_\mathrm{Ncr}$, R_fp describes the positive variation of mass of the tissue's solid phase, we notice that the factor

$$\left[1 - \frac{\delta_1\langle\wp\rangle_+}{\delta_2 + \langle\wp\rangle_+}\right]$$

accounts for mechanotransduction through the action of the stress $\langle\wp\rangle_+$. Comparing this result with the works of Mascheroni et al. [166] and Di Stefano et al. [62], we notice that our model suggests a slightly different interpretation of mechanotransduction. Indeed, while Mascheroni et al. [166] and Di Stefano et al. [62] prescribe $\wp$ as $\wp = -(1/3)\mathrm{tr}(\boldsymbol{g}\boldsymbol{\sigma}_{\mathrm{sc}})$, where $\boldsymbol{\sigma}_{\mathrm{sc}} = J^{-1}\boldsymbol{P}_{\mathrm{sc}}\boldsymbol{F}^{\mathrm{T}}$ is the constitutive part of the solid phase Cauchy stress, and, accordingly, $\boldsymbol{P}_{\mathrm{sc}}$ is defined by

$$\boldsymbol{P}_{\mathrm{sc}} = J_\gamma \left(\rho_{\mathrm{s}0}\Phi_{\mathrm{s}\nu}\boldsymbol{g}^{-1}\frac{\partial\hat{\Psi}_{\mathrm{s}}^{(\mathrm{st})}}{\partial\boldsymbol{F}_{\mathrm{e}}}(\boldsymbol{F}\boldsymbol{F}_\gamma^{-1}\boldsymbol{F}_{\mathrm{p}}^{-1})\boldsymbol{F}_{\mathrm{p}}^{-\mathrm{T}}\boldsymbol{F}_\gamma^{-\mathrm{T}} \right) \equiv \boldsymbol{\mathcal{P}}_{\mathrm{sc}}(\boldsymbol{F}, \boldsymbol{F}_\gamma, \boldsymbol{F}_{\mathrm{p}}), \tag{6.64}$$

in our approach $\wp$ is taken as $\wp = -(1/3)\mathrm{tr}(\boldsymbol{g}\boldsymbol{\sigma}_{\mathrm{eff}})$ (see also [56]), with

$$\begin{aligned} \boldsymbol{\sigma}_{\mathrm{eff}} &= \boldsymbol{\sigma}_{\mathrm{sc}} + \frac{1}{J_{\mathrm{e}}}\boldsymbol{g}^{-1}\boldsymbol{F}_{\mathrm{e}}^{-\mathrm{T}}\boldsymbol{\eta}\boldsymbol{\Sigma}_\nu^{(\mathrm{n\text{-}st})}\boldsymbol{F}_{\mathrm{e}}^{\mathrm{T}} \\ &= \frac{1}{J_{\mathrm{e}}}\boldsymbol{g}^{-1}\boldsymbol{F}_{\mathrm{e}}^{-\mathrm{T}}\boldsymbol{\eta}\boldsymbol{\Sigma}_\nu^{(\mathrm{st})}\boldsymbol{F}_{\mathrm{e}}^{\mathrm{T}} + \frac{1}{J_{\mathrm{e}}}\boldsymbol{g}^{-1}\boldsymbol{F}_{\mathrm{e}}^{-\mathrm{T}}\boldsymbol{\eta}\boldsymbol{\Sigma}_\nu^{(\mathrm{n\text{-}st})}\boldsymbol{F}_{\mathrm{e}}^{\mathrm{T}} \\ &= \frac{1}{J_{\mathrm{e}}}\boldsymbol{g}^{-1}\boldsymbol{F}_{\mathrm{e}}^{-\mathrm{T}}\boldsymbol{\eta}\boldsymbol{\Sigma}_\nu\boldsymbol{F}_{\mathrm{e}}^{\mathrm{T}}. \end{aligned} \tag{6.65}$$

In other words, while the works done by Mascheroni et al. [166] and Di Stefano et al. [62] the stress used to express the mechanotransduction is the classical $\boldsymbol{\sigma}_{\mathrm{sc}}$, we propose here to adopt the *effective Cauchy stress*, $\boldsymbol{\sigma}_{\mathrm{eff}}$, which captures both $\boldsymbol{\sigma}_{\mathrm{sc}}$ and the non-standard, purely configurational contribution $\boldsymbol{\Sigma}_\nu^{(\mathrm{n\text{-}st})}$. Our point is that, since in our approach $\boldsymbol{\Sigma}_\nu$ is (power-)conjugate to the growth rate $\dot{\gamma}/\gamma$ (through R_{s}) and to $\dot{\varepsilon}_{\mathrm{p}}$ (see (6.32)), it might be a more natural representative of the stress responsible for modulating growth. This consideration notwithstanding, for the parameters chosen in our simulations, the contribution of $\boldsymbol{\Sigma}_\nu^{(\mathrm{n\text{-}st})}$ is very marginal with respect to the standard measures of stress, and its contribution is thus not much appreciable.

6.5.2 Benchmark problem

The benchmark problem is essentially the same as the one computed in Di Stefano et al. [62], with the major difference that we are now considering also plastic distortions and the role of micro-plasticity. Hence, by adapting a study originally designed by Ambrosi and Mollica[10], we consider the case of volumetric growth in a cylindrical sample of isotropic material. For this purpose, we introduce the systems of cylindrical coordinates (R, Θ, Z) and (r, θ, z), which cover the reference and current configuration, respectively. For both systems, the first coordinate is radial, the second one is circumferential, and the third one is axial.

We assume that the radius of the specimen is preserved, and that only its length varies along the axial direction. Hence, we eliminate any rigid rotation about the principal axis. These restrictions imply that the momentum balance law

(6.60a) reduces to a scalar equation in Z, and that the deformation gradient tensor becomes $\boldsymbol{F} = \boldsymbol{e}_r \otimes \boldsymbol{E}^R + \boldsymbol{e}_\theta \otimes \boldsymbol{E}^\Theta + (1 + \frac{\partial u}{\partial Z})\boldsymbol{e}_z \otimes \boldsymbol{E}^Z$, where u is the field of axial displacements. We note that $\{\boldsymbol{E}^R, \boldsymbol{E}^\Theta, \boldsymbol{E}^Z\}$ and $\{\boldsymbol{e}_r, \boldsymbol{e}_\theta, \boldsymbol{e}_z\}$ are the co-vector and vector bases associated with the system of cylindrical coordinates (R, Θ, Z) and (r, θ, z), respectively.

We impose the following boundary conditions on Equations (6.60a)–(6.60h)

$$
\begin{aligned}
&(-Jp\boldsymbol{g}^{-1}\boldsymbol{F}^{-\mathrm{T}} + \boldsymbol{P}_{\mathrm{sc}}).\boldsymbol{N}_{\mathrm{A}} = \boldsymbol{0}, && \text{on } (\partial\mathscr{B})_{\mathrm{Left}} \text{ and } (\partial\mathscr{B})_{\mathrm{Right}}, && (6.66\mathrm{a})\\
&p = 0, && \text{on } (\partial\mathscr{B})_{\mathrm{Left}} \text{ and } (\partial\mathscr{B})_{\mathrm{Right}}, && (6.66\mathrm{b})\\
&(-\boldsymbol{K}\,\mathrm{Grad}\,p).\boldsymbol{N}_{\mathrm{C}} = 0, && \text{on } (\partial\mathscr{B})_{\mathrm{C}}, && (6.66\mathrm{c})\\
&(-\rho_{\mathrm{f}}\boldsymbol{D}\mathrm{Grad}\,\omega_{\mathrm{N}}).\boldsymbol{N}_{\mathrm{C}} = 0, && \text{on } (\partial\mathscr{B})_{\mathrm{C}}, && (6.66\mathrm{d})\\
&\omega_{\mathrm{N}} = \omega_{\mathrm{Nenv}}, && \text{on } (\partial\mathscr{B})_{\mathrm{Left}} \text{ and } (\partial\mathscr{B})_{\mathrm{Right}}, && (6.66\mathrm{e})\\
&(\gamma B_\nu \boldsymbol{B}_{\mathrm{p}}\mathrm{Grad}\mathfrak{e}_{\mathrm{p}}).\boldsymbol{N} = 0, && \text{on } \partial\mathscr{B}, && (6.66\mathrm{f})
\end{aligned}
$$

where $\partial\mathscr{B} = (\partial\mathscr{B})_{\mathrm{Left}} \cup (\partial\mathscr{B})_{\mathrm{C}} \cup (\partial\mathscr{B})_{\mathrm{Right}}$, $(\partial\mathscr{B})_{\mathrm{C}}$ is the lateral boundary of the cylinder, $(\partial\mathscr{B})_{\mathrm{Left}}$ and $(\partial\mathscr{B})_{\mathrm{Right}}$ are the left and right surface cross-sections at $Z = -L/2$ and $Z = L/2$, respectively, and L is the initial length of the cylinder. Moreover, $\boldsymbol{N}_{\mathrm{A}}$, $\boldsymbol{N}_{\mathrm{C}}$, and $\boldsymbol{N}$ are fields of unit vectors normal to $(\partial\mathscr{B})_{\mathrm{Left}}$ and $(\partial\mathscr{B})_{\mathrm{Right}}$, $(\partial\mathscr{B})_{\mathrm{C}}$, and $\partial\mathscr{B}$, respectively.

Equations (6.66a) and (6.66b) mean that the left and right ends of the cylinder are free boundaries. The relations (6.66c) and (6.66d) are enforced to express that $(\partial\mathscr{B})_{\mathrm{C}}$ is undeformable and impermeable to the fluid and to the nutrients, respectively. Equation (6.66e) is a Dirichlet condition specifying that there always exists a constant availability of nutrients on the boundaries $(\partial\mathscr{B})_{\mathrm{Left}}$ and $(\partial\mathscr{B})_{\mathrm{Right}}$. Finally, the boundary condition (6.66f) is introduced following Anand et al. [15].

To complete the mathematical formulation of the problem, we prescribe the initial conditions,

$$
\begin{aligned}
&\chi^r(R, \Theta, Z, 0) = R, && (6.67\mathrm{a})\\
&\chi^\vartheta(R, \Theta, Z, 0) = \Theta, && (6.67\mathrm{b})\\
&\chi^z(R, \Theta, Z, 0) = Z, && (6.67\mathrm{c})\\
&p(R, \Theta, Z, 0) = 0, && (6.67\mathrm{d})\\
&\omega_{\mathrm{N}}(R, \Theta, Z, 0) = \omega_{\mathrm{Nenv}}, && (6.67\mathrm{e})\\
&\gamma(R, \Theta, Z, 0) = 1, && (6.67\mathrm{f})\\
&\omega_{\mathrm{p}}(R, \Theta, Z, 0) = 1, && (6.67\mathrm{g})\\
&\varepsilon_{\mathrm{p}}(R, \Theta, Z, 0) = 0, && (6.67\mathrm{h})\\
&\mathfrak{e}_{\mathrm{p}}(R, \Theta, Z, 0) = 0, && (6.67\mathrm{i})
\end{aligned}
$$

with $R \in [0, R_{\mathrm{b}}]$, $\Theta \in [0, 2\pi[$ and $Z \in [-L/2, L/2]$. The conditions (6.67a)–(6.67i) have to be valid in the whole domain $\mathscr{B}$.

The material parameters $k_{0\mathrm{R}}$, m_0, m_1, and $d_{0\mathrm{R}}$, the coefficients ζ_{pn}, ζ_{fp}, ζ_{nf}, and ζ_{Np} as well as the constants ω_{Nenv}, ω_{Ncr}, ω_{N0}, δ_1, δ_2, σ_{th}, and λ_{p} are given in Table 6.1.

In Table 6.1, the length of the cylindric specimen, L, and the radius of its cross section, R_{b}, are chosen within a plausible physical range. However, it is necessary to motivate the choice of the parameters ω_{Nenv}, ω_{Ncr}, and ω_{N0}, which are all taken from Di Stefano et al. [62]. These quantities are adapted from [166], where they were set equal to $\omega_{\mathrm{Nenv}} = 7.0 \cdot 10^{-6}$, $\omega_{\mathrm{Ncr}} = 2.0 \cdot 10^{-6}$, and $\omega_{\mathrm{N0}} = 4.2 \cdot 10^{-6}$, respectively. With the exception of ω_{Ncr}[3], in the work of Mascheroni et al. [166] these values come from experiments performed on tumour spheroids and associated with geometry, size, diffusion length scales and nutrients' characteristic mass fractions that are very different from those considered in our work. Indeed, an essential feature of the benchmark problem investigated by Mascheroni et al. [166] is that, because of the spherical geometry of the tumour, and because of the nutrients being distributed homogeneously on the tumour's surface, the diffusion of the nutrients occurs isotropically, from the boundary to the center of the spheroid, in radial direction. In our problem, instead, the nutrients can diffuse only along the axial direction of the tumour, and they have to travel the length L, which is much larger than the radius, of about 20 μm, of the spheroids considered Mascheroni et al. [166]. Due to these geometric and size aspects, if we used the values of ω_{Nenv}, ω_{Ncr} and ω_{N0} suggested Mascheroni et al., we would generate a situation in which the replenishment of the nutrients "eaten" by the cells would be too slow for the tumour to grow. Indeed, especially in the middle of the tumour, the nutrients' mass fraction would go below the threshold value, ω_{Ncr}, after few hours. Therefore, to avoid a fast inhibition of growth, we have increased the value of ω_{Nenv} of three orders of magnitude in our experiment *in silico*. Note that there is a certain freedom in the choice of ω_{Nenv}, since prescribing its value amounts to preparing the bath of nutrients in which the tumour is immersed. This freedom notwithstanding, the value assigned to ω_{Nenv} should take into account the characteristic length of the tumour —in our case, L— in order to ensure that the effects of growth remain active over a sufficiently long time scale. In principle, ω_{Ncr} and ω_{N0} should be determined experimentally. Still, since we are not aware of any experimental value of ω_{Ncr}, we have calibrated it so that ω_{Ncr} be smaller than ω_{Nenv}, but big enough to allow for a transition from the stage of tumour growth, for $\omega_{\mathrm{Ncr}} < \omega_{\mathrm{N}} \leq \omega_{\mathrm{Nenv}}$, to the stage of no growth, for $\omega_{\mathrm{N}} \leq \omega_{\mathrm{Ncr}} < \omega_{\mathrm{Nenv}}$. This reasoning has led us to choose ω_{Ncr} three orders of magnitude greater than the value assigned Mascheroni et al. [166]. Finally, the value given to ω_{N0} in our work (see Table 6.1) is two orders of

[3] Note that the values attributed to ω_{Ncr} by Mascheroni et al. [166] for all the considered studies are never referenced, the only exception being the growth of a tumour spheroid. In this case, however, the reference is a typographical error.

magnitude greater than the one prescribed by Mascheroni et al. [166]. This choice allows us to be consistent with the scale of the nutrients' mass fraction imposed in our work.

6.6 Some computational aspects

The system (6.60a)–(6.60h) features both ordinary differential equations (ODEs) in time, and partial differential equations (PDEs). All the ODEs of our model, including those obtained after that the finite element discretisation of the PDEs is performed, have been discretised adaptively in time, and have been solved by means of a four-step Backward Differentiation Formula (BDF4). This is an implicit linear multistep method, which generalises the implicit Euler method. Since the BDF4 is implicit, it requires in general the solution of nonlinear equations at each time integration step. The BDF4 is available in COMSOL Multiphysics®, which has been used to run our simulations.

The PDEs have been put in weak form and solved by means of Finite Element techniques. In particular, classical methods have been used for (6.60b), (6.60d), and (6.60h), while a "special treatment" has been reserved to the momentum balance law (6.60a), for which the Hu-Washizu method [33] has been employed.

Looking more closely at the PDEs (6.60b), (6.60d), and (6.60h), we notice that (6.60b) is a generalised Poisson equation in the pressure, p, with a time-dependent right-hand-side, $\dot{J}$, which represents the volume change of the solid phase due to the changes in porosity accompanying the flow of the fluid. Equation (6.60d), instead, is a nonlinear diffusion-advection-reaction equation in the mass fraction of the nutrients, ω_N, with the nonlinearity being nested in the reaction terms, R_Np and R_s. Both for (6.60b) and for (6.60d), the Finite Element Method leads to a set of ODEs in which the unknowns are the nodal pressures and the nodal mass fractions of the nutrients, respectively. Finally, Equation (6.60h) is an equation of Helmholtz type and, in this case, the Finite Element method yields a set of algebraic equations in the nodal values of $\mathfrak{e}_\mathrm{p}$, which are anyway time-dependent. In the following, we do not fuss over the procedure for obtaining the set of nodal equations associated with (6.60b), (6.60d), and (6.60h), since such procedure is rather standard.

To sketch the formulation of the Hu-Washizu method, we add together the expressions of the stress tensors $\boldsymbol{P}_\mathrm{f}$ and $\boldsymbol{P}_\mathrm{s}$, and we notice that the weak form of the momentum balance law (6.60a) admits the compact form

$$\int_{\mathscr{B}} (\boldsymbol{P}_\mathrm{f} + \boldsymbol{P}_\mathrm{s}) : \boldsymbol{g}\,\mathrm{Grad}\,\boldsymbol{U}_\mathrm{s} = \int_{\mathscr{B}} \left(-Jp\,\boldsymbol{g}^{-1}\boldsymbol{F}^{-\mathrm{T}} + \boldsymbol{P}_\mathrm{sc}\right) : \boldsymbol{g}\,\mathrm{Grad}\,\boldsymbol{U}_\mathrm{s} = 0, \tag{6.68}$$

where $\boldsymbol{U}_\mathrm{s}$ is the virtual velocity of the solid, expressed as a function of the points X of $\mathscr{B}$.

One of the main drawbacks of this formulation is that, once a Finite Element scheme is used for solving (6.68), the "limitations" of the interpolations adopted for χ [33], $\boldsymbol{F}$, and $\boldsymbol{F}_{\mathrm{p}}$ are transferred to $\boldsymbol{P}_{\mathrm{sc}}$ through its constitutive representation, $\boldsymbol{\mathcal{P}}_{\mathrm{sc}}(\boldsymbol{F}, \boldsymbol{F}_\gamma, \boldsymbol{F}_{\mathrm{p}})$. This ill behaviour persists even increasing the order of the basis functions used for the discretisation of χ, and may lead to a remarkable deterioration of the resolution of $\boldsymbol{P}_{\mathrm{sc}}$, with consequent loss of accuracy of the employed numerical method. A possible way to contain the occurrence of the just depicted numerical phenomenon is supplied by the Hu-Washizu method [33], which we implement for our purposes in its three-field-formulation. Although the Hu-Washizu method is well known in the computational community, we briefly explain here how we adapt it to the case under investigation in this work.

Together with the motion, χ, which is an unknown of the model, we introduce two tensor-valued auxiliary variables, which we regard as additional independent fields of our model: these are an auxiliary "deformation gradient tensor", $\boldsymbol{F}^{\mathrm{HW}}$, and an auxiliary first Piola-Kirchhoff stress tensor, $\boldsymbol{P}_{\mathrm{sc}}^{\mathrm{HW}}$ (note that the superscript "HW" stands for "Hu-Washizu"). Although being independent, $\boldsymbol{F}^{\mathrm{HW}}$ and $\boldsymbol{P}_{\mathrm{sc}}^{\mathrm{HW}}$ must be consistent with the *true* deformation gradient tensor and with the *true* first Piola-Kirchhoff stress tensor, respectively, and are thus bound to satisfy the constraints

$$\boldsymbol{F}^{\mathrm{HW}} = \boldsymbol{F}, \tag{6.69a}$$

$$\boldsymbol{P}_{\mathrm{sc}}^{\mathrm{HW}} = \boldsymbol{\mathcal{P}}_{\mathrm{sc}}(\boldsymbol{F}^{\mathrm{HW}}, \boldsymbol{F}_\gamma, \boldsymbol{F}_{\mathrm{p}}). \tag{6.69b}$$

To proceed with the Hu-Washizu method, we rephrase Equations (6.69a) and (6.69b) in weak form. Hence, we write

$$\int_{\mathscr{B}} \Big\{ \Big[\boldsymbol{F} - \boldsymbol{F}^{\mathrm{HW}}\Big] : \boldsymbol{\Pi} + \Big[\boldsymbol{\mathcal{P}}_{\mathrm{sc}}(\boldsymbol{F}^{\mathrm{HW}}, \boldsymbol{F}_\gamma, \boldsymbol{F}_{\mathrm{p}}) - \boldsymbol{P}_{\mathrm{sc}}^{\mathrm{HW}}\Big] : \boldsymbol{\Lambda} \Big\} = 0, \tag{6.70}$$

where $\boldsymbol{\Pi}$ and $\boldsymbol{\Lambda}$ denote the virtual variations of $\boldsymbol{P}_{\mathrm{sc}}^{\mathrm{HW}}$ and $\boldsymbol{F}^{\mathrm{HW}}$, respectively, and represent a virtual stress rate and a virtual velocity gradient. Equation (6.70) is now appended to (6.68), which has to be reformulated in terms of the Hu-Washizu auxiliary fields, thereby obtaining

$$\begin{aligned} \int_{\mathscr{B}} \{ \Big[\boldsymbol{P}_{\mathrm{sc}}^{\mathrm{HW}} - (\det \boldsymbol{F}^{\mathrm{HW}}) p \boldsymbol{g}^{-1} (\boldsymbol{F}^{\mathrm{HW}})^{-\mathrm{T}}\Big] : \boldsymbol{g}\, \mathrm{Grad}\, \boldsymbol{U}_{\mathrm{s}} + \Big[\boldsymbol{F} - \boldsymbol{F}^{\mathrm{HW}}\Big] : \boldsymbol{\Pi} \\ + \Big[\boldsymbol{\mathcal{P}}_{\mathrm{sc}}(\boldsymbol{F}^{\mathrm{HW}}, \boldsymbol{F}_\gamma, \boldsymbol{F}_{\mathrm{p}}) - \boldsymbol{P}_{\mathrm{sc}}^{\mathrm{HW}}\Big] : \boldsymbol{\Lambda} \} = 0. \end{aligned} \tag{6.71}$$

After performing the interpolation of all the fields introduced so far, the algebraic form of (6.71) consists of a block system, in which one block corresponds to the balance of momentum, one block is associated with (6.69a), and one with (6.69b).

6.7 Results

To weigh the effects of the non-local theory of remodelling on the benchmark problem presented in Section 6.5.2, we perform two different simulations: one is done by excluding micro-plasticity, and is thus said to be "standard"; the other one, instead, accounts for micro-plasticity, and refers to the "non-standard" model.

The standard model (ST) is obtained by setting A_ν, B_ν, and Z_ν equal to zero, so that Equation (6.60h) is always satisfied and the evolution law for $\varepsilon_{\rm p}$ only takes into account the first term of the right-hand-side of (6.60f), with $\mathbf{\Sigma}_\nu \equiv \mathbf{\Sigma}_\nu^{(\rm st)}$. In the non-standard model (NST), the parameters A_ν, B_ν, and Z_ν are different from zero (see Table 6.2), and the full system of equations (6.60a)–(6.60h) has to be solved.

Since, to the best of our knowledge, no measurements for A_ν, B_ν, and Z_ν are available in the scientific literature on soft tissues, we have chosen such parameters after several trials. For this reason, the values used to obtain Figures 6.4–6.3 may be unrealistic for describing a true biological situation. Moreover, we remark that the convergence of the system (6.60a)–(6.60h) was achieved only for $Z_\nu \leq 1$ and $A_\nu > B_\nu$, whereas our computations never converged for $Z_\nu > 1$, regardless of the tested values of A_ν and B_ν. We also emphasise that, for the cases in which the model converged, the results of the simulations featured no remarkable difference.

To report the results of our model, we display the numerical solutions of the displacement, the growth parameter, γ, the mass fraction of the proliferating cells, $\omega_{\rm p}$, the pressure, p, and the axial component of the effective Cauchy stress tensor, $\sigma_{\rm eff}^{zz}$. We plot all these quantities versus the axial coordinate of the specimen, and at the times $t = 10$ d and $t = 20$ d.

Figure 6.4 shows the displacement of the tumour (left panel) and the growth parameter, γ (right panel). Both quantities are computed only for the case of growth without "plasticity" (remodelling) (NP), i.e., for $\boldsymbol{F}_{\rm p} = \boldsymbol{I}$, $\varepsilon_{\rm p} = 0$, $\mathfrak{e}_{\rm p} = 0$, and for the case in which "plasticity" (remodelling) is active. Moreover, "plasticity" is accounted for as prescribed by the non-standard model (NST). In fact, we could have also used the standard one (ST), but it would have led to imperceptible differences with respect to the non-standard model. As expected, both the displacement and the growth parameter increase as time goes by, but we observe a drastic reduction of their spatiotemporal evolution when remodelling is active. The results presented in Figure 6.4 confirm the ones obtained by Mascheroni et al. [166] and Di Stefano et al. [62], and have been re-computed with the purpose of highlighting the important role that remodelling may play on growth.

To further investigate the possible role of remodelling on growth and, in particular, the switch from the standard to the non-standard approach, we study the evolution of $\omega_{\rm p}$ (Figure 6.2), p (Figure 6.5), and $\sigma_{\rm eff}^{zz}$ (Figure 6.3).

Figure 6.2 displays, in the left panel, the progression of the mass fraction of the proliferating cells, $\omega_{\rm p}$, and, in the right panel, the absolute value of the difference between $\omega_{\rm p}^{\rm ST}$ and $\omega_{\rm p}^{\rm NST}$, which denote the mass fractions of the proliferating cells computed with the standard model (ST) and the non-standard model (NST), respectively. In the left panel, we notice that, at time $t = 10$ d, the differences between $\omega_{\rm p}^{\rm ST}$ and $\omega_{\rm p}^{\rm NST}$ are irrelevant. However, at $t = 20$ d, a slight, yet appreciable, difference starts to appear. We visualise this difference in the right panel of Figure

6.2. Here, we notice that, due to the Dirichlet boundary condition imposed on ω_p at $Z = L/2$, such difference cannot be pronounced for values of the axial coordinate tending to $L/2$. On the other hand, $|\omega_\mathrm{p}^\mathrm{ST} - \omega_\mathrm{p}^\mathrm{NST}|$ becomes relatively more visible in the portion of the specimen in which growth is inhibited (see Figure 6.4(right)). This is due to a limited availability of nutrients (data not shown).

In the left panel of Figure 6.5, we show the pressure, p, both for the ST model and for the NST one. For both models, the same behaviour is attained, i.e., the pressure drops from the tumour boundary towards its centre, where it takes negative values. In the right panel of Figure 6.5, we report the absolute value of the difference, at time $t = 20$ d, between p^ST and p^NST, i.e., the pressures computed with the ST model and the NST model, respectively. The differences between p^ST and p^NST are relatively small, but visible, in almost all of the half domain and at both times. They are clearly zero at the Dirichlet boundary $Z = L/2$ and, at $t = 20$ d, the maximum of $|p^\mathrm{ST} - p^\mathrm{NST}|$ is reached at a point between 0.4 cm and 0.5 cm.

Parameter	Unit	Value	Equation	Reference
L	[cm]	1.000	—	[62]
R_b	[cm]	$1.000 \cdot 10^{-2}$	—	[62]
$k_{0\mathrm{R}}$	[mm^4/(N s)]	0.4875	(6.62a)	[138]
m_0	[−]	0.0848	(6.62a)	[138]
m_1	[−]	4.6380	(6.62a)	[138]
$d_{0\mathrm{R}}$	[m^2/s]	$3.200 \cdot 10^{-9}$	(6.62b)	[216]
σ_th	[Pa]	$1.000 \cdot 10^{-7}$	(6.53)	[112]
λ_p	[m s/kg]	$7.000 \cdot 10^{-7}$	(6.54)	[112]
λ	[Pa]	$1.333 \cdot 10^4$	(6.42)	[220]
μ	[Pa]	$1.999 \cdot 10^4$	(6.42)	[220]
ω_Ncr	[−]	$1.000 \cdot 10^{-3}$	(6.63a)	[62]
ω_Nenv	[−]	$7.000 \cdot 10^{-3}$	(6.63b)	[62]
ω_N0	[−]	$1.480 \cdot 10^{-4}$	(6.63e)	[62]

Table 6.1: Numerical values of the parameters used both for the standard and for the non-standard model.

Moreover, in Figure 6.3, the axial component of the constitutive part of the Cauchy stress tensor, σ_sc^{zz}, is shown. Indeed, due to the imposed boundary conditions and the symmetry restrictions of the considered problem, the balance of momentum (6.60a) amounts to requiring $-p+\sigma_\mathrm{sc}^{zz} = 0$ everywhere in the specimen. Hence, it holds that $\sigma_\mathrm{sc}^{zz} = p$. In addition, the axial component of the stress used to model the mechanotransduction, σ_eff^{zz}, is different from σ_sc^{zz}, as it features $\partial \mathfrak{e}_\mathrm{p}/\partial Z$

(see Equation (6.65)). However, since this derivative is very small, it occurs that $\sigma_{\mathrm{eff}}^{zz}$ can be safely approximated with $\sigma_{\mathrm{sc}}^{zz}$ and, thus, with p. The above discussion answers the research question 6.1.

A last comment concerns the evolution of $\mathfrak{e}_{\mathrm{p}}$ and ε_{p}. As reported in Figure 6.6, both ε_{p} and $\mathfrak{e}_{\mathrm{p}}$ are increasing functions of time and space. If we focus on ε_{p}, we note that, as time goes by, the remodelling strains augment and accumulate in a neighbourhood of the boundaries of the specimen. This is highlighted by the fact that the slope of the curves corresponding to ε_{p} tends to raise when it approaches the edge. However, as predicted by the theory, $\mathfrak{e}_{\mathrm{p}}$ plays a smoothing role on the remodelling distortions and, in fact, it distributes itself more uniformly along the specimen. A relevant aspect of this result is that, while the curves corresponding to ε_{p} at $t = 10$ d and $t = 20$ d are almost coincident at the centre of the specimen, the curves determining $\mathfrak{e}_{\mathrm{p}}$ are distinguishable from one another. The above discussion answers the research question 6.2.

6.8 Conclusions

In this work, we study an idealised biological tissue that grows and remodels. As tissue we consider a tumour in avascular stage, and we assume that its remodelling —or structural reorganisation— occurs through a two-scale plasticity-like phenomenon. Following [15], we distinguish a coarse and a fine scale, and we resolve this phenomenon, at the coarse scale, by means of the accumulated remodelling strain, ε_{p}, and, at the fine scale, by means of $\mathfrak{e}_{\mathrm{p}}$. The latter is the representative of the so-called *micro-"plasticity"* and, being related to ε_{p} through a Helmholtz-like equation, it makes ε_{p} non-local [15]. Within this framework, we have set ourselves the scope of evaluating if, how, and to what extent the micro-"plasticity" influences the growth of the tumour. In our approach, such influence can occur both directly and indirectly. The direct way is due to the fact that the *effective* Cauchy stress, $\boldsymbol{\sigma}_{\mathrm{eff}}$, modulates the source of mass R_{fp}, and thus also R_{s}, by giving rise to mechanotransduction. The indirect way, instead, manifests itself through the slight, and to a certain extent visible, changes that the non-local plastic-like distortions induce in some of the physical quantities that characterise the growth of the tumour, as reported in Section 6.7.

It is important to emphasise that the results shown in this work (see Figures 6.4–6.3) are obtained for numerical values of the "non-standard" parameters A_ν, B_ν, and Z_ν (see Table 6.2), which could be far beyond the physical range. Therefore, for the time being, our results aim at being a qualitative contribution to a unified strain-gradient theory of growth and remodelling. However, they are quantitative in evaluating the impact of the considered theory on growth.

We remark that, following an idea put forward by Epstein [66], Di Stefano et al. [62] proposed a model of strain-gradient growth, in which the evolution of γ is governed by a generalised diffusion-reaction equation. Such equation was obtained by accounting for the growth-induced scalar curvature, κ_γ[4], which features the spatial derivatives of γ up to the second order. However, in that model we considered no remodelling. In the present work, instead, we have neglected the role of κ_γ, but we have focussed our attention on strain-gradient remodelling in order to quantify its effect on growth. The role of κ_γ in the current framework can be recovered by simply re-activating $r_{\mathrm{p}\gamma}$ and $r_{\mathrm{n}\gamma}$ in (5.9a) and (5.9b) (see Di Stefano et al. [62] for the definition of these terms as functions of κ_γ).

Apart from the obvious fact that the topics under study necessitate further investigations from our side, two comments are in order: firstly, we have not hypothesised a strain-softening behaviour of the considered material, and no formation of shear bands can be observed that justifies from the outset the use of a strain-gradient regularisation; secondly, the benchmark problem adopted in this work might be inappropriate, since it does not produce the desired/expected localisation of the accumulated plastic strain, ε_p, which calls for the employment of a strain-gradient theory. Nevertheless, our model is able to capture the regularising effect that the microscale descriptor $\mathfrak{e}_\mathrm{p}$ has on the accumulated remodelling distortions (cf. Figure 6.6).

It is known that the internal structural changes occurring in heterogeneous materials influence their overall macroscopic behaviour. For example, in bones, the change of orientation of the lamellae's collagen fibres modifies the bone's longitudinal effective Young's modulus [229, 205]. In the present work, we attempt to know how, and to what extent, the microscopic plastic-like (remodelling) effects are significant for the macroscopic evolution of the tissue. To the best of our knowledge, there are no experimental studies showing the influence of the microscopic plastic effects on the tissue behaviour. However, one can think of an experiment where, at some level, there can be a relatively strong localisation of the accumulated "plastic" strain, $\mathfrak{e}_\mathrm{p}$, because of the presence of constraints (e.g. contact of the tissue with much stiffer materials). In this respect, we hope that our work contributes to understand the interactions between growth and remodelling by merging the theories of multiphasic materials and of strain-gradient plasticity.

To the best of our understanding, another important difference between our work and previous publications (see e.g. [50, 48, 47]) resides in the definition of the internal and external mechanical powers. Indeed, looking for instance at [48], these powers feature only the generalised velocities associated with the "classical" degrees of freedom of a body[5], while the time derivatives of the tensors associated with the

[4]The growth distortions, $\boldsymbol{F}_\gamma = \gamma \boldsymbol{I}$, induce the Riemannian metric tensor $\boldsymbol{C}_\gamma = \gamma^2 \boldsymbol{G}$, which yields Christoffel symbols that allow to determine a Levi-Civita connection with nontrivial fourth-order curvature tensor [165, 106] and, thus, with nontrivial associated Ricci curvature tensor, $\mathfrak{R}_\gamma$. Hence, it is possible to define the scalar curvature as $\kappa_\gamma := \mathfrak{R}_\gamma : \boldsymbol{C}_\gamma^{-1}$ (see [62] for details).

[5]These are the body velocity, $\boldsymbol{V}$, the time derivative of the deformation gradient tensor, $\dot{\boldsymbol{F}}$,

body's structural changes appear in the study of the dissipation inequality through the derivative of the body's Helmholtz free energy density. In our case, instead, following a philosophy outlined in other papers [122, 44, 60, 123, 15], we introduce the structural kinematic descriptors both constitutively, i.e., as arguments of the solid phase Helmholtz free energy density, and in the formulation of the overall virtual powers of the problem, that is, jointly with the "classical" ones.

In our work, the tensor $\tilde{\boldsymbol{\Sigma}}_\nu$ is entirely determined by mechanical quantities (cf. Equation (6.33a)) and this property is inherited by its associated direction tensor, $\boldsymbol{N}_\nu = \tilde{\boldsymbol{\Sigma}}_\nu / \|\tilde{\boldsymbol{\Sigma}}_\nu\|_{\boldsymbol{\eta}}$. Consequently, the hypothesis of co-directionality of $\tilde{\boldsymbol{D}}_{\mathrm{p}}$ and $\tilde{\boldsymbol{\Sigma}}_\nu$ implies that the direction of the plastic flow is exclusively dictated by mechanical stress, the latter being augmented by the non-standard contribution $\tilde{\boldsymbol{\Sigma}}_\nu^{(\text{n-st})}$. However, in more general situations, it is possible to define generalised Mandel stress tensors featuring bio-chemical contributions, i.e., depending explicitly on the mass fraction of the nutrients (and on its gradient). In such cases, tensor $\boldsymbol{N}_\nu$ defines the direction of the plastic flow on the basis of chemo-mechanical guidance.

A last comment is on the design of an adequate benchmark problem. Indeed, when Anand et al. [15] developed their theory, they wrote that $\mathfrak{e}_{\mathrm{p}}$ *"is introduced for the purpose of regularisation of numerical simulations of shear band formation under strain softening conditions"*. To achieve this objective, they called for the concept of micro-scale plasticity, and admitted a physics described by ε_{p}, $\mathfrak{e}_{\mathrm{p}}$, and $\mathrm{Grad}\mathfrak{e}_{\mathrm{p}}$. Then, in order to determine these quantities, they established a thermodynamically consistent framework, rather than simply improving the equations that were problematic from the numerical point of view. In our work, we have extended such thermodynamic set-up to a growth problem, by admitting that its physical meaning goes beyond the necessity of solving numerical issues. Nevertheless, we have seen only a very marginal impact of this modelling choice on our results and we argue that it is of fundamental importance to design benchmark problems capable of capturing the physics behind it. This is part of our ongoing research.

We summarise the answers to the research questions 6.1—6.3 in the following way:

- The result obtained from the numerical simulations of the model presented in this chapter do not show significant differences with the results obtained by numerically simulating the "standard" model. With "standard model" we refer to the one in which the contributions associated with the strain gradient formulation are neglected.

- We note that, as time goes by, the accumulated remodelling strain ε_{p} increases as it approaches the boundary of the specimen, with a rapidly raising of its slope. However, as predicted by the theoretical framework outlined in this

and the time derivative of the second gradient of the deformation, i.e., $\overline{\mathrm{Grad}\boldsymbol{F}}^{\boldsymbol{\cdot}}$ [48].

chapter, the micro-scale plasticity parameter $\mathfrak{e}_{\mathrm{p}}$ guarantees a smoothing of the remodelling distortions and, in fact, it distributes itself more uniformly along the specimen.

- To properly clarify the type of remodelling studied in this chapter, we consider, as an example, the inelastic rearrangement of a multicellular spheroid, following an experiment discussed in [86].

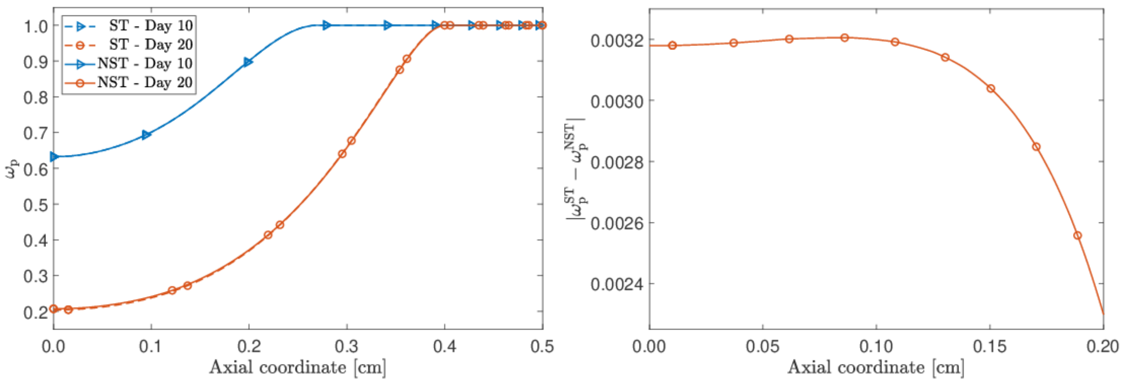

Figure 6.2: *Left panel*: spatial profile of the mass fraction of the proliferating cells, ω_{p}. Since the problem is symmetric, only the half $[0, L/2]$ of the domain is shown. *Right panel*: spatial profile of the absolute value of the difference between $\omega_{\mathrm{p}}^{\mathrm{ST}}$ and $\omega_{\mathrm{p}}^{\mathrm{NST}}$, i.e., the mass fractions of the proliferating cells computed with the standard model (ST) and the non-standard model (NST), respectively. The picture refers to the portion of the half domain in which $|\omega_{\mathrm{p}}^{\mathrm{ST}} - \omega_{\mathrm{p}}^{\mathrm{NST}}|$ is greater than, approximatively, $2.25 \cdot 10^{-3}$, and is computed at time $t = 20$ day.

Parameter	Unit	Value	Equation	Reference
δ_1	[−]	$7.138 \cdot 10^{-1}$	(6.63b)	[167]
δ_2	[Pa]	$1.541 \cdot 10^{3}$	(6.63b)	[167]
ζ_{pn}	[kg/(m^3 s)]	$1.500 \cdot 10^{-3}$	(6.63a)	[45]
ζ_{fp}	[kg/(m^3 s)]	$1.343 \cdot 10^{-3}$	(6.63b)	[45]
ζ_{nf}	[kg/(m^3 s)]	$1.150 \cdot 10^{-5}$	(6.63d)	[45]
ζ_{Np}	[kg/(m^3 s)]	$3.000 \cdot 10^{-4}$	(6.63e)	[41]
A_ν	[Pa]	$1.0 \cdot 10^{-9}$	(6.33c)	
B_ν	[Pa m^2]	$1.0 \cdot 10^{-14}$	(6.33d)	
Z_ν	[Pa]	$1.0 \cdot 10^{-2}$	(6.60f)	

Table 6.2: Numerical values of the parameters used both for the standard and for the non-standard model.

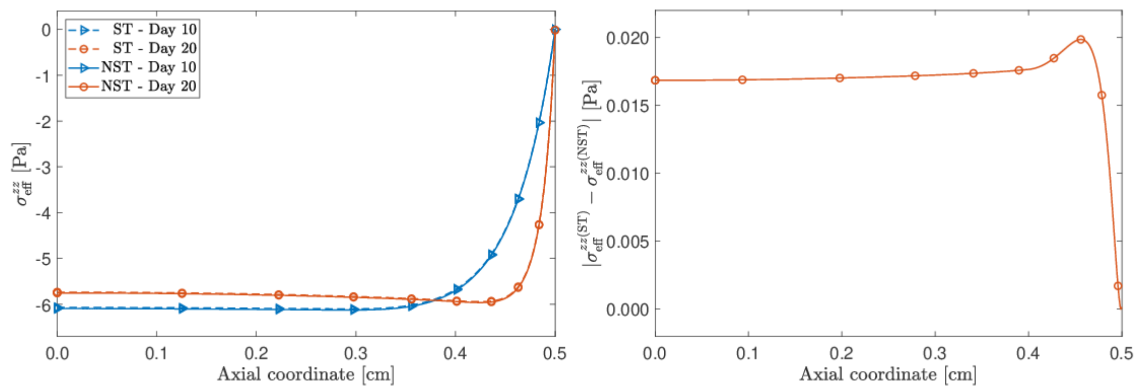

Figure 6.3: *Left panel*: spatial profile of the axial component of the effective Cauchy stress tensor, $\sigma_{\mathrm{eff}}^{zz}$. *Right panel*: spatial profile of the absolute value of the difference between $\sigma_{\mathrm{eff}}^{zz(\mathrm{ST})}$ and $\sigma_{\mathrm{eff}}^{zz(\mathrm{NST})}$, which denote the stress computed with the standard model (ST) and the non-standard model (NST), respectively. The picture is computed at time $t = 20$ day. Since the problem is symmetric, in both panels only the half $[0, L/2]$ of the domain is shown.

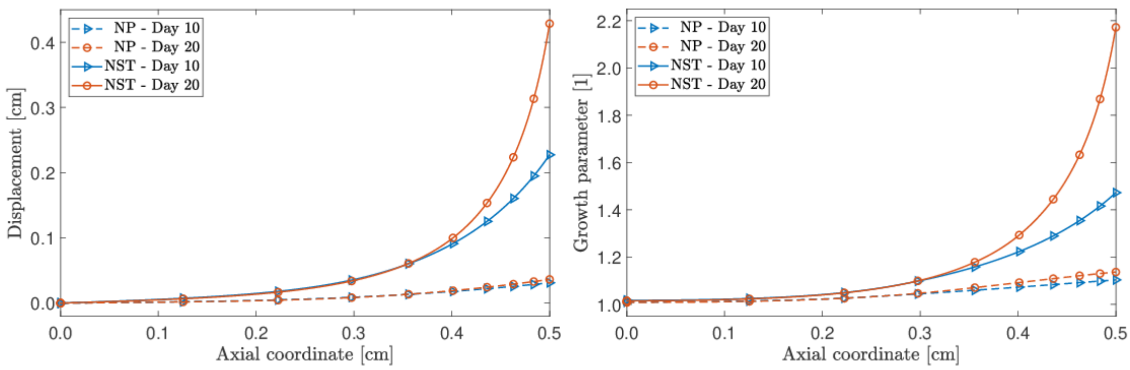

Figure 6.4: *Left panel*: spatial profile of the displacement. *Right panel*: spatial profile of the growth parameter, γ. Since the problem is symmetric, in both panels only the half $[0, L/2]$ of the domain is shown.

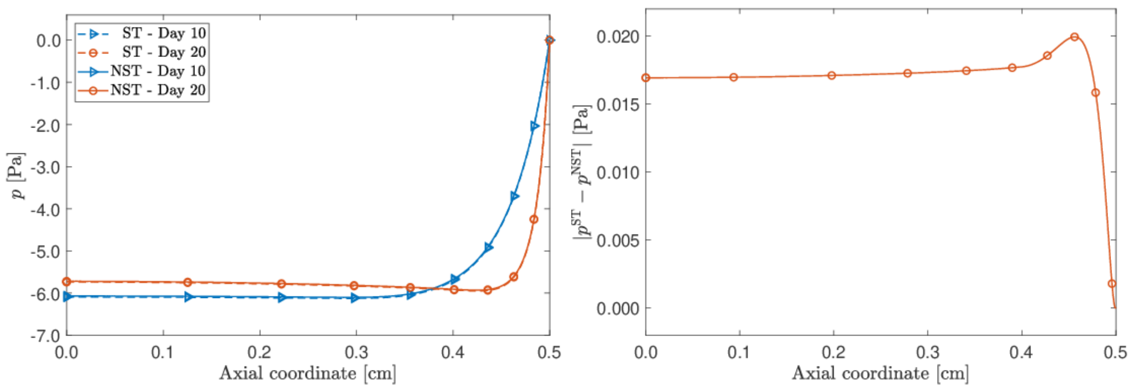

Figure 6.5: *Left panel*: spatial profile of the pressure, p. *Right panel*: spatial profile of the absolute value of the difference between p^{ST} and p^{NST}, which denote the pressure computed with the standard model (ST) and the pressure computed with the non-standard model (NST). The picture is computed at time $t = 20$ day. Since the problem is symmetric, in both panels only the half $[0, L/2]$ of the domain is shown.

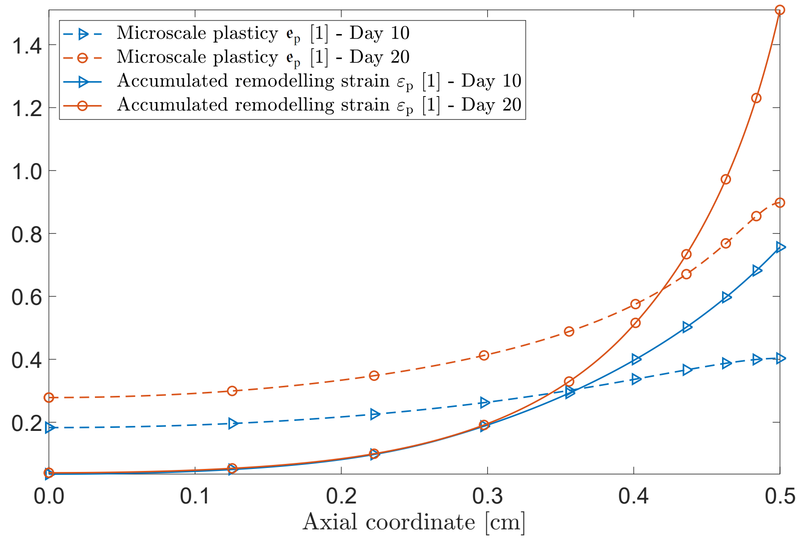

Figure 6.6: Spatial profiles of the accumulated remodelling strain ε_{p} and of the microscale plasticity $\mathfrak{e}_{\mathrm{p}}$. Since the problem is symmetric, only the half $[0, L/2]$ of the domain is shown.

Chapter 7

Growth and remodelling in the light of of Noether's Theorem

The work reported in this chapter has been previously published in [113].

7.1 *Internal time* in growth mechanics

Starting from the observation that the growth of a body breaks the time translation symmetry of the body's dynamics, we determine a scalar field, called *internal time*, that defines an indicator of the intrinsic time scale of the growth-related body's structural evolution. By recasting the theory of growth for monophasic media within a variational framework, we obtain the internal time as the solution of a partial differential equation descending from Noether's Theorem. We do this by considering two approaches, one formulated in terms of internal variables and one adopting the concept of augmented kinematics.

The mechanics of volumetric growth studies the variation of mass and the concomitant structural evolution of biological tissues [210, 222, 72]. Such processes are often conceived as anelastic, and are described by a generally non-integrable tensor field, $\boldsymbol{F}_\gamma$, referred to as *growth tensor*.

The role of $\boldsymbol{F}_\gamma$ in the modelling of growth is not unique, and its interpretation depends on the theory within which it is introduced. To the best of our knowledge, there exist at least two ways of interpreting $\boldsymbol{F}_\gamma$: it can be viewed either as an *internal* variable (see e.g. [72]) or as a *kinematic* variable (see e.g. [60]). The conceptual difference between these two approaches affects all the relations governing the dynamics of a body, especially the one representing the evolution of its internal structure.

The way in which the dissipation is studied in [72] and [60] plays a major role in this work. In the sequel, indeed, we employ the dissipation inequality to show that a growing body possesses an intrinsic time scale, defined by the chosen theory. To this end, we take inspiration from Vakulenko's concept of *"endochronic thermodynamics"* [227, 176], and we demonstrate that the body's intrinsic time scale is related to a generalised force, hereafter denoted by $\mathcal{F}_0$ and termed *time-like inhomogeneity force* [168]. In our framework, $\mathcal{F}_0$ plays a role similar to that played by the material inhomogeneity forces in Eshelby's theory of inclusions [74] and, more generally, in the mechanics of materials with inhomogeneities [168], as is the case of growing media [72].

Vakulenko's theory addresses the thermodynamics of anelastic processes [227, 176], and is said to be *"endochronic"* since it associates a given anelastic process with a scalar-valued function, the *"thermodynamic time"*, defined from the outset as the time integral of a suitable function of the entropy production [176].

Quite differently, in our work we identify the *internal time* of growth of a body, hereafter denoted by τ, with the solution of the partial differential equation [117]

$$\mathcal{N}_0(\tau) := \mathcal{H}\,\dot{\tau} - (\boldsymbol{P}^{\mathrm{T}}\boldsymbol{v})\,\mathrm{Grad}\,\tau - \mathcal{F}_0\,\tau = 0, \tag{7.1}$$

where $\mathcal{H}$ is the body's total energy density, $\boldsymbol{P}$ is the first Piola-Kirchhoff stress tensor and $\boldsymbol{v}$ is the Lagrangian velocity field.

Equation (7.1) was deduced in [117] as a consequence of Noether's Theorem, and τ was defined as a deformation of time depending on material points and on time itself. More specifically, τ was introduced to highlight how the occurrence of growth in a body is a symmetry breaking, spoiling the invariance of the body's dynamics under time translations and yielding the failure of the conservation of energy [117]. This symmetry breaking results in the arising of $\mathcal{F}_0$ and manifests itself as the loss of the homogeneity of time.

In this work, we deeply reformulate the mathematical framework of [117] and, after polishing it from some formal imprecisions, we propose the following novelties: (a) we retrieve Equation (7.1) within the two different pictures of growth given in [72] and [60], respectively; (b) for both pictures, we compute *explicitly* the internal time, τ, and we show that the quantity $\tau_{\mathrm{c}} := 1 - \tau/\tau_0$, where τ_0 is a reference value, is analogous to endochronic time in that it increases monotonically in time and may thus represent an intrinsic time-scale associated with growth; (c) within the formulation presented in [60], we describe mechanotransduction through the conceptually systematic approach of Theoretical Mechanics. Our results also apply to remodelling.

7.2 Growth in monophasic continua

We consider the simplest possible formulation of the volumetric growth of a body. In particular, we assume the body to be hyperelastic and we employ the Bilby-Kröner-Lee decomposition of the deformation gradient tensor, i.e., $\boldsymbol{F} = \boldsymbol{\Phi}\boldsymbol{F}_{\gamma}$, so that the body's material response is described by the strain energy density function

$$\Psi(X,t) = \hat{\Psi}(\boldsymbol{F}(X,t), \boldsymbol{F}_\gamma(X,t)) = J_\gamma \hat{\Psi}_\nu(\boldsymbol{\Phi}(X,t)), \tag{7.2}$$

where $\boldsymbol{\Phi} := \boldsymbol{F}\boldsymbol{F}_\gamma^{-1}$ is the elastic part of the deformation gradient tensor, $\hat{\Psi}_\nu$ is the strain energy density expressed per unit volume of the body in its stress-free state, and $J_\gamma := \det \boldsymbol{F}_\gamma > 0$.

In local form, and with respect to the body's reference configuration, $\mathscr{B}$, the mass balance law is given by $\dot{\varrho}_\mathrm{R} = \Pi$, where ϱ_R is the mass density of the body per unit volume of $\mathscr{B}$, the superimposed dot denotes partial differentiation with respect to time, and Π is the source or sink of mass that describes growth. As in [72, 7], we write $\varrho_\mathrm{R} = J_\gamma \varrho_\nu$, where ϱ_ν is the mass density of the body in its stress-free state, and we require the conditions

$$\frac{\dot{J}_\gamma}{J_\gamma} = \mathrm{tr}(\boldsymbol{F}_\gamma^{-1}\dot{\boldsymbol{F}}_\gamma) = \tfrac{1}{2}\mathrm{tr}(\dot{\boldsymbol{C}}_\gamma \boldsymbol{C}_\gamma^{-1}) = \frac{\Pi}{J_\gamma \varrho_\nu} =: \Gamma, \tag{7.3}$$

where $\boldsymbol{C}_\gamma := \boldsymbol{F}_\gamma^\mathrm{T}.\boldsymbol{F}_\gamma$ is the metric tensor induced by $\boldsymbol{F}_\gamma$, Γ measures the relative variation of ϱ_R, and ϱ_ν is regarded as a time independent field specified from the outset.

Within the quasi-static limit, and neglecting all inertial and long-range body forces, such as gravity, the local form of the momentum balance law reads

$$\mathrm{Div}\, \boldsymbol{P} = \boldsymbol{0}, \tag{7.4a}$$

$$\boldsymbol{P} = \frac{\partial \hat{\Psi}}{\partial \boldsymbol{F}} \circ (\boldsymbol{F}, \boldsymbol{F}_\gamma) = J_\gamma \left[\frac{\partial \hat{\Psi}_\nu}{\partial \boldsymbol{\Phi}} \circ \boldsymbol{\Phi} \right] \boldsymbol{F}_\gamma^{-\mathrm{T}}, \tag{7.4b}$$

where Div is the material divergence operator and $\boldsymbol{P}$ is the first Piola-Kirchhoff stress tensor. The balance law (7.4a) should be regarded as an equation for the motion of the body, χ, whose partial derivatives define the components of $\boldsymbol{F}$. To determine $\boldsymbol{F}_\gamma$, an additional, independent equation is needed.

7.2.1 Tensor $\boldsymbol{F}_\gamma$ viewed as internal variable

The tensor field $\boldsymbol{F}_\gamma$ shares several formal analogies with the inverse of the tensor field referred to as *"uniformity mapping"* in [72]. Hence, if $\boldsymbol{F}_\gamma$ is regarded as an internal variable, the theory exposed in [72] can be employed to develop a criterion for determining an admissible evolution law for $\boldsymbol{F}_\gamma$. In particular, by invoking the representation theorem for tensor-valued functions [155], it can be shown that, in the case of isotropy, $\boldsymbol{F}_\gamma$ satisfies

$$\mathrm{sym}[\boldsymbol{C}_\gamma \boldsymbol{\mathfrak{L}}_\gamma] = \sum_{n=0}^{2} (J_\gamma)^{-n} \beta_n \boldsymbol{\mathfrak{E}}^n \boldsymbol{C}_\gamma, \tag{7.5}$$

where $\mathfrak{L}_\gamma := \boldsymbol{F}_\gamma^{-1}\dot{\boldsymbol{F}}_\gamma$, $\mathfrak{E}$ is Eshelby's stress tensor,

$$\mathfrak{E} := \Psi \boldsymbol{I}^{\mathrm{T}} - \boldsymbol{F}^{\mathrm{T}}\boldsymbol{P} \equiv \boldsymbol{F}_\gamma^{\mathrm{T}} \left(\frac{\partial \hat{\Psi}}{\partial \boldsymbol{F}_\gamma} \circ (\boldsymbol{F}, \boldsymbol{F}_\gamma) \right), \tag{7.6}$$

and $\{\beta_n\}_{n=0}^2$ are to be expressed constitutively through functions of J_γ, Ψ, the three principal invariants of $\mathfrak{E}$, and other quantities, possibly required by phenomenology.

In Equation (7.5), the convention $\mathfrak{E}^0 = \boldsymbol{I}^{\mathrm{T}}$ is used, where $\boldsymbol{I}^{\mathrm{T}}$ is the transpose of the material identity tensor, $\boldsymbol{I}$. Moreover, because of isotropy, $\mathfrak{E}\boldsymbol{C}_\gamma$ is symmetric, and so is also $\mathfrak{E}^2\boldsymbol{C}_\gamma = \mathfrak{E}\boldsymbol{C}_\gamma\mathfrak{E}^{\mathrm{T}}$ [169]. Finally, the functions $\{\beta_n\}_{n=0}^2$ have to comply with the dissipation inequality

$$\mathcal{D}_{\mathrm{IV}} = \Psi \,\mathrm{tr}(\mathfrak{L}_\gamma) - \mathfrak{E} : \mathfrak{L}_\gamma + \mathcal{D}_{\mathrm{nc}} \geq 0. \tag{7.7}$$

Here, $\mathcal{D}_{\mathrm{nc}}$ is said to be the *"non-compliant"* contribution to the dissipation [106] and is attributed to processes accompanying growth but not explicitly accounted for in the model. Moreover, the subscript "IV" in $\mathcal{D}_{\mathrm{IV}}$ stands for "internal variable" to remark that in Equation (7.7) $\boldsymbol{F}_\gamma$ is viewed as an internal variable.

In order to model the material inhomogeneities associated with growth, Epstein and Maugin [72] introduce a Lagrangian density function, $\mathcal{L}$, whose constitutive representation depends on material points and time through $\boldsymbol{F}_\gamma$. Hence, within the quasi-static limit, in which the identification $\mathcal{L} = -\Psi$ applies, and by mimicking the theory of material uniformity [72], we can write

$$\mathcal{L} = \check{\mathcal{L}} \circ (\boldsymbol{F}, \mathcal{X}, \mathcal{T}) = \hat{\mathcal{L}} \circ (\boldsymbol{F}, \boldsymbol{F}_\gamma) = -\hat{\Psi} \circ (\boldsymbol{F}, \boldsymbol{F}_\gamma), \tag{7.8}$$

where $\mathcal{X} : \mathscr{B} \times \mathbb{R} \to \mathscr{B}$ and $\mathcal{T} : \mathscr{B} \times \mathbb{R} \to \mathbb{R}$ are auxiliary functions defined by $\mathcal{X}(X, t) = X$ and $\mathcal{T}(X, t) = t$, and introduced to account for the explicit dependence of $\check{\mathcal{L}}$ on material points and time [78], i.e.,

$$\mathcal{L}(X, t) = \check{\mathcal{L}}(\boldsymbol{F}(X, t), X, t) = -\hat{\Psi}(\boldsymbol{F}(X, t), \boldsymbol{F}_\gamma(X, t)). \tag{7.9}$$

Equations (7.8) and (7.9) permit to determine the *time-like inhomogeneity force*, $\mathcal{F}_0$ (see also [3], where it is referred to as *"energy release rate"*), which, recalling the definition $\mathfrak{L}_\gamma := \boldsymbol{F}_\gamma^{-1}\dot{\boldsymbol{F}}_\gamma$, reads

$$\begin{aligned} \mathcal{F}_0 := & \frac{\partial \check{\mathcal{L}}}{\partial \mathcal{T}} \circ (\boldsymbol{F}, \mathcal{X}, \mathcal{T}) = -\left(\frac{\partial \hat{\Psi}}{\partial \boldsymbol{F}_\gamma} \circ (\boldsymbol{F}, \boldsymbol{F}_\gamma) \right) : \dot{\boldsymbol{F}}_\gamma \\ = & - \mathfrak{E} : \mathfrak{L}_\gamma = \mathcal{D}_{\mathrm{IV}} - \mathcal{D}_{\mathrm{nc}} - \Psi \,\mathrm{tr}(\mathfrak{L}_\gamma). \end{aligned} \tag{7.10}$$

Thus, τ is determined by Equation (7.1) with $\mathcal{H} = \Psi$.

7.2.2 Tensor $\boldsymbol{F}_\gamma$ viewed as kinematic variable

A different approach to the mechanics of growth is provided in [60], where the structural transformation of a body corresponds to the activation of *structural degrees of freedom* describing the body's internal kinematics. From this perspective, $\boldsymbol{F}_\gamma$ and $\dot{\boldsymbol{F}}_\gamma$ acquire the meaning of tensor-valued kinematic descriptors that, together with χ, $\boldsymbol{v} = \dot{\chi}$ and $\operatorname{Grad}\boldsymbol{v} = \dot{\boldsymbol{F}}$, define the overall kinematics of the body.

Restricting our considerations to a material of first grade in χ and zeroth grade in $\boldsymbol{F}_\gamma$ [60], it is natural to define the body's configuration manifold as a suitable set of pairs $(\chi, \boldsymbol{F}_\gamma)$ describing the overall evolution of the body. Accordingly, the bundle of the body's virtual velocities is given by the set of triples $(\boldsymbol{\mathfrak{v}}, \operatorname{Grad}\boldsymbol{\mathfrak{v}}, \boldsymbol{Z})$ that represent all the admissible realisations of the generalised velocities associated with the "standard" motion, i.e., $\boldsymbol{\mathfrak{v}}$ and $\operatorname{Grad}\boldsymbol{\mathfrak{v}}$, and with the structural evolution, $\boldsymbol{Z}$, respectively.

By duality, it is natural to introduce the generalised forces expending virtual power on $\boldsymbol{\mathfrak{v}}$, $\operatorname{Grad}\boldsymbol{\mathfrak{v}}$, and $\boldsymbol{Z}$. Hence, the Principle of Virtual Powers, specialised here to the case of no external forces dual to $\boldsymbol{\mathfrak{v}}$ (i.e., neither inertial nor body forces), reads

$$\int_{\mathscr{B}} \{\boldsymbol{P} : \operatorname{Grad}\boldsymbol{\mathfrak{v}} + \boldsymbol{F}_\gamma^{-\mathrm{T}}\boldsymbol{Y}_{\mathrm{i}} : \boldsymbol{Z}\} = \int_{\mathscr{B}} \boldsymbol{F}_\gamma^{-\mathrm{T}}\boldsymbol{Y}_{\mathrm{e}} : \boldsymbol{Z}, \tag{7.11}$$

where $\boldsymbol{Y}_{\mathrm{i}}$ and $\boldsymbol{Y}_{\mathrm{e}}$ are an internal and an external generalised force dual to $\boldsymbol{F}_\gamma^{-1}\boldsymbol{Z}$, respectively, and $\boldsymbol{Z}$ is the virtual counterpart of $\dot{\boldsymbol{F}}_\gamma$. The strong form of (7.11) consists of the force balances

$$\operatorname{Div}\boldsymbol{P} = \boldsymbol{0}, \tag{7.12a}$$

$$\boldsymbol{Y}_{\mathrm{i}} = \boldsymbol{Y}_{\mathrm{e}}. \tag{7.12b}$$

To close the model, we prescribe $\boldsymbol{Y}_{\mathrm{i}}$ constitutively, in compliance with the dissipation inequality

$$\mathcal{D}_{\mathrm{KV}} = -\boldsymbol{\mathfrak{E}} : \boldsymbol{\mathfrak{L}}_\gamma + \boldsymbol{Y}_{\mathrm{i}} : \boldsymbol{\mathfrak{L}}_\gamma = \boldsymbol{Y}_{\mathrm{id}} : \boldsymbol{\mathfrak{L}}_\gamma \geq 0, \tag{7.13}$$

where $\boldsymbol{Y}_{\mathrm{id}} := \boldsymbol{Y}_{\mathrm{i}} - \boldsymbol{\mathfrak{E}}$ is said to be the *dissipative part* of $\boldsymbol{Y}_{\mathrm{i}}$ [44, 60] and the subscript "KV" reminds that Equation (7.13) is obtained by regarding $\boldsymbol{F}_\gamma$ as a kinematic variable.

In the sequel, we admit that $\boldsymbol{Y}_{\mathrm{id}}$ depends constitutively on $\boldsymbol{F}$, $\boldsymbol{F}_\gamma$ and $\dot{\boldsymbol{F}}_\gamma$, and, because of isotropy, we express such dependence as a function $\bar{\boldsymbol{Y}}_{\mathrm{id}}$ of $\boldsymbol{F}$, $\boldsymbol{C}_\gamma$ and $\dot{\boldsymbol{C}}_\gamma$, i.e., $\boldsymbol{Y}_{\mathrm{id}} = \bar{\boldsymbol{Y}}_{\mathrm{id}} \circ (\boldsymbol{F}, \boldsymbol{C}_\gamma, \dot{\boldsymbol{C}}_\gamma)$. Thus, we rewrite (7.12b) as

$$\boldsymbol{Y}_{\mathrm{e}} - \bar{\boldsymbol{Y}}_{\mathrm{id}} \circ (\boldsymbol{F}, \boldsymbol{C}_\gamma, \dot{\boldsymbol{C}}_\gamma) = \boldsymbol{\mathfrak{E}}, \tag{7.14}$$

thereby obtaining the equation of "motion" for $\boldsymbol{F}_\gamma$. To supply an explicit expression for $\bar{\boldsymbol{Y}}_{\mathrm{id}}$, we rewrite it as a function of $\boldsymbol{\mathfrak{L}}_\gamma$, i.e., $\bar{\boldsymbol{Y}}_{\mathrm{id}} \circ (\boldsymbol{F}, \boldsymbol{C}_\gamma, \dot{\boldsymbol{C}}_\gamma) = \check{\boldsymbol{Y}}_{\mathrm{id}} \circ (\boldsymbol{F}, \boldsymbol{F}_\gamma, \boldsymbol{\mathfrak{L}}_\gamma)$, and we notice that, because of isotropy, the tensor $\boldsymbol{Y}_{\mathrm{e}} - \boldsymbol{Y}_{\mathrm{id}}$ in Equation (7.14) must have the same symmetry property as $\boldsymbol{\mathfrak{E}}$, i.e., $\boldsymbol{C}_\gamma^{-1}(\boldsymbol{Y}_{\mathrm{e}} - \boldsymbol{Y}_{\mathrm{id}}) = (\boldsymbol{Y}_{\mathrm{e}}^{\mathrm{T}} - \boldsymbol{Y}_{\mathrm{id}}^{\mathrm{T}})\boldsymbol{C}_\gamma^{-1}$. Here, without much loss of generality, we hypothesise that such property holds, independently, both for $\boldsymbol{Y}_{\mathrm{id}}$ and for $\boldsymbol{Y}_{\mathrm{e}}$, and, by further assuming $\check{\boldsymbol{Y}}_{\mathrm{id}}$ to be linear in $\boldsymbol{\mathfrak{L}}_\gamma$, we prescribe (cf. e.g. [110, 178] and references therein)

$$\boldsymbol{C}_\gamma^{-1}[\check{\boldsymbol{Y}}_{\mathrm{id}} \circ (\boldsymbol{F}, \boldsymbol{F}_\gamma, \boldsymbol{\mathfrak{L}}_\gamma)] = \mathbb{D} : \mathrm{sym}(\boldsymbol{C}_\gamma \boldsymbol{\mathfrak{L}}_\gamma), \tag{7.15}$$

where $\mathbb{D}$ is a fourth-order tensor function given by

$$\mathbb{D} = 3J_\gamma d_{\mathrm{v}} \mathbb{K}^\sharp + 2J_\gamma d_{\mathrm{m}} \mathbb{M}^\sharp. \tag{7.16}$$

Here, d_{v} and d_{m} are scalar constitutive functions to be specified, $\mathbb{K}^\sharp$ and $\mathbb{M}^\sharp$ are defined as (analogous operators have been introduced in [77, 110])

$$\mathbb{K}^\sharp = \tfrac{1}{3}\boldsymbol{C}_\gamma^{-1} \otimes \boldsymbol{C}_\gamma^{-1}, \tag{7.17a}$$

$$\mathbb{M}^\sharp = \tfrac{1}{2}[\boldsymbol{C}_\gamma^{-1} \underline{\otimes} \boldsymbol{C}_\gamma^{-1} + \boldsymbol{C}_\gamma^{-1} \overline{\otimes} \boldsymbol{C}_\gamma^{-1}] - \mathbb{K}^\sharp, \tag{7.17b}$$

and the tensor products "$\underline{\otimes}$" and "$\overline{\otimes}$" are defined in [57]. By using the identity $\mathrm{sym}(\boldsymbol{C}_\gamma \boldsymbol{\mathfrak{L}}_\gamma) = \frac{1}{2}\dot{\boldsymbol{C}}_\gamma$, we find (cf. [183])

$$\mathbb{D} : \tfrac{1}{2}\dot{\boldsymbol{C}}_\gamma = \boldsymbol{C}_\gamma^{-1}[\boldsymbol{Y}_{\mathrm{e}} - \boldsymbol{\mathfrak{E}}], \tag{7.18}$$

thereby supplying six independent differential equations in the six independent components of $\boldsymbol{C}_\gamma$. Moreover, we split Equation (7.18) into the two independent equations

$$J_\gamma d_{\mathrm{v}} \mathrm{tr}\Big(\tfrac{1}{2}\dot{\boldsymbol{C}}_\gamma \boldsymbol{C}_\gamma^{-1}\Big) = \tfrac{1}{3}\mathrm{tr}\,\boldsymbol{Y}_{\mathrm{e}} - \tfrac{1}{3}\mathrm{tr}\,\boldsymbol{\mathfrak{E}}, \tag{7.19a}$$

$$2J_\gamma d_{\mathrm{m}} \mathrm{dev}\Big(\tfrac{1}{2}\dot{\boldsymbol{C}}_\gamma \boldsymbol{C}_\gamma^{-1}\Big) = \mathrm{dev}\,\boldsymbol{Y}_{\mathrm{e}} - \mathrm{dev}\,\boldsymbol{\mathfrak{E}}. \tag{7.19b}$$

Once the external force $\boldsymbol{Y}_{\mathrm{e}}$ is identified, and $\boldsymbol{C}_{\boldsymbol{F}_\gamma}$ is computed by solving (7.18), the term Γ in the mass balance law (7.3) is determined by $\Gamma = \mathrm{tr}\,\boldsymbol{\mathfrak{L}}_\gamma = \frac{1}{2}\mathrm{tr}(\dot{\boldsymbol{C}}_\gamma \boldsymbol{C}_\gamma^{-1})$. Finally, $\mathcal{F}_0$ becomes

$$\mathcal{F}_0 = -\boldsymbol{\mathfrak{E}} : \boldsymbol{\mathfrak{L}}_\gamma = (\boldsymbol{Y}_{\mathrm{id}} - \boldsymbol{Y}_{\mathrm{e}}) : \boldsymbol{\mathfrak{L}}_\gamma, \tag{7.20}$$

and the equation for τ takes on the form

$$\Psi\,\dot{\tau} - (\boldsymbol{P}^{\mathrm{T}}\boldsymbol{v})\,\mathrm{Grad}\,\tau + [(\boldsymbol{Y}_{\mathrm{e}} - \boldsymbol{Y}_{\mathrm{id}}) : \boldsymbol{\mathfrak{L}}_\gamma]\tau = 0. \tag{7.21}$$

Before proceeding, we remark that Equation (7.15) is *not* the most general constitutive law relating $\boldsymbol{Y}_{\mathrm{id}}$ with $\boldsymbol{\mathfrak{L}}_\gamma$, or $\dot{\boldsymbol{C}}_\gamma$. The main property of (7.15) is that, being invertible, if $\boldsymbol{\mathfrak{L}}_\gamma$ is null, then $\boldsymbol{Y}_{\mathrm{id}}$ is null too, thereby implying $\boldsymbol{Y}_{\mathrm{e}} = \boldsymbol{\mathfrak{E}}$. Moreover, due to invertibility, it is true that, when $\boldsymbol{Y}_{\mathrm{id}}$ is null, also $\boldsymbol{\mathfrak{L}}_\gamma$ has to vanish, which means that the balance between $\boldsymbol{Y}_{\mathrm{e}}$ and $\boldsymbol{\mathfrak{E}}$ leads to a stop of the growth process. However, in the case of a tumour, this last result need not be true (see e.g. [7]), as it may well happen that, if no nutrients are available for the tumour cells, $\boldsymbol{\mathfrak{L}}_\gamma$ vanishes also when $\boldsymbol{Y}_{\mathrm{id}}$ is not null, a situation that, according to Equation (7.19a), requires d_{v} to diverge for finite values of $\boldsymbol{Y}_{\mathrm{id}} := \boldsymbol{Y}_{\mathrm{e}} - \boldsymbol{\mathfrak{E}}$.

7.3 A Noether-like framework

Equation (7.1) can be obtained by framing growth within a Noether-like approach. To show this, we introduce the *action*

$$\mathcal{A} := \int_{\mathscr{B}\times\mathscr{I}} \mathcal{L},$$

where $\mathscr{I} \subseteq [0, +\infty[$ is an interval of time, and the notation $\int_{\mathscr{B}\times\mathscr{I}} f \equiv \int_{\mathscr{I}} \{\int_{\mathscr{B}} f \,\mathrm{d}V\} \,\mathrm{d}t$ applies.

7.3.1 $\boldsymbol{F}_\gamma$ considered as internal variable: internal time

When $\boldsymbol{F}_\gamma$ is regarded as an internal variable, the Lagrangian density function is defined in Equation (7.9), and the first-order total variation of the action reads

$$D\mathcal{A} = \int_{\mathscr{B}\times\mathscr{I}} \left[\boldsymbol{\mathcal{E}}\boldsymbol{h} + \mathrm{Div}(-\boldsymbol{\mathfrak{C}}^{\mathrm{T}}\boldsymbol{W} - \boldsymbol{P}^{\mathrm{T}}\boldsymbol{u})\right], \tag{7.22}$$

where $\boldsymbol{W}$ is a vector field, valued in the tangent bundle of $\mathscr{B}$, that at each time t maps the points X of $\mathscr{B}$ into $\tilde{X} = X + \varepsilon \boldsymbol{W}(X,t)$, with ε being a real smallness parameter, $\boldsymbol{h}$ is the vector field describing the variation of χ when the points X are held fixed, $\boldsymbol{u} := \boldsymbol{h} + \boldsymbol{F}\boldsymbol{W}$ is the vector field representing the *total variation* of χ, and $\boldsymbol{\mathcal{E}}\boldsymbol{h} = \mathcal{E}_a h^a$ is the contraction of the co-vector field $\boldsymbol{\mathcal{E}} := \mathrm{Div}\,\boldsymbol{P}$ with $\boldsymbol{h}$ (see [78] for a derivation in a notation similar to that adopted here). In addition, we denote by $\boldsymbol{\mathcal{J}} := -\boldsymbol{\mathfrak{C}}^{\mathrm{T}}\boldsymbol{W} - \boldsymbol{P}^{\mathrm{T}}\boldsymbol{u}$ *Noether's current density*, which is the sum of a fully material current density, $\boldsymbol{\mathcal{J}}^{(\mathrm{m})} = -\boldsymbol{\mathfrak{C}}^{\mathrm{T}}\boldsymbol{W}$, and a "spatial" current density, $\boldsymbol{\mathcal{J}}^{(\mathrm{s})} = -\boldsymbol{P}^{\mathrm{T}}\boldsymbol{u}$ (note that, although $\boldsymbol{\mathcal{J}}^{(\mathrm{s})}$ is a material field too, we call it "spatial" because it is generated by the spatial vector field $\boldsymbol{u}$).

Upon setting $\boldsymbol{W} = \boldsymbol{0}$ in $\mathscr{B}$ and $\boldsymbol{h}_{|\partial\mathscr{B}} = \boldsymbol{u}_{|\partial\mathscr{B}} = \boldsymbol{0}$ for all times, Hamilton's Principle of Stationary Action [150] requires $D\mathcal{A} = 0$, which leads to $\boldsymbol{\mathcal{E}} = \mathrm{Div}\,\boldsymbol{P} = \boldsymbol{0}$ in $\mathscr{B}$ and $\boldsymbol{P}.\boldsymbol{N} = \boldsymbol{0}$ on $\partial_N\mathscr{B}$, where $\boldsymbol{N}$ is the field of unit vectors normal to the Neumann boundary of $\mathscr{B}$, $\partial_N\mathscr{B}$.

For χ and $\boldsymbol{F}_\gamma$ satisfying $\boldsymbol{\mathcal{E}} = \boldsymbol{0}$, we look at Equation (7.22) under the light shed by Noether's Theorem [136]. Hence, we search for conservation laws, and we obtain [117]

$$\mathrm{Div}\,\boldsymbol{\mathcal{J}}^{(\mathrm{s})} = -\boldsymbol{P} : \mathrm{Grad}\,\boldsymbol{u}, \tag{7.23a}$$

$$\mathrm{Div}\,\boldsymbol{\mathcal{J}}^{(\mathrm{m})} = \boldsymbol{\mathcal{F}}\boldsymbol{W} - \boldsymbol{\mathfrak{C}} : \mathrm{Grad}\,\boldsymbol{W} =: \mathcal{N}(\boldsymbol{W}), \tag{7.23b}$$

where $\boldsymbol{\mathcal{F}} := \frac{\partial \check{\mathcal{L}}}{\partial \mathcal{X}} \circ (\boldsymbol{F}, \mathcal{X}, \mathcal{T}) = -[\frac{\partial \hat{\Psi}}{\partial \boldsymbol{F}_\gamma} \circ (\boldsymbol{F}, \boldsymbol{F}_\gamma)] : \mathrm{Grad}\,\boldsymbol{F}_\gamma$ is referred to as *"material inhomogeneity force"* [73, 71, 168] and $\boldsymbol{\mathcal{F}}\boldsymbol{W} = \mathcal{F}_A W^A$. We remark that, more generally, the integrand in Equation (7.22) should feature a summand consisting of the divergence of a vector field independent of $\boldsymbol{F}$, and descending from the so-called *"divergence transformation"* of the Lagrangian density function [136, 168, 78]. However, as in [136], this summand can be omitted for the type of symmetries addressed here.

In Equation (7.23a), $\boldsymbol{P} : \mathrm{Grad}\,\boldsymbol{u}$ vanishes identically in three cases: when $\boldsymbol{u}$ is null, when $\boldsymbol{u}$ represents a uniform translation, or when $\boldsymbol{u}$ takes on the form $\boldsymbol{u} = \boldsymbol{g}^{-1}\boldsymbol{\omega}[\chi - x_0]$, where $\boldsymbol{\omega}$ is a uniform skew-symmetric tensor, x_0 is a fixed point of space and $\boldsymbol{g}^{-1}$ is the inverse of the spatial metric tensor, $\boldsymbol{g}$. The second case is consistent with the fact that $\check{\mathcal{L}}$ is independent of χ, so that the system is invariant under translations in space and, thus, linear momentum is conserved. The third case, instead, stems from the symmetry of $\boldsymbol{g}^{-1}\boldsymbol{P}\boldsymbol{F}^{\mathrm{T}}$, which ensures $\boldsymbol{P} : \mathrm{Grad}\,\boldsymbol{u} = (\boldsymbol{g}^{-1}\boldsymbol{P}\boldsymbol{F}^{\mathrm{T}}) : \boldsymbol{\omega} = 0$ and is equivalent to the conservation of angular momentum. In conclusion, for the mentioned choices of $\boldsymbol{u}$, $\mathrm{Div}\,\boldsymbol{\mathcal{J}}^{(\mathrm{s})}$ is zero, which implies that $\boldsymbol{\mathcal{J}}^{(\mathrm{s})}$ is conserved.

We turn now to Equation (7.23b), and we notice that it is obtained by using the relation $-\mathrm{Div}\,\boldsymbol{\mathfrak{C}} = \boldsymbol{\mathcal{F}}$. This result follows from the computation of the divergence of $\boldsymbol{\mathfrak{C}}$, and characterises the *fully material* force balance describing the *"inverse dynamics"* of the body [168, 72]. It stipulates that the "spatial" part of the body's energy-momentum tensor, $-\boldsymbol{\mathfrak{C}}$, is not conserved. This is a manifestation of the symmetry breaking due to the material inhomogeneity of the body, reflected by $\mathcal{N}(\boldsymbol{W})$. This quantity plays the role of an *effective* source term for $\boldsymbol{\mathcal{J}}^{(\mathrm{m})}$ [117] and is such that the variation of the action becomes $D\mathcal{A} = \int_{\mathscr{B}\times\mathscr{I}} \mathcal{N}(\boldsymbol{W})$. Therefore, in order to search for the class of fields $\boldsymbol{W}$ such that $\boldsymbol{\mathcal{J}}^{(\mathrm{m})}$ is conserved and the action is invariant, i.e., $D\mathcal{A} = 0$, one has to impose [117]

$$\begin{aligned}\mathcal{N}(\boldsymbol{W}) &= -\boldsymbol{\mathfrak{C}} : \mathrm{Grad}\,\boldsymbol{W} + \boldsymbol{\mathcal{F}}\boldsymbol{W} \\ &= -\boldsymbol{\mathfrak{C}} : \Big[\mathrm{Grad}\,\boldsymbol{W} + (\boldsymbol{F}_\gamma^{-1}\mathrm{Grad}\,\boldsymbol{F}_\gamma)\boldsymbol{W}\Big] = 0. \end{aligned} \tag{7.24}$$

We remark that relations of the type (7.24) are sometimes referred to as *"Noetherian identities"* [196].

Apart from the trivial solution $\boldsymbol{W} = \boldsymbol{0}$, a uniform field $\boldsymbol{W}$ does not generally satisfy Equation (7.24) and, thus, the action is not invariant under uniform translations of the material points. This result is another evidence of the symmetry breaking emerging because of $\boldsymbol{\mathcal{F}}$. Clearly, if $\boldsymbol{F}_\gamma$ is uniform, so that $\mathrm{Grad}\,\boldsymbol{F}_\gamma = \boldsymbol{0}$, then $\boldsymbol{W}$ can be uniform too. When this occurs, $\boldsymbol{\mathcal{F}}$ vanishes identically and, in the jargon of [168], one obtains the conservation of *"canonical pseudo-momentum"*. Let us now look at the identity

$$\dot{\Psi} - \mathrm{Div}(\boldsymbol{P}^{\mathrm{T}}\boldsymbol{v}) = -\mathcal{F}_0, \tag{7.25}$$

which is the *non*-conservation of energy for $\mathcal{H} = \Psi = -\mathcal{L}$ (i.e., in the quasi-static limit), and let us multiply Equation (7.25) by a scalar field $\tau : \mathscr{B} \times \mathscr{I} \to \mathbb{R}$

describing a point- and time-dependent *deformation* of time [117]. Then, recalling the definition of $\mathcal{F}_0$ given in (7.10), we find (cf. [168])

$$\begin{aligned} &\overline{\Psi\tau}^{\boldsymbol{\cdot}} + \mathrm{Div}(-\boldsymbol{P}^{\mathrm{T}}\boldsymbol{v}\tau) \\ &= \Psi\dot{\tau} - (\boldsymbol{P}^{\mathrm{T}}\boldsymbol{v})\,\mathrm{Grad}\,\tau + (\boldsymbol{\mathfrak{E}} : \boldsymbol{\mathfrak{L}}_\gamma)\tau =: \mathcal{N}_0(\tau). \end{aligned} \tag{7.26}$$

By analogy with Equation (7.23b), we call $\mathcal{N}_0(\tau)$ *effective source* of Noether's energy current density, defined by the time-like component $\Psi\tau$ and the flux vector $-\boldsymbol{P}^{\mathrm{T}}\boldsymbol{v}\tau$. As noticed for $\mathcal{N}(\boldsymbol{W})$, the presence of $\mathcal{F}_0 = -\boldsymbol{\mathfrak{E}} : \boldsymbol{\mathfrak{L}}_\gamma$ implies that $\mathcal{N}_0(\tau)$ does not vanish for nonzero constant fields τ. Hence, to conserve Noether's energy current density, we enforce the condition anticipated by Equation (7.1), i.e.,

$$\mathcal{N}_0(\tau) = \Psi\dot{\tau} - (\boldsymbol{P}^{\mathrm{T}}\boldsymbol{v})\mathrm{Grad}\,\tau + (\boldsymbol{\mathfrak{E}} : \boldsymbol{\mathfrak{L}}_\gamma)\tau = 0, \tag{7.27}$$

in which $\boldsymbol{\mathfrak{E}} : \boldsymbol{\mathfrak{L}}_\gamma$ is now regarded as the generator of τ.

7.3.2 $\boldsymbol{F}_\gamma$ considered as a kinematic variable: internal time

Equations (7.6), (7.8) and (7.14) allow to rephrase the force balances (7.12a) and (7.12b) as

$$\mathrm{Div}\,\boldsymbol{P} \equiv -\mathrm{Div}\left(\frac{\partial\hat{\mathcal{L}}}{\partial\boldsymbol{F}} \circ (\boldsymbol{F}, \boldsymbol{F}_\gamma)\right) = \boldsymbol{0}, \tag{7.28a}$$

$$-\boldsymbol{\mathfrak{E}} \equiv \quad \boldsymbol{F}_\gamma^{\mathrm{T}}\left(\frac{\partial\hat{\mathcal{L}}}{\partial\boldsymbol{F}_\gamma} \circ (\boldsymbol{F}, \boldsymbol{F}_\gamma)\right) = \boldsymbol{Y}_{\mathrm{id}} - \boldsymbol{Y}_{\mathrm{e}}. \tag{7.28b}$$

Looking at (7.28b), we notice that a relevant case occurs when there exists a potential $\mathcal{U} = \hat{\mathcal{U}} \circ (\boldsymbol{F}, \boldsymbol{F}_\gamma)$ such that

$$\frac{\partial\hat{\mathcal{U}}}{\partial\boldsymbol{F}} \circ (\boldsymbol{F}, \boldsymbol{F}_\gamma) = \boldsymbol{0}, \quad \frac{\partial\hat{\mathcal{U}}}{\partial\boldsymbol{F}_\gamma} \circ (\boldsymbol{F}, \boldsymbol{F}_\gamma) = \boldsymbol{F}_\gamma^{-\mathrm{T}}\boldsymbol{Y}_{\mathrm{e}}, \tag{7.29}$$

where the first requirement of Equation (7.29) prevents $\hat{\mathcal{U}}$ from introducing an unphysical contribution to $\boldsymbol{P}$. Thus, Eqs. (7.28a) and (7.28b) become

$$-\mathrm{Div}\left(\frac{\partial\hat{\mathcal{L}}_{\mathrm{eff}}}{\partial\boldsymbol{F}} \circ (\boldsymbol{F}, \boldsymbol{F}_\gamma)\right) = \boldsymbol{0}, \tag{7.30a}$$

$$\boldsymbol{F}_\gamma^{\mathrm{T}}\left(\frac{\partial\hat{\mathcal{L}}_{\mathrm{eff}}}{\partial\boldsymbol{F}_\gamma} \circ (\boldsymbol{F}, \boldsymbol{F}_\gamma)\right) = \boldsymbol{Y}_{\mathrm{id}}, \tag{7.30b}$$

with $\mathcal{L}_{\mathrm{eff}} := \mathcal{L} + \mathcal{U}$ being referred to as *effective Lagrangian density function*. Note that, although Equation (7.29) may be too restrictive for biologically meaningful situations, it is possible to think of $\boldsymbol{Y}_{\mathrm{e}}$ as the sum of an integrable and a non-integrable force, with the former one admitting a potential like $\hat{\mathcal{U}}$. For this reason, in this work we concentrate on the limiting case in which $\boldsymbol{Y}_{\mathrm{e}}$ is integrable.

By defining the effective action, $\mathcal{A}_{\mathrm{eff}} = \int_{\mathscr{B}\times\mathscr{I}} \mathcal{L}_{\mathrm{eff}}$, the first-order total variation of $\mathcal{A}_{\mathrm{eff}}$ is given by

$$D\mathcal{A}_{\mathrm{eff}} = \int_{\mathscr{B}\times\mathscr{I}} \left[\boldsymbol{F}_\gamma^{-\mathrm{T}}\boldsymbol{Y}_{\mathrm{id}} : \boldsymbol{\Upsilon} + \mathrm{Div}(\boldsymbol{\mathcal{J}}^{(\mathrm{s})} + \boldsymbol{\mathcal{J}}^{(\mathrm{m})}_{\mathrm{eff}})\right], \tag{7.31}$$

with $\boldsymbol{\mathcal{J}}^{(\mathrm{s})} = -\boldsymbol{P}^{\mathrm{T}}\boldsymbol{u}$, $\boldsymbol{\mathcal{J}}^{(\mathrm{m})}_{\mathrm{eff}} = -\boldsymbol{\mathfrak{E}}^{\mathrm{T}}_{\mathrm{eff}}\boldsymbol{W}$, the effective Eshelby stress tensor $\boldsymbol{\mathfrak{E}}_{\mathrm{eff}} = -(\mathcal{L}_{\mathrm{eff}}\boldsymbol{I}^{\mathrm{T}} + \boldsymbol{F}^{\mathrm{T}}\boldsymbol{P})$ and $\boldsymbol{\Upsilon}$ being the variation of $\boldsymbol{F}_\gamma$ when the points X are "held fixed".

Upon taking $\mathrm{Div}\,\boldsymbol{\mathcal{J}}^{(\mathrm{s})} = 0$, as done in Section 7.3.1, a direct calculation yields

$$\mathrm{Div}\,\boldsymbol{\mathcal{J}}^{(\mathrm{m})}_{\mathrm{eff}} = \boldsymbol{\mathcal{F}}_{\mathrm{eff}}\boldsymbol{W} - \boldsymbol{\mathfrak{E}}_{\mathrm{eff}} : \mathrm{Grad}\,\boldsymbol{W}, \tag{7.32}$$

where we call $\boldsymbol{\mathcal{F}}_{\mathrm{eff}} := \left(\boldsymbol{F}_\gamma^{-\mathrm{T}}\boldsymbol{Y}_{\mathrm{id}} : \mathrm{Grad}\,\boldsymbol{F}_\gamma\right)$ *effective inhomogeneity force*, and Equation (7.31) reduces to

$$D\mathcal{A}_{\mathrm{eff}} = \int_{\mathscr{B}\times\mathscr{I}} [\boldsymbol{F}_\gamma^{-\mathrm{T}}\boldsymbol{Y}_{\mathrm{id}} : \boldsymbol{Q} - \boldsymbol{\mathfrak{E}}_{\mathrm{eff}} : \mathrm{Grad}\,\boldsymbol{W}], \tag{7.33}$$

with $\boldsymbol{Q} := \boldsymbol{\Upsilon} + (\mathrm{Grad}\boldsymbol{F}_\gamma)\boldsymbol{W}$ being the total variation of $\boldsymbol{F}_\gamma$. If we set $\boldsymbol{W} = \boldsymbol{0}$, Equation (7.33) returns Rayleigh-Hamilton Principle [150, 58], which states that the first-order variation of the action is equal to the integral of the work $\boldsymbol{F}_\gamma^{-\mathrm{T}}\boldsymbol{Y}_{\mathrm{id}} : \boldsymbol{Q}$. Thus, if we reinterpret Equation (7.33) on the basis of this result, we find that the class of fields $\boldsymbol{W}$ satisfying $D\mathcal{A}_{\mathrm{eff}} = \int_{\mathscr{B}\times\mathscr{I}} \boldsymbol{F}_\gamma^{-\mathrm{T}}\boldsymbol{Y}_{\mathrm{id}} : \boldsymbol{Q}$ is given by all the solutions of the equation

$$-\boldsymbol{\mathfrak{E}}_{\mathrm{eff}} : \mathrm{Grad}\,\boldsymbol{W} = 0. \tag{7.34}$$

In contrast to (7.24), Equation (7.34) is satisfied by nontrivial uniform fields $\boldsymbol{W}$. To see the implications of this result, let us consider the situation in which $\boldsymbol{Y}_{\mathrm{id}}$ is null. Hence, it follows that $\boldsymbol{\mathfrak{E}} = \boldsymbol{Y}_{\mathrm{e}}$, $\mathrm{Div}\,\boldsymbol{\mathcal{J}}^{(\mathrm{m})}_{\mathrm{eff}} = -\boldsymbol{\mathfrak{E}}_{\mathrm{eff}} : \mathrm{Grad}\,\boldsymbol{W}$, and Equation (7.33) becomes $D\mathcal{A}_{\mathrm{eff}} = \int_{\mathscr{B}\times\mathscr{I}}[-\boldsymbol{\mathfrak{E}}_{\mathrm{eff}} : \mathrm{Grad}\,\boldsymbol{W}]$. In this case, uniform fields $\boldsymbol{W}$ leave the action invariant, i.e., $D\mathcal{A}_{\mathrm{eff}} = 0$, and represent symmetry transformations. This constitutes a symmetry restoration and is due to the fact that, since $\boldsymbol{Y}_{\mathrm{id}}$ is null, $\boldsymbol{\mathfrak{E}}$ is entirely "balanced" by $\boldsymbol{Y}_{\mathrm{e}}$, which plays the role of compensating field. In fact, this results follows from Equation (7.30b), which, for $\boldsymbol{Y}_{\mathrm{id}} = \boldsymbol{0}$, implies $\boldsymbol{\mathcal{F}}_{\mathrm{eff}} := \left(\frac{\partial\hat{\mathcal{L}}_{\mathrm{eff}}}{\partial\boldsymbol{F}_\gamma} \circ (\boldsymbol{F}, \boldsymbol{F}_\gamma)\right) : \mathrm{Grad}\,\boldsymbol{F}_\gamma = \boldsymbol{0}$ even though it holds that $\boldsymbol{\mathcal{F}} = -\boldsymbol{\mathfrak{E}} : \boldsymbol{F}_\gamma^{-1}\mathrm{Grad}\,\boldsymbol{F}_\gamma \neq \boldsymbol{0}$.

As done in Section 7.3.1, we consider the identity

$$\dot{\Psi}_{\mathrm{eff}} - \mathrm{Div}(\boldsymbol{P}^{\mathrm{T}}\boldsymbol{v}) = -\boldsymbol{Y}_{\mathrm{id}} : \boldsymbol{\mathfrak{L}}_\gamma = -\mathcal{D}_{\mathrm{KV}}, \tag{7.35}$$

where $\Psi_{\mathrm{eff}} := -\mathcal{L}_{\mathrm{eff}}$ denotes the effective energy density associated with the body and, by multiplying (7.35) by τ, we obtain

$$\begin{aligned}&\overset{\cdot}{\overline{\Psi_{\mathrm{eff}}\tau}} + \mathrm{Div}(-\boldsymbol{P}^{\mathrm{T}}\boldsymbol{v}\tau)\\&= \Psi_{\mathrm{eff}}\dot{\tau} - (\boldsymbol{P}^{\mathrm{T}}\boldsymbol{v})\,\mathrm{Grad}\,\tau - \mathcal{D}_{\mathrm{KV}}\,\tau =: \mathcal{N}_{0\mathrm{eff}}(\tau).\end{aligned} \tag{7.36}$$

Equation (7.35) describes the non-conservation of Ψ_{eff}, while Equation (7.36) defines $\mathcal{N}_{0\mathrm{eff}}(\tau)$ as the effective source of Noether's energy current density with time-like component $\Psi_{\mathrm{eff}}\tau$ and flux vector $-\boldsymbol{P}^{\mathrm{T}}\boldsymbol{v}\tau$. Hence, to conserve Noether's energy current density, the condition

$$\mathcal{N}_{0\mathrm{eff}}(\tau) = \Psi_{\mathrm{eff}}\dot{\tau} - (\boldsymbol{P}^{\mathrm{T}}\boldsymbol{v})\,\mathrm{Grad}\,\tau - \mathcal{D}_{\mathrm{KV}}\,\tau = 0 \tag{7.37}$$

has to be imposed. Equation (7.37) prescribes that $\mathcal{D}_{\mathrm{KV}}$ is the generator of τ. Therefore, $\mathcal{D}_{\mathrm{KV}}$ can be thought of as an *effective time-like inhomogeneity force*, i.e., $\mathcal{F}_{0\mathrm{eff}} := \mathcal{D}_{\mathrm{KV}}$, which vanishes in the non-dissipative limit. If this is the case, a constant field τ satisfies $\mathcal{N}_{0\mathrm{eff}}(\tau) = 0$ and, consequently, Eq. (7.36) and (7.37) is satisfied as a conservation law. This is a crucial difference with Equations (7.21) and (7.27), in which the generator of τ is given by $-\mathcal{F}_0 = \boldsymbol{Y}_{\mathrm{e}} - \boldsymbol{Y}_{\mathrm{id}} = \boldsymbol{\mathfrak{E}} : \boldsymbol{\mathfrak{L}}_\gamma$ and need not vanish even when the dissipation is zero. The above discussion answers the research question 7.2.

7.4 A proof of concept

To supply a proof of concept of the theory discussed so far, we take a benchmark problem from [7]. Specifically, we study a tumour modelled as a monophasic, isotropic, solid body of cylindric shape, confined by an undeformable lateral wall, and allowed to expand uniformly along its axial direction, with traction-free terminal cross sections. Moreover, we assume the growth tensor, $\boldsymbol{F}_\gamma$, to be spherical. By using cylindrical coordinates, these hypotheses imply that the only nonzero component of the velocity, $\boldsymbol{v}$, is the axial one, v^z, and that $\boldsymbol{F}$, $\boldsymbol{F}_\gamma$, $\boldsymbol{\mathfrak{L}}_\gamma = \boldsymbol{F}_\gamma^{-1}\dot{\boldsymbol{F}}_\gamma$, $\boldsymbol{P}$ and $\boldsymbol{\mathfrak{E}}$ admit the diagonal matrix representations

$$[F] = \mathrm{diag}\{1,1,\mathfrak{f}\}, \tag{7.38a}$$
$$[F_\gamma] = \gamma\,\mathrm{diag}\{1,1,1\}, \tag{7.38b}$$
$$[\mathfrak{L}_\gamma] = \gamma^{-1}\dot{\gamma}\,\mathrm{diag}\{1,1,1\}, \tag{7.38c}$$
$$[P] = \mathrm{diag}\{P_r{}^R, P_\varphi{}^\Phi, P_z{}^Z\}, \tag{7.38d}$$
$$[\mathfrak{E}] = \mathrm{diag}\{\Psi - P_r{}^R, \Psi - P_\varphi{}^\Phi, \Psi - \mathfrak{f}\,P_z{}^Z\}. \tag{7.38e}$$

We remark that, since $\mathrm{Div}\,\boldsymbol{P} = \boldsymbol{0}$ reduces to $\partial P_z{}^Z/\partial Z = 0$, and the terminal cross sections of the body are free of tractions [7], $P_z{}^Z$ is zero at all the points of the tumour. This implies that the energy flux $\boldsymbol{P}^{\mathrm{T}}\boldsymbol{v}$ vanishes identically, i.e., $\boldsymbol{P}^{\mathrm{T}}\boldsymbol{v} = \boldsymbol{0}$ and $P_z{}^Z v^z = 0$. Moreover, as in [7], we adopt the Blatz-Ko strain energy density

$$\Psi = J_\gamma \tfrac{1}{2}\mu \left[(I_1 - 3) - \tfrac{1}{q/2}(I_3{}^{q/2} - 1) \right], \tag{7.39}$$

with $I_1 = \mathrm{tr}(\boldsymbol{C}\boldsymbol{C}_\gamma^{-1})$, $I_3 = J_\gamma^{-2}\det\boldsymbol{C}$ and material constants $\mu > 0$ and $q < 0$. Due to Equation (7.39), the constitutive expression of $P_z{}^Z$ is such that [7]

$$P_z{}^Z = \mu\frac{\gamma^3}{\mathfrak{f}}\left[\frac{\mathfrak{f}^2}{\gamma^2} - \left(\frac{\mathfrak{f}}{\gamma^3}\right)^q\right] = 0 \;\Rightarrow\; \mathfrak{f} = \gamma^{\frac{2-3q}{2-q}}. \tag{7.40}$$

Therefore, any constitutive function of $\mathfrak{f}$ and γ can be rephrased as a function of γ alone. For, example, in the case of Eshelby stress, one has $\boldsymbol{\mathfrak{E}} = \hat{\boldsymbol{\mathfrak{E}}}(\mathfrak{f},\gamma) \equiv \boldsymbol{\mathfrak{H}}(\gamma)$ and

$$\mathfrak{H}(\gamma) := \tfrac{1}{3}\mathrm{tr}\,\boldsymbol{\mathfrak{H}}(\gamma) = \Psi - \tfrac{1}{3}(P_r{}^R + P_\varphi{}^\Phi) = \tfrac{1}{3}\mathrm{tr}\,\boldsymbol{\mathfrak{E}}. \tag{7.41}$$

First, we consider the case in which $\boldsymbol{F}_\gamma$ is an internal variable [72] and we refer to this model as "IV Model". We notice that, in order to recover the growth law proposed in [7] from Equation (7.5), we have to set $\beta_n = 0$, for $n \neq 0$, thereby obtaining

$$\dot{\gamma} = \beta_0\gamma, \quad \beta_0 = \tfrac{1}{3}\Gamma, \tag{7.42}$$

where, in general, β_0 depends on mechanical stress through the principal invariants of $\boldsymbol{\mathfrak{E}}$. However, if β_0 is assumed to be a positive constant, and if the initial distribution of γ, denoted by γ_{in}, is independent of material points, γ is uniform and increases exponentially in time [7], i.e., $\gamma(t) = \gamma_{\mathrm{in}}\exp(\beta_0 t)$ (see the line marked with triangles, and referred to as "IV Model", in Fig. 7.1). Moreover, according to Equation (7.40), also $\mathfrak{f}$ is independent of material points. In the case under study, the material inhomogeneity force $\boldsymbol{\mathcal{F}}$ is null, so that uniform fields $\boldsymbol{W} = \boldsymbol{W}_0$ satisfy Equation (7.24) and, since the identity $\boldsymbol{\mathfrak{E}} : \boldsymbol{\mathfrak{L}}_\gamma = \dot{\Psi}$ holds true, Equation (7.27) becomes

$$\mathcal{N}_0(\tau) = \Psi\dot{\tau} + \dot{\Psi}\tau = \dot{\overline{\Psi\tau}} = 0. \tag{7.43}$$

Coherently with Equation (7.26), this result implies that the time-like component of Noether's current density, $\Psi\tau$, is conserved, and the internal time is given by

$$\Psi(t)\tau(t) = \Psi_0\tau_0 \;\Rightarrow\; \tau(t) = \frac{\tau_0\Psi_0}{\Psi(t)}, \tag{7.44}$$

where Ψ_0 and τ_0 are reference constant values, and $\Psi(t)$ is rescaled so that $\Psi(0) = \Psi_0$. The trend of τ is reported in Fig. 7.2 and corresponds to the solid line marked with triangles and referred to as "τ/τ_0 IV Model". The product $\Psi_0\tau_0$ defines the negative of a reference value of the action, i.e., $\mathcal{A}_0 := -\Psi_0\tau_0$, which is invariant.

Now, we regard $\boldsymbol{F}_\gamma$ as a kinematic variable [60] and we call this model "KV Model". In this case, the evolution of γ is given by Equations (7.19a) and (7.19b), which yield

$$\frac{\dot{\gamma}}{\gamma} = \frac{1}{3\gamma^3 d_{\mathrm{v}}} \left[Y_{\mathrm{e}} - \mathfrak{H}(\gamma) \right], \tag{7.45}$$

with $Y_{\mathrm{e}} := \frac{1}{3}\mathrm{tr}\,\boldsymbol{Y}_{\mathrm{e}}$ and $\mathrm{dev}\,\boldsymbol{Y}_{\mathrm{e}} = \mathbf{0}$. Within the present variational setting, we choose a constant Y_{e}, so that it can be obtained by differentiation of the potential $\hat{\mathcal{U}} \circ (\boldsymbol{F}, \boldsymbol{F}_\gamma) = Y_{\mathrm{e}} \ln(\det \boldsymbol{F}_\gamma)$, and the numerical solution of Equation (7.45), obtained for constant d_{v}, is reported in Fig. 7.1 (see the solid line marked with open circles and referred to as "KV Model - Linear Case").

Since it holds true that $\boldsymbol{P}^{\mathrm{T}}\boldsymbol{v} = \mathbf{0}$, Equation (7.35) prescribes $\mathcal{D}_{\mathrm{KV}} = -\dot{\Psi}_{\mathrm{eff}}$ and, consequently, Equation (7.37) becomes

$$\mathcal{N}_{0\mathrm{eff}} = \Psi_{\mathrm{eff}}\dot{\tau} + \dot{\Psi}_{\mathrm{eff}}\tau = \overline{\Psi_{\mathrm{eff}}\tau}^{\boldsymbol{\cdot}} = 0. \tag{7.46}$$

Therefore, the internal time, τ, is given by

$$\Psi_{\mathrm{eff}}(t)\tau(t) = \Psi_{\mathrm{eff}0}\tau_0 \;\Rightarrow\; \tau(t) = \frac{\tau_0 \Psi_{\mathrm{eff}0}}{\Psi_{\mathrm{eff}}(t)}, \tag{7.47}$$

with τ_0 and $\Psi_{\mathrm{eff}0}$ being reference constants, and $\Psi_{\mathrm{eff}}(t)$ rescaled so that $\Psi_{\mathrm{eff}}(0) = \Psi_{\mathrm{eff}0}$. In spite of the similarity with Equation (7.44), in the present case $\tau(t)$ depends on Y_{e}. Its evolution is shown in Fig. 7.2 and corresponds to the solid line marked with open circles.

7.5 Discussion

In the IV Model, the coefficient β_0 in Equation (7.42) is assumed to be constant. Although this choice may be too restrictive, it describes the limit case in which, to activate growth, it is sufficient that the nutrient substances in the tumour exceed a certain threshold. Clearly, more general models, which include the feedback of stress on growth (mechanotransduction), can be obtained by considering Equation (7.5) in full, or by expressing β_0 as a phenomenological function of the stress.

In the KV Model, which descends from Equation (7.15), (7.19a) and (7.45), γ is coupled with $Y_{\mathrm{id}} := \frac{1}{3}\mathrm{tr}\,\boldsymbol{Y}_{\mathrm{id}} = Y_{\mathrm{e}} - \mathfrak{H}(\gamma)$, rather than with stress alone, and this coupling may appear both directly, i.e., in the right-hand-side of Equation (7.45), and indirectly, i.e., through the coefficient d_{v}, which can be taken as a function of the principal invariants of $\boldsymbol{Y}_{\mathrm{id}}$. To the best of our understanding, this could be a possible interpretation of the *"Eshelbian coupling"* mentioned in [60]. In this respect, we also notice that, even within our variational setting, mechanotransduction can be accounted for by suitably interpreting Y_{e}. This can be achieved by relating $\dot{\gamma}/\gamma$ to a term of the type [166, 62]

$$M(\mathfrak{H}) := 1 - \frac{c_0 \mathfrak{E}}{c_0 Y_\mathrm{e} + \mathfrak{E}} = 1 - \frac{\mathfrak{E}}{Y_\mathrm{e}} + o\left(\frac{\mathfrak{E}}{Y_\mathrm{e}}\right), \tag{7.48}$$

where $c_0 \in]0,1[$ is a model parameter and $\mathfrak{E} = \frac{1}{3}\mathrm{tr}\,\boldsymbol{\mathfrak{E}} = \mathfrak{H}(\gamma)$. By setting $M_\mathrm{lin}(\mathfrak{E}) := 1 - \mathfrak{E}/Y_\mathrm{e}$, Equation (7.45) can be rewritten as $\dot{\gamma}/\gamma = M_\mathrm{lin}(\mathfrak{E})/3\gamma^3\bar{\tau}$, where $\bar{\tau}$ is a characteristic time scale and $d_\mathrm{v} \equiv \bar{\tau} Y_\mathrm{e}$. The solution to this equation, or, equivalently, to Equation (7.45), corresponds to the solid line marked with open circles in Fig. 7.1, where it is compared with the solution to the equation $\dot{\gamma}/\gamma = M(\mathfrak{E})/3\gamma^3\bar{\tau}$. The latter is represented by the solid line marked with triangles in Fig. 7.1, and refers to a phenomenological model in which the mechanotransduction term, $M(\mathfrak{E})$, is not linearised. Looking at the magnified inset in Fig. 7.1, we notice that a constant and integrable Y_e, although being restrictive, leads to reasonable results for the first days in which the tumour grows, i.e., as long as the ratio $\mathfrak{E}/Y_\mathrm{e}$ remains sufficiently small. For longer times, however, the solution to Equation (7.45) ceases to be acceptable. Indeed, it tends towards a stationary value, corresponding to the force balance $Y_\mathrm{e} = \mathfrak{H}(\gamma)$, which contradicts the hypothesis $\mathfrak{E}/Y_\mathrm{e} \to 0$. The solution of the nonlinear model, instead, keeps increasing in time, and is qualitatively closer to the dashed curve marked with open circles that describes the trend of γ in the case of a reference model available in the literature [62]. The above discussion answers the research question 7.3.

The main result of this work is the introduction of the internal time, τ, that, for the considered benchmark problem, is obtained by solving Equation (7.44) for the IV Model and Equation (7.47) for the KV Model. The solutions, expressed in terms of the ratio τ/τ_0, are reported in Fig. 7.2 and correspond to the solid lines marked with asterisks and open circles, respectively. We notice that, since both Ψ and Ψ_eff increase with γ, and since γ increases with time, τ/τ_0 decreases monotonically for both models. In particular, since γ is computed by solving Equation (7.45), which admits a stationary solution, τ/τ_0 reaches a plateau for long times, and the solution predicted by the IV Model tends to converge to the one supplied by the KV Model. Finally, we notice that the function $\tau_\mathrm{c} = 1 - \tau(t)/\tau_0$ is monotonically increasing, and might thus be taken as a natural characteristic time scale of growth, just as the endochronic time in Plasticity [176]. The above discussion answers the research question 7.1.

7.6 Conclusions

In this work, we have studied a problem of volumetric growth in a continuum body within the quasi-static limit. In doing this, we have followed two paths: the one that views the growth tensor, $\boldsymbol{F}_\gamma$, as an internal variable, and the one that defines $\boldsymbol{F}_\gamma$ as a kinematic variable. We have cast the problem in a variational setting

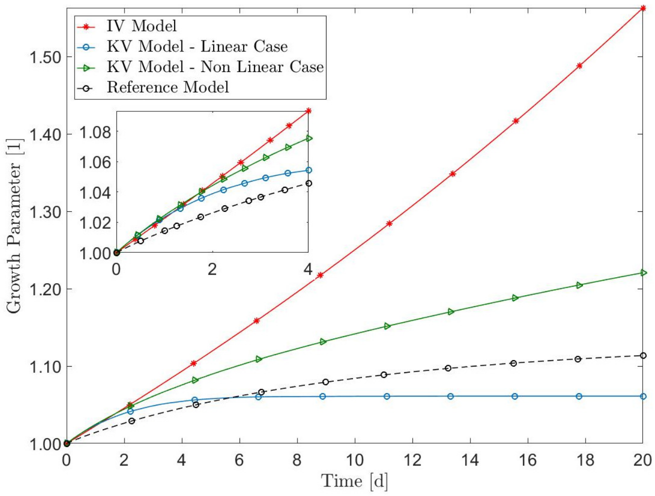

Figure 7.1: Time evolution of γ. The model parameters are $\Gamma = 2.68 \cdot 10^{-2}\,\mathrm{s}^{-1}$, for the IV-model, and $c_0 = 0.7138$, $Y_\mathrm{e} = 2.159\,\mathrm{kPa}$ and $\bar{\tau} = 10^6\,\mathrm{s}$, for the KV-model. For both models, we set $\mu = 1.999\,\mathrm{kPa}$, $q = -1$, $k_\mathrm{in} = 1$, $\tau_0 = 1\,\mathrm{s}$.

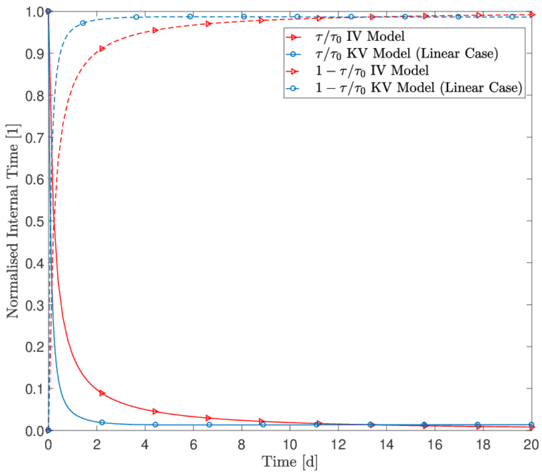

Figure 7.2: Time evolution of τ . The values of the model parameters are declared in the caption of Fig. 7.1.

and we have employed the framework of Noether's Theorem in order to reveal some subtle implications of the two theories of growth exploited in the manuscript, especially in terms of material inhomogeneities and conservation laws.

Hence, we have shown that Noether's current is not conserved, in general, for the classes of transformations that would represent material symmetries if the body were homogeneous. This has been reflected, in fact, by the condition $\mathcal{N}(\boldsymbol{W}) = 0$, imposed to annihilate the effective source of Noether's current [117].

We have focussed on the non-conservation of energy. This has led us to adopt the conditions $\mathcal{N}_0(\tau) = 0$ and $\mathcal{N}_{0\text{eff}}(\tau) = 0$, respectively, to search for transformations capable of defining a characteristic time scale for growth, termed *internal time*.

We summarise the answers to the research questions 7.1—7.3 in the following way:

- The internal time, τ, for the considered benchmark problem is computed as the solution of two differential equations relying on two different models of growth. For both models, the normalised internal time τ/τ_0 is an increasing function of time and it reaches a *plateau*, since the equation for the growth parameter, γ, admits a stationary solution. However, the KV model, which regards the growth tensor as a kinematic variable predicts that the stationary state is attained faster than in the case of IV model, in which the growth tensor is viewed as an internal parameter,

- One of the main advantages of using variational principles within the study of growth is the possibility of giving a unifying definition of internal time, which results to be independent on the specific theory of growth that one decides to adhere to. In fact, the internal time can be defined as the solution of a differential equation, descending from Noether's Theorem and whose formulation is, in fact, independent on the mathematical model used to describe growth.

- Although we have adhered to variational principles for studying the growth in monophasic continua, we have shown that it is possible to address the issue of "mechanotrasduction". Therefore, in spite of some technical limitations that require *ad hoc* hypotheses, we have recast in a some evolution laws for the growth parameter, which are usually declared to be phenomenological, in a variational framework

Chapter 8

Future perspectives

The work outlined in this Thesis addresses the mathematical modelling of some key problems in the field of Biomechanics, by focusing on theoretical and computational aspects of Nonlinear Continuum Mechanics.

Although relevant technical aspects have been solved in a different manner, depending on the problem at hand, we have always tried to harmonise all the diverse theoretical visions emerging in our works and to find a physico-mathematical link able to disclose a common theoretical substrate.

In this respect, in the works presented in Chapter 2 and in Chapter 3 we have employed a mathematical framework in which the distortion tensor, $\boldsymbol{F}_{\mathrm{p}}$ (or, equivalently, its inverse $\boldsymbol{H}$), and the growth tensor, $\boldsymbol{F}_{\gamma}$, are treated as internal variables. Moreover, the evolution laws for $\boldsymbol{F}_{\mathrm{p}}$ and for $\boldsymbol{F}_{\gamma}$ are are in part phenomenological. In particular, in the case of $\boldsymbol{F}_{\mathrm{p}}$, its equation is derived by the Dissipation Inequality, while, for $\boldsymbol{F}_{\gamma}$, its evolution is imposed from the outset, in accordance with experimental evidences.

On the contrary, in Chapter 3 and in Chapter 6, the tensors $\boldsymbol{F}_{\mathrm{p}}$ and $\boldsymbol{F}_{\gamma}$ are regarded as kinematic variables. In this sense, their evolution laws are deduced from a balance of generalised forces, dual to suitable generalised velocities and all the phenomenological assumptions are employed as kinematic constraints.

Beyond the differences characterising the "internal variables" approach and the "kinematic variables" approach discussed so far, we have wondered about the possibility of identifying a bridge between these two ways of proceeding. A first step in this direction is presented in Chapter 7 with the employment of Noether's Theorem and the introduction of the internal time as a thermodynamic indicator of anelastic processes.

In general, for all the specific problems studied in this Thesis, the formulation adopted for developing our works has been characterised by the employment of Differential Geometry in order to satisfy two requirements. The first one, according to the conception of a deep relationship between Mechanics and Geometry, relies on the adoption of the Covariant Formalism of Continuum Mechanics as a fundamental “language” to proceed with our scientific studies. The choice of such way of proceeding makes it particularly easy to disclose duality for defining the (generalised) forces acting on a mechanical system as dual entities of a specified (generalised) kinematics. Second, to study a certain class of problems in the field of Biomechanics, it raises the necessity to “enrich” their kinematic description and, in our framework, this has been achieved by having recourse to some classical tools of Differential Geometry, as explained in Chapters 2, 3, 5 and 6.

Starting from the framework outlined in Chapters 2 and 3, the remodelling can be understood as the occurrence of two types of events: one consists of the reorientation of the fibres and, the other one relies on the production of inelastic distortions at the tissue scale. It is assumed that the fibres are oriented accordingly to a probability density function, whose functional form is prescribed. The inelastic distortions, which can be associated with the rupture and formation of bonds among the tissue cells, are represented by means of a second-order tensor and studied by means of the Bilby–Kröner–Lee decomposition of the deformation gradient tensor. An evolution law for the tensor of inelastic distortions is prescribed.

In general, the evolution law for the tensor of inelastic distortions is written by considering only the symmetric part of the inelastic distortions tensor and it is assumed that its rotational component reduces to the identity tensor. One possibility is to investigate mathematical models of structural reorganisation in which the role of the inelastic rotations is explicitly considered. From the modelling point of view, this choice requires to individuate a suitable geometrical quantity able to be represent the kinematics associated with the inelastic rotations. Consequently, the overall framework should be rephrased to account for the new kinematics, which enriches the standard one previously employed.

In the modelling framework of gradient theories, one could employ a different model of the fluid flow. More in detail, instead of making use of Darcy’s law one could refer to Brinkman-like models, which involve the gradient of the fluid velocity [146, 34, 63]. This will allow, on the one hand, to relax the hypothesis of negligibility of the dissipative part of the stress tensor of the fluid phase and, on the other hand, to resolve the fluid-structure interactions as well as boundary effects, which cannot be accounted for by Darcy-based models.

In Chapter 6, a mathematical model to investigate how a tumour tissue grows and remodels in response to growth has been proposed. For our scopes, it has been assumed that remodelling is characterised by a coarse and a fine length scale, and a kinematic variable that resolves the fine scale inhomogeneities induced by remodelling have been introduced . With respect to this variable, a strain-gradient framework of remodelling has been developed.

One research line, starting from the work presented in Chapter 6, could be to investigate a tumour growth inside a host tissue, in order to resolve the mechanical interactions at the interface between the two media.

Finally, the model of growth employed in Chapter 5 and in Chapter 6 could be developed and extended to describe other biological situations. For instance, the approach presented in this two chapters for isotropic media could be adapted for describing a tumour growing in anisotropic tissues. Moreover, we could investigate the coupling with other remodelling phenomena, introduced in term of cellular reorganisation, fibre reorientation or onset of degenerative phenomena.

Appendix A

The notation adopted in the following is taken from [77]. Let $[T\mathscr{B}]^1{}_1$, $[T\mathscr{B}]_1{}^1$, $[T\mathscr{B}]^2_0$, and $[T\mathscr{B}]^0_2$ denote the spaces of all second-order tensors which, as bilinear maps, read

$$\boldsymbol{A} : T^\star\mathscr{B} \times T\mathscr{B} \to \mathbb{R}, \tag{8.1a}$$

$$\boldsymbol{B} : T\mathscr{B} \times T^\star\mathscr{B} \to \mathbb{R}, \tag{8.1b}$$

$$\boldsymbol{T} : T^\star\mathscr{B} \times T^\star\mathscr{B} \to \mathbb{R}, \tag{8.1c}$$

$$\boldsymbol{Q} : T\mathscr{B} \times T\mathscr{B} \to \mathbb{R}, \tag{8.1d}$$

respectively. Let also $([T\mathscr{B}]^2_0, \mathrm{sym})$ and $([T\mathscr{B}]^0_2, \mathrm{sym})$ be, respectively, the subspaces of $[T\mathscr{B}]^2_0$ and $[T\mathscr{B}]^0_2$ of all symmetric, second-order tensors. The elements of $[T\mathscr{B}]^1{}_1$ and $[T\mathscr{B}]_1{}^1$ can be written as linear maps from $T\mathscr{B}$ into itself, and from $T^\star\mathscr{B}$ into itself, respectively, while the elements of $[T\mathscr{B}]^2_0$, and $[T\mathscr{B}]^0_2$ can be written as linear maps from $T^\star\mathscr{B}$ into $T\mathscr{B}$, and from $T\mathscr{B}$ into $T^\star\mathscr{B}$, respectively.

Let us also consider the spaces $[T\mathscr{B}]^2{}_2$ and $[T\mathscr{B}]_2{}^2$ of all fourth-order tensors of the type

$$\mathbb{T} \in [T\mathscr{B}]^2{}_2,\ \ \mathbb{T} : T^\star\mathscr{B} \times T^\star\mathscr{B} \times T\mathscr{B} \times T\mathscr{B} \to \mathbb{R},$$
$$\mathbb{Q} \in [T\mathscr{B}]_2{}^2,\ \ \mathbb{Q} : T\mathscr{B} \times T\mathscr{B} \times T^\star\mathscr{B} \times T^\star\mathscr{B} \to \mathbb{R}.$$

An element of $[T\mathscr{B}]^2{}_2$ can also be represented as a linear map from $[T\mathscr{B}]^2_0$ into $[T\mathscr{B}]^2_0$. Analogously, an element of $[T\mathscr{B}]_2{}^2$ can be represented as a linear map from $[T\mathscr{B}]^0_2$ into $[T\mathscr{B}]^0_2$. For instance, the fourth-order tensor

$$\mathbb{I} : [T\mathscr{B}]^2_0 \to ([T\mathscr{B}]^2_0, \mathrm{sym}), \quad \mathbb{I} = \tfrac{1}{2} \left(\boldsymbol{I} \,\underline{\otimes}\, \boldsymbol{I} + \boldsymbol{I} \,\overline{\otimes}\, \boldsymbol{I} \right), \tag{8.3}$$

where $\boldsymbol{I} : T\mathscr{B} \to T\mathscr{B}$ is the identity tensor in $T\mathscr{B}$, returns the symmetric part of the element of $[T\mathscr{B}]^2_0$ to which it is applied. Given two tensors $\boldsymbol{A}, \boldsymbol{D} \in [T\mathscr{B}]^1{}_1$, the representation of the tensor products $\boldsymbol{A} \underline{\otimes} \boldsymbol{D}$ and $\boldsymbol{A} \overline{\otimes} \boldsymbol{D}$ in index notation reads $[\boldsymbol{A} \underline{\otimes} \boldsymbol{D}]^{AB}{}_{MN} = A^A{}_M D^B{}_N$ and $[\boldsymbol{A} \overline{\otimes} \boldsymbol{D}]^{AB}{}_{MN} = A^A{}_N D^B{}_M$ [57]. Accordingly, in index notation, $\mathbb{I}$ is represented by the expression

$$\mathbb{I}^{AB}{}_{MN} = \tfrac{1}{2} \left(\delta^A{}_M \delta^B{}_N + \delta^A{}_N \delta^B{}_M \right). \tag{8.4}$$

Thus, for every $\boldsymbol{T} \in [T\mathscr{B}]^2_0$, it holds that

$$\mathbb{I} : \boldsymbol{T} = \tfrac{1}{2}\left(\boldsymbol{T} + \boldsymbol{T}^{\mathrm{T}}\right) = \mathrm{sym}(\boldsymbol{T}), \tag{8.5}$$

where the symbol ":" stands for "double contraction". In index notation, it reads $(\mathbb{I} : \boldsymbol{T})^{AB} = \mathbb{I}^{AB}{}_{MN} T^{MN} = [\mathrm{sym}(\boldsymbol{T})]^{AB}$. By definition, $\mathbb{I}$ is the identity fourth-order tensor over the space $([T\mathscr{B}]^2_0, \mathrm{sym})$. From here on, we consider only the restrictions of the fourth-order tensors of $[T\mathscr{B}]^2_0$ onto $([T\mathscr{B}]^2_0, \mathrm{sym})$.

For every $\boldsymbol{T} \in ([T\mathscr{B}]^2_0, \mathrm{sym})$, the fourth-order tensor

$$\begin{aligned} &\mathbb{K}^* : ([T\mathscr{B}]^2_0, \mathrm{sym}) \to ([T\mathscr{B}]^2_0, \mathrm{sym}), \\ &\mathbb{K}^* = \tfrac{1}{3}\boldsymbol{C}^{-1} \otimes \boldsymbol{C} \end{aligned} \tag{8.6}$$

extracts the spherical part of $\boldsymbol{T}$ with respect to the metric $\boldsymbol{C}$, i.e.,

$$\mathbb{K}^* : \boldsymbol{T} = \tfrac{1}{3}\mathrm{tr}(\boldsymbol{C}\boldsymbol{T})\boldsymbol{C}^{-1}. \tag{8.7}$$

The deviatoric part of $\boldsymbol{T}$ with respect to the metric $\boldsymbol{C}$ is obtained by substracting $\mathbb{K}^* : \boldsymbol{T}$ to $\boldsymbol{T}$. This operation can be represented by the application of the fourth-order tensor

$$\begin{aligned} &\mathbb{M}^* : ([T\mathscr{B}]^2_0, \mathrm{sym}) \to ([T\mathscr{B}]^2_0, \mathrm{sym}) \\ &\mathbb{M}^* = \mathbb{I} - \mathbb{K}^*, \end{aligned} \tag{8.8}$$

to $\boldsymbol{T}$ i.e.,

$$\mathbb{M}^* : \boldsymbol{T} = (\mathbb{I} - \mathbb{K}^*) : \boldsymbol{T} = \boldsymbol{T} - \tfrac{1}{3}\mathrm{tr}(\boldsymbol{C}\boldsymbol{T})\boldsymbol{C}^{-1}. \tag{8.9}$$

Clearly, it holds that $\mathrm{tr}\left[\boldsymbol{C}\,(\mathbb{M}^* : \boldsymbol{T})\right] = 0$. We remark that, by their own definition, $\mathbb{K}^*$ and $\mathbb{M}^*$ constitute the partition of unity, i.e., $\mathbb{I} = \mathbb{K}^* + \mathbb{M}^*$.

In analogous manner, we introduce the identity fourth-order tensor over the space $([T\mathscr{B}]^0_2, \mathrm{sym})$, i.e.,

$$\begin{aligned} &\mathbb{I}^{\mathrm{T}} : ([T\mathscr{B}]^0_2, \mathrm{sym}) \to ([T\mathscr{B}]^0_2, \mathrm{sym}), \\ &\mathbb{I}^{\mathrm{T}} = \tfrac{1}{2}\left(\boldsymbol{I}^{\mathrm{T}} \,\underline{\otimes}\, \boldsymbol{I}^{\mathrm{T}} + \boldsymbol{I}^{\mathrm{T}} \,\overline{\otimes}\, \boldsymbol{I}^{\mathrm{T}}\right), \end{aligned} \tag{8.10}$$

where $\boldsymbol{I}^{\mathrm{T}} : T^{\star}\mathscr{B} \to T^{\star}\mathscr{B}$ is the identity tensor in $T^{\star}\mathscr{B}$. For every $\boldsymbol{Q} \in ([T\mathscr{B}]^0_2, \mathrm{sym})$ it holds that

$$\mathbb{I}^{\mathrm{T}} : \boldsymbol{Q} = \tfrac{1}{2}\left(\boldsymbol{Q} + \boldsymbol{Q}^{\mathrm{T}}\right) \equiv \boldsymbol{Q}. \tag{8.11}$$

The spherical and the deviatoric parts of $\boldsymbol{Q}$ with respect to the inverse metric $\boldsymbol{C}^{-1}$ are extracted by employing the fourth-order tensors

$$\mathbb{K}^{*\mathrm{T}} : ([T\mathscr{B}]^0_2, \mathrm{sym}) \to ([T\mathscr{B}]^0_2, \mathrm{sym}),$$

$$\mathbb{K}^{*\mathrm{T}} = \tfrac{1}{3}\boldsymbol{C} \otimes \boldsymbol{C}^{-1}, \tag{8.12}$$

and

$$\begin{aligned} &\mathbb{M}^{*\mathrm{T}} : ([T\mathscr{B}]^0_2, \mathrm{sym}) \to ([T\mathscr{B}]^0_2, \mathrm{sym}), \\ &\mathbb{M}^{*\mathrm{T}} = \mathbb{I}^{\mathrm{T}} - \mathbb{K}^{*\mathrm{T}}, \end{aligned} \tag{8.13}$$

respectively, which are such that

$$\mathbb{K}^{*\mathrm{T}} : \boldsymbol{Q} = \tfrac{1}{3}\mathrm{tr}(\boldsymbol{C}^{-1}\boldsymbol{Q})\boldsymbol{C}, \tag{8.14}$$

$$\mathbb{M}^{*\mathrm{T}} : \boldsymbol{Q} = (\mathbb{I}^{\mathrm{T}} - \mathbb{K}^{*\mathrm{T}}) : \boldsymbol{Q} = \boldsymbol{Q} - \tfrac{1}{3}\mathrm{tr}(\boldsymbol{C}^{-1}\boldsymbol{Q})\boldsymbol{C}. \tag{8.15}$$

In this case, it holds that $\mathrm{tr}\left[\boldsymbol{C}^{-1}\left(\mathbb{M}^{*\mathrm{T}} : \boldsymbol{Q}\right)\right] = 0$.

Finally, we introduce the fourth-order tensor

$$\begin{aligned} &\mathbb{I}^{\sharp *} : ([T\mathscr{B}]^0_2, \mathrm{sym}) \to ([T\mathscr{B}]^2_0, \mathrm{sym}), \\ &\mathbb{I}^{\sharp *} = \tfrac{1}{2}\left(\boldsymbol{C}^{-1} \underline{\otimes}\, \boldsymbol{C}^{-1} + \boldsymbol{C}^{-1} \overline{\otimes}\, \boldsymbol{C}^{-1}\right). \end{aligned} \tag{8.16}$$

For every $\boldsymbol{Q} \in ([T\mathscr{B}]^0_2, \mathrm{sym})$, it holds that

$$\mathbb{I}^{\sharp *} : \boldsymbol{Q} = \boldsymbol{C}^{-1}\boldsymbol{Q}\boldsymbol{C}^{-1}. \tag{8.17}$$

In index notation, Equation (8.17) implies $(\mathbb{I}^{\sharp *} : \boldsymbol{Q})^{AB} = (\boldsymbol{C}^{-1})^{AM} Q_{MN} (\boldsymbol{C}^{-1})^{NB}$, which means that $\mathbb{I}^{\sharp *}$ raises the indices of $\boldsymbol{Q}$ through the inverse metric tensor $\boldsymbol{C}^{-1}$ rather than through $\boldsymbol{G}^{-1}$, the latter being the inverse of the metric tensor $\boldsymbol{G}$ in the undeformed configuration. In analogy with $\mathbb{K}^*$ and $\mathbb{M}^*$, we also consider the fourth-order tensors

$$\begin{aligned} &\mathbb{K}^{\sharp *} : ([T\mathscr{B}]^0_2, \mathrm{sym}) \to ([T\mathscr{B}]^2_0, \mathrm{sym}), \\ &\mathbb{K}^{\sharp *} = \tfrac{1}{3}\boldsymbol{C}^{-1} \otimes \boldsymbol{C}^{-1}, \end{aligned} \tag{8.18a}$$

$$\begin{aligned} &\mathbb{M}^{\sharp *} : ([T\mathscr{B}]^0_2, \mathrm{sym}) \to ([T\mathscr{B}]^2_0, \mathrm{sym}), \\ &\mathbb{M}^{\sharp *} = \mathbb{I}^{\sharp *} - \mathbb{K}^{\sharp *}. \end{aligned} \tag{8.18b}$$

For every $\boldsymbol{Q} \in ([T\mathscr{B}]^0_2, \mathrm{sym})$, we obtain

$$\mathbb{K}^{\sharp *} : \boldsymbol{Q} = \tfrac{1}{3}\mathrm{tr}(\boldsymbol{C}^{-1}\boldsymbol{Q})\boldsymbol{C}^{-1}, \tag{8.19a}$$

$$\mathbb{M}^{\sharp *} : \boldsymbol{Q} = \boldsymbol{C}^{-1}\boldsymbol{Q}\boldsymbol{C}^{-1} - \tfrac{1}{3}\mathrm{tr}(\boldsymbol{C}^{-1}\boldsymbol{Q})\boldsymbol{C}^{-1}. \tag{8.19b}$$

Note that the second-order tensor $\mathbb{M}^{\sharp *} : \boldsymbol{Q}$ is deviatoric in the sense that $\mathrm{tr}[\boldsymbol{C}(\mathbb{M}^{\sharp *} : \boldsymbol{Q})] = 0$.

Bibliography

[1] M. Bongué -Boma, L. Sudak, and S. Federico. "Gradient Dependent Constitutive Laws For A Model Of Microcracked Bodies". In: *International Journal for Multiscale Computational Engineering* 10.6 (2012), pp. 581–597. DOI: `10.1615/intjmultcompeng.2012002781`.

[2] T. Alarcón, H. M. Byrne, and P. K. Maini. "A cellular automaton model for tumour growth in inhomogeneous environment". In: *Journal of Theoretical Biology* 225.2 (Nov. 2003), pp. 257–274. DOI: `10.1016/s0022-5193(03)00244-3`.

[3] M. F. Alhasadi, M. Epstein, and S. Federico. "Eshelby force and power for uniform bodies". In: *Acta Mechanica* 230.5 (Jan. 2019), pp. 1663–1684. DOI: `10.1007/s00707-018-2353-6`.

[4] G. Allaire and M. Briane. "Multiscale convergence and reiterated homogenisation". In: *Proceedings of the Royal Society of Edinburgh: Section A Mathematics* 126.2 (1996), pp. 297–342. DOI: `10.1017/s0308210500022757`.

[5] D. Ambrosi and F. Guana. "Stress-modulated growth". In: *Math. Mech. Solids* 12 (2007), pp. 319–342. DOI: `10.1177/1081286505059739`.

[6] D. Ambrosi, A. Guillou, and E. S. Di Martino. "Stress-modulated remodelling of a non-homogeneous body". In: *Biomechanics and Modeling in Mechanobiology* 1 (2007), pp. 63–76. DOI: `10.1007/s10237-007-0076-z`.

[7] D. Ambrosi and F. Mollica. "On the mechanics of a growing tumor". In: *Int. J. Eng. Sci.* 40 (2002), pp. 1297–1316. DOI: `10.1016/S0020-7225(02)00014-9`.

[8] D. Ambrosi and F. Mollica. "The role of stress in the growth of a multicell spheroid". In: *J. Math. Biol.* 49 (2004), pp. 477–499. DOI: `10.1007/s00285-003-0238-2`.

[9] D. Ambrosi and L. Preziosi. "Cell adhesion mechanisms and stress relaxation in the mechanics of tumours". In: *Biomechanics and Modeling in Mechanobiology* 8 (2009), pp. 397–413. DOI: `10.1007/s10237-008-0145-y`.

[10] D. Ambrosi and L. Preziosi. "On the closure of mass balance models for tumor growth". In: *Mathematical Models and Methods in Applied Sciences* 12.05 (May 2002), pp. 737–754. DOI: 10.1142/s0218202502001878.

[11] D. Ambrosi, L. Preziosi, and G. Vitale. "The insight of mixtures theory for growth and remodeling". In: *Z. Angew. Math. Phys.* 61 (2010), pp. 177–191. DOI: 10.1007/s00033-009-0037-8.

[12] D. Ambrosi, L. Preziosi, and G. Vitale. "The interplay between stress and growth in solid tumors". In: *Mech. Res. Commun.* 42 (2012), pp. 87–91. DOI: 10.1016/j.mechrescom.2012.01.002.

[13] D. Ambrosi et al. "Perspectives on biological growth and remodeling". In: *J. Mech. Phys. Solids* 59(4) (2011), pp. 863–883. DOI: 10.1016/j.jmps.2010.12.011.

[14] D. Ambrosi et al. "Solid tumors are poroelastic solids with a chemo-mechanical feedback on growth". In: *J. Elast.* 129 (2017), pp. 107–124. DOI: 10.1007/s10659-016-9619-9.

[15] L. Anand, O. Aslan, and A. Chester. "A large-deformation gradient theory for elastic-plastic materials: Strain softening and regularization of shear bands". In: *International Journal of Plasticity* 30–31 (2012), pp. 116–143. DOI: 10.1016/j.ijplas.2011.10.002.

[16] R. P. Araujo and D. L. McElwain. "A history of the study of solid tumour growth: the contribution of mathematical modelling". In: *Bulletin of Mathematical Biology* (May 2004). DOI: 10.1016/s0092-8240(03)00126-5.

[17] G. A. Ateshian. "On the theory of reactive mixtures for modeling biological growth". In: *Biomechanics and Modeling in Mechanobiology* 6.6 (Jan. 2007), pp. 423–445. DOI: 10.1007/s10237-006-0070-x.

[18] G. A. Ateshian and J. D. Humphrey. "Continuum Mixture Models of Biological Growth and Remodeling: Past Successes and Future Opportunities". In: *Annual Review of Biomedical Engineering* 14.1 (Aug. 2012), pp. 97–111. DOI: 10.1146/annurev-bioeng-071910-124726.

[19] G. A. Ateshian and J. A. Weiss. "Anisotropic hydraulic permeability under finite deformation". In: *J. Biomech. Engng.* 132 (2010), pp. 111004-1–111004-7. DOI: 10.1115/1.4002588.

[20] J. L. Auriault, C. Boutin, and C. Geindreau. *Homogenization of Coupled Phenomena in Heterogenous Media.* ISTE, Jan. 2009. DOI: 10.1002/978047-\\0612033.

[21] F. Baaijens, C. Bouten, and N. Driessen. "Modeling cartilage remodeling". In: *J. Biomech.* 43 (2010), pp. 166–175. DOI: 10.1016/j.jbiomech.2009.09.022.

[22] N. M. Bachrach, V. C. Mow, and F. Guilak. "Incompressibility of the solid matrix of articular cartilage under high hydrostatic pressures". In: *Journal of Biomechanics* 31 (1998), pp. 445–451. DOI: 10.1016/S0021-9290(98)00035-9.

[23] N. Bakhvalov and G. Panasenko. *Homogenisation: Averaging Processes in Periodic Media*. Springer Netherlands, 1989. DOI: 10.1007/978-94-009-2247-1.

[24] A. D. Bazykin. *Nonlinear dynamics of interacting populations*. World Scientific Publishing, Singapore New Jersey London Hong Kong, 1998. DOI: 10.1142/2284.

[25] J. Bear and Y. Bachmat. *Introduction to Modeling of Transport Phenomena in Porous Media*. Kluwer, Dordrecht, 1990. DOI: 10.1007/978-94-009-1926-6.

[26] N. Bellomo and L. Preziosi. "Modelling and mathematical problems related to tumor evolution and its interaction with the immune system". In: *Mathematical and Computer Modelling* 32.3-4 (Aug. 2000), pp. 413–452. DOI: 10.1016/s0895-7177(00)00143-6.

[27] L. Schreyer Bennethum, M. A. Murad, and J. H. Cushman. "Macroscale thermodynamics and the chemical potential for swelling porous media". In: *Transport in Porous Media* 39.2 (2000), pp. 187–225. DOI: 10.1023/a:1006661330427.

[28] A. Bensoussan, J. L. Lions, and G. Papanicolaou. *Asymptotic Analysis for Periodic Structures*. AMS Chelsea Publishing, 1978. DOI: 10.1115/1.3424588.

[29] Y. Benveniste. "A general interface model for a three-dimensional curved thin anisotropic interphase between two anisotropic media". In: *Journal of the Mechanics and Physics of Solids* 54.4 (Apr. 2006), pp. 708–734. DOI: 10.1016/j.jmps.2005.10.009.

[30] Y. Benveniste and T. Miloh. "Imperfect soft and stiff interfaces in two-dimensional elasticity". In: *Mechanics of Materials* 33.6 (June 2001), pp. 309–323. DOI: 10.1016/s0167-6636(01)00055-2.

[31] X. Bi et al. "A novel method for determination of collagen orientation in cartilage by Fourier transform infrared imaging spectroscopy (FT-IRIS)". In: *Osteoarthr. Cartil.* 13 (2005), pp. 1050–1058. DOI: 10.1016/j.joca.2005.07.008.

[32] M. Bongué Boma, M. Epstein, and S. Federico. "A continuum model of negatively charged rods finely dispersed in a positively charged fluid". In: *Mechanics Research Communications* 38.8 (Dec. 2011), pp. 574–578. DOI: 10.1016/j.mechrescom.2011.08.002.

[33] J. Bonet and R. D. Wood. *Nonlinear Continuum Mechanics for Finite Element Analysis*. Cambridge University Press, New York, 2008. DOI: `10.1017/CBO9780511755446`.

[34] H. C. Brinkman. “A calculation of the viscous force exerted by a flowing fluid on a dense swarm of particles”. In: *Flow, Turbulence and Combustion* 1.1 (Dec. 1949). DOI: `10.1007/bf02120313`.

[35] R. Burridge and J. B. Keller. “Poroelasticity equations derived from microstructure”. In: *The Journal of the Acoustical Society of America* 70.4 (Oct. 1981), pp. 1140–1146. DOI: `10.1121/1.386945`.

[36] H. M. Byrne and M. A. J. Chaplain. “Growth of nonnecrotic tumors in the presence and absence of inhibitors.” In: *Mathematical biosciences* 130 (2 Dec. 1995), pp. 151–181. ISSN: 0025-5564. DOI: `10.1016/0025-5564(94)00117-3`.

[37] H. M. Byrne and D. Drasdo. “Individual-based and continuum models of growing cell populations: a comparison”. In: *Journal of Mathematical Biology* 58.4-5 (Oct. 2009), pp. 657–687. DOI: `10.1007/s00285-008-0212-0`.

[38] H. M. Byrne and L. Preziosi. “Modelling solid tumour growth using the theory of mixtures”. In: *Mathematical Medicine and Biology* 20.4 (Dec. 2003), pp. 341–366. DOI: `10.1093/imammb/20.4.341`.

[39] G. Capriz. *Continua with Microstructure*. Springer, New York, 1989. DOI: `10.1007/978-1-4612-3584-2`.

[40] M. Carfagna and A. Grillo. “The Spherical Design Algorithm in the numerical simulation of biological tissues with statistical fibre-reinforcement”. In: *Computing and Visualization in Science* (2017), pp. 1–28. ISSN: 1433-0369. DOI: `10.1007/s00791-017-0278-6`.

[41] J. J. Casciari, S. V. Sotirchos, and R. M. Sutherland. “Mathematical modelling of microenvironment and growth in EMT6/Ro multicellular tumour spheroids”. In: *Cell Proliferation* 25.1 (Jan. 1992), pp. 1–22. DOI: `10.1111/j.1365-2184.1992.tb01433.x`.

[42] J. J. Casciari, Stratis V. Sotirchos, and R. M. Sutherland. “Variations in tumor cell growth rates and metabolism with oxygen concentration, glucose concentration, and extracellular pH”. In: *Journal of Cellular Physiology* 151.2 (May 1992), pp. 386–394. DOI: `10.1002/jcp.1041510220`.

[43] P. Ponte Castañeda. “The effective mechanical properties of nonlinear isotropic composites”. In: *Journal of the Mechanics and Physics of Solids* 39.1 (1991), pp. 45–71. DOI: `10.1016/0022-5096(91)90030-r`.

[44] P. Cermelli, E. Fried, and S. Sellers. “Configurational stress, yield and flow in rate-independent plasticity”. In: *Proc. R. Soc. Lond. A* 457 (2001), pp. 1447–1467. DOI: `10.1098/rspa.2001.0786`.

[45] M. A. J. Chaplain, L. Graziano, and L. Preziosi. “Mathematical modelling of the loss of tissue compression responsiveness and its role in solid tumour development”. In: *Mathematical Medicine and Biology: A Journal of the IMA* 23.3 (Sept. 2006), pp. 197–229. DOI: `10.1093/imammb/dql009`.

[46] V. Ciancio et al. “Uniform materials and the multiplicative decomposition of the deformation gradient in finite elasto-plasticity”. In: *J. Non-Equilib. Thermodyn.* 33(3) (2008), pp. 199–234. DOI: `10.1515/JNETDY.2008.009`.

[47] P. Ciarletta, D. Ambrosi, and G. A. Maugin. “Configurational forces for growth and shape regulations in morphogenesis”. In: *Bulletin of the Polish Academy of Sciences –Technical Sciences* 60(2) (2012), pp. 253–257. DOI: `10.2478/v10175-012-0034-5`.

[48] P. Ciarletta, D. Ambrosi, and G. A. Maugin. “Mass transport in morphogenetic processes: A second gradient theory for volumetric growth and material remodeling”. In: *J. Mech. Phys. Solids* 60 (2012), pp. 432–450. DOI: `10.1016/j.jmps.2011.11.011`.

[49] P. Ciarletta, M. Destrade, and A. L. Gower. “On residual stresses and homeostasis: an elastic theory of functional adaptation in living matter”. In: *Scientific Reports* 6.1 (Apr. 2016). DOI: `10.1038/srep24390`.

[50] P. Ciarletta and G. A. Maugin. “Elements of a finite strain-gradient thermomechanical theory for material growth and remodeling”. In: *Int. J. Non-Lin. Mech.* 46 (2011), pp. 1341–1346. DOI: `10.1016/j.ijnonlinmec.2011.07.004`.

[51] P. Ciarletta et al. “Mechano-transduction in tumour growth modelling”. In: *Eur. Phys. J. E* 36 (2013), p. 23. DOI: `10.1140/epje/i2013-13023-2`.

[52] D. Cioranescu and P. Donato. *An introduction to homogenization.* Oxford University Press, 1999.

[53] S. Cleja-Tigoiu and G. A. Maugin. “Eshelby’s stress tensors in finite elastoplasticity”. In: *Acta Mechanica* 139.1-4 (Mar. 2000), pp. 231–249. DOI: `10.1007/bf01170191`.

[54] J. Collis et al. “Effective equations governing an active poroelastic medium”. In: *Proceedings of the Royal Society A: Mathematical, Physical and Engineering Sciences* 473.2198 (Feb. 2017), p. 20160755. DOI: `10.1098/rspa.2016.0755`.

[55] S. C. Cowin. “How is a tissue built?” In: *J. Biomech. Eng.* 122 (2000), pp. 553–569. DOI: `10.1115/1.1324665`.

[56] E. Crevacore, S. Di Stefano, and A. Grillo. “Coupling among deformation, fluid flow, structural reorganisation and fibre reorientation in fibre-reinforced, transversely isotropic biological tissues”. In: *International Journal of Non-Linear Mechanics* 111 (May 2019), pp. 1–13. DOI: 10.1016/j.ijnonlinmec.2018.08.022.

[57] A. Curnier, Q. C. He, and P. Zysset. “Conewise linear elastic materials”. In: *J. Elasticity* 37 (1995), pp. 1–38. DOI: 10.1007/BF00043417.

[58] F. dell’Isola and L. Placidi. “Variational principles are a powerful tool also for formulating field theories”. In: *Variational Models and Methods in Solid and Fluid Mechanics*. Ed. by F. dell’Isola and S. Gavrilyuk. Springer-Verlag, 2011, pp. 1–15. DOI: 10.1007/978-3-7091-0983-0_1.

[59] M. Destrade et al. “At least three invariants are necessary to model the mechanical response of incompressible, transversely isotropic materials”. In: *Comput. Mech.* 52 (2013), pp. 959–969. DOI: 10.1007/s00466-013-0857-4.

[60] A. Di Carlo and S. Quiligotti. “Growth and balance”. In: *Mechanics Research Communications* 29.6 (Nov. 2002), pp. 449–456. DOI: 10.1016/s0093-6413(02)00297-5.

[61] S. Di Stefano et al. “Anelastic reorganisation of fibre-reinforced biological tissues”. In: *Computing and Visualization in Science* 20.3-6 (June 2019), pp. 95–109. DOI: 10.1007/s00791-019-00313-1.

[62] S. Di Stefano et al. “Self-influenced growth through evolving material inhomogeneities”. In: *International Journal of Non-Linear Mechanics* 106 (Nov. 2018), pp. 174–187. DOI: 10.1016/j.ijnonlinmec.2018.08.003.

[63] H. J. G. Diersch and O. Kolditz. “Variable-density flow and transport in porous media: approaches and challenges”. In: *Advances in Water Resources* 25.8-12 (Aug. 2002), pp. 899–944. DOI: 10.1016/s0309-1708(02)00063-5.

[64] N.J.B. Driessen et al. “A computational model for collagen fibre remodelling in the arterial wall”. In: *J. Theor. Biol.* 226 (2004), pp. 53–64. DOI: 10.1016/j.jtbi.2003.08.004.

[65] W. Ehlers et al. “Inverse poroelasticity as a fundamental mechanism in biomechanics and mechanobiology”. In: *Nat. Commun.* 1002(8) (2017), pp. 1–10. DOI: 10.1038/s41467-017-00801-3.

[66] M. Epstein. “Self-Driven continuous Dislocations and Growth”. In: *Mechanics of Material Forces. Advances in Mechanics and Mathematics*. Ed. by Maugin G.A. Steinmann P. Vol. 11. Springer, Boston, MA, 2005, pp. 129–139. DOI: 10.1007/0-387-26261-x_13.

[67] M. Epstein. *The geometric language of continuum mechanics*. Cambridge University Press, 2010. DOI: 10.1017/CBO9780511762673.

[68] M. Epstein. “The split between remodelling and aging”. In: *International Journal of Non-Linear Mechanics* 44.6 (July 2009), pp. 604–609. DOI: 10.1016/j.ijnonlinmec.2009.02.005.

[69] M. Epstein and M. Elżanowski. *Material Inhomogeneities and their Evolution — A Geometric Approach*. 1st ed. Springer-Verlag Berlin Heidelberg, 2007. DOI: 10.1007/978-3-540-72373-8.

[70] M. Epstein and G. A. Maugin. “On the geometrical material structure of anelasticity”. In: *Acta Mechanica* 115.1-4 (Mar. 1996), pp. 119–131. DOI: 10.1007/bf01187433.

[71] M. Epstein and G. A. Maugin. “The energy-momentum tensor and material uniformity in finite elasticity”. In: *Acta Mechanica* 83 (1990), pp. 127–133. DOI: 10.1007/BF01172974.

[72] M. Epstein and G. A. Maugin. “Thermomechanics of volumetric growth in uniform bodies”. In: *International Journal of Plasticity* 16.7-8 (June 2000), pp. 951–978. DOI: 10.1016/s0749-6419(99)00081-9.

[73] J. D. Eshelby. “The elastic energy-momentum tensor”. In: *J. Elasticity* 5 (1975), pp. 321–35. DOI: 10.1007/BF00126994.

[74] J. D. Eshelby. “The force on an elastic singularity”. In: *Philos. T. R. Soc. A* 244A (1951), pp. 87–112. DOI: 10.1098/rsta.1951.0016.

[75] Z. Fang et al. “Homogenization of heterogeneous tissue scaffold: A comparison of mechanics, asymptotic homogenization, and finite element approach”. In: *Applied Bionics and Biomechanics* 2.1 (Jan. 2005), pp. 17–29. DOI: 10.1533/abbi.2004.0002.

[76] T. Farquhar, P. R. Dawson, and P. A. Torzilli. “A Microstructural Model for the Anisotropic Drained Stiffness of Articular Cartilage”. In: *Journal of Biomechanical Engineering* 112.4 (Nov. 1990), pp. 414–425. DOI: 10.1115/1.2891205.

[77] S. Federico. “Covariant formulation of the tensor algebra of non-linear elasticity”. In: *Int. J. Nonlinear Mech.* 47 (2012), pp. 273–284. DOI: 10.1016/j.ijnonlinmec.2011.06.007.

[78] S. Federico, M. F. Alhasadi, and A. Grillo. “Eshelby’s inclusion theory in light of Noether’s theorem”. In: *Mathematics and Mechanics of Complex Systems* 7.3 (Dec. 2019), pp. 247–285. DOI: 10.2140/memocs.2019.7.247.

[79] S. Federico and T. C. Gasser. “Non-Linear Elasticity of Biological Tissues with Statistical Fibre Orientation”. In: *Journal of the Royal Society Interface* 7 (2010), pp. 955–966. DOI: 10.1098/rsif.2009.0502.

[80] S. Federico and A. Grillo. “Elasticity and Permeability of Porous Fibre-Reinforced Materials Under Large Deformations”. In: *Mechanics of Materials* 44 (2012), pp. 58–71. DOI: 10.1016/j.mechmat.2011.07.010.

[81] S. Federico and A. Grillo. “Linear Elastic Composites with Statistically Oriented Spheroidal Inclusions”. In: *Micromechanics and Nanomechanics of Composite Solids*. Springer International Publishing, July 2017, pp. 307–346. DOI: 10.1007/978-3-319-52794-9_11.

[82] S. Federico and W. Herzog. “On the Anisotropy and Inhomogeneity of Permeability in Articular Cartilage”. In: *Biomechanics and Modeling in Mechanobiology* 7 (2008), pp. 367–378. DOI: 10.1007/s10237-007-0091-0.

[83] S. Federico and W. Herzog. “On the Permeability of Fibre-Reinforced Porous Materials”. In: *International Journal of Solids and Structures* 45 (2008), pp. 2160–2172. DOI: 10.1016/j.ijsolstr.2007.11.014.

[84] S. Federico and W. Herzog. “Towards an Analytical Model of Soft Tissues”. In: *Journal of Biomechanics* 41 (2008), pp. 3309–3313. DOI: 10.1016/j.jbiomech.2008.05.039.

[85] S. Federico et al. “A transversely isotropic, transversely homogeneous microstructural- statistical model of articular cartilage”. In: *Journal of Biomechanics* 38 (2005), pp. 2008–2018. DOI: 10.1016/j.jbiomech.2004.09.020.

[86] G. Forgacs et al. “Viscoelastic Properties of Living Embryonic Tissues: a Quantitative Study”. In: *Biophysical Journal* 74 (1998), pp. 2227–2234. DOI: 10.1016/S0006-3495(98)77932-9.

[87] R.A. Foty et al. “Surface tensions of embryonic tissues predict their mutual envelopment behavior”. In: *Development* 122 (1996), pp. 1611–1620.

[88] A. J. Sophia Fox, A. Bedi, and S. A. Rodeo. “The Basic Science of Articular Cartilage: Structure, Composition, and Function”. In: *Sports Health: A Multidisciplinary Approach* 1.6 (Nov. 2009), pp. 461–468. DOI: 10.1177/1941738109350438.

[89] Hunter J.H. Fry. “The interlocked stresses of articular cartilage”. In: *British Journal of Plastic Surgery* 27.4 (Oct. 1974), pp. 363–364. DOI: 10.1016/0007-1226(74)90040-x.

[90] H. Fujie, S. Morishita, and S. Yarimitsu. “Effect of collagen-induced residual stress on the frictional property of articular cartilage”. In: *Biosurface and Biotribology* 4.2 (June 2018), pp. 68–71. DOI: 10.1049/bsbt.2018.0008.

[91] Y. C. Fung. *Biomechanics. Motion, flow, stress, and growth.* Springer, New York, 1990. DOI: 10.1007/978-1-4419-6856-2.

[92] Y. C. Fung. "Stress, Strain, growth, and remodeling of living organisms". In: *Theoretical, Experimental, and Numerical Contributions to the Mechanics of Fluids and Solids*. Birkhäuser Basel, 1995, pp. 469–482. DOI: 10.1007/978-3-0348-9229-2_25.

[93] Y. C. Fung. "What are the residual stresses doing in our blood vessels?" In: *Annals of Biomedical Engineering* 19.3 (May 1991), pp. 237–249. DOI: 10.1007/bf02584301.

[94] W. Jones G and S. J. Chapman. "Modeling Growth in Biological Materials". In: *SIAM Review* 54.1 (Jan. 2012), pp. 52–118. DOI: 10.1137/080731785.

[95] J. F. Ganghoffer. "A kinematically and thermodynamically consistent volumetric growth model based on the stress-free configuration". In: *International Journal of Solids and Structures* 50.20-21 (Oct. 2013), pp. 3446–3459. DOI: 10.1016/j.ijsolstr.2013.06.011.

[96] J. F. Ganghoffer. "On Eshelby tensors in the context of the thermodynamics of open systems: application to volumetric growth". In: *International Journal of Engineering Science* 48(12) (2010), pp. 2081–2098. DOI: 10.1016/j.ijengsci.2010.04.003.

[97] D. Garcia et al. "A three-dimensional elastic plastic damage constitutive law for bone tissue". In: *Biomech. Model. Mechanobiol.* 8(2) (2009), pp. 149–165. DOI: 10.1007/s10237-008-0125-2.

[98] K. Garikipati et al. "A continuum treatment of growth in biological tissue: the coupling of mass transport and mechanics". In: *J. Mech. Phys. Solids* 52 (2004), pp. 1595–1625. DOI: 10.1016/j.jmps.2004.01.004.

[99] K. Garikipati et al. "Biological remodelling: Stationary energy, configurational change, internal variables and dissipation". In: *Journal of the Mechanics and Physics of Solids* 54 (2006), pp. 1493–1515. DOI: 10.1016/j.jmps.2005.11.011.

[100] T. C. Gasser, R. W. Ogden, and G. A. Holzapfel. "Hyperelastic modelling of arterial layers with distributed collagen fibre orientations". In: *Journal of the Royal Society Interface* 3 (2006), pp. 15–35. DOI: 10.1098/rsif.2005.0073.

[101] M. Gei, F. Genna, and D. Bigoni. "An Interface Model for the Periodontal Ligament". In: *Journal of Biomechanical Engineering* 124.5 (2002), p. 538. DOI: 10.1115/1.1502664.

[102] G. Giantesio, A. Musesti, and D. Riccobelli. "A Comparison Between Active Strain and Active Stress in Transversely Isotropic Hyperelastic Materials". In: *Journal of Elasticity* 137.1 (Dec. 2018), pp. 63–82. DOI: 10.1007/s10659-018-9708-z.

[103] Thomas Gibson and W. Brian Davis. "The distortion of autogenous cartilage grafts: Its cause and prevention". In: *British Journal of Plastic Surgery* 10 (1957), pp. 257–274. DOI: 10.1016/s0007-1226(57)80042-3.

[104] C. Giverso and L. Preziosi. "Modelling the compression and reorganization of cell aggregates". In: *Math. Med. Biol.* 29(2) (2012), pp. 181–204. DOI: 10.1093/imammb/dqr008.

[105] C. Giverso, M. Scianna, and A. Grillo. "Growing avascular tumours as elasto-plastic bodies by the theory of evolving natural configurations". In: *Mech. Res. Commun.* 68 (2015), pp. 31–39. DOI: http://dx.doi.org/10.1016/j.mechrescom.2015.04.004.

[106] A. Goriely. *The Mathematics and Mechanics of Biological Growth.* Springer New York, 2016. DOI: 10.1007/978-0-387-87710-5.

[107] A. Grillo, M. Carfagna, and S. Federico. "An Allen–Cahn approach to the remodelling of fibre-reinforced anisotropic materials". In: *Journal of Engineering Mathematics* 109.1 (Apr. 2018), pp. 139–172. ISSN: 1573-2703. DOI: 10.1007/s10665-017-9940-8.

[108] A. Grillo, M. Carfagna, and S. Federico. "Non-Darcian flow in fibre-reinforced biological tissues". In: *Meccanica* 52 (2017), pp. 3299–3320. DOI: 10.1007/s11012-017-0679-0.

[109] A. Grillo, M. Carfagna, and S. Federico. "The Darcy-Forchheimer law for modelling fluid flow in biological tissues". In: *Theoret. Appl. Mech. TEOPM7* 41(4) (2014), pp. 283–322. DOI: 10.2298/TAM1404281G.

[110] A. Grillo, S. Federico, and G. Wittum. "Growth, mass transfer, and remodeling in fiber-reinforced, multi-constituent materials". In: *International Journal of Non-Linear Mechanics* 47 (2012), pp. 388–401. DOI: 10.1016/j.ijnonlinmec.2011.09.026.

[111] A. Grillo, R. Prohl, and G. Wittum. "A generalised algorithm for anelastic processes in elastoplasticity and biomechanics". In: *Mathematics and Mechanics of Solids* 22(3) (2017), pp. 502–527. DOI: 10.1177/1081286515598661.

[112] A. Grillo, R. Prohl, and G. Wittum. "A poroplastic model of structural reorganisation in porous media of biomechanical interest". In: *Continuum Mechanics and Thermodynamics* 28 (2016), pp. 579–601. DOI: 10.1007/s00161-015-0465-y.

[113] A. Grillo, S. Di Stefano, and S. Federico. "Growth and remodelling from the perspective of Noether's theorem". In: *Mechanics Research Communications* 97 (Apr. 2019), pp. 89–95. DOI: 10.1016/j.mechrescom.2019.04.012.

[114] A. Grillo et al. “A study of growth and remodeling in isotropic tissues, based on the Anand-Aslan-Chester theory of strain-gradient plasticity”. In: *GAMM-Mitteilungen* (May 2019), e201900015. DOI: `10.1002/gamm.201900015`.

[115] A. Grillo et al. “Mass transport in porous media with variable mass”. In: *Numerical Analysis of Heat and Mass Transfer in Porous Media*. Ed. by J. M. P. Q. Delgado et al. Berlin, Heidelberg, Germany: Springer-Verlag, 2012, pp. 27–61. DOI: `10.1007/978-3-642-30532-0-2`.

[116] A. Grillo et al. “Remodelling in statistically oriented fibre-reinforced materials and biological tissues”. In: *Math. Mech. Solids* 20(9) (2015), pp. 1107–1129. DOI: `10.1177/1081286513515265`.

[117] A. Grillo et al. “Restoration of the symmetries broken by reversible growth in hyperelastic bodies”. In: *Theoret. Appl. Mech.* 30(4) (2003), pp. 311–331. DOI: `10.2298/TAM0304311G`.

[118] M. Grynpas. “Age and disease-related changes in the mineral of bone”. In: *Calcified Tissue International* 53.S1 (Feb. 1993), S57–S64. DOI: `10.1007/bf01673403`.

[119] A. Guerra et al. “Phase transitions in tumor growth VI: Epithelial–Mesenchymal transition”. In: *Physica A: Statistical Mechanics and its Applications* 499 (June 2018), pp. 208–215. DOI: `10.1016/j.physa.2018.01.040`.

[120] A. Guillou and R. W. Ogden. “Growth in Soft Biological Tissue and Residual Stress Development”. In: *Mechanics of Biological Tissue*. Springer-Verlag, 2006, pp. 47–62. DOI: `10.1007/3-540-31184-x_4`.

[121] R. Guinovart-Díaz et al. “Effective elastic properties of a periodic fiber reinforced composite with parallelogram-like arrangement of fibers and imperfect contact between matrix and fibers”. In: *International Journal of Solids and Structures* 50.13 (June 2013), pp. 2022–2032. DOI: `10.1016/j.ijsolstr.2013.02.019`.

[122] M. E. Gurtin. “Generalized Ginzburg-Landau and Cahn-Hilliard equations based on a microforce balance”. In: *Physica D* 92 (1994), pp. 178–192. DOI: `10.1016/0167-2789(95)00173-5`.

[123] M. E. Gurtin and L. Anand. “A theory of strain-gradient plasticity for isotropic, plastically irrotational materials. Part II: Finite deformations”. In: *International Journal of Plasticity* 21 (2005), pp. 2297–2318. DOI: `10.1016/j.ijplas.2005.01.006`.

[124] M. E. Gurtin, E. Fried, and L. Anand. *The Mechanics and Thermodynamics of Continua*. Cambridge University Press, 2010. DOI: `10.1017/CBO9780511762956`.

[125] D. A. Hammer and M. Tirrell. “Biological Adhesion at Interfaces”. In: *Annual Review of Materials Science* 26.1 (Aug. 1996), pp. 651–691. DOI: 10.1146/annurev.ms.26.080196.003251.

[126] R. H. Hardin and N. J. A. Sloane. “McLaren’s improved Snub cube and other new spherical designs in three dimensions”. In: *Discrete Comput. Geom.* 15 (1996), pp. 429–441. DOI: 10.1007/BF02711518.

[127] I. Hariton et al. “Stress-driven collagen fiber remodeling in arterial walls”. In: *Biomech. Model. Mechanobiol.* 6(3) (2007), pp. 163–175. DOI: 10.1007/s10237-006-0049-7.

[128] Z. Hashin. “Thermoelastic properties of fiber composites with imperfect interface”. In: *Mechanics of Materials* 8.4 (Feb. 1990), pp. 333–348. DOI: 10.1016/0167-6636(90)90051-g.

[129] Z. Hashin. “Thin interphase/imperfect interface in elasticity with application to coated fiber composites”. In: *Journal of the Mechanics and Physics of Solids* 50.12 (Dec. 2002), pp. 2509–2537. DOI: 10.1016/s0022-5096(02)00050-9.

[130] K. Hashlamoun and S. Federico. “Transversely isotropic higher-order averaged structure tensors”. In: *Z. Angew. Math. Phys.* 68(4) (2017), pp. 113–145. DOI: 10.1007/s00033-017-0830-8.

[131] K. Hashlamoun, A. Grillo, and S. Federico. “Efficient evaluation of the material response of tissues reinforced by statistically oriented fibres”. In: *Z. Angew. Math. Phys.* 67 (2016), pp. 113–145. DOI: 10.1007/s10237-006-0049-7.

[132] S. M. Hassanizadeh. “Derivation of basic equations of mass Transp. Porous Med., Part 2. Generalized Darcy’s and Fick’s laws”. In: *Adv. Water Resour.* 9 (1986), pp. 207–222. DOI: 10.1016/0309-1708(86)90025-4.

[133] P. Haupt. *Continuum Mechanics and Theory of Materials.* Springer, 2000. DOI: 10.1007/978-3-662-04775-0.

[134] H. Hedlund et al. “Stereologic studies on collagen in bovine articular cartilage”. In: *APMIS* 101.1-6 (Jan. 1993), pp. 133–140. DOI: 10.1111/j.1699-0463.1993.tb00092.x.

[135] G. Helmlinger et al. “Solid stress inhibits the growth of multicellular tumor spheroids”. In: *Nature Biotechnology* 15.8 (Aug. 1997), pp. 778–783. DOI: 10.1038/nbt0897-778.

[136] E. L. Hill. “Hamilton’s principle and the conservation theorems of mathematical physics”. In: *Reviews of Modern Physics* 23(3) (1951), pp. 253–260. DOI: 10.1103/RevModPhys.23.253.

[137] M. H. Holmes. *Introduction to perturbation methods*. Ed. by New York. Springer Science & Business Media Springer-Verlag. 1995. DOI: 10.1007/978-1-4614-5477-9.

[138] M. H. Holmes and V. C. Mow. “The nonlinear characteristics of soft gels and hydrated connective tissues in ultrafiltration.” In: *Journal of biomechanics* 23 (11 1990), pp. 1145–1156. ISSN: 0021-9290. DOI: 10.1016/0021-9290(90)90007-P.

[139] G. A. Holzapfel, T. C. Gasser, and R. W. Ogden. “A new constitutive framework for arterial wall mechanics and a comparative study of material models”. In: *J. Elast.* 61(1-3) (2000), pp. 1–48. DOI: 10.1023/A:1010835316564.

[140] G. A. Holzapfel and R. W. Ogden. “On Fiber Dispersion Models: Exclusion of Compressed Fibers and Spurious Model Comparisons”. In: *J. Elast.* 129(1-2) (2017), pp. 49–68. DOI: 10.1007/s10659-016-9605-2.

[141] M. Hori and S. Nemat-Nasser. “On two micromechanics theories for determining micro–macro relations in heterogeneous solids”. In: *Mechanics of Materials* 31.10 (Oct. 1999), pp. 667–682. DOI: 10.1016/s0167-6636(99)00020-4.

[142] J. D. Humphrey. “Towards a Theory of Vascular Growth and Remodeling”. In: *Mechanics of Biological Tissue*. Ed. by Holzapfel G.A. and Ogden R.W. Springer-Verlag, 2006, pp. 3–15. DOI: 10.1007/3-540-31184-x_1.

[143] J. M. Huyghe, R. Van Loon, and F.T.P. Baaijens. “Fluid-solid mixtures and electrochemomechanics: the simplicity of Lagrangian mixture theory”. In: *Clinics* 23.2-3 (Dec. 2004). DOI: 10.1590/s1807-03022004000200008.

[144] R. K. Jain, J. D. Martin, and T. Stylianopoulos. “The role of mechanical forces in tumor growth and therapy”. In: *Annual Review of Biomedical Engineering* 16 (2014), pp. 321–346. DOI: 10.1146/annurev-bioeng-071813-105259.

[145] A. Javili, P. Steinmann, and E. Kuhl. “A novel strategy to identify the critical conditions for growth-induced instabilities”. In: *Journal of the Mechanical Behavior of Biomedical Materials* 29 (Jan. 2014), pp. 20–32. DOI: 10.1016/j.jmbbm.2013.08.017.

[146] A. R. A. Khaled and K. Vafai. “The role of porous media in modeling flow and heat transfer in biological tissues”. In: *International Journal of Heat and Mass Transfer* 46.26 (Dec. 2003), pp. 4989–5003. DOI: 10.1016/s0017-9310(03)00301-6.

[147] A. Klarbring, T. Olsson, and J. Stålhand. “Theory of residual stresses with application to an arterial geometry”. In: *Arch. Mech.* 59(4–5) (2007), pp. 341–364.

[148] E. Kröner. "Allgemeine Kontinuumstheorie der Versetzungen und Eigenspannungen". In: *Archive for Rational Mechanics and Analysis* 4.1 (Jan. 1959), pp. 273–334. DOI: `10.1007/bf00281393`.

[149] E. Kuhl and G. A. Holzapfel. "A continuum model for remodeling in living structures". In: *Journal of Materials Science* 42.21 (July 2007), pp. 8811–8823. DOI: `10.1007/s10853-007-1917-y`.

[150] C. Lanczos. *The Variational Principles of Mechanics*. Dover Publications, Inc., Mineola, New York, 1970.

[151] Y. Lanir. "Constitutive equations for fibrous connective tissues". In: *Journal of Biomechanics* 16 (1983), pp. 1–12. DOI: `10.1016/0021-9290(83)90041-6`.

[152] M. Lefik and B. Schrefler. "FE modelling of a boundary layer corrector for composites using the homogenization theory". In: *Engineering Computations* 13.6 (Sept. 1996), pp. 31–42. DOI: `10.1108/02644409610128391`.

[153] A. Leyrat, A. Duperray, and C. Verdier. "Adhesion Mechanisms in Cancer Metastasis". In: *Cancer Modelling and Simulation*. CRC Press, June 2003. DOI: `10.1201/9780203494899.ch8`.

[154] W.J. Lin et al. "Growth and remodeling with application to abdominal aortic aneurysms". In: *J. Eng. Math.* In press (2017), pp. 1–25. DOI: `https://doi.org/10.1007/s10665-017-9915-9`.

[155] I. S. Liu. *Continuum Mechanics*. Springer, 2002. DOI: `10.1007/978-3-662-05056-9`.

[156] I. S. Liu. "Method of Lagrange multipliers for exploitation of the entropy principle". In: *Archive Rational Mech. Anal.* 46 (1972), pp. 131–148. DOI: `10.1007/BF00250688`.

[157] B. Loret and F.M.F. Simões. "A framework for deformation, generalized diffusion, mass transfer and growth in multi-species multi-phase biological tissues". In: *Eur. J. Mech. A* 24 (2005), pp. 757–781. DOI: `10.1016/j.euromechsol.2005.05.005`.

[158] B. Loret and F. M. F. Simões. "Articular cartilage with intra- and extrafibrillar waters: a chemo-mechanical model". In: *Mechanics of Materials* 36.5-6 (May 2004), pp. 515–541. DOI: `10.1016/s0167-6636(03)00074-7`.

[159] Y. Lu and T. Lekszycki. "Modelling of bone fracture healing: influence of gap size and angiogenesis into bioresorbable bone substitute". In: *Mathematics and Mechanics of Solids* 0.0 (2016). DOI: `10.1177/1081286516653272`.

[160] V.A. Lubarda and A. Hoger. "On the mechanics of solids with a growing mass". In: *International Journal of the Mechanics and Physics of Solids* 39 (2002), pp. 4627–4664. DOI: `10.1016/S0020-7683(02)00352-9`.

[161] J. Lubliner. *Plasticity Theory*. Dover Publications, Inc., Mineola, New York, 2008. DOI: 10.1115/1.2899459.

[162] V. Lukeš and E. Rohan. "Microstructure based two-scale modelling of soft tissues". In: *Mathematics and Computers in Simulation* 80.6 (Feb. 2010), pp. 1289–1301. DOI: 10.1016/j.matcom.2009.02.016.

[163] D. Lukkassen and G. W. Milton. "On hierarchical structures and reiterated homogenization". In: *Function Spaces, Interpolation Theory and Related Topics*. 2002.

[164] P. Macklin et al. "Multiscale modelling and nonlinear simulation of vascular tumour growth". In: *Journal of Mathematical Biology* 58.4-5 (Sept. 2009), pp. 765–798. DOI: 10.1007/s00285-008-0216-9.

[165] J.E. Marsden and T.J.R. Hughes. *Mathematical Foundations of Elasticity*. Dover Publications, Inc., Mineola, New York, 1983.

[166] P. Mascheroni et al. "An avascular tumor growth model based on porous media mechanics and evolving natural states". In: *Mathematics and Mechanics of Solids* 23.4 (June 2018), pp. 686–712. DOI: 10.1177/1081286517711217.

[167] P. Mascheroni et al. "Predicting the growth of glioblastoma multiforme spheroids using a multiphase porous media model". In: *Biomech. Model. Mechanobiol.* 15.5 (Jan. 2016), pp. 1215–1228. DOI: 10.1007/s10237-015-0755-0.

[168] G. A. Maugin. *Material Inhomogeneities in Elasticity*. CRC Press, Boca Raton, FL, USA, 1993. DOI: 10.1007/978-1-4899-4481-8.

[169] G. A. Maugin and M. Epstein. "Geometrical material structure of elastoplasticity". In: *Int. J. Plasticity* 14(1-3) (1998), pp. 109–115. DOI: 10.1016/S0749-6419(97)00043-0.

[170] A. V. Melnik, H. B. Da Rocha, and A. Goriely. "On the modeling of fiber dispersion in fiber-reinforced elastic materials". In: *Int. J. Nonlinear Mech.* 75 (2015), pp. 92–106. DOI: http://dx.doi.org/10.1016/j.ijnonlinmec.2014.10.006.

[171] A. Menzel. "A fibre reorientation model for orthotropic multiplicative growth. Configurational driving stresses, kinematics-based reorientation and algorithmic aspects". In: *Biomechan. Model. Mechanobiol.* 6(5) (2007), pp. 303–320. DOI: 10.1007/s10237-006-0061-y.

[172] A. Menzel. "Modelling of anisotropic growth in biological tissues — A new approach and computational aspects". In: *Biomechan. Model. Mechanobiol.* 3 (2005), pp. 147–171. DOI: 10.1007/s10237-004-0047-6.

[173] A. Menzel and E. Kuhl. “Frontiers in growth and remodeling”. In: *Mechanics Research Communications* 42 (2012), pp. 1–14. DOI: 10.1016/j.mechrescom.2012.02.007.

[174] J. Merodio. “On constitutive equations for fiber-reinforced nonlinearly viscoelastic solids”. In: *Mech. Res. Commun.* 33 (2006), pp. 764–770. DOI: 10.1016/j.mechrescom.2006.03.009.

[175] J. Merodio, R. W. Ogden, and J. Rodríguez. “The influence of residual stress on finite deformation elastic response”. In: *Int. J. Nonliner Mech.* 56 (2013), pp. 43–49. DOI: 10.1016/j.ijnonlinmec.2013.02.010.

[176] M. Mićunović. *Thermomechanics of Viscoplasticity*. Springer New York, 2009. DOI: 10.1007/978-0-387-89490-4.

[177] G. W. Milton. *The Theory of Composites*. Ed. by Cambridge University Press . 2002. DOI: 10.1017/CBO9780511613357.

[178] M. Minozzi et al. “Growth-induced compatible strains”. In: *Math. Mech. Solids* 22.1 (Aug. 2017), pp. 62–71. DOI: 10.1177/1081286515570510.

[179] J. Mollenhauer et al. “X-Ray Diffraction of the Molecular Substructure of Human Articular Cartilage”. In: *Connective Tissue Research* 44 (2003), pp. 201–207. DOI: 10.1080/03008200390244005.

[180] F. Mpekris et al. “Stress-mediated progression of solid tumors: effect of mechanical stress on tissue oxygenation, cancer cell proliferation, and drug delivery”. In: *Biomech. Model. Mechanobiol.* 14.6 (May 2015), pp. 1391–1402. DOI: 10.1007/s10237-015-0682-0.

[181] P. Neff. “A finite-strain elastic-plastic Cosserat theory for polycrystals with grain rotations”. In: *Int. J. Eng. Sci.* 44 (2006), pp. 574–594. DOI: 10.1016/j.ijengsci.2006.04.002.

[182] R. D. O’Dea, S. L. Waters, and H. M. Byrne. “A multiphase model for tissue construct growth in a perfusion bioreactor”. In: *Mathematical Medicine and Biology* 27.2 (Oct. 2010), pp. 95–127. DOI: 10.1093/imammb/dqp003.

[183] T. Olsson and A. Klarbring. “Residual stresses in soft tissue as a consequence of growth and remodeling: application to an arterial geometry”. In: *Eur. J. Mech. A* 27(6) (2008), pp. 959–974. DOI: 10.1016/j.euromechsol.2007.12.006.

[184] G. Panasenko. *Multi-Scale Modelling for Structures and Composites*. Springer Verlag GMBH, Feb. 9, 2005. 398 pp. DOI: 10.1007/1-4020-2982-9.

[185] W. J. Parnell et al. “Analytical methods to determine the effective mesoscopic and macroscopic elastic properties of cortical bone”. In: *Biomechanics and Modeling in Mechanobiology* 11.6 (Nov. 2011), pp. 883–901. DOI: 10.1007/s10237-011-0359-2.

[186] R Penta et al. “Can a continuous mineral foam explain the stiffening of aged bone tissue? A micromechanical approach to mineral fusion in musculoskeletal tissues”. In: *Bioinspiration & Biomimetics* 11.3 (May 2016), p. 035004. DOI: 10.1088/1748-3190/11/3/035004.

[187] R. Penta, D. Ambrosi, and R. J. Shipley. “Effective governing equations for poroelastic growing media”. In: *The Quarterly Journal of Mechanics and Applied Mathematics* 67.1 (Jan. 2014), pp. 69–91. DOI: 10.1093/qjmam/hbt024.

[188] R. Penta and A. Gerisch. “An Introduction to Asymptotic Homogenization”. In: *Lecture Notes in Computational Science and Engineering*. Springer International Publishing, 2017, pp. 1–26. DOI: 10.1007/978-3-319-73371-5_1.

[189] R. Penta and A. Gerisch. “Investigation of the potential of asymptotic homogenization for elastic composites via a three-dimensional computational study”. In: *Computing and Visualization in Science* 17.4 (Aug. 2015), pp. 185–201. DOI: 10.1007/s00791-015-0257-8.

[190] R. Penta and J. Merodio. “Homogenized modeling for vascularized poroelastic materials”. In: *Meccanica* 52.14 (Feb. 2017), pp. 3321–3343. DOI: 10.1007/s11012-017-0625-1.

[191] R. Penta et al. “Effective balance equations for elastic composites subject to inhomogeneous potentials”. In: *Continuum Mechanics and Thermodynamics* 30.1 (Aug. 2017), pp. 145–163. DOI: 10.1007/s00161-017-0590-x.

[192] L. E. Persson et al. *The homogenization method. An introduction.* Ed. by Lund. Studentlitteratur. 1993. DOI: 10.1007/BFb0106742.

[193] S. Pezzuto and D. Ambrosi. “Active contraction of the cardiac ventricle and distortion of the microstructural architecture”. In: *International Journal for Numerical Methods in Biomedical Engineering* 30(12) (2014), pp. 1578–1596. DOI: 10.1002/cnm.2690.

[194] D. M. Pierce, T. Ricken, and G. A. Holzapfel. “A hyperelastic biphasic fibre-reinforced model of articular cartilage considering distributed collagen fibre orientations: continuum basis, computational aspects and applications”. In: *Comput. Methods Biomech. Biomed. Eng.* 16 (2013), pp. 1344–1361. DOI: 10.1080/10255842.2012.670854.

[195] D. M. Pierce et al. “A microstructurally based continuum model of cartilage viscoelasticity and permeability incorporating measured statistical fiber orientations”. In: *Biomech. Model. Mechanobiol.* 15 (2016), pp. 229–244. DOI: 10.1007/s10237-015-0685-x.

[196] P. Podio-Guidugli. “Configurational balances via variational arguments”. In: *Interface Free Bound.* 3 (2001), pp. 323–332. DOI: 10.4171/IFB/39.

[197] S. Preston and M. Elżanowski. “Material Uniformity and the Concept of the Stress Space”. In: *Continuous Media with Microstructure*. Ed. by Bettina Albers. 1st ed. Springer-Verlag Berlin Heidelberg, 2010, pp. 91–101. DOI: 10.1007/978-3-642-11445-8.

[198] L. Preziosi, D. Ambrosi, and C. Verdier. “An elasto-visco-plastic model of cell aggregates”. In: *J. Theor. Biol.* 262(1) (2010), pp. 35–47. DOI: 10.1016/j.jtbi.2009.08.023.

[199] L. Preziosi and A. Farina. “On Darcy’s law for growing porous media”. In: *Int. J. Non-Linear Mech.* 37(3) (2002), pp. 485–491. DOI: 10.1016/S0020-7462(01)00022-1.

[200] L. Preziosi and G. Vitale. “A multiphase model of tumor and tissue growth including cell adhesion and plastic reorganization”. In: *Math. Models Methods Appl. Sci.* 21.09 (Sept. 2011), pp. 1901–1932. DOI: 10.1142/S021820251-1005593.

[201] E. Pruchnicki. “Hyperelastic homogenized law for reinforced elastomer at finite strain with edge effects”. In: *Acta Mechanica* 129.3-4 (Sept. 1998), pp. 139–162. DOI: 10.1007/bf01176742.

[202] S. Quiligotti, G. A. Maugin, and F. dell’Isola. “An Eshelbian approach to the nonlinear mechanics of constrained solid-fluid mixtures”. In: *Acta Mech.* 160 (2003), pp. 45–60. DOI: 10.1007/s00707-002-0968-z.

[203] T. M. Quinn and V. Morel. “Microstructural modeling of collagen network mechanics and interactions with the proteoglycans gel in articular cartilage”. In: *Biomech. Model. Mechanobiol.* 6 (2007), pp. 73–82. DOI: 10.1007/s10237-006-0036-z.

[204] A. Ramírez-Torres et al. “Action of body forces in tumor growth”. In: *International Journal of Engineering Science* 89 (Apr. 2015), pp. 18–34. DOI: 10.1016/j.ijengsci.2014.11.009.

[205] A. Ramírez-Torres et al. “An asymptotic homogenization approach to the microstructural evolution of heterogeneous media”. In: *International Journal of Non-Linear Mechanics* 106 (Nov. 2018), pp. 245–257. DOI: 10.1016/j.ijnonlinmec.2018.06.012.

[206] A. Ramírez-Torres et al. “Mathematical modeling of anisotropic avascular tumor growth”. In: *Mechanics Research Communications* 69 (Oct. 2015), pp. 8–14. DOI: 10.1016/j.mechrescom.2015.06.002.

[207] A. Ramírez-Torres et al. “Three scales asymptotic homogenization and its application to layered hierarchical hard tissues”. In: *International Journal of Solids and Structures* 130-131 (Jan. 2018), pp. 190–198. DOI: 10.1016/j.ijsolstr.2017.09.035.

[208] P. Reimer et al. *Clinical MR Imaging*. Springer Berlin Heidelberg, 2010. DOI: 10.1007/978-3-540-74504-4.

[209] R. O. Ritchie, Markus J. Buehler, and Paul Hansma. "Plasticity and toughness in bone". In: *Physics Today* 62.6 (June 2009), pp. 41–47. DOI: 10.1063/1.3156332.

[210] E. K. Rodríguez, A. Hoger, and A. D. McCullogh. "Stress-dependent finite growth in soft elastic tissues". In: *Journal of Biomechanics* 27 (1994), pp. 455–467. DOI: 10.1016/0021-9290(94)90021-3.

[211] E. Rohan, Robert Cimrman, and Vladimìr Lukeš. "Numerical modelling and homogenized constitutive law of large deforming fluid saturated heterogeneous solids". In: *Computers & Structures* 84.17-18 (June 2006), pp. 1095–1114. DOI: 10.1016/j.compstruc.2006.01.008.

[212] T. Roose, S. J. Chapman, and P. K. Maini. "Mathematical Models of Avascular Tumor Growth". In: *SIAM Review* 49.2 (Jan. 2007), pp. 179–208. DOI: 10.1137/s0036144504446291.

[213] S. Sadik and A. Yavari. "On the origins of the idea of the multiplicative decomposition of the deformation gradient". In: *Mathematics and Mechanics of Solids* 22.4 (Oct. 2017), pp. 771–772. DOI: 10.1177/1081286515612280.

[214] E. Sanchez-Palencia. "Non-homogeneous media and vibration theory". In: *Lecture Notes in Physics, 127*. Springer-Verlag, Berlin, 1980. DOI: 10.1007/3-540-10000-8.

[215] G. Sciarra, G. A. Maugin, and K. Hutter. "A variational approach to a microstructured theory of solid-fluid mixtures". In: *Archive of Applied Mechanics* 73 (2003), pp. 194–224. DOI: 10.1007/s00419-003-0279-4.

[216] G Sciumè et al. "A multiphase model for three-dimensional tumor growth". In: *New Journal of Physics* 15.1 (Jan. 2013), p. 015005. DOI: 10.1088/1367-2630/15/1/015005.

[217] R. Serpieri and F. Travascio. *Variational continuum multiphase poroelasticity*. Springer Singapore, 2017. DOI: 10.1007/978-981-10-3452-7.

[218] J.C. Simo and T.J.R. Hughes. *Computational Inelasticity*. Springer, New York, 1998. DOI: 10.1007/b98904.

[219] T. Stylianopoulos et al. "Causes, consequences, and remedies for growth-induced solid stress in murine and human tumors". In: *PNAS* 109(38) (2012), pp. 15101–15108.

[220] T. Stylianopoulos et al. "Coevolution of Solid Stress and Interstitial Fluid Pressure in Tumors During Progression: Implications for Vascular Collapse". In: *Cancer Research* 73.13 (Apr. 2013), pp. 3833–3841. DOI: 10.1158/0008-5472.can-12-4521.

[221] P. M. Suquet. “Introduction”. In: *Homogenization Techniques for Composite Media*. Springer Berlin Heidelberg, pp. 193–198. DOI: 10.1007/3-540-17616-0_15.

[222] L.A. Taber. “Biomechanics of Growth, Remodeling, and Morphogenesis”. In: *Appl. Mech. Rev.* 48.8 (1995), p. 487. DOI: 10.1115/1.3005109.

[223] M. Taffetani et al. “Biomechanical modelling in nanomedicine: multiscale approaches and future challenges”. In: *Archive of Applied Mechanics* 84.9-11 (July 2014), pp. 1627–1645. DOI: 10.1007/s00419-014-0864-8.

[224] J. J. Telega, A. Gałka, and S. Tokarzewski. “Application of the reiterated homogenization to determination of effective noduli of a compact bone”. In: *Journal of Theoretical and Applied Mechanics* 37.3 (1999), pp. 687–706.

[225] A. Tomic, A. Grillo, and S. Federico. “Poroelastic Materials Reinforced by Statistically Oriented Fibres - Numerical Implementation and Application to Articular Cartilage”. In: *IMA Journal of Applied Mathematics* 79 (2014), pp. 1027–1059. DOI: 10.1093/imamat/hxu039.

[226] D. Tsalis et al. “Homogenization of elastoplastic composites with generalized periodicity in the microstructure”. In: *International Journal of Plasticity* 51 (Dec. 2013), pp. 161–187. DOI: 10.1016/j.ijplas.2013.05.006.

[227] A. A. Vakulenko. “Superposition in continuum rheology (in Russian)”. In: *Izv. AN SSSR Mekhanika Tverdogo Tela* 1 (1970), pp. 69–74.

[228] M. Vasta, A. Gizzi, and A. Pandolfi. “On three- and two-dimensional fiber distributed models of biological tissues”. In: *Probabilist. Eng. Mech.* 37 (2014), pp. 170–179. DOI: http://dx.doi.org/10.1016/j.probengmech.2014.05.003.

[229] T.J. Vaughan, C.T. McCarthy, and L.M. McNamara. “A three-scale finite element investigation into the effects of tissue mineralisation and lamellar organisation in human cortical and trabecular bone”. In: *Journal of the Mechanical Behavior of Biomedical Materials* 12 (Aug. 2012), pp. 50–62. DOI: 10.1016/j.jmbbm.2012.03.003.

[230] C. Voutouri et al. “Role of Constitutive Behavior and Tumor-Host Mechanical Interactions in the State of Stress and Growth of Solid Tumors”. In: *PLoS ONE* 9.8 (Aug. 2014). Ed. by Pankaj K. Singh, e104717. DOI: 10.1371/journal.pone.0104717.

[231] L. J. Walpole. “Elastic Behavior of Composite Materials: Theoretical Foundations”. In: *Advances in Applied Mechanics* 21 (1981), pp. 169–242. DOI: 10.1016/S0065-2156(08)70332-6.

[232] L. J. Walpole. “Fourth-Rank Tensors of the Thirty-Two Crystal Classes: Multiplication Tables”. In: *Proceedings of the Royal Society of London Series A* 391 (1984), pp. 149–179. DOI: 10.1098/rspa.1984.0008.

[233] W. Wilson, J.M. Huyghe, and C.C. van Donkelaar. "A composition-based cartilage model for the assessment of compositional changes during cartilage damage and adaptation". In: *Osteoarthr. Cartil.* 14 (2006), pp. 554–560. DOI: `10.1016/j.joca.2005.12.006`.

[234] W. Wilson et al. "Prediction of collagen orientation in articular cartilage by a collagen remodeling algorithm". In: *Osteoarthr. Cartil.* 14 (2006), pp. 1196–1202. DOI: `10.1016/j.joca.2006.05.006`.

[235] A. Yavari. "A geometric theory of growth mechanics". In: *J. Nonlinear Sci.* 20 (2010), pp. 781–830. DOI: `10.1007/s00332-010-9073-y`.

[236] A. Yavari and A. Goriely. "Weyl geometry and the nonlinear mechanics of distributed point defects". In: *Proc. R. Soc. A* 468 (2012), pp. 3902–3922. DOI: `10.1098/rspa.2012.0342`.

This Ph.D. thesis has been typeset by means of the TeX-system facilities. The typesetting engine was pdfLaTeX. The document class was `toptesi`, by Claudio Beccari, with option `tipotesi=scudo`. This class is available in every up-to-date and complete TeX-system installation.